Characterizing the Structural Influence of Electromagnetic Field Application Geometry on Biological Systems

By

Trevor N. Carniello

A thesis submitted in partial fulfillment
of the requirements for the degree of
Doctor of Philosophy (PhD) in Biomolecular Sciences

The Faculty of Graduate Studies
Laurentian University
Sudbury, Ontario, Canada

THESIS DEFENCE COMMITTEE/COMITÉ DE SOUTENANCE DE THÈSE
Laurentian Université/Université Laurentienne
Faculty of Graduate Studies/Faculté des études supérieures

Title of Thesis Titre de la thèse	Characterizing the Structural Influence of Electromagnetic Field Application Geometry on Biological Systems
Name of Candidate Nom du candidat	Carniello, Trevor
Degree Diplôme	Doctor of Philosophy
Department/Program Département/Programme	Biomolecular Sciences
Date of Defence Date de la soutenance	January 14, 2020

APPROVED/APPROUVÉ

Thesis Examiners/Examinateurs de thèse:

Dr. Robert Lafrenie
(Supervisor/Directeur de thèse)

Dr. Blake Dotta
(Committee member/Membre du comité)

Dr. Jeffrey Gagnon
(Committee member/Membre du comité)

Approved for the Faculty of Graduate Studies
Approuvé pour la Faculté des études supérieures
Dr. David Lesbarrères
Monsieur David Lesbarrères
Dean, Faculty of Graduate Studies
Doyen, Faculté des études supérieures

Dr. Rodney O'Connor
(External Examiner/Examinateur externe)

Dr. Joy Gray-Munro
(Internal Examiner/Examinateur interne)

ACCESSIBILITY CLAUSE AND PERMISSION TO USE

Abstract

There is growing literature that describes the effects that exposures to different forms of magnetic and electromagnetic fields have on biological systems. Some robust effects have been reported when the temporal structure of the electromagnetic field is patterned after what has been observed biologically. However, there has been little effort devoted to ascertaining the role for that physical application geometry, the structure through that current is presented, plays in the bio-effectivity of patterned EMF. Here we devised a series of investigations that compared 4 unique geometric organizations of copper wire based application devices to generate patterned EMFs in order to discern if application geometry has any impact on biological responses from cell systems treated with exposure to EMF. Furthermore, we examined the structural pattern of a burst-firing EMF in order to characterize that parameters are important in optimizing the proportion of cells that can be induced to bear plasma membrane extensions in a cell model of induced neuritogenesis. Results of the experiments conducted within this thesis show that the pattern of the EMF applied to PC-12 cells is the most important factor to promote neurite outgrowth. Other parameters such as: the intensity of the applied field, the timing of the field, exposure duration, and whether or not the pattern in constantly or intermittently (i.e., rotated) exposed to PC-12 cells treated with forskolin do not appreciably impact the growth of neurites. Investigations using different magnetic geometries (e.g., structures around that copper wire is wound) were able to show that the physical structure of the EMF-generating device contribute to the efficacy of neurogenesis of PC-12 cells exposed to burst-firing pattern. Furthermore, unique EMF-generating devices influenced spectral profiles of ultra-weak photons emitted from B16-BL6 cells. The differences obtained between magnetic field generating devices suggest that the more heterogeneous the patterned EMF the more impactful it is on the structural and functional aspects of the biological system under investigation. Rigorous physical experimentation examining the features associated with

unique structures around that copper wire is wound, showed that if the EMF-generating device approaches the structure of a dome, it has the capacity to reduce background magnetic field intensity and may provide insight (e.g., a mechanism) as to the efficaciousness of observed effects when a patterned EMF is generated through this device.

Keywords

Electromagnetic fields, pheochromocytoma (PC-12), B16-BL6, ultra-weak photon emission, neuritogenesis, application geometry.

Co-Authorship (where applicable)

The candidate acknowledges that written work is the product of the individual whose name is attached to this dissertation. We do not disclose any additional authorship, nor contribution outside of the primary author, in the formalization of this document.

Acknowledgements

The actualization of a Ph.D. thesis requires the dedication of not only the student who aims to bring their labours to fruition, but also the unrelenting support offered by their colleagues, mentors, and supervisors. For the continued positive support offered by members of Laurentian University's Neuroscience Research Group, past and present, I am forever grateful. I have been fortunate to have been engrossed in a creative, intelligent, and challenging environment that has fostered an insatiable pursuit of the unknown that has highlighted my experience as a graduate student. Furthermore, to all my graduate and ungraduated colleagues with whom I have had the pleasure of becoming acquainted and with whom I have grown, I am immensely thankful. It was our deep, creative, esoteric, and dare I say fringe, conversations that served as my source of motivation to continue my pursuits regardless of the trials and tribulations they offered. I have been, and will continue to be, inspired by the insights and creativity of my colleagues.

The course of development from an undergraduate and even graduate student into a Ph.D., involves the investment, care, and nurturance of an excellent committee. I could not have asked for a better group of doctors to join me on this journey and to facilitate these pursuits. To my supervisors, Dr. Lafrenie and Dr. Dotta, the amount of time and encouragement that was provided by you over this transformative experience, coming at a time of departmental reorganization, was well beyond what any other supervisor would have done. I appreciate the structure and positive reinforcement that our weekly meetings provided, as well as the challenging feedback necessary to appropriately capture the essence that this storied thesis encompasses. I am indebted to you for our lengthy office discussions related to personal development beyond the laboratory and academia. I have come to value of the benefit of life experience and the wisdom it offers and am glad have been able to gain this insight from the

two of you. Dr. Gagnon, your insight in terms of addressing aspects of mechanism of action and offers to collaborate greatly assisted in tackling the nuances of this project. It is my intention to continue to collaborate with you and your lab and enjoy the inquiry of scientific discovery. Finally, to my mentor Dr. Michael Persinger, I wish to extend a most heartfelt thank you for taking a risk on me as a student. I was able to experience a lot of learning from you, doc, and I will cherish our corrective feedback chats, philosophical discussions, chalkboard sessions, and a good King Fish and Lilly-fly joke. Many thanks for emphasizing the power of the scientific method, challenging preconceived notions, and promoting the pursuit of the unknown.

Table of Contents

List of Figures

List of Tables

List of Appendices

List of Abbreviations

AC (alternating current); AM (amplitude modulated); BDNF (brain-derived neurotrophic factor); cAMP (cyclic adenosine monophosphate); CREB (cAMP response element binding protein); DAC (digital-to-analog converter); DC (direct current); EAE (experimental allergic encephalomyelitis); EEG (electroencephalograph); ELF (extremely-low frequency); EMF (electromagnetic field); ERK (extracellular signal-regulated kinase); FM (frequency modulated); HF (high frequency); IR (infrared); ISI (inter-stimulus interval); LSD (lysergic acid diethylamide); LTP (long-term potentiation); MAPK (mitogen activated protein kinase); MF (magnetic field); NGF (nerve growth factor); PC-12 (pheochromocytoma); PD (point duration); PME (plasma membrane extension); PKA (cAMP dependent protein kinase A); rMF (rotating magnetic field); SEM (standard error of the mean); UPE (ultra-weak photon emission); UV (ultraviolet)

Chapter 1

1.1 Non-Ionizing, Electromagnetic Field Effects on Biological Systems: An Introduction

Electromagnetic fields used in research can be dichotomized as either 1) static or 2) dynamic (time-varying). Each subdivision has its own unique features that contribute to the efficacy of the field under examination. A static magnetic field, as exemplified by a bar magnet, is generated by the alignment of magnetic moments/dipoles that are contained within the material of the magnetic body. The greater the homogeneity of magnetic moment alignment, the greater the intensity that is generated from the material and ultimately experienced by whatever matter (system) is interposed within the magnetic lines of force. The alignment of magnetic moments can be used to explain a number of observed phenomena associated with exposures to a static magnet including polarity and the consequences of bifurcating the material. Magnetic polarity is the result of having a magnetic dipole whose force lines, that are representations of magnetic force, extend from one pole of the particle (i.e., North pole) and bends to return to the other, opposite, pole (i.e., South pole). Secondly, the act of bisecting a bar magnet results in the formation of 2 smaller, equally intense magnets that observe a conserved polarity (i.e., North and South poles). In actual fact, what happens when one bisects a bar magnet is that the available aligned magnetic moments are equally divided and distributed into separated halves provided that the material is a homogenous substrate and if we were able to re-fuse the halves, the intensity and polarity would be restored.

The second category of magnetic field, that of dynamic or time-varying magnetic fields, is not generated by the alignment of magnetic moments but rather by the movement (rate of change) of charged particles. Displacement of a charged particle as a function of some temporal increment (time) generates a current. According to the Biot-Savart law, a current generated in

a conducting wire generates a perpendicularly radiating magnetic field around that wire in a direction parallel to the axis of current flow. The relationship between the movement of a charged particle and the generation of a perpendicular magnetic field is exemplified by the description provided by a Lorenz force, or more colloquially electromagnetic force (Dahl, 1997; Burke 2012). The electromagnetic force comprises 1 of the 4 fundamental forces known in our Universe and results from the interaction between electrically charged particles and is carried by the electromagnetic field.

The relationship between electricity and magnetism has been extensively researched by Volta, Ampere, Gauss, and most notably, Faraday. Maxwell summarized Faraday's findings that mathematically describe the operation of electromagnetic fields. Dynamic (time-varying) magnetic fields can be further sub-categorized into 1) rotating magnetic (rMF) fields and 2) propagating electromagnetic fields (EMF). rMF are created by the axial rotation of a static magnetic. Consider the case of 2 horseshoe magnets that are being rotated in a counter clockwise fashion by way of a rotary motor. Field lines are described as being attractive between opposing poles and repulsive when presented with paired polarity. When we activate the rotary device, the field lines are torqued and twisted alternating between periods of attraction and repulsion generating regions of amplified and depressed intensity with the potential of even creating magnetic "dead zones" (nodes) when the 2 horseshoe magnets are oriented perpendicularly. The complex interaction between rotating magnetic material not only creates opposing and attractive forces but alterations in the experienced intensity of any object that is placed within their rotational space. The rate at that the magnets are rotated, a feature that we operationalize as frequency or pattern, also contributes to the experienced intensity and potential for biologically-relevant field effects. A second method of generating a rMF is by rotating a propagating EMF. Consider an array of equally spaced solenoids arranged

circumferentially (i.e., in a circular array). When current is supplied to each of the solenoids they will generate a magnetic field. Now, consider that if we were to delay the presentation of current to each subsequent solenoid sequentially by some arbitrary temporal increment such that all of the solenoids are not presented simultaneously, then we will have created an artificially rotating electromagnetic field. Furthermore, we would be able to visualize the rotational component of the magnetic field by placing a metal spinning top in the center of the apparatus and initializing the delayed-sequence field presentation to the series of solenoids. A similar piece of equipment as described, has been developed by Persinger and Koren and has been used to experimentally elicit excess correlation between human pairs, physiochemical reactions, and pH deviations in aqueous solutions (Persinger et al., 2003; Richards et al., 2002; Dotta et al., 2012; Persinger and Koren, 2016).

Propagating EMFs result from current injections into a magnetic field-generating device, typically composed of a series of wires wound in a particular geometry (i.e., solenoid, toroid, etc.), in that the presentation of the respective current is varied in terms of frequency (time of presentation) and amplitude (amount of current presented). Most electronic devices in North America generate a 60 Hz, patterned EMF as the result of the standard alternating current supplied by electrical power grids. An EMF generated by the application of a sine wave is categorized as a symmetrically patterned EMF whose rate of change between adjacent points, or rise time, is gradual. Conversely, when the increment of time (frequency) between successive current applications or the intensity (amplitude) of successive current injections are variable and abrupt, the patterned EMF is defined as being asymmetrical. Notably, changing the frequency of current presentation or the amount of current being supplied to the field-generating device would be likened to frequency and amplitude modulations for a given EMF, a feature that is central to radio communication systems. Amplitude and frequency modulation,

static versus dynamic, propagating versus rotating, and the concept of symmetrical versus asymmetrical constructs of EMF represent features that can comprise the "application geometry" of EMF research. Additional features that can be categorized in terms of application geometry include the physical apparatus through that the resulting EMF has been generated and phase modulation of the resulting EMF.

Little evidence has been gathered to address the impact that EMF application geometry has on biological systems or to address the contribution of physical application geometry as a variable in EMF research. In biology, structure is said to dictate function as evidenced by the development/differentiation of specialized cells (i.e., neurons, neutrophils, macrophages, erythrocytes, etc.) that are designed to execute specific function(s). In this chapter, the evidence that different forms (sources) of MF/EMF energy can elicit different effects on cells will be reviewed. In addition, research suggests that even though the exposure apparatus may be the same, different temporal organizations (patterns) of stimulus presentations can also produce different effects. Both the source of the MF/EMF energy and temporal construction of the stimulus can be argued to be forms of "structure" of an EMF. In later chapters, we will investigate the bio-effectivity provided by the physical structure of EMF-generating devices in terms of EMF effects on cell systems.

1.2 Static MF

The characteristics of MF/EMF applications are of importance in order to differentiate their effects. In this section, we categorize static MF as being derived from the alignment of magnetic domains (clusters of magnetic moments) that are contained within the structure of a material. Static MF effects are derived from the application of traditional bar magnets or their equivalents. Persinger (1976) summarized a number of effects that were associated with the

application of a static MF, whose intensities ranged from 10 G to 5 kG. For example, rats exposed to static MF showed differences in the mass of visceral organs, disease susceptibility, and endocrine physio-chemistry. Furthermore, Pelyhe et al., (1973) demonstrated that exposure to static MF applications (8 kG) affected conditioned avoidance training in rats. It was determined that there was a delay in criterion learning for those animals that were exposed to the static MF conditions as compared to their sham-exposed counterparts. In addition, the orientation of migratory birds can be altered when they are exposed to strong static MFs (Ossenkopp and Barbeito, 1978; Saunders, 2005).

Static MFs have been shown to impact cell structure and function. For instance, exposures to a strong, static MF of Tesla level intensities (10 kG) can regulate orientation of matrix proteins, such as collagen and fibrin fibers, as well as cells (Bigham et al., 2009; Leesungbok et al., 2013) while higher intensity fields (8 T) have been shown to impact osteoblastic cell formation (Kotani et al., 2002). Kotani et al., (2002) observed the presence of rod-like osteoblastic cell formations aligned in the direction of the field and concomitant cell differentiation and matrix synthesis pathway activation following 60-hour exposures to static MF in *in vitro* and *in vivo* models of bone formation. Bidal (2018) demonstrated that prolonged exposure to static MFs (0.16 T) can alter calcium crystal formation in samples of spring water that were maintained in darkened environments. Time-dependent changes in membrane structure (i.e., cell surface damage) and *E. coli* colony formation following exposure to static MF were observed by Ji et al., (2009). Weaker static MF intensities (0 – 118 μT) were shown by Binhi et al., (2001) to promote anomalous viscosity time-dependencies in ion-protein complexes. The authors determined that there were differences in this measure when the specimens were rotated at 18 Hz while being exposed to the field. Exposures to a 220 mT static MF increased ethanol production by 3.4-fold in fermenting *S. cerevisiae* (da Motta et al., 2004; Muniz et al., 2007).

The authors also reported a 2.5-fold increase in biomass associated with static MF treatment and ethanol production.

1.3 Rotating MF

For the purpose of this thesis, we defined a rotating MF (rMF) as falling under the umbrella of a static (bar) magnet, or equivalent, that has been subjected to concentric displacement (i.e., rotation). Therefore, the discussion herein is limited to the biological effects observed following exposure to a rMF and excludes experiments and observations made on biological substrates subjected to rotation within a static field.

Rotating MFs have been shown to successfully impact functional (behavioural) and structural aspects of animals when exogenous fields are applied during natal development. For example, Persinger (1969) demonstrated a reduction in the ambulatory behaviour of rats that had been continuously exposed to a 0.5 Hz rMF of intensity 3-30 G as compared to sham-treated controls. Additionally, Persinger and Pear (1971) demonstrated statistically significant suppression of response rates in a conditioned suppression test specifically for those animals with a history of rMF exposure as compared to control-treated animals. The authors suggested that the data supported the concept that rMF-treated animals are more reactive to aversive stimuli. In a series of investigations, Kavaliers and Ossenkopp (1985, 1986) examined the synergism between rMF treatment and analgesic responses in mice. They determined that mice, both the CF1 and C57-BL strains, treated for 60 min with 0.5 Hz rMF (intensity: 0.5 G, 1-90 G) had reduced locomotion and analgesia produced by morphine. The observed changes were dose-dependent and were maintained in both day-time analgesia and nocturnal analgesia (Ossenkopp and Kavaliers, 1983; Kavaliers and Ossenkopp, 1984; Kavaliers and Ossenkopp, 1985). The authors were able to demonstrate that application of EGTA (a calcium chelator)

removed field effects while administration of a calcium ionophore A21387 potentiated inhibition. Similarly, mice exposed to 0.5 Hz rMF (1 – 8 G) demonstrated a significant reduction in analgesic effects mediated by μ and κ opiate agonists in a manner similar to naloxone, as well as an inhibition in the endogenous opioid mediated responses, to warm- and cold-stress induced nociception. No effects were observed for animals treated with saline solutions (Kavaliers and Ossenkopp, 1987). These data support Persinger and Pear's hypothesis that rMF enhances behavioural reactivity in animals. One possibility that may arise from a decreased threshold for reactivity is the enhanced capacity to discern discrete stimuli. Investigations conducted by Blomme and colleagues (1990) demonstrated that pigeons could accurately discriminate between the presence or absence of an rMF and that task accuracy could be interrupted by sudden changes in ambient lighting, an alternative form of electromagnetic radiation. Accuracy of discrimination was a function of individual differences.

Mulligan and Persinger (1998) exposed rats to 0.5 Hz rMF at 3 – 30 G prenatally, and showed reduced cell density in the medial preoptic nucleus of the male, but not the female rats, suggesting that prenatal rMF exposure may alter sexually dimorphic characteristics and circadian cycle features. Reductions in pineal melatonin, a neurohormone associated with circadian cycle and sleep-wakefulness, was demonstrated in rats who were continuously exposed to a 50 Hz rMF at 1, 5, 50, and 250 **μT** for 6 weeks (Kato et al., 1993). Ossenkopp et al., (1972) demonstrated intensity- and duration-dependent changes in testicular and thyroid weights in adult male rats that had been prenatally exposed to 0.5 Hz rMF at 0.5-3 and 3-15 G intensities. Furthermore, prolonged exposure to 0.5 Hz rMF, with intensities of 0.5 – 3 and 3 – 30 G, resulted in progressive changes in body weight, thyroid weight, water consumption, adrenal weight, and circulating eosinophil counts (Persinger et al., 1972). Persinger et al., (1972) further explored these changes by exposing rats continuously to 2 field intensities (0.5

– 3 G, 3 – 30 G) of 0.5 Hz rMF for 5, 10, or 26 days. Water consumption was greater in rats exposed for longer durations (10 and 26 days versus 5 days) while increased weight gains and decreased thyroid weight was observed in animals exposed for 10 days or less while longer exposure durations were associated with increased testicular weight.

Structural and functional changes secondary to rMF exposure have been observed in bacterial cultures. In one experiment, Fijalowski et al., (2013) showed frequency-dependent changes in growth rates, metabolic activity, and biofilm formation in *E. coli* and *S. aureus* cultures following 60-min exposures to rMFs ranging in frequency between 1 – 50 Hz and intensities of 22-34 μT. These same biological features were measured following a 60 min rMF exposure of 8 different bacterial species (*S. aureus, E. coli, A. bauminnii, P. aeruginosa, S. marcessans, S. mutans, K. oxytoca,* and *S xylosus*). Results indicated that field treatment stimulated growth, biofilm formation, and metabolism in 6 of the 8 species with inhibition of metabolism and biofilm production also observed in *A. bauminnii* and *P. aeruginosa* **(**Fijalowski et al., 2015). rMF exposures have differential impacts on different biological systems that are contingent on the duration of exposure and the frequency of rotation.

1.4 Propagating EMF

Propagating EMF is defined as a field generated by the movement of charge (current or voltage) presented through a material designed to serve as the EMF application device. The creation of time-varying electric fields are able to generate a changing magnetic field in accordance with Maxwell's descriptions. This section is divided into sub-categories based upon the parameters of manipulation.

1.4.1 DC-EMF

We define DC-EMF as belonging to one of two categorical constructs; those that result from the constant application of non time-varying (static) current and those where the current's rate of change is less than 1 Hz in frequency. Exposures to DC-EMF has been shown to impact motor activity in a number of animals especially when intensities fall within the range of 10s of mT (Kholodov, 1967, 1969, 1975, 1979). Reductions in excitation thresholds and slowing of action potentials were reported by Volobuev et al. (1985) when samples of sciatic nerves were exposed to 5.5 mT DC-EMF. Altering the intensity of DC-EMF, to between 0.8 and 2.0 T resulted in alterations in fluorescein transport in nervous tissues (Bresler et al., 1978). Additional alterations at the level of the nervous system were observed when the intensity of the DC-EMF fell within 20 – 30 mT and when exposures lasted for 1 hour as described by Aleksandrovsknja and Kholodov (1966). The authors reported an increase in the number of stained astroglia, oligodendrocytes, and microglia in the sensorimotor neocortex of rabbits, sparring an impact on the structure of neurons. Artjwikhina (1988) showed that daily, 2-hour exposures to DC-EMF for 1, 3, 6, 14, and 21 days caused animals to show alterations of neuron, glial, vasculature, and synapse morphology. The structural alterations were determined to be a function of exposure duration, or the number of exposures. The impact of DC-EMF on the functional activity in the brain was assessed by Luk'janova (1969) who exposed rabbits to 90 mT DC-EMF and measured activity in neurostructural aggregates (e.g., hippocampus, thalamus, etc.) that showed an inhibitory action on the pulse rate of these structures. For human brain activity, electroencephalographic (EEG) slow wave and alpha spindles were recorded by Shpil'berg and Vjalov (1972) after prolonged exposure to DC-EMF whose intensity was greater than 10 mT. Prolonged, systemic, exposure to DC-EMF in the 10s of mT range, is associated with fatigue, dizziness, sleeplessness, headache, and somatic symptoms in workers in industrial settings as documented by Vjalov (1971). Others showed that short-term exposure

(~10 min) of humans to 93 µT DC-EMF increased EEG delta activity (0-3 Hz) over central parietal channels (Bell et al. 1991). Fuller et al., (1995) measured increased epileptiform activity (i.e., aberrant electrical activity) over the medial temporal lobe of individuals that were exposed to 1-2 mT DC-EMF for 5 min.

In cell models, exposure to DC-EMF for 2 – 4 min at an intensity of 20 – 200 µT reduced antibody secretion from spleen cell suspensions with maximal inhibition observed at an intensity of 50 µT (Podkolzin and Dontsov, 1994). Exposures to DC-EMF at 1.1 T intensity was determined to orchestrate the formation of an artificial lipid bilayer from egg lecithin in such a way that the field oriented parallel to the substrate negatively impacted bilayer formation while bilayer formation was facilitated when the field was oriented perpendicular to the substrate. In terms of cancer treatment, Anisimov et al. (1996) reported that exposures to a 300 µT DC-EMF promoted mammary carcinogenesis in outbred female rats provided that exposures were presented for 3 hours a day for 14 days.

Synergisms are observed when DC-EMF are coupled to AC fields. Shuvalova et al., (1991) showed that the rates of calmodulin-dependent phosphorylation of myosin by light chains myosin kinase could be altered, when exposed for 20 minutes, to 20.9 µT DC-EMF coupled to 20.9 µT, 8 – 20 Hz AC EMF. Regenerating planarian exposed to 20.9 µT DC-EMF and 38.6 uT, 16 Hz AC EMF for 4 – 240 hours showed increased mitosis rates in postblastema and an acceleration of blastemal growth (Tiras et al., 1996). Shorter duration exposures (~20 min) to 21 mT DC-EMF and 140 uT, 16 Hz AC EMF maximized heart beat power spectra in *Daphnia magna* at the 16 Hz frequency if and only if the 2 fields were presented simultaneously (Chemeris and Safranova, 1993). Blackman et al., (1994) and Lednev (1996) suggested that the existence of amplitude windows, described as alternating between strengthening and

weakening of the effects when the amplitude of the AC modulation was increased, as a possible source of variance to describe the observed results.

1.4.2 ELF-EMF

Extremely-low frequency (ELF) EMFs are defined as those EMFs whose frequency component, presented through an EMF-generating device, falls within the range of 1 – 100 Hz. Included in this sub-section are those EMFs that have been amplitude modulated (AM) or frequency modulated (FM) provided that the frequency range is restricted to the 1 – 100 Hz bin. Special attention is paid when describing AM features.

There is evidence to suggest that exposures to ELF-EMF, either sinusoidally patterned or organized in a way to reflect the activity of biological systems, can affect chemical and cellular processes. For instance, Lazar and Barca (1969) found that exposures to a weak intensity-pulsated magnetic field increased uptake of potassium ions and decreased uptake of sodium ions in tissue compared to exposure to a static magnet that demonstrated an opposite effect. Charge transfer and reaction rates for Na, K-ATPase and cytochrome oxidase can be modulated in response to ELF-EMF application (Blank, 1992; Blank and Soo, 1993; Blank and Soo, 1998; Blank and Soo 1998a; Blank and Soo, 1998b; Blank and Soo, 2001a). Blank and Soo (2001b), found that the presence of a 60 Hz, 28 μT ELF-EMF altered a Belousov-Zhanotinski reaction. Under normal conditions, the rate of the reaction is positively correlated to temperature while in the presence of the EMF an increase in the temperature decreased the overall rate of reaction in a model consistent with Moving Charge Interaction model. When samples of spring water are exposed to a bulk angular decelerating/accelerating velocity EMF with accelerating/decelerating phase velocity EMFs the latency of the response to injections of a weak proton donor is increases (it takes longer to respond) (Dotta et al., 2013). Exposure of

spring water to a different patterned EMF (Thomas) caused an increase in alkalinity over the course of a 12-hour exposure regimen (Murugan et al., 2014). Cultured cells have shown alterations in cAMP levels caused by exposure to ELF-EMF in a duration-specific manner (Schimmelpfeng and Dertinger, 1993). Exposures to pulsated fields between 130 µsec to 3 secs, at intensities up to 200 G for periods of 1.5 hrs per day for 30 days, and to more continuous exposures, have been reported to affect Glucose-6-Phosphate activity, ATP/ADP ratios, serum glutamic oxalacetic transaminase levels, and follicle size (Proumb, 1971; Neaga and Lazar, 1972). Furthermore, exposures to ELF-EMF have been reported to mitigate the effects of ionizing radiation (Barnothy 1963a; Amer and Tobias, 1965; Zecca et al., 1984). Additional evidence suggests that weak (less than 1 G), low frequency fields can influence bone healing (Basset, 1994), regeneration of peripheral nerves (Sisken et al., 1993; Sisken et al., 1995), alterations in cellular levels of calcium (Liburdy, 1992; Liburdy et al., 1993), increases in transcript levels of the early response genes myc, jun, and fos (Lin et al., 1994; Lin and Goodman, 1995; Lin et al., 1996; Jin et al., 1997; Phillips et al., 1992; Rao and Henderson, 1996), HSP-70 (Goodman and Blank, 1998), and electron-transfer rates (Blank and Goodman, 2004).

Buckner et al., (2015, 2017, 2018) demonstrated that daily 1-hour exposure of cultured cells to an ELF-EMF, Thomas-EMF, was able to inhibit the growth of malignant, but not non-malignant, cells *in vitro* and *in vivo*. Further investigations were able to demonstrate an increase in calcium influx by activation of voltage-gated T-type calcium channels as the driving force behind the observed Thomas-EMF effect. Using the same target field, Dotta et al., (2014) demonstrated reliable differences in spectral power densities of ultra-weak photon emission from B16-BL6 cells corresponding to intensities of 0.9 and 1.8 µT but not others. These differences were enhanced when samples were pre-exposed to a complex patterned EMF for 4

min prior to exposure to Thomas-EMF. The authors indicated that the peak frequencies affected by the application of these EMF sequences correspond to the energy difference obtained between the orbital-spin magnetic moment as derived from the Rydberg atoms corresponding to these intensities. Employing this target pattern (i.e., Thomas-EMF) in more complex biological systems, Tessaro and Persinger (2013) demonstrated an enhancement in the rate of regeneration of bisected planaria. Conversely, exposure of whole planaria to the combination of Thomas-EMF (0.1 to 2 uT) for 6.5 hours per day for 5 days followed by an exposure for an additional 6.5 hours to a complex, amplitude modulated EMF (0.5 to 5 uT) with exponentially increasing spectral power, designed to mimic sudden-storm onset of the Earth's geomagnetic field, was able to elicit complete fragmentation of the planaria (Murugan et al., 2013).

Exposures to different field configurations can lead to differential effects. For example, Piacentini et al., (2008) exposed differentiating neural stem/progenitor cells to a 1 mT 50 Hz EMF and observed increased spontaneous firing of voltage-gated calcium channels in response to treatment with KCl. Murugan et al., (2014b) exposed human breast cancer cells to either morphine or burst-firing EMF at an intensity of 1 μT and demonstrated, by systematic investigations with chemical inhibitors, that both treatments affected mu opioid receptors and could be blocked by classical antagonists, but only morphine was able to activate molecular pathways associated with cell proliferation. Exposure to 50 Hz EMF for two months resulted in more sensitive responses of catalases, glutathione reductase, and the overall capability to neutralize peroxyl radicals in the land snail *Helix aspersa* (Regoli et al., 2005). Blackman et al., (1993a) reported enhanced neurite outgrowth of differentiated PC-12 cells exposed to a 50 Hz, 7.9 μT EMF for 22 hours. However, in another cell isolate of PC-12s, the same exposure conditions reduced neurite outgrowth (Blackman et al., 1993b). Investigations using isolated microtubule preparations revealed spectral power density changes in biophoton emission, and

not mean number of photons emitted, when exposed to a patterned EMF designed to facilitate LTP in hippocampal slices (Dotta et al., 2014b). Work examining the utility of simultaneously exposing pairs of either cell cultures or human beings to the same complex pattern of accelerating/decelerating bulk angular velocity field with contradictory or opposing (decelerating/accelerating) phase velocity fields, revealed coherent responses to light flashes in both pairs, when only 1 target received light application although they were spatially isolated (Dotta et al., 2011).

In bacteria, ELF-EMF exposures have been shown to alter chromatin conformation in *E. coli* and stimulate growth especially when the frequency of the applied EMF fell within the range of 7 – 11 Hz (Belyaev, 2011; Alipov and Belyaev, 1996). Other investigations by Belyaev and Alipov, (2001) demonstrated that exposures to 9 and 16 Hz resonant frequencies were observed for *E coli* (GE499), while 8.5 Hz was effective for the GE500 strain. In human cells, the frequency windows for resonant-like features were determined to be within the 8 and 58 Hz frequency bands. It was suggested that the data supported the ion cyclotron resonance model, where the angular frequency response of acceleration that is experienced when ions are placed in a magnetic field driven by the Lorenz force, for several biologically relevant ions. Tessaro et al., (2015) exposed 4 species of bacteria (2 gram-positive and 2 gram-negative) to 6 EMF conditions: 3 variations of the Thomas-EMF, strong static magnets (5000 G), oppositely rotating strong magnets (5000 G, 30 rpm), and a strong dynamic MF generator (Resonator, average intensity ~ 250 uT) all exposures were maintained for 12-hour durations. ELF-EMF treatments significantly impacted the growth rates of bacterial cultures while the static magnets did not. The Resonator increased growth in 3 of the selected bacterial species but slowed the growth rates of *S. marcescens*.

Exposure of organisms to ELF-EMF has been shown to be associated with a variety of behavioural changes (Persinger, Ossenkopp, & Glavin, 1972: Ludwig et al., 1968; Friedman, Becker, & Bachman, 1967; Reiter, 1964; Konig, 1962) and have been implicated as possible "zeitgebers" for circadian rhythms in man (Wever, 1967, 1968). Intermittent exposure to ELF-EMF have been shown to delay hatching in ducks and produce unfavourable albumin biosynthesis as compared to exposure to a static MF of the same intensity that had no effects (Ossenkopp and Shapiro, 1973). Reille (1968) reported that pigeons exposed for 5 sec to 0.15 G at 0.3 Hz, 0.5 Hz, and higher frequency fields before the onset of an electric shock, began to show increases in heart rate after the presentation of the field but before the shock. Similar findings were reported by Yakovleva and Medvedeva (1974). Neurodevelopmental changes in the hippocampus, as well as in contextual fear learning in response to ELF-EMF administration in rats was investigated by Fournier et al., (2012). Rats were exposed to 4 different intensities of complex patterned EMF (5 – 20 nT, 30 – 50 nT, 90 – 580 nT, and 590 – 1200 nT) that was designed specifically to interfere with brain development during gestation and their histochemistry was examined. The results indicated that a narrow band intensity was capable of reducing cell density in the CA1 and CA3 hippocampal subfields. Conversely, Dupont et al., (2004) demonstrated some alterations in cell density within the parasolitary nucleus following treatment with a 0.5 Hz square wave complex magnetic fields with hourly alterations in amplitude and intensity ranges falling within the nT spectrum.

Seizures have been described as aberrant electrical discharges within specific brain structures (Bodde et al., 2009), ultimately altering their electrical sensitivity (Varro et al., 2009; Csernansky et al., 1988; Gaetz, 2004). ELF-EMFs have been shown to induce increased electrical lability in treated cells and it should be possible to disrupt or affect the function of these more labile structures and observe large scale behavioural changes. Bureau and Persinger

(1995) demonstrated a reduction (68% as compared to 100%) of overt behavioural displays contingent on lithium-pilocarpine-induced stage 5 seizures for animals that received 20 pairings of 4-min of burst-firing EMF for 1s every 4 seconds. Another study with 24 male rats with histories of limbic seizures, involved exposures to 10 different variations of point duration and inter-stimulus interval in two different, patterned EMFs (Thomas and burst-firing) for 5 min and revealed that animals receiving treatments of the Thomas pattern with point duration and inter-stimulus interval set to 3 msec, displayed significantly more Racine level 5 seizures (Persinger and Belanger-Chellew, 1999). Furthermore, application of a 7 Hz, 5 nT ELF-EMF to rats during prenatal development impacted post-seizure mortality when ELF-EMF treated rats were adults (St-Pierre et al., 2007).

The perception of nociceptive stimuli (i.e., pain) has implications for learning and survival, while pain, secondary to organic or non-organic (psychogenic) conditions, can negatively impact the quality of life (Weich et al., 2008; Bär et al., 2005). The potential to mitigate the perception of nociceptive stimuli with ELF-EMF treatment has received great attention. Del Sepia (2007) reviewed evidence that exposure to weak, time-varying ELF-EMF can elevate nociceptive thresholds, alternatively producing analgesia, in a variety of vertebrates and invertebrates. Fleming et al., (1994) experimentally compared the effectiveness of morphine (4mg/kg), naloxone (10 mg/kg), and exposure to burst-firing EMF (5 μT for 1 sec every 4 seconds) across 3 successive days and found that the burst-firing pattern elicited a more prolonged and larger analgesic effect than the other treatments. The effect size obtained was argued to be therapeutically relevant for potential clinical interventions. Ryczko and Persinger (2002), compared the latency of nociceptive responses in female Wistar rats at 30 and 60 minutes following a 30 min exposure to either; 1) burst-firing EMF or 2) Activity Pulse by Emmers (another patterned EMF theoretically designed to produce analgesia) at an intensity of

1 μT. Results indicated relative increases in nociceptive response latencies for animals treated with the burst-firing EMF but not the Activity Pulse EMF at 30 and 60 minutes after exposure. The effectiveness of the burst-firing patterns was significantly greater than the effects observed for naloxone or naloxone in combination field-treated animals. In a series of experiments spanning 2 years, Martin and colleagues further described the specificity, timing, application geometry, intensity, and most effective patterns of ELF-EMF to induce analgesia. Martin and Persinger's (2003) first endeavour compared the efficacy of 2 different EMF patterns (burst-firing and Thomas) generated from either a heterogeneous EMF-generating device (solenoid) or a homogeneous source generator (Helmholtz coil) to produce analgesia in response to thermal nociception. Results indicated that those animals receiving EMF treatment generated from a heterogeneous application device exhibited strong analgesia immediately and 30 minutes following ELF-EMF treatment. These authors also demonstrated that treatment with clonidine in the presence of a 1 μT burst-firing ELF-EMF enhanced analgesic responses in animals challenged with thermal nociceptive stimulation in a dose-dependent manner, while the same EMF configuration in combination with prazosin, phenylephrine, and yohimbine had no effect (Martin and Persinger, 2004). Subsequently, Martin et al., (2004a) systematically investigated the potential of polarity (positive, negative, bipolar) of the burst-firing EMF to reduce nociceptive responses to thermal insult, and demonstrated that the burst-firing EMF presented with positive polarity or bipolar organizations had the strongest analgesic responses when presented over 30 min for 1 sec every 4 sec. Further investigations demonstrated an intensity dependence, and augmentation of analgesic responses associated with pre-injections of morphine (4mg/kg) or agmatine (10mg/kg) but was blocked by naloxone (1 mg/kg) in rats treated with burst-firing EMF for 1 sec every 4 sec over the duration of 30 min (Martin et al., 2004b). The observed effects were conserved when using the Thomas-EMF, that is also capable of eliciting analgesia, albeit with an onset occurring much more quickly. In a follow-up study

comparing the most effective ELF-EMF capable of producing analgesia in rats, burst-firing EMF (that mimics LTP) in combination with nimodipine, but not when presented in combination with Haldol, Chlorpromazine, and prednisolone (Martin and Persinger, 2005) Finally, Martin et al., (2005) altered the parameters of magnetic field stimulation to determine that components were important to maximize the effectiveness of the analgesic response in male rats: the successive time delay of burst-firing presentations, the total exposure duration, and the point duration (i.e., the length of time each current value was presented) that composed the pattern were systematically investigated. Results demonstrated that maximum analgesia was produced when the combination of 30 min exposures with presentations lasting 690 msec presented ever 4 seconds. Further findings demonstrated elevated nociceptive thresholds in seized rats for at least one week after a single exposure. Two other fields, the Thomas EMF and a chaos pattern derived from the May algorithm, produced similar levels of analgesia (Martin et al. 2005).

One structure that has been associated with remarkable sensitivity to electrical insult has been the hippocampus (Andersen et al., 2006**).** The underlying function of the hippocampus is concerned with the formation of new and retrieval of old memories (Andersen et al., 2006; Crosby et al., 1962). The antecedent processes that convert newly acquired memory into longer term representations within the interconnections between dendritic spines has been reported to be affected by electrical and magnetic mechanisms (McFadden, 2013). An ELF-EMF modeled after theta burst-firing neurons in the hippocampus (a pattern of activity that can induce LTP in hippocampal slices (Rose, Diamond, Pang, & Dunwiddie, 1988), had powerful effects on learning. Data collected from rats exposed to low intensity (200 to 500 nT) theta-burst EMF modelled after current equivalents demonstrated the capacity to induce long-term potentiation in hippocampal slices either immediately before or after training using a radial arm maze task.

Results were suggestive of an impairment in spatial memory (commissions of reference errors) in animals that were exposed to the LTP-patterned EMF immediately after training (McKay and Persinger, 2000). Conversely, an observed reduction in the speed of responding was associated with animals that had received ELF-EMF exposure prior to training. Using the same patterned ELF-EMF presented for 30-min either before or following fear conditioning resulted in a marked attenuation of freezing behaviour during contextual extinction 24 hours later, specifically for those animals that had received the treatment following training (McKay et al., 2000). In an experiment aimed to ascertain potential synergisms between treatment with ELF-EMF and with chemical stimulation on disrupting contextual fear learning, McKay and Persinger (2003) reported that the combination of 4mg/kg amagmatine and 30 min exposures to LTP EMF immediately following learning significantly decreased freezing behaviour. Increased performance in radial arm maze cued recall, where the cue was a static magnet, was reported in rats exposed to LTP ELF-EMF when the inter-stimulus interval was set to 4000 msec (McKay and Persinger, 2005). Delparte and Persinger (2007) found that exposures to LTP patterned ELF-EMF elicited amnesic effects for contextual stimuli in rats that were exposed to LTP ELF-EMF for 15 min per day for 6 days in a paradigm of food-induced conditioned place preference. Rats exposed to LTP patterned ELF-EMF for 30 min before training displayed impairments in memory performance in operant tasks while a facilitation of performance on a timed inhibitory task was observed in animals that were exposed to this pattern during task acquisition (Mach and Persinger, 2009). Animals that have been induced to have chronic (limbic) seizures followed by treatment with ketamine behave similarly to controls although the underlying structure of the brain demonstrates distinct alterations (McKay and Persinger, 2004; Fournier and Persinger, 2004). When ketamine-treated lithium-pilocarpine seized rats were exposed to a complex sequence of magnetic fields during 8 days of radial arm maze acquisition, followed by 14 days of constant exposure to the Thomas pattern

before retention testing, where no training occurred, there was a slower response duration as compared to all other treatment conditions (McKay and Persinger, 2006). If alterations in hippocampal structure are associated with the acquisition of memories (und Halbach, 2009; Geinisman, 2009), then any change that positively or negatively impacts the encoding of new information should also elicit structural changes in the hippocampus. Whissel et al., (2009) demonstrated that acquisition of conditioned fear was inhibited in animals exposed to a LTP patterned ELF-EMF, with a concomitant decrease in cell density in the CA2 hippocampal sub-field when intensities were greater than 10 nT while there was an increase in cell density in Somer's sector (the CA1 hippocampal sub-field) when intensity ranged from 10 – 50 nT as well as reduction in cell density in the medial preoptic nucleus that was linearly dependent on field intensity.

In humans, exposures to ELF-EMF have been reported to impact measures of electroencephalographic activity, sensation, subjective and empirical measures of mood and performance. Ruttan et al., (1990) exposed human participants to pulsed EMFs with frequencies of 4, 9, and 16 Hz with intensities between 0.3 to 1.0 mG (100 nT) at the level of the temporal lobes. Participants receiving field applications displayed enhanced vestibular, depersonalization, and imagining experiences, as well as an increased number of temporal lobe spikes correlated with self-reported pleasantness scores. Using a different EMF configuration, Glover and colleagues (2007) were able to produce vertigo in 30% of their participants. Volunteers exposed to successive 3-min bursts of different types of weak, patterned EMF reported the sense of a presence while an exceptional subject with a history of accurately discerning the health and history of people when handling their photos also reported an increased number of events associated with this capacity when the fields were present (Cook and Persinger, 1997). In a study examining 50 men and 50 women exposed to 5-min-off and

10-min-on cycles of burst-firing EMF for 35 min, Persinger (2003) demonstrated significantly more experiences of a sensed presence for women, as compared to men, while the men were more likely to consider these experiences as “intrusions” from an external source. The possibility that exposures to ELF-EMF can enhance intrinsic features in a unique individual was investigated with the artist Ingo Swann, who is reported to recreate and describe randomly selected photos that were sealed in envelopes and placed in another location. Koren and Persinger (2002) assessed the ability of Swann to accurately depict target photographs that were treated with repeated presentations of ELF-EMF of 1) a sine wave of decreasing amplitude or 2) a sequence based upon the Fibonacci series, generated from either 1) WINDOWS or 2) DOS systems, at intensities that were less than 20 nT over the target image. Results revealed that WINDOWS, but not DOS, generated patterns significantly and negatively impacted Mr. Swann’s reporting accuracy.

Alterations in human brain electroencephalographic power in response to exposures to ELF-EMF application was conducted by Richards et al., (2002). The experiment consisted of the application of Thomas-EMF across an 8 solenoid array placed circumferentially around the head of volunteers and the target ELF-EMF pattern was presented sequentially between the 8 solenoids with a rotation duration of 20 msec. Results indicated a 30% increase in spectral power density in the transcerebral EEG theta band, with a 20% increase in right hemispheric power as compared to the left. The capacity of ELF-EMF as a therapeutic for mood disorders has been demonstrated to be effective in normal individuals and in those who have sustained a head injury. In one study, Baker-Price and Persinger (1996) examined the treatment efficacy of weekly, 30 min exposure to weak (1 uT) burst-firing EMF across the temporal lobes for a duration 5 weeks in 4 depressed patients who had sustained traumatic brain injuries and exhibited mild-to-moderate brain impairment (as assessed with standardized tests). The results

described significant improvements in depression and a reduction in phobias but not in the physical symptoms or other complaints. In a second study, Baker-Price and Persinger (2003), examined the differences in depression scores for 14 patients that reported chronic depression lasting for more than 1 year following a closed head injury, after being exposed to burst-firing EMF (1 uT) either over the frontal or temporal lobes (bilaterally) for 30 min sessions once a week for 6 weeks. Clients treated with burst-firing ELF-EMF reported a significant reduction in depression scores as compared to those receiving no ELF-EMF intervention. The changes in depression scores were present irrespective of location of application. Also salient was a concomitant reduction in complex partial epileptic-like experiences, only from those individuals that received burst-firing ELF-EMF treatments that were directed over their temporal lobes, while EEG measures that assessed the spectral power over the frontal, temporal, and occipital lobes showed increased power within the 16 – 18 Hz range 6 weeks after treatment cessation. Corradini and Persinger (2013) exposed normal individuals to burst-firing EMF for 30 – 60 min and measured alterations in quantitative electroencephalographic profiles and correlated these features with psychometric measures of depression. Results indicated that exposure to burst-firing EMF significantly reduced subjective measures of depression in normal individuals while concomitant increases in EEG beta power over the prefrontal regions and left temporo-parietal regions were observed. Tsang et al., (2009), reported that individuals exposed to ELF-EMF lowered levels of self-reported psychometric fatigue after 20 min exposures, 1 time per week over three sessions to either burst-firing, complex sequence, or LTP EMFs, while only exposures to burst-firing was determined to improve mood and vigour scores.

1.4.3. HF-EMF

High frequency (HF) EMFs are operationalized as an EMF whose frequency characteristics exceed 100 Hz.

High frequency EMFs have been demonstrated to affect chemical and cellular dynamics. For instance, Mudrick et al., (1995) investigated the effect of the application of 42.19, 46.84, and 53.53 GHz, 1 mW/cm^2 EMF for 30 min on the intensity of barium sulphate-induced luminol chemoluminescence in human erythrocytes. Exposures to 42.19 GHz HF-EMF had maximal effects showing that the phenomenon was frequency-dependent. Adey and colleagues (1982) observed increased calcium efflux from the cortical cells of anesthetized cat cortices after 60 min exposures to 450 MHz, sinusoidally, amplitude-modulated EMF at 16 Hz. Intensity-dependent changes in *c-fos* gene expression were observed in PC-12 cells treated for 20 min with packet-modulated radio frequency EMF in combination with nerve growth factor (NGF; Ivaschuk et al., 1997). Bioluminescent intensities of the *Photobacterim leiognathi* demonstrated frequency-dependent suppression (~15%) when exposed to HF-EMF between 36.2 and 55.9 GHz, and intensities of 1.3 to 48.0 μW/cm^2 (Berzhanskaya et al., 1995).

Changes in cell growth, chemical resistance, and survivability have also been demonstrated to be impacted by HF-EMF treatment. Grundler and colleagues (1977, 1982, 1988) demonstrated that HF-EMF frequency, and not intensity, was important in the enhancement or inhibition of *S. cerevisiae* growth when they were exposed to EMF whose frequency swept between 41.8 – 42.0 GHz. *S. cerevisiae* showed similar synchronous fluctuations in growth rates and bud

formation in response to treatment with 0.03, W/cm^2, 46 GHz EMF for 50 min (Golant et al., 1994). Bulgakova et al., (1996) exposed *S. aureus* to either 54 or 42.195 GHz, or 66-78 GHz band EMF with 1 GHz steps at 10 mW/cm^2 for 1.5 to 60 minutes. In over 1000 experiments examining 14 different antibiotic agents, these researchers were able to demonstrate differences in growth when cells were exposed to EMF and antibiotics that affect cell membrane but not when the inhibitors altered cell wall synthesis, DNA-dependent RNA synthesis, RNA polymerase and RNA synthesis, or protein biosynthesis. While Levina et al., (1989) demonstrated that *Spirostum spirulina* cell populations could be affected by exposures to a 7.1-mm wavelength of HF-EMF at an intensity of 1.5 mW/cm^2 when exposures were conducted between days 2 and 11 of growth. Cultures exposed to EMF on days 2, 4, or 7 entered the stationary growth phase on day 9, while exposures on day 9 and 11 postponed population death by 5 days. Exposures occurring on day 2 increased the proliferation rate and by day 7 cell density had doubled. In the yeast, *C. albicans*, narrow band frequency and modulation-dependent changes in growth (i.e., 15% reduction) was observed when exposures consisted of 72 GHz fields that were modulated at 1 kHz (Dardononi et al., 1985). Exposure of ultraviolet light treated *E. coli* to 61 GHz, 1 mW/cm^2 EMF increased cell survival (Rojavin and Ziskin, 1995).

Exposure of animals and plants to HF-EMF have revealed some interesting results. Mahmoudi et al., (2018) demonstrated that short (2 hour) exposures of rats treated with pentylentetrazol (in a model of epilepsy), to 2.65 GHz EMF from Wi-Fi sources produced an enhancement in seizure activity, although the authors cautioned the interpretation of these results. Brovkovich et al., (1991) reported that exposures to a 61 GHz 4 mW/cm^2 HF-EMF can activate calcium pumps in the sarcoplasmic reticulum of skeletal and heart muscle cells in rats. Chromosomal changes were identified in *Acricotopus lucidus* salivary glands following exposure to 67.2 and

68.2 GHz EMF at an intensity of 5 mW/cm^2 (Kremer et al., 1988). With respect to plants, Tambiev and colleagues (1989) found that treatment with 2.2 mW/cm^2, 7.1-mm wavelength EMF for 30 min enhanced growth in blue-green algae *Spirulina platensis* by 50%. Barley seeds exposed to 61.5 GHz 0.1mW/cm^2 EMF for 20 min demonstrated an increase in synchronization of cell division of about 36% (Shestopalova et al., 1995).

Exposure to HF-EMF has been demonstrated to affect human task performance and EEG measures. For instance, Preece (1999) found that exposures to 915 MHz continuous wave HF-EMF at 1 W intensity, did not impact immediate word recall and picture presentation tasks. However, exposures to a 915 MHz HF-EMF pulsed at 217 Hz with an intensity of 0.125 W was found to negatively impact performance of choice reaction times, although it did not affect simple reaction time, digit vigilance, spatial working memory, numeric working memory, delayed word recall, delayed word recognition, or delayed picture recognition. In two experiments, Koivisto et al., (2000a; 2000b) showed that exposure to a 2.0 W, 902 MHz HF-EMF pulsed at 217 Hz resulted in a decrease in reaction time performance (i.e., longer response times) and a decrease in false alarms in a vigilance task when exposures lasted 30 min, while 60 min exposures only negatively affected reaction time. Using a similar methodology, Koivisto et al., (2001) found that self-report measures of somatic symptom severity from individuals was not impacted by experimental HF-EMF treatment.

Alterations in EEG activity have been reported during and following prolonged periods of exposure to low-level sinusoidally and pulse-modulated radio- and microwave fields (Servantie et al., 1975; Bawin et al., 1973; Bawin et al., 1975 Takashima et al., 1979). Eulitz et al., (1998) used a 917.2 MHz field modulated at 217 Hz at an intensity of 2.8 W, and demonstrated a reduction in the P300 event-related potential over the central parietal region. Adding to this,

Freude (1998; 2000) and colleagues exposed individuals to a 916.2 MHz field with 217 Hz modulation at an intensity of 2.0 W for 3 – 5 min, and demonstrated a reduction in EEG slow-wave potentials over the central parietal, temporal, and occipital regions but not over the frontal regions. Krause et al., (2000a) found an increase in relative EEG power within the 8 – 10 Hz band associated with the retrieval portion of working memory in individuals exposed to a 902 MHz EMF pulsed at 217 Hz with an intensity of 2.0 W for 30 min. In a follow-up study, Krause et al., (2000b) demonstrated that event-related potential alpha activity was modulated when subjects were exposed to 903 MHz HF-EMF pulsed at 217 Hz at a 2.0 W intensity for 30 min. However, no effects on reaction time or on the performance of tasks of visual working memory were observed. In contrast, Roschke et al., (1997) observed significant changes in event-related potentials (ERP) and tasks related to EEG in individuals exposed to a 900 MHz, 8.0 W EMF with 217 Hz modulation for 3.5 min.

There is some evidence to support the use of specific configurations of HF-EMF as a therapeutic intervention for radiation contamination, tumorigenesis, and wound healing. Detalvs et al., (1993, 1994, 1995, 1996) rigorously studied the effects of exposures to HF-EMF on wound healing by assessing the degree of granulation fibrous tissue formation. Data suggested that 30 min daily exposure to 53.53 or 42.19 GHz continuous wave EMF or 42.19 GHz with 200 MHz modulation significantly decreased granulation fibrous tissue formation and suppressed the inflammatory process in the former cases, while the latter application enhanced inflammation. Further, Zemskov et al., (1998) investigated the potential of HF-EMF treatment to enhance wound healing in septic conditions. Animals exposed to 37 or 46 GHz continuous wave EMF for 30 min twice daily for 5 days had decreased swellings, enhanced leukocyte infiltration, and a rapidly reduced wound area in the first 24 hours, as well as increased phagocytosis and reduced bacterial contamination. Peripheral nerve regeneration

was enhanced by 20-day treatment course with 54 GHz HF-EMF for 10 minutes every third day that demonstrated a statistically greater regeneration length, greater conduction velocity, but no change in the amplitude or duration of the action potential, in regenerating peripheral nerves (Kolosova et al., 1996). Chernov et al., (1989) demonstrated that rats inoculated with Walker 256 tumor cells and exposed to 8-mm wavelength EMF pulsed 43 times at 40-s intervals had a 1.5-fold reduction in tumor size and an increased lifespan (17-25 days).

Previous research has shown that exposure to low-intensity HF-EMF could mitigate the impact of X-ray radiation (Gubkina et al., 1996). HF-EMF exposure consisted of a frequency-sweep (38-53 GHz) at 7 mW/cm^2 for 30 min/day over the course of 23 days. Rats were then exposed to keV X-rays during the last 8 days of treatment up to a total dose of 24 Roentgens ($3.0 \cdot 10^{-3}$ C/kg). X-rays treatment alone enhanced serum glucose levels, but when animals were presented with prophylactic EMF glucose levels returned to normal. Similar effects were determined for soluble and fibrillary forms of the acidic glial fibrillary protein. Kuzmanova and Ivanov (1995) studied changes in the surface electrical charge of erythrocytes after HF-EMF and gamma-ray exposure in rats. Animals were exposed to 5.6-mm wavelength EMF for 10 days, for a duration of 20 minutes per day at an intensity of 1.1 mW/cm^2 followed by 6 Gy whole body exposures to Cobalt 137 gamma-rays. Exposure to gamma-rays alone altered erythrocyte surface charge while treatment with HF-EMF radiation prior to gamma-ray exposure returned these measures to control levels. Finally, Tstutsaeva et al., (1995) found that treatment with HF-EMF increased survivability of mice following a lethal dose of X-rays. The HF-EMF was pulse modulated at 1 $\mu W/cm^2$ and presented either 80 or 24 hours prior to the X-ray exposure. Exposures occurring 80-h prior to ionizing radiation treatment delayed X-ray related death until day 14 as compared to ~7 days without prophylactic intervention, with a 50% mortality seen on day 30 and 100% mortality by day 96. Prophylactic treatment 24-hours

prior to X-ray exposure did not increase the longevity of animals as defined as the date of first death (day 8) with 50% of animals dying within the first 30 days, however animals that survived until day 30 were still alive at the termination of the experiment. Simultaneous exposure of HF-EMF and lethal X-ray resulted in a fivefold increase in mouse survival and longevity.

1.4.4 Naturally Occurring EMF

The effects of manipulating the intensity of Earth's ambient magnetic field have been studied. In addition, applied exogenous fields designed to mimic magnetic perturbations that naturally occur in the geomagnetic field have been examined. Geomagnetic field effects have been associated with a disturbance in human embryonic fibroblast division (Kaznacheev and Mikhajliva, 1985), as well as with increased sensitivity of cells challenged with poisoning agents (Kanacheev et al., 1989). The amplitude and duration of incurrent geomagnetic storms have been associated with bacterial bioluminescence intensity (Berzhanskaja et al., 1995). Work by Brown et al., (1967) demonstrated that maximal alterations in snail behaviour occurred at EMF intensities that were close to that of the geomagnetic field while Becker (1963) found similar changes in animal behaviour. Orientation to the geomagnetic field is widely observed in birds (Yeagley, 1947; Kholodov, 1975; Kirschvink et al., 1985; Barnes, 1996), that can be disrupted by marked alterations in field intensity. Other authors have observed that the geomagnetic field, and associated disruptions, are associated with plant root system development (Bogatina et al., 1986), root metabolism (Beljavaskaja et al., 1992), cell proliferation (Fomichjova, 1992), and plant branching (Govorun et al., 1992). Alterations in geomagnetic activity may be amplified and maintained in unique geographic locations and could be dependent upon local geological and physical properties. For instance, Persinger and Dotta (2011) observed a protracted 150 – 200 nT increase in the orthogonal magnetic vector following a geomagnetic storm (K-index = 7), in the Sudbury basin. These alterations were

maintained and may contribute to unique experiences by different individuals and social groups that may be reflected in local culture.

Natural periodicities in geomagnetic activity have also been demonstrated to impact the behaviour of animals. Bureau and Persinger (1995) identified a relationship between the latency of overt behavioural displays corresponding to limbic seizures and increases in geomagnetic intensity (nT), associated with geomagnetic storms, with a 12% decrease in the onset time when global geomagnetic activity exceeded 20-25 nT. There was an increase in occurrence of sudden unexpected deaths by lithium-pilocarpine seized rats with chronic limbic seizures provided that the daily measure of geomagnetic activity exceeded 50 nT, especially at night (Persinger, 1995).

The presence of geomagnetic storm occurrence was associated with changes in human behaviour that was correlated with an increased number of mistakes committed by pilots (Derjapa et al., 1986; Usenko et al., 1989), an increased number of instantaneous deaths from cardiovascular disease, (Gnevyshev et al., 1982) and the promoting of anxiety, irritability, lower attention, and accuracy at work leading to an increase in motor vehicle accidents (Ashikaliev et al., 1995). Persinger (1995b) demonstrated that an increase in individual self-reports of "leaving" or being detached from one's body by 128 men and women, that were exposed only once to an experimental manipulation that enhances awareness of cognitive processes, was correlated with changes in geomagnetic intensity. More specifically, greater reports and experiences were reported when the geomagnetic activity on the day of the experiment was greater than 15 nT but did not exceed 45 nT. The most intense experiences of detachment were observed in individuals who had the greatest proportion of complex partial epileptic-like signs. Factors that contribute to geomagnetic periodicities (e.g., solar cycles)

were associated with deterioration of the human nervous system (Belisheva et al., 1995), increased psychotic episodes (Rudakov et al., 1984), and hospitalization for schizophrenia, alcohol induced psychosis, and epileptic patients (Samokhvalov, 1989). Geomagnetic periodicities were also associated with the risk of breast cancer in women (Rjabykh and Bodrova, 1992), sudden infant death (Zaĭtseva and Pudovkin, 1995). criminal offences (Chibirkin et al., 1995a), volumes of issued currency (Chibrikin et al., 1995b), sociopolitical events (e.g., wars, economy, crises, etc.), and intellectual creativity (Vladimirsky and Kislovsky, 1995).

Human brains fixed in preparations of formaldehyde and ethanol-formalin-acetic acid were able to show specific release of biophotons in response to ambient geomagnetic field intensities. Even though metabolic activity had ceased, aggregates of nervous tissue in a quasi-stable geomagnetic environment demonstrated conserved reactivity to fluctuations in geomagnetic intensity. Costa et al., (2016) demonstrated increased photon emission from the right hemisphere, but not the left, when fixed post-mortem human brains were dark adapted, exposed to ambient light conditions, assessed, and responded with right hemispheric photon emission that was strongly correlated to geomagnetic field intensity. Similar alterations in right hemispheric photon emission and quantitative electroencephalographic measures were observed in living humans (Mulligan et al., 2010; Mulligan and Persinger, 2012**)**. Asymmetry in cellular organizations of the parasolitary nucleus were observed in rats that were exposed to EMF whose strength and frequency components were correlated with the geomagnetic field configurations associated with sudden infant death syndrome (Dupont et al., 2004).

Fluctuations and enhancements of ambient geomagnetic intensity are capable of impacting aspects of biological structure and function. Depression of the geomagnetic field intensity, by

shielding in Faraday cages, can also promote unique changes in biological responses. Podkhovin (1995) observed an increase in epinephrine and histamine levels with a concomitant decrease in serotonin levels in Guinea pigs following 30 min exposures to weakened (1/10) geomagnetic field intensities. Shielding of the geomagnetic field has also been related to a risk of embryological teratomas (Shibab et al., 1987; Asashima et al., 1991). Exposures to a weakened geomagnetic environment was shown to affect the building behaviour of termites (Becker, 1976), Several authors have remarked on the depression of vital functions of bacteria when the geomagnetic environment was dampened (Achkasova, 1972; Alfjorov and Kuznetsova, 1981).

Although changes in geomagnetic activity can be correlated with changes in behaviour, this does not support the idea that the changes cause the observation. Therefore, rigorous scientific experimentation with successive approximation, allows us to collect enough data to support the idea that the relationship is being driven by one factor. Mulligan et al., (2012) demonstrated a synergistic relationship between sub-micromolar and micromolar concentrations of melatonin and an experimental EMF designed to mimic geomagnetic activity in their ability to reduce planaria motility. The exposure protocol was such that the experimental field was presented once an hour for 6 min over 8 successive hours. The relationship between geomagnetic activity and seizure behaviour was investigated by Persinger (1996) who intermittently exposed chronic (limbic) epileptic rats to experimental EMFs (for one to three nights consecutively) designed to simulate geomagnetic activity with 2 different intensities (50 nT and 500 nT) and ripple frequencies (7 and 40 Hz) over a 200-day period Results indicated a 3.1 fold increase in overt seizures following food presentation when the field was administered for 1 or 2, but not 3, nights.

Geomagnetic activity has been associated with the onset, progression, and symptom severity of multiple sclerosis (Papathanasopoulos et al., 2016; Persinger, 2006; Resch, 1995). Cook and Persinger (2000) exposed female Lewis rats subjected to protocols to induce experimental allergic encephalomyelitis (EAE) to either a 7 or 40 Hz amplitude-modulated EMF whose temporal structure was designed to mimic geomagnetic sudden storm commencement at 2 intensities (30 – 50 nT and 500 nT) for 6 minutes every hour for 8 hours across 2 weeks and demonstrated reductions in overt EAE signs. These reductions were specific to the 30-50 nT, 7 Hz pattern. Histological analysis revealed a reduction in mononuclear cell infiltration foci in animals exposed to the most effective configuration of intensity and pattern. Additional analysis indicated that the 50 nT, 7 Hz EMF treatments were associated with a greater cell infiltration in the left thalamus while the 500 nT, 40 Hz EMF had more right thalamic foci. Alteration in the presence of mast cells in the thalamus were observed as a function of treatment. Following these initial studies, Kinoshemeg and Persinger (2004), exposed female Lewis rats to 50 nT, 7 Hz amplitude-modulated EMF for 6 minutes an hour for 8 hours, after induction of EAE across days 1-7, days 8-16, days 1-16, or days 9 and 10 following EAE induction. Results suggested that animals exposed to EMF on nights 1-7 and on days 9 and 10 displayed more severe clinical symptoms of EAE as compared to animals receiving treatments on nights 8-16 and nights 1-16. The authors discussed the importance of the timing of intervention following the onset of diseased states in affecting the therapeutic value of the treatment.

1.5 Light/EM radiation:

Here we aim to examine data generated from the direct application of light emitting units or EMFs generated by current presentations that correspond to frequencies that fall within the infra-red (IR) to ultraviolet (UV) spectrum of electromagnetic radiation.

The hypothesis that applied EMF corresponding to UV-visible spectrum wavelengths can be generated by biological systems has long been theorized since the initial investigations conducted by Gurwitsch who observed that mitotic radiation can be induced by adjacent cells (Cifra et al., 2014; Gurwitsch and Gurwitsch, 1959; Gurwitsch, 1988). Light as a measure of biological function/change has been heavily researched (Popp et al., 1988; Popp 2003a; Popp, 2003b; VanWijk, 2001). For instance, it is possible to discriminate between malignant and non-malignant cell lines based on the differences in the spectral power density profiles emitted by cells (Dotta et al, 2016).

The use of photo-multiplier tubes to detect the quantity of light being emitted, has allowed the detection of magnetically coupled physio-chemical reactions (Dotta and Persinger, 2012) and demonstrated a doubling of ultra-weak emission, when samples were exposed to a unique configuration of bulk accelerating/decelerating EMFs with decelerating/accelerating phase velocities (Dotta et al., 2013). In terms of biology, Cosic et al., (1991) demonstrated that specific wavelengths of light corresponded to specific protein-protein and protein-DNA interactions as derived by assigning amino acid sequences pseudo-potentials.

Experimental verification that light could impact cell or protein activity would be directly relevant. Choi et al., (2012) applied a brief 710 nm LED treatment to the eyes of patients following ischemia and demonstrated neurite outgrowth that was associated with enhancement of mitogen-activated protein kinase (MAPK) pathways, while retinal wound healing was observed subsequent to 670 nm, light therapy that was associated with activation of signal transduction (Eells et al., 2004). Conversely, Masoumipoor et al., (2013) demonstrated that neuropathic pain could be attenuated in patients treated with low-level laser therapy at a

wavelength of 660 nm, a 10 nm difference in wavelength from that which promoted peripheral neurogenesis. Wu and Persinger (2011) showed that only applications of 880 nm light at an intensity of 1 mW/m^2 increased mobility and regeneration rates in amputated planaria. Folta and Childers (2008) examined the potential of artificial light applications to enhance growth of plants, observing that those specimens that received a mixture of red and blue light had greater total fresh weight, root mass, and vegetative growth.

While light alone demonstrates bio-effectivity, combinations of light coupled to the presence of other forms of EM stimuli may elicit unique synergies. Olcese and Reuss (1986) found that rats exposed to a weak (1 lux) red light enhanced the animal's ability to discriminate between the presence or absence of an ELF-EMF. Karbowski et al., (2016) reported that cells treated with a combination of pulsed blue light (470 nm; 1 msec durations) and the presentation of a weak, complex EMF for 1 hour promoted light production with spectral characteristics demonstrating a 10^2-10^3fold increase in power, peaking approximately 70 min following exposure and decreasing after 100 min. The authors quantified the energy of the emitted light as being equal to the energy stored within the applied EMF and was emitted at a wavelength of 470 nm, as assessed by spectrophotometry. Murugan et al., (2017) examined the effect of the combination of 3 different wavelengths (blue, green, red) coupled to a weak physiologically patterned EMF (Thomas-EMF) on both planaria regeneration and on the suppression of melanoma cell proliferation. Results suggested that the combination of blue light and Thomas-EMF was able to enhance melanoma cell growth suppression while red light (alone), blue light (alone), Thomas-EMF, and the combination of the Thomas-EMF with both red and blue light facilitated planaria regeneration. Conversely, treatment with green light (alone) did not appreciably alter melanoma cell proliferation and eliminated the growth suppression elicited by Thomas-EMF when presented together. Meli and Persinger (2009) examined the

effectiveness of combining different wavelengths of light and the degree of spectrum saturation (red, green, white) with exposure to a burst-firing patterned EMF in a protocol that has been shown to reliably elicit a sensed presence in participants. Results were suggestive of increased visual sensations along the right side for participants exposed to red light, as well as more reports of dizziness, sensed presence, "ego-alien" thoughts, and detachment from body. Meanwhile, green light facilitated more left-sided visual sensations in participants.

The previous chapter was devoted to reviewing the effects that magnetic and electromagnetic field exposures have on biological systems. This is important because any system under observation is continually subjected to natural and artificial MF/EMFs present in the environment. It has been previously demonstrated that experimental and ambient MF/EMF exposures can affect biological systems with the different sources used to generate these fields leading to distinct outcomes. Furthermore, the response of biological systems to MF/EMF exposure is maximized when the structure of the applied field (i.e., the pattern) mimics what is observed biologically in a manner similar to the way that psychotropic drugs affect behaviour. Consider the activation of the nervous system in response to psychedelics (e.g., lysergic acid diethylamide; LSD). The mechanism of action by that LSD produces its effects is the result of receptor activation by endogenous neurotransmitters that the psychotropic mimics. In this example, the resultant experiential changes associated with LSD only occur because the structure of the molecule resembles the structure of naturally occurring neurotransmitters (i.e., serotonin). In fact, if there was no exclusive receptor for LSD to act on and therefore its effects, mediated by endogenous receptors that bind neurotransmitter with structures that mimic LSD, would not occur. Similarly, patterned EMFs designed to mimic what is occurring biologically are efficacious, while those EMFs whose patterns are different from naturally occurring processes, do not elicit a response or result in a response that is different.

We can liken effects observed as a consequence of EMF exposure, at least partially, as being similar to the effects observed when the system is presented with pharmacological interventions. As in the development of novel pharmaceutical therapies, it is important to understand the mechanisms through that EMFs work in order to produce their effects, as well as that components of EMFs are important to initiate or sustain the mechanism of action. Identifying the structural components of the EMF that most contribute to any change would be similar to identifying functional groups of chemicals. In order to demonstrate the mechanism through that EMFs produce their effects we must identify a system(s) that reliably and consistently responds to a particular EMF configuration. Identifying these model systems would provide a basis to allow for systematic experimentation to investigate the functional salience of distinct EMF parameters including pattern, intensity, modulation (amplitude, frequency, phase), exposure duration, equipment, etc. In our review, we have found that B16-BL6 cells reliably respond to a frequency-modulated EMF (i.e., Thomas-EMF) and these responses can be measured in a number of different ways (i.e., ultra-weak photon emission, proliferation, calcium uptake). In this thesis, we will develop another cell system to evaluate the mechanisms underlying EMF effects.

Having knowledge that exposure to a particular EMF configuration can result in unique outcomes does not provide us with an understanding of the mechanism of action. It would be prudent to associate known structural and functional changes (e.g., changes in protein kinetics, protein channel activation, conformational of receptors, etc.) at the level of the cell and provide a series of events that results from EMF exposure in order to effectively identify a mechanism of action. Understanding the molecular mechanisms associated with EMF exposure would

provide the unique opportunity to examine pharmaco-magneto synergisms, that could be used to develop alternative and cost-effective treatments for a myriad of health concerns.

1.6 References:

Achkasova YuN. 1973. Metabolism and rate of reproduction of microorganisms developing at shielding electric and magnetic fields. In: Effects of weak electromagnetic fields on biological objects. Kharkov: Kharkov Medical Institute. p 51-52.

Adey, W. R., Bawin, S. M., & Lawrence, A. F. (1982). Effects of weak amplitude-modulated microwave fields on calcium efflux from awake cat cerebral cortex. *Bioelectromagnetics: Journal of the Bioelectromagnetics Society, The Society for Physical Regulation in Biology and Medicine, The European Bioelectromagnetics Association*, *3*(3), 295-307.

Aleksandrovskaia, M. M., & Kholodov, I. (1966). The possible role of the neuroglia in the formation of a bioelectric reaction of the brain to a constant magnetic field. *Doklady Akademii nauk SSSR*, *170*(2), 482.

Alfjorov, O. A., & Kuznetsova, T. V. (1981). Influence of weakened geomagnetic field on the stability of Escherichia coli to ultraviolet rays. *Kosmicheskaja Biologija i Aviakosmicheskaja Meditsina (Cosmic biology and aviation and cosmic medicine)*, *4*, 57-58.

Alipov, Y. D., & Belyaev, I. Y. (1996). Difference in frequency spectrum of extremely-low-frequency effects on the genome conformational state of AB1157 and EMG2 E. coli cells. *Bioelectromagnetics: Journal of the Bioelectromagnetics Society, The Society for Physical Regulation in Biology and Medicine, The European Bioelectromagnetics Association*, *17*(5), 384-387.

Amer NM, Tobias CA. 1965. Analysis of the combined effect of magnetic fields, temperature, and radiation on development. Radiat Res 25:172a.

Andersen, P., Morris, R., Amaral, D., Bliss, T., & O'Keefe, J. (Eds.). (2006). *The hippocampus book*. Oxford university press.

Anisimov, V. N., Zhukova, O. V., Veniashvili, D., Bilanishvili, V. G., Menabde, M. Z., & Gupta, D. (1996). Effect of the light regime and electromagnetic fields on mammary carcinogenesis in female rats. *Biofizika*, *41*(4), 807-814.

Artjukhina, NI. (1988). Reactions of structural elements of the rat's brain to the action of magnetic fields. In: Kholodov YuA, lebedeva, NN, editors. Problems of electromagnetic neurobiology. Moscow: Nauka (Science). p 48-64.

Asashima M, Shimada K, Pfeiffer CJ. 1991. Magnetic shielding induces early developmental abnormalities in the newt. Bioelectromagnetics 12:215–224.

Ashikaliev YaF, Drob'jev VI, Somsikov VM, Turkeeva VA, Yakovets TK. 1995. The influence of heliogeophysical parameters on ecology. Biofizika (Biophysics) 40: 1031-1037.

Baker-Price, L. A., & Persinger, M. A. (1996). Weak, but complex pulsed magnetic fields may reduce depression following traumatic brain injury. *Perceptual and motor skills*, *83*(2), 491-498.

Baker-Price, L., & Persinger, M. A. (2003). Intermittent burst-firing weak (1 microTesla) magnetic fields reduce psychometric depression in patients who sustained closed head injuries: A replication and electroencephalographic validation. *Perceptual and Motor Skills*, *96*(3), 965-974.

Bär, K. J., Brehm, S., Boettger, M. K., Boettger, S., Wagner, G., & Sauer, H. (2005). Pain perception in major depression depends on pain modality. *Pain*, *117*(1-2), 97-103.

Barnes FS. 1996. Interaction of DC and ELF electric fields with biological materials and systems. In: Polk C, Postow E, editors. The CRC handbook on biological effects of electromagnetic fields. Boca Raton, Florida: CRC Press. p 103-147.

Barnothy MF. 1963. Reduction of radiation mortality through magnetic pre-treatment. Nature 200:279–280.

Barnwell, F. H., & Brown, F. A. (1964). Responses of planarians and snails. In *Biological effects of magnetic fields* (pp. 263-278). Springer, Boston, MA.

Bassett, A. (1994). Therapeutic uses of electric and magnetic fields in orthopedics. *Biological effects of electric and magnetic fields—beneficial and harmful effects*, *2*, 13-48.

Bawin, S. M., Gavalas-Medici, R. J., & Adey, W. R. (1973). Effects of modulated very high frequency fields on specific brain rhythms in cats. *Brain Research*, *58*(2), 365-384.

Bawin, S. M., Kaczmarek, L. K., & Adey, W. R. (1975). Effects of modulated VHF fields on the central nervous system. *Annals of the New York Academy of Sciences*, *247*(1), 74-81.

Becker, R. O. (1963). Relationship of geomagnetic environment to human biology. *New York state journal of medicine, 63*, 2215.

Becker, G. (1967). Die Temperatur-Abhangigkeit der Frasstatigkeit einiger Termitenarten. *Zeitschrift fur Angewandte Entomologie* 60, 90 – 123.

Becker, G. (1971). Physiological influences on wood-destroying insects of wood compounds and substances produced by microorganisms. *Wood science and technology*, *5*(3), 236-246.

Belisheva NK, Popov AN, Petukhova NV, Pavlova LP, Osipov KS, Tkachenko SE, Baranova TI. 1995. Qualitative and quantitative estimation of influence of geomagnetic field variations on functional state of the human brain. Biofizika (Biophysics) 40:1005±1012.

Beljavskaja, N. A., Fomichjova, V. N., Govorun, R. D., & Danilov, V. I. (1992). Structural and functional organization of meristem cells of pea, flax and lentil roots under conditions of the geomagnetic field shielding. *Biofizika (Biophysics)*, *37*, 745-749.

Belyaev, I. (2011). Toxicity and SOS-response to ELF magnetic fields and nalidixic acid in E. coli cells. *Mutation Research/Genetic Toxicology and Environmental Mutagenesis*, *722*(1), 56-61.

Belyaev, I. Y., & Alipov, E. D. (2001). Frequency-dependent effects of ELF magnetic field on chromatin conformation in Escherichia coli cells and human lymphocytes. *Biochimica et Biophysica Acta (BBA)-General Subjects*, *1526*(3), 269-276.

Bell, G. B., Marino, A. A., & Chesson, A. L. (1992). Alterations in brain electrical activity caused by magnetic fields: detecting the detection process. *Electroencephalography and clinical Neurophysiology*, *83*(6), 389-397.

LYu, B., Berzhanskii, V. N., & OYu, B. (1995). Effect of electromagnetic fields on the activity of bioluminescence in bacteria. *Biofizika*, *40*, 974-977.

Berzhanskaja LYu, Berzhansky VN, Beloplotova OYu, Pil'nikova TG, Metljaev TN. 1995. Bioluminescent activity of bacteria as an indicator of geomagnetic disturbances. Biofizika (Biophysics) 40:778-781.

Bidal. R. (2018). Spontaneous aggregation of non-living and living matter in aqueous environments subjected to a static electromagnetic field: potential link to the next step of abiogenesis (**Master's of Science in Biology**). Laurentian University. Sudbury, Canada.

Bigham, A. S., Shadkhast, M., & Dehghani, S. N. (2009). Autogenous bone marrow concurrent with static magnetic field effects on bone-defect healing: radiological and histological study. *Comparative Clinical Pathology*, *18*(2), 163.

Binhi, V. N., Alipov, Y. D., & Belyaev, I. Y. (2001). Effect of static magnetic field on E. coli cells and individual rotations of ion–protein complexes. *Bioelectromagnetics: Journal of the Bioelectromagnetics Society, The Society for Physical Regulation in Biology and Medicine, The European Bioelectromagnetics Association*, *22*(2), 79-86.

Blackman, C. F., Benane, S. G., & House, D. E. (1993a). Evidence for direct effect of magnetic fields on neurite outgrowth. *The FASEB journal*, *7*(9), 801-806.

Blackman, C. F., Benane, S. G., House, D. E., & Pollock, M. M. (1993b). Action of 50 Hz magnetic fields on neurite outgrowth in pheochromocytoma cells. *Bioelectromagnetics*, *14*(3), 273-286.

Blackman, C. F., Blanchard, J. P., Benane, S. G., & House, D. E. (1994). Empirical test of an ion parametric resonance model for magnetic field interactions with PC-12 cells. *Bioelectromagnetics: Journal of the Bioelectromagnetics Society, The Society for Physical Regulation in Biology and Medicine, The European Bioelectromagnetics Association*, *15*(3), 239-260.

Blank, M., & Goodman, R. (2004). Initial interactions in electromagnetic field-induced biosynthesis. *Journal of cellular physiology*, *199*(3), 359-363.

Blank, M., Soo, L., & Abbott, R. E. (1979). Erythrocyte membrane proteins: a modified Gorter-Grendel experiment. *The Journal of membrane biology*, *47*(2), 185-193.

Blank, M. A. R. T. I. N. (1992). Na, K-ATPase function in alternating electric fields. *The FASEB journal*, *6*(7), 2434-2438.

Blank, M., & Soo, L. (1992). The threshold for alternating current inhibition of the Na, K-ATPase. *Bioelectromagnetics*, *13*, 329-333.

Blank, M., & Soo, L. (1993). The Na, K-ATPase as a model for electromagnetic field effects on cells. *Bioelectrochemistry and bioenergetics*, *30*, 85-92.

Blank, M., & Soo, L. (1998a). Enhancement of cytochrome oxidase activity in 60 Hz magnetic fields. *Bioelectrochemistry and bioenergetics*, *45*(2), 253-259.

Blank, M., & Soo, L. (1998b). Frequency dependence of cytochrome oxidase activity in magnetic fields. *Bioelectrochemistry and Bioenergetics*, *46*(1), 139-143.

Blank, M., & Soo, L. (2001a). Optimal frequencies for magnetic acceleration of cytochrome oxidase and Na, K-ATPase reactions. *Bioelectrochemistry*, *53*(2), 171-174.

Blank, M., & Soo, L. (2001b). Electromagnetic acceleration of electron transfer reactions. *Journal of cellular biochemistry*, *81*(2), 278-283.

Blomme, C. G., Parker, G. H., & Persinger, M. A. (1990). Operant Detection of Extremely Low Frequency Magnetic Fields by the Domestic Pigeon Columba livia. *Bird Behavior*, *8*(2), 73-78.

Bogatina NI, Litvin VM, Travkin MP. 1986. Wheat roots orientation under the effect of geomagnetic field. Biofizika (Biophysics) 31:886-890.

Bresler, S. E., Bresler, V. M., Vasil'eva, N. N., & Kazbekov, E. N. (1978). Effect of strong magnetic fields on active transport in the choroid plexus. *Dokl. Biol. Sci. (Engl. Transl.) ;(United States)*, *242*.

Brovkovich, V. M., Kurilo, N. B., & Barishpol'ts, V. L. (1991). Action of millimeter-range electromagnetic radiation on the Ca pump of sarcoplasmic reticulum. *Radiobiologiia*, *31*(2), 268-271.

Brown Jr, F. A., Barnwell, F. H., & Webb, H. M. (1964). Adaptation of the magnetoreceptive mechanism of mud-snails to geomagnetic strength. *The Biological Bulletin*, *127*(2), 221-231.

Brown Jr, F. A., & Park, Y. H. (1967). Association-formation between photic and subtle geophysical stimulus patterns—a new biological concept. *The Biological Bulletin*, *132*(3), 311-319.

Buckner, C. A., Buckner, A. L., Koren, S. A., Persinger, M. A., & Lafrenie, R. M. (2015). Inhibition of cancer cell growth by exposure to a specific time-varying electromagnetic field involves T-type calcium channels. *PLoS One*, *10*(4), e0124136.

Buckner, C. A., Buckner, A. L., Koren, S. A., Persinger, M. A., & Lafrenie, R. M. (2017). The effects of electromagnetic fields on B16-BL6 cells are dependent on their spatial and temporal character. *Bioelectromagnetics*, *38*(3), 165-174.

Buckner, C. A., Buckner, A. L., Koren, S. A., Persinger, M. A., & Lafrenie, R. M. (2018). Exposure to a specific time-varying electromagnetic field inhibits cell proliferation via cAMP and ERK signaling in cancer cells. *Bioelectromagnetics*, *39*(3), 217-230.

Bulgakova, V. G., Grushina, V. A., Orlova, T. I., Petrykina, Z. M., Polin, A. N., Noks, P. P., ... & Rubin, A. B. (1996). The effect of millimeter-band radiation of nonthermal intensity on sensitivity of Staphylococcus to various antibiotics. *Biofizika*, *41*(6), 1289-1293.

Bureau, Y. R. J., & Persinger, M. A. (1995). Decreased incidence of limbic motor seizures following twenty pairings of subclinical lithium-pilocarpine injections and a complex "burst-firing" magnetic field. *Electro-and Magnetobiology*, *14*(1), 1-6.

Bureau, Y. R. J., & Persinger, M. A. (1995). Decreased latencies for limbic seizures induced in rats by lithium-pilocarpine occur when daily average geomagnetic activity exceeds 20 nanoTesla. *Neuroscience letters*, *192*(2), 142-144.

Burke, H. E. (2012). *Handbook of magnetic phenomena*. Springer Science & Business Media.

Chemeris, N. K., & Safronova, V. G. (1993). A weak low-frequency magnetic field initiates the frequency dependent fluctuations of Daphnia magna heart contraction period. *Biofizika*, *38*(3), 511-519.

Chernov, Z. S., Faikin, V. V., & Bernashevskii, G. A. (1989). Experimental study of the effect of nanosecond EHF pulses on malignancies. *Millimeter Waves in Medicine and Biology." Moscow: Radioelectronica*, 121-127.

Chibrikin VM, Samovichev EG, Kashinskaja IV, Udal'tsova NY. 1995a. Dynamics of social processes and geomagnetic activity. 1. Periodic components in variations of the number of crimes registered in Moscow. Biofizika (Biophysics) 40:1050-1053.

Chibrikin VM, Kashinskaja IV, Udal'tsova NY. 1995b. Dynamics of social processes and geomagnetic activity. 2. Geomagnetic response in money issue. Biofizika (Biophysics) 40:1054-1059.

Choi, D. H., Lee, K. H., Kim, J. H., Kim, M. Y., Lim, J. H., & Lee, J. (2012). Effect of 710 nm visible light irradiation on neurite outgrowth in primary rat cortical neurons following ischemic insult. *Biochemical and biophysical research communications*, *422*(2), 274-279.

Cifra, M., & Pospíšil, P. (2014). Ultra-weak photon emission from biological samples: definition, mechanisms, properties, detection and applications. *Journal of Photochemistry and Photobiology B: Biology*, *139*, 2-10.

COSIC, I., HODDER, A. N., AGUILAR, M. I., & HEARN, M. T. (1991). Resonant recognition model and protein topography: model studies with myoglobin, hemoglobin and lysozyme. *European journal of biochemistry*, *198*(1), 113-119.

Cook, C. M., & Persinger, M. A. (1997). Experimental induction of the “sensed presence” in normal subjects and an exceptional subject. *Perceptual and Motor Skills*, *85*(2), 683-693.

Cook, L. L., & Persinger, M. A. (2000). Suppression of experimental allergic encephalomyelitis is specific to the frequency and intensity of nocturnally applied, intermittent magnetic fields in rats. *Neuroscience letters*, *292*(3), 171-174.

Corradini, P. L., & Persinger, M. A. (2013). Brief Cerebral Applications of Weak, Physiologically-patterned Magnetic Fields Decrease Psychometric Depression and Increase Frontal Beta Activity in Normal Subjects. *J Neurol Neurophysiol*, *4*, 175.

Costa, J. N., Rouleau, N., & Persinger, M. A. (2016). Differential spontaneous photon emissions from cerebral hemispheres of fixed human brains: Asymmetric coupling to geomagnetic activity and potentials for examining post-mortem intrinsic photon information. *Neuroscience and Medicine*, *7*(02), 49.

Crosby, E. C. T., Humphrey and EW Lauer 1962 Correlative Anatomy of the Nervous System.

Csernansky, John G., Julia Mellentin, Linda Beauclair, and Leon Lombrozo. "Mesolimbic dopaminergic supersensitivity following electrical kindling of the amygdala." *Biological psychiatry* 23, no. 3 (1988): 285-294.

Dahl, P. F. (1997). *Flash of the Cathode Rays: A History of JJ Thomson's Electron*. CRC Press.

da Motta MA, Muniz JBF, Schuler A, Da Motta M. Static magnetic fields enhancement of Saccharomyces cerevisae ethanolic fermentation. Biotechnol Prog. 2004; 20:393–6.

Dardanonl, L., Torregrossa, M. V., & Zanforlin, L. (1985). Millimeter-wave effects on Candida albicans cells. *Journal of Bioelectricity*, *4*(1), 171-176.

Delparte, J. J., & Persinger, M. A. (2007). Brief exposures to theta-burst magnetic fields impair the consolidation of food-induced conditioned place preference. *International Journal of Neuroscience*, *117*(2), 295-299.

Del Seppia, C., Ghione, S., Luschi, P., Ossenkopp, K. P., Choleris, E., & Kavaliers, M. (2007). Pain perception and electromagnetic fields. *Neuroscience & Biobehavioral Reviews*, *31*(4), 619-642.

Derjapa NR, Kopanev CI, Usenko GA. 1986. Effects of factors of solar flares and geomagnetic disturbance on the functional and physiological possibilities of a pilot. Bjulleten' SO AMN SSSR (Bulletin of the Siberian Department of the Academy of Science of the USSR) 5:83±88.

Detlav, I. E., Shkirmante, B. K., Dombrovska, L. E., Pahegle, I. V., & Slutskii, L. I. (1993). Biochemical parameters of developing granulo-fibrous tissue after the effect of an extremely high-frequency electromagnetic field. *Millimetrovie Volni v Biologii i Meditcine*, *2*, 43-50.

Detlavs, I., Dombrovska, L., Klavinsh, I., Turauska, A., Shkirmante, B., & Slutskii, L. (1994). Experimental study of the effect of electromagnetic fields' in the early stage of wound healing. *Bioelectrochemistry and Bioenergetics*, *35*(1-2), 13-17.

Detlavs, I., Dombrovska, L., Shkirmante, B., Turauska, A., & Slutskii, L. (1995). Some biological effects of mm-wave electromagnetic fields on the granulation-fibrous tissue in a healing wound. In *Moscow, Russia: 10th Russian Symposium "Millimeter Waves in Medicine and Biology," April* (pp. 117-119).

Detlavs, I., Dombrovska, L., Turauska, A., Shkirmante, B., & Slutskii, L. (1996). Experimental study of the effects of radiofrequency electromagnetic fields on animals with soft tissue wounds. *Science of the total environment*, *180*(1), 35-42.

Dotta, B. T., Buckner, C. A., Cameron, D., Lafrenie, R. M., & Persinger, M. A. (2011). Biophoton emissions from cell cultures: biochemical evidence for the plasma membrane as the primary source. *General Physiology and Biophysics*, *30*(3), 301.

Dotta, B. T., & Persinger, M. A. (2012). "Doubling" of local photon emissions when two simultaneous, spatially-separated, chemiluminescent reactions share the same magnetic field configurations. *Journal of Biophysical Chemistry*, *3*(01), 72.

Dotta, B. T., Koren, S. A., & Persinger, M. A. (2013). Demonstration of entanglement of "pure" photon emissions at two locations that share specific configurations of magnetic fields: implications for translocation of consciousness. *Journal of Consciousness Exploration & Research*, *4*(1).

Dotta, B. T., Murugan, N. J., Karbowski, L. M., & Persinger, M. A. (2013). Excessive correlated shifts in pH within distal solutions sharing phase-uncoupled angular accelerating magnetic fields: macro-entanglement and information transfer. *International Journal of Physical Sciences*, *8*(36), 1783-1787.

Dotta, B. T., Lafrenie, R. M., Karbowski, L. M., & Persinger, M. A. (2014a). Photon emission from melanoma cells during brief stimulation by patterned magnetic fields: is the source

coupled to rotational diffusion within the membrane. *General Physiology and Biophysics*, *33*, 63-73.

Dotta, B. T., Vares, D. A., Buckner, C. A., Lafrenie, R. M., & Persinger, M. A. (2014b). Magnetic field configurations corresponding to electric field patterns that evoke long-term potentiation shift power spectra of light emissions from microtubules from non-neural cells. *Open Journal of Biophysics*, *4*(04), 112.

Dotta, B. T., Karbowski, L. M., Murugan, N. J., Vares, D. A. E., & Persinger, M. A. (2016). Ultra-weak Photon Emissions Differentiate Malignant Cells from Non-Malignant Cells In Vitro. *Archives of Cancer Res*, *4*(2).

Dupont, M. J., McKay, B. E., Parker, G., & Persinger, M. A. (2004). Geophysical variables and behavior: XCIX. Reductions in numbers of neurons within the parasolitary nucleus in rats exposed perinatally to a magnetic pattern designed to imitate geomagnetic continuous pulsations: implications for sudden infant death. *Perceptual and motor skills*, *98*(3), 958-966.

Eells, J. T., Wong-Riley, M. T., VerHoeve, J., Henry, M., Buchman, E. V., Kane, M. P., ... & Margolis, D. (2004). Mitochondrial signal transduction in accelerated wound and retinal healing by near-infrared light therapy. *Mitochondrion*, *4*(5-6), 559-567.

Eulitz, C., Ullsperger, P., Freude, G., & Elbert, T. (1998). Mobile phones modulate response patterns of human brain activity. *Neuroreport*, *9*(14), 3229-3232.

Fijalkowski, K., Nawrotek, P., Struk, M., Kordas, M., & Rakoczy, R. (2013). The effects of rotating magnetic field on growth rate, cell metabolic activity and biofilm formation by Staphylococcus aureus and Escherichia coli. *Journal of Magnetics*, *18*(3), 289-296.

Fijałkowski, K., Nawrotek, P., Struk, M., Kordas, M., & Rakoczy, R. (2015). Effects of rotating magnetic field exposure on the functional parameters of different species of bacteria. *Electromagnetic biology and medicine*, *34*(1), 48-55.

Fleming, J. L., Persinger, M. A., & Koren, S. A. (1994). Magnetic pulses elevate nociceptive thresholds: Comparisons with opiate receptor compounds in normal and seizure-induced brain-damaged rats. *Electro-and Magnetobiology*, *13*(1), 67-75.

Folta, K. M., & Childers, K. S. (2008). Light as a growth regulator: Controlling plant biology with narrow-bandwidth solid-state lighting systems. *HortScience*, *43*(7), 1957-1964.

Fomichjova, V. M. (1992). Proliferation activity and cell reproduction in meristems of root seedlings of pea, flax and lentil under conditions of shielding the geomagnetic field. *Biofizika*, *37*, 745-749.

Fournier, N. M., & Persinger, M. A. (2004). The neuromatrix and the epileptic brain: behavioral and learning preservation in limbic epileptic rats treated with ketamine but not acepromazine. *Epilepsy & Behavior*, *5*(1), 119-127.

Fournier, N. M., Mach, Q. H., Whissell, P. D., & Persinger, M. A. (2012). Neurodevelopmental anomalies of the hippocampus in rats exposed to weak intensity complex magnetic fields throughout gestation. *International Journal of Developmental Neuroscience*, *30*(6), 427-433.

Friedman, H., Becker, R. O., & Bachman, C. H. (1967). Effect of magnetic fields on reaction time performance. *Nature*, *213*(5079), 949-950.

Freude, G., Ullsperger, P., Eggert, S., & Ruppe, I. (1998). Effects of microwaves emitted by cellular phones on human slow brain potentials. *Bioelectromagnetics: Journal of the Bioelectromagnetics Society, The Society for Physical Regulation in Biology and Medicine, The European Bioelectromagnetics Association*, *19*(6), 384-387.

Freude, G., Ullsperger, P., Eggert, S., & Ruppe, I. (2000). Microwaves emitted by cellular telephones affect human slow brain potentials. *European journal of applied physiology*, *81*(1-2), 18-27.

Fuller, M., Dobson, J., Wieser, H. G., & Moser, S. (1995). On the sensitivity of the human brain to magnetic fields: evocation of epileptiform activity. *Brain research bulletin*, *36*(2), 155-159.

Gaetz, M. (2004). The neurophysiology of brain injury. *Clinical neurophysiology*, *115*(1), 4-18.

Geinisman, Y. (2000). Structural synaptic modifications associated with hippocampal LTP and behavioral learning. *Cerebral Cortex*, *10*(10), 952-962.

Glover, P. M., Cavin, I., Qian, W., Bowtell, R., & Gowland, P. A. (2007). Magnetic-field-induced vertigo: a theoretical and experimental investigation. *Bioelectromagnetics: Journal of the Bioelectromagnetics Society, The Society for Physical Regulation in Biology and Medicine, The European Bioelectromagnetics Association*, *28*(5), 349-361.

Golant, M. B., Kuznetsov, A. P., & Bozhanova, T. P. (1994). The mechanism of synchronizing yeast cell cultures with EHF-radiation. *Biofizika*, *39*(3), 490-495.

Goodman R, Blank M. 1998. Magnetic field stress induces expression of hsp70. Cell Stress Chap 3:74–88.

Govorun, R. D. (1992). Influence of geomagnetic field fluctuations and its shielding on early periods of higher plant germination. *Biofizika*, *37*, 738-744.

Gnevyshev MN, Novikova KF, Ol' AI, Tokareva NV. 1982. Instantaneous death at cardiovascular disease and solar activity. In: Problems of solar-biospheric connections. Novosibirsk. p 179-187.

Grundler, W., Keilmann, F., & Fröhlich, H. (1977). Resonant growth rate response of yeast cells irradiated by weak microwaves. *Physics letters A*, *62*(6), 463-466.

Grundler, W., Keilmann, F., Putterlik, V., & Strube, D. (1982). Resonant-like dependence of yeast growth rate on microwave frequencies. *The British journal of cancer. Supplement*, *5*, 206.

Grundler, W., Jentzsch, U., Keilmann, F., & Putterlik, V. (1988). Resonant cellular effects of low intensity microwaves. In *Biological coherence and response to external stimuli* (pp. 65-85). Springer, Berlin, Heidelberg.

Gubkina, E. A., Kushnir, A. E., Bereziuk, S. K., Potapov, V. A., & Lepekhin, E. A. (1996). Effects of low-intensity electromagnetic radiation of extremely high-frequency on the animal organism in combination with whole-body low-dose X-ray irradiation. *Radiats Biol Radioecol*, *36*, 722-726.

Gurwitsch, A. G., & Gurwitsch, L. D. (1959). Mito-genetic radiation. *Mito-genetic radiation.*

Gurwitsch, A. A. (1988). A historical review of the problem of mitogenetic radiation. *Experientia*, *44*(7), 545-550.

Ivaschuk, O. I., Jones, R. A., Ishida-Jones, T., Haggren, W., Adey, W. R., & Phillips, J. L. (1997). Exposure of nerve growth factor-treated PC-12 rat pheochromocytoma cells to a modulated radiofrequency field at 836.55 MHz: Effects on c-jun and c-fos expression. *Bioelectromagnetics: Journal of the Bioelectromagnetics Society, The Society for Physical Regulation in Biology and Medicine, The European Bioelectromagnetics Association*, *18*(3), 223-229.

Ji, W., Huang, H., Deng, A., & Pan, C. (2009). Effects of static magnetic fields on Escherichia coli. *Micron*, *40*(8), 894-898.

Jin, M., Lin, H., Han, L., Opler, M., Maurer, S., Blank, M., & Goodman, R. (1997). Biological and technical variables in myc expression in HL60 cells exposed to 60 Hz electromagnetic fields. *Bioelectrochemistry and Bioenergetics*, *44*(1), 111-120.

Kato, M., Honma, K. I., Shigemitsu, T., & Shiga, Y. (1993). Effects of exposure to a circularly polarized 50-Hz magnetic field on plasma and pineal melatonin levels in rats. *Bioelectromagnetics*, *14*(2), 97-106.

Karbowski, L. M., Murugan, N. J., & Persinger, M. A. (2016). Experimental evidence that specific photon energies are “stored” in malignant cells for an hour: the synergism of weak magnetic field-LED wavelength pulses. *Biology and Medicine*, *8*(1), 1.

Kavaliers, M., Ossenkopp, K. P., & Hirst, M. (1984). Magnetic fields abolish the enhanced nocturnal analgesic response to morphine in mice. *Physiology & Behavior*, *32*(2), 261-264.

Kavaliers, M., & Ossenkopp, K. P. (1985). Exposure to rotating magnetic fields alters morphine-induced behavioral responses in two strains of mice. *Neuropharmacology*, *24*(4), 337-340.

Kavaliers, M., & Ossenkopp, K. P. (1986). Stress-induced opioid analgesia and activity in mice: inhibitory influences of exposure to magnetic fields. *Psychopharmacology*, *89*(4), 440-443.

Kavaliers, Martin, and Klaus-Peter Ossenkopp. "Calcium channel involvement in magnetic field inhibition of morphine-induced analgesia." *Naunyn-Schmiedeberg's archives of pharmacology* 336, no. 3 (1987): 308-315.

Kaznacheev VP, Mikhajlova LP. 1985. Extra weak irradiation in cellular interactions. Novosibirsk: Nauka (Science).

Kaznacheev VP, Mikhajlova LP, Ivanova MP, Zajtsev YuA, Kharina NI. 1989. Growth and behavior of the cell monolayer in the hypomagnetic field. In: Gnevyshev MN, Ol' AI, editors. Problems of cosmic biology, Vol 65, Biophysical and clinical aspects of heliobiology. Leningrad: Nauka (Science). p 189-195.

Kholodov, I. A. (1967). *The effect of electromagnetic and magnetic fields on the central nervous system* (Vol. 459). National Aeronautics and Space Administration.

Kholodov, J. A., Alexandrovskaya, M. M., Lukjanova, S. N., & Udarova, N. S. (1969). Investigations of the reactions of mammalian brain to static magnetic fields. In *Biological effects of magnetic fields* (pp. 215-225). Springer, Boston, MA.

Kholodov, Y. A. (1975). Reactions of the nervous system to electromagnetic fields.

Kholodov, Y. A., & Shishlo, M. A. (1979). Electromagnetic fields in neurophysiology. *Moscow: Science*, *168*.

Kinoshameg, S. A., & Persinger, M. A. (2004). Suppression of experimental allergic encephalomyelitis in rats by 50-nT, 7-Hz amplitude-modulated nocturnal magnetic fields depends on when after inoculation the fields are applied. *Neuroscience letters*, *370*(2-3), 166-170.

Kirschvink JL, Jones DS, McFadden BJ, editors. 1985. Magnetite biomineralization and magnetoreception in organisms. A new biomagnetism. New York and London: Plenum Press

Koivisto, M., Revonsuo, A., Krause, C., Haarala, C., Sillanmäki, L., Laine, M., & Hämäläinen, H. (2000a). Effects of 902 MHz electromagnetic field emitted by cellular telephones on response times in humans. *Neuroreport*, *11*(2), 413-415.

Koivisto, M., Krause, C. M., Revonsuo, A., Laine, M., & Hämäläinen, H. (2000b). The effects of electromagnetic field emitted by GSM phones on working memory. *Neuroreport*, *11*(8), 1641-1643.

Koivisto, M., Haarala, C., Krause, C. M., Revonsuo, A., Laine, M., & Hämäläinen, H. (2001). GSM phone signal does not produce subjective symptoms. *Bioelectromagnetics: Journal of the Bioelectromagnetics Society, The Society for Physical Regulation in Biology and Medicine, The European Bioelectromagnetics Association, 22*(3), 212-215.

Kolosova, L. I., Akoev, G. N., Avelev, V. D., Riabchikova, O. V., & Babu, K. S. (1996). Effect of low-intensity millimeter wave electromagnetic radiation on regeneration of the sciatic nerve in rats. *Bioelectromagnetics: Journal of the Bioelectromagnetics Society, The Society for Physical Regulation in Biology and Medicine, The European Bioelectromagnetics Association, 17*(1), 44-47.

König, H. L. (1962). Ueber den Einfluss besonders niederfrequenter elektrischer Vorgaenge in der Atmosphäre auf die Umwelt. *Z. angew. Bиет,-u. Klimaheilk, 9*, 481-501.

Koren, S. A., & Persinger, M. A. (2002). Possible disruption of remote viewing by complex weak magnetic fields around the stimulus site and the possibility of accessing real phase space: A pilot study. *Perceptual and Motor Skills*, *95*(3), 989-998.

Kotani H, Kawaguchi H, Shimoaka T, Iwasaka M, Ueno S, Ozawa H et al (2002) Strong static magnetic field stimulates bone formation to a definite orientation in vitro. J Bone Miner Res 17:1814–1821 doi: 10.1359/jbmr.2002.17.10.1814

Krause, C. M., Sillanmäki, L., Koivisto, M., Häggqvist, A., Saarela, C., Revonsuo, A., ... & Hämäläinen, H. (2000a). Effects of electromagnetic field emitted by cellular phones on the EEG during a memory task. *Neuroreport*, *11*(4), 761-764.

M. Krause, L. Sillanmäki, M. Koivisto, A. Häggqvist, C. Saarela, A. Revonsuo, M. Laine, H. Hämäläinen, C. (2000b). Effects of electromagnetic fields emitted by cellular phones on the electroencephalogram during a visual working memory task. *International Journal of Radiation Biology*, *76*(12), 1659-1667.

Kremer, F., Santo, L., Poglitsch, A., Koschnitzke, C., Behrens, H., & Genzel, L. (1988). The influence of low intensity millimetre waves on biological systems. In *Biological coherence and response to external stimuli* (pp. 86-101). Springer, Berlin, Heidelberg.

Kuzmanova, M., & St, I. (1995, April). Effect of millimeter waves and gamma-radiation on the surface electrical charge of erythrocyte membranes. In *Millimeter Waves in Medicine and*

Biology," Digest of papers of the 10th Russian Symposium with International Participation (pp. 24-26).

Lazar, M., & Barca, C. (1969). Influence of electromagnetic field of small intensity and of the homogenous field of large intensity on the ions of chicken tissue. *An. Stiint. Univ. Al. I Cuza Iasi. Sea. II Biol*, *15*, 1-7.

Lednev, V. V., Srebnitskaya, L. K., Ilyasova, E. N., Rogdestvenskaya, Z. E., Klimov, A. A., Belova, N. A., & Kiras, K. P. (1996). Magnetic parametric resonance in biosystems: Experimental verification of the theoretical predictions with the use of regenerating planarians Dugesia tigrina as a test-system. *Biofizika*, *41*(4), 815-825.

Leesungbok, R., Ahn, S. J., Lee, S. W., Park, G. H., Kang, J. S., & Choi, J. J. (2013). The effects of a static magnetic field on bone formation around a sandblasted, large-grit, acid-etched–treated titanium implant. *Journal of Oral Implantology*, *39*(s1), 248-255.

Levina, M. Z., Veselago, I. A., Belaya, T. I., Gapochka, L. D., Mantrova, G. M., & Yakovleva, M. N. (1989). Influence of low-intensity VHF irradiation on growth and development of protozoa cultures. *Millimeter Waves in Medicine and Biology." Moscow: Radioelectronica*, 189-195.

Liburdy, R. P. (1992). Calcium signaling in lymphocytes and ELF fields evidence for an electric field metric and a site of interaction involving the calcium ion channel. *FEBS letters*, *301*(1), 53-59.

Liburdy, R. P., Callahan, D. E., Harland, J., Dunham, E., Sloma, T. R., & Yaswen, P. (1993). Experimental evidence for 60 Hz magnetic fields operating through the signal transduction cascade: effects on calcium influx and c-MYC mRNA induction. *FEBS letters*, *334*(3), 301-308.

Lin, H., Goodman, R., & Shirley-Henderson, A. (1994). Specific region of the c-myc promoter is responsive to electric and magnetic fields. *Journal of Cellular Biochemistry*, *54*(3), 281-288.

Lin, H., & Goodman, R. (1995). Electric and magnetic noise blocks the 60 Hz magnetic field enhancement of steady state c-myc transcript levels in human leukemia cells. *Bioelectrochemistry and Bioenergetics*, *36*(1), 33-37.

Lin, H., Blank, M., Jin, M., & Goodman, R. (1996). Electromagnetic field stimulation of biosynthesis: changes in c-myc transcript levels during continuous and intermittent exposures. *Bioelectrochemistry and bioenergetics*, *39*(2), 215-220.

Ludwig, H. W., Mecke, R., and Seelewind, H. (1968). Elektroklimatologie. Arch. Meteorol., Geophys. Bioklimatol

Luk'janova SN. 1969. Analysis of reactions of the central nervous system to the static magnetic field. Author's abstract of Candidate. Dissertation. Moscow.

Mach, Quoc Hao, and Michael A. Persinger. "Behavioral changes with brief exposures to weak magnetic fields patterned to stimulate long-term potentiation." *Brain research* 1261 (2009): 45-53.

Mahmoudi, A., Shojaeifard, M. B., Nematollahii, S., Mortazavi, S. M. J., & Mehdizadeh, A. R. (2018). Effect of Microwave Wi-Fi Radiation at Frequency of 2.4 GHz on Epileptic Behavior of Rats. *Journal of biomedical physics & engineering*, *8*(2), 185.

Martin, L. J., & Persinger, M. A. (2003). Spatial heterogeneity not homogeneity of the magnetic field during exposures to complex frequency-modulated patterns facilitates analgesia. *Perceptual and motor skills*, *96*(3), 1005-1012.

Martin, L. J., & Persinger, M. A. (2004). Thermal analgesia induced by 30-min exposure to 1 μT burst-firing magnetic fields is strongly enhanced in a dose-dependent manner by the α2 agonist clonidine in rats. *Neuroscience letters*, *366*(2), 226-229.

Martin, L. J., Koren, S. A., & Persinger, M. A. (2004a). Influence of a complex magnetic field application in rats upon thermal nociceptive thresholds: The importance of polarity and timing. *International Journal of Neuroscience*, *114*(10), 1259-1276.

Martin, L. J., Koren, S. A., & Persinger, M. A. (2004b). Thermal analgesic effects from weak, complex magnetic fields and pharmacological interactions. *Pharmacology Biochemistry and Behavior*, *78*(2), 217-227.

Martin, L. J., S. A. Koren, and M. A. Persinger. "Thermal analgesic effects from weak, complex magnetic fields: critical parameters." *Electromagnetic biology and medicine* 24, no. 2 (2005): 65-85.

Martin, L. J., and M. A. Persinger. "The influence of various pharmacological agents on the analgesia induced by an applied complex magnetic field treatment: a receptor system potpourri." *Electromagnetic Biology and Medicine* 24, no. 2 (2005): 87-97.

Masoumipoor, M., Jameie, S. B., Janzadeh, A., Nasirinezhad, F., Kerdari, M., & Soleimani, M. (2014). Effects of 660 nm low level laser therapy on neuropathic pain relief following chronic constriction injury in rat sciatic nerve. *Archives of Neuroscience*, *1*(2), 76-81.

McFadden, J. (2013). The CEMI field theory closing the loop. *Journal of Consciousness Studies*, *20*(1-2), 153-168.

McKay, B. E., & Persinger, M. A. (2000). Application timing of complex magnetic fields delineates windows of posttraining-pretesting vulnerability for spatial and motivational behaviors in rats. *International Journal of Neuroscience*, *103*(1-4), 69-77.

McKay, B. E., Persinger, M. A., & Koren, S. A. (2000). Exposure to a theta-burst patterned magnetic field impairs memory acquisition and consolidation for contextual but not discrete conditioned fear in rats. *Neuroscience Letters*, *292*(2), 99-102.

McKay, B. E., & Persinger, M. A. (2003). Combined effects of complex magnetic fields and agmatine for contextual fear learning deficits in rats. *Life sciences*, *72*(22), 2489-2498.

McKay, B. E., & Persinger, M. A. (2004). Normal spatial and contextual learning for ketamine-treated rats in the pilocarpine epilepsy model. *Pharmacology Biochemistry and Behavior*, *78*(1), 111-119.

McKay, B. E., & Persinger, M. A. (2005). Complex magnetic fields enable static magnetic field cue use for rats in radial maze tasks. *International journal of neuroscience*, *115*(5), 625-648.

McKay, B. E., & Persinger, M. A. (2006). Weak, physiologically patterned magnetic fields do not affect maze performance in normal rats, but disrupt seized rats normalized with ketamine: Possible support for a neuromatrix concept?. *Epilepsy & Behavior*, *8*(1), 137-144.

Meli, S. C., & Persinger, M. A. (2009). Red light facilitates the sensed presence elicited by application of weak, burst-firing magnetic fields over the temporal lobes. *International Journal of Neuroscience*, *119*(1), 68-75.

Mudrick, D. G., Golant, M. B., Izvol'skaia, V. E., Slutzkii, E. M., & Oganezova, R. A. (1995). Chemoluminescence of human blood leukocytes after exposure to a low-intensity extremely-high frequency electromagnetic field. In *Moscow, Russia: 10th Russian Symposium "Millimeter Waves in Medicine and Biology," April* (pp. 109-111).

Mulligan, S., & Persinger, M. A. (1998). Perinatal exposures to rotating magnetic fieldsdemasculinize'neuronal density in the medial preoptic nucleus of male rats. *Neuroscience letters*, *253*(1), 29-32.

Mulligan, B. P., Hunter, M. D., & Persinger, M. A. (2010). Effects of geomagnetic activity and atmospheric power variations on quantitative measures of brain activity: replication of the Azerbaijani studies. *Advances in Space Research*, *45*(7), 940-948.

Mulligan, B. P., & Persinger, M. A. (2012). Experimental simulation of the effects of sudden increases in geomagnetic activity upon quantitative measures of human brain activity: validation of correlational studies. *Neuroscience Letters*, *516*(1), 54-56.

Mulligan, B. P., Gang, N., Parker, G. H., & Persinger, M. A. (2012). Magnetic field intensity/melatonin-molarity interactions: Experimental support with planarian (Dugesia sp.) activity for a resonance-like process. *Open Journal of Biophysics*, *2*(04), 137.

Muniz JB, Marcelino M, da Motta M, Schuler A, da Motta MA. Influence of static magnetic fields on S-cerevisae biomass growth. Braz Arch Biol Technol. 2007; 50:515–20.

Murugan, Nirosha J., Lukasz M. Karbowski, Robert M. Lafrenie, and Michael A. Persinger. "Temporally-patterned magnetic fields induce complete fragmentation in planaria." *PloS one* 8, no. 4 (2013): e61714.

Murugan, N. J., Karbowski, L. M., & Persinger, M. A. (2014a). Serial pH increments (~ 20 to 40 milliseconds) in water during exposures to weak, physiologically patterned magnetic fields: implications for consciousness. *Water*, *6*, 45-60.

Murugan, N. J., Karbowski, L. M., & Persinger, M. A. (2014b). Weak burst-firing magnetic fields that produce analgesia equivalent to morphine do not initiate activation of proliferation pathways in human breast cells in culture. *Integrative Cancer Science and Therapeutics*, *1*(3), 47-50.

Murugan, N. J., Karbowski, L. M., & Persinger, M. A. (2017). Synergistic interactions between temporal coupling of complex light and magnetic pulses upon melanoma cell proliferation and planarian regeneration. *Electromagnetic biology and medicine*, *36*(2), 141-148.

NEAGA, N., and LAZAR, M., Histological changes in the thyroids of chicks after treatment with a pulsing magnetic field. *Stud. Cevoet. Biol. Ser. Zool., 24*, 119–124.

Olcese, J., & Reuss, S. (1986). Magnetic field effects on pineal gland melatonin synthesis: comparative studies on albino and pigmented rodents. *Brain research*, *369*(1-2), 365-368.

Ossenkopp, K. P., Koltek, W. T., & Persinger, M. A. (1972). Prenatal exposure to an extremely low frequency-low intensity rotating magnetic field and increases in thyroid and testicle weight in rats. *Developmental Psychobiology: The Journal of the International Society for Developmental Psychobiology*, *5*(3), 275-285.

Ossenkopp, K. P., & Barbeito, R. (1978). Bird orientation and the geomagnetic field: A review. *Neuroscience & Biobehavioral Reviews*, *2*(4), 255-270.

Ossenkopp, K. P., Kavaliers, M., & Hirst, M. (1983). Reduced nocturnal morphine analgesia in mice following a geomagnetic disturbance. *Neuroscience letters*, *40*(3), 321-325.

Ossenkopp, K. P., & Kavaliers, M. (1987). Morphine-induced analgesia and exposure to low-intensity 60-Hz magnetic fields: inhibition of nocturnal analgesia in mice is a function of magnetic field intensity. *Brain Research*, *418*(2), 356-360.

Ossenkopp, K. P., & Shapiro, L. J. (1972, January). EFFECTS OF PRENATAL EXPOSURE TO A 0.5 HZ LOW-INTENSITY ROTATING MAGNETIC-FIELD ON WHITE PEKING DUCKLINGS. In *AMERICAN ZOOLOGIST* (Vol. 12, No. 4, pp. 650-650). 1313 DOLLEY MADISON BLVD, NO 402, MCLEAN, VA 22101 USA: SOC INTEGRATIVE COMPARATIVE BIOLOGY.

Persinger, M. A., Glavin, G. B., & Ossenkopp, K. P. (1972). Physiological changes in adult rats exposed to an ELF rotating magnetic field. *International journal of biometeorology*, *16*(2), 163-172.

Papathanasopoulos, P., Preka-Papadema, P., Gkotsinas, A., Dimisianos, N., Hillaris, A., Katsavrias, C., ... & Papachristou, P. (2016). The possible effects of the solar and geomagnetic activity on multiple sclerosis. *Clinical neurology and neurosurgery*, *146*, 82-89.

Persinger, M. A., & Pear, J. J. (1972). Prenatal exposure to an ELF-rotating magnetic field and subsequent increase in conditioned suppression. *Developmental Psychobiology: The Journal of the International Society for Developmental Psychobiology*, *5*(3), 269-274.

Persinger, M. A., & Psych, C. (1995a). Sudden unexpected death in epileptics following sudden, intense, increases in geomagnetic activity: prevalence of effect and potential mechanisms. *International Journal of Biometeorology*, *38*(4), 180-187.

Persinger, M. A. (1995b). Out-of-body-like experiences are more probable in people with elevated complex partial epileptic-like signs during periods of enhanced geomagnetic activity: a nonlinear effect. *Perceptual and Motor Skills*, *80*(2), 563-569.

Persinger, M. A. (1996). Enhancement of limbic seizures by nocturnal application of experimental magnetic fields that simulate the magnitude and morphology of increases in geomagnetic activity. *International journal of neuroscience*, *86*(3-4), 271-280.

Persinger, M. A., & Belanger-Chellew, G. (1999). Facilitation of seizures in limbic epileptic rats by complex 1 microTesla magnetic fields. *Perceptual and motor skills*, *89*(2), 486-492.

Persinger, M. A. (2003). The sensed presence within experimental settings: implications for the male and female concept of self. *The Journal of Psychology*, *137*(1), 5-16.

Persinger, M. A., Koren, S. A., & Tsang, E. W. (2003). Enhanced power within a specific band of theta activity in one person while another receives circumcerebral pulsed magnetic fields: a mechanism for cognitive influence at a distance?. *Perceptual and Motor Skills*, *97*(3), 877-894.

Persinger, M. A. (2006). A potential multiple resonance mechanism by that weak magnetic fields affect molecules and medical problems: the example of melatonin and experimental "multiple sclerosis". *Medical hypotheses*, *66*(4), 811-815.

Persinger, M. A., & Dotta, B. T. (2011). A transient but protracted geomagnetic anomaly in the Sudbury Basin following two near-contiguous intense geomagnetic storms. *International Journal of Geosciences*, *2*(03), 363.

Persinger, M. A., & Koren, S. A. (2016). The Aharanov-Bohm phase shift and magnetic vector potential "A" could accommodate for optical coupler, digital-to-analogue magnetic field

excess correlations of photon emissions within living aqueous systems. *Journal: JOURNAL OF ADVANCES IN PHYSICS*, *11*(5).

Pelyhe I, Meszaros I, Sarvari E (1973): Effect of static magnetic field on the establishment of conditioned electrodefensive reflex in the rat. Acta Physiol Acad Sci Hung 43:125-132.

Phillips JL, Haggren W, Thomas WJ, Ishida-Jones T, Adey WR. 1992. Magnetic field induced changes in specific gene transcription. Biochim Biophys Acta 1132:140–144.

Piacentini, R., Ripoli, C., Mezzogori, D., Azzena, G. B., & Grassi, C. (2008). Extremely low-frequency electromagnetic fields promote in vitro neurogenesis via upregulation of Cav1-channel activity. *Journal of cellular physiology*, *215*(1), 129-139.

Podkolzin, A. A., & Dontsov, V. I. (1994). Immunomodulating action of weak magnetic fields on formation of antibodies in mice. *Bjulleten'Experimental'noj Biologii i Meditsiny (Bulletin of experimental biology and medicine)*, *117*, 482-483.

Podkovkin VG. 1995. Response of hormonal and mediator regulation systems to the weak geomagnetic field after the ionizing radiation action. Radiatsionnaja Biologija. Radioekologija (Radiation Biology. Radioecology) 35:906-909.

Popp, F. A., Li, K. H., Mei, W. P., Galle, M., & Neurohr, R. (1988). Physical aspects of biophotons. *Experientia*, *44*(7), 576-585.

Popp, F. A. (2003a). Properties of biophotons and their theoretical implications.

Popp, F. A. (2003b). Biophotons—background, experimental results, theoretical approach and applications. In *Integrative biophysics* (pp. 387-438). Springer, Dordrecht.

Porumb, S. (1971). The influence of an electromagnetic field on glucose-6-phosphate dehydrogenase activity in rabbit red blood cells. *Stud. Cerc. Biol. Ser. Zool.*, *23*, 239-242.

Preece, A. W. (1999). Effect of a 915-MHz simulated mobile phone signal on cognitive function in man. *International journal of radiation biology*, *75*(4), 447-456.

Rao S, Henderson AS. 1996. Regulation of c-fos is affected by electromagnetic fields. J Cell Biochem 63:358–365.

Reille, A. (1968). Essai de mise en évidence d'une sensibilité du pigeon au champ magnétique à l'aide d'un conditionnement nociceptif. *J. Physiol.(Paris)*, *60*, 85-92.

Reiter, R. (1964). Atmospheric electricity and natural radioactivity. *Medical climatology*. *New York: Waverly*, 280-316.

Regoli, F., Gorbi, S., Machella, N., Tedesco, S., Benedetti, M., Bocchetti, R., ... & Principato, G. (2005). Pro-oxidant effects of extremely low frequency electromagnetic fields in the land snail Helix aspersa. *Free Radical Biology and Medicine*, *39*(12), 1620-1628.

Resch, J. (1995). Geographic distribution of multiple sclerosis and comparison with geophysical values. *Sozial-und Praventivmedizin*, *40*(3), 161-171.

Richards, M. A., Koren, S. A., & Persinger, M. A. (2002). Circumcerebral application of weak complex magnetic fields with derivatives and changes in electroencephalographic power spectra within the theta range: implications for states of consciousness. *Perceptual and Motor Skills*, *95*(2), 671-686.

Rojavin, M. A., & Ziskin, M. C. (1995). Effect of millimeter waves on survival of UVC-exposed Escherichia coli. *Bioelectromagnetics*, *16*(3), 188-196.

Röschke, J., & Mann, K. (1997). No short-term effects of digital mobile radio telephone on the awake human electroencephalogram. *Bioelectromagnetics: Journal of the Bioelectromagnetics Society, The Society for Physical Regulation in Biology and Medicine, The European Bioelectromagnetics Association*, *18*(2), 172-176.

Rose, G. M., David M. Diamond, K. Pang, and T. V. Dunwiddie. "Primed burst potentiation: lasting synaptic plasticity invoked by physiologically patterned stimulation." In *Synaptic plasticity in the hippocampus*, pp. 96-98. Springer, Berlin, Heidelberg, 1988.

Rudakov YaYa, Mansurov SM, Mansurova LG, Portnov AA, Poleshchuk YuI, Mazursky MB. 1984. Significance of sector structure of the interplanetary magnetic field in synchronization of psycho-physiological regulation in human beings. In: Electromagnetic fields in biosphere: electromagnetic fields in the earth's atmosphere and their biological significance. Moscow: Nauka (Science), Vol 1. p 150-159.

Ruttan, L. A., Persinger, M. A., & Koren, S. (1990). Enhancement of temporal lobe-related experiences during brief exposures to milligauss intensity extremely low frequency magnetic fields. *Journal of Bioelectricity*, *9*(1), 33-54.

Ryczko, M. C., & Persinger, M. A. (2002). Increased analgesia to thermal stimuli in rats after brief exposures to complex pulsed 1 microTesla magnetic fields. *Perceptual and motor skills*, *95*(2), 592-598.

Ryabykh, T. P., & Bodrova, N. B. (1992). CORRELATION OF THE RISK OF ONCOLOGICAL BREAST DISEASE AND SOLAR-ACTIVITY. *Biofizika*, *37*(4), 710-715.

Samokhvalov VP. 1989. Effects of cosmic fluctuations on mental diseases. In: Gnevyshev MN, Ol' AI, editors. Problems of Cosmic Biology, Vol 65, Biophysical and clinical aspects of heliobiology. Leningrad: Nauka (Science). p 65-80.

Saunders, R. (2005). Static magnetic fields: animal studies. *Progress in biophysics and molecular biology*, *87*(2-3), 225-239.

Schimmelpfeng, J., & Dertinger, H. (1993). The action of 50 Hz magnetic and electric fields upon cell proliferation and cyclic AMP content of cultured mammalian cells. *Bioelectrochemistry and bioenergetics*, *30*, 143-150.

Servantie, B., Servantie, A. M., & Etienne, J. (1975). Synchronization of cortical neurons by a pulsed microwave field as evidenced by spectral analysis of electrocorticograms from the white rat. *Annals of the New York Academy of Sciences*, *247*(1), 82-86.

Shestopalova, N. G., Makarenko, B. I., Golovina, L. N., Timoshenko YuP, B. T., Vinokurova, L., & Miroshnichenko, V. (1995, April). Modification of synchronizing effect of millimeter waves on first mitoses by different temperature regimens of germination. In *10th Russian Symposium Millimeter Waves in Medicine and Biology, IRE RAN, Moscow, Russia* (pp. 236-237).

Shibab, K., Brock, M., Gosztonyi, G., Erne, S. E., Hahlbohm, H. D., & Schoknecht, G. (1987). The geomagnetic field: a factor in cellular interactions. *Neurological Research*, *9*, 225-235.

Shpil'berg PI, Vjalov AM. (1972). EEG changes at rhythmic light ¯ashes in the human persons subjected to action of magnetic fields during the production process. In: Clinics and problems of examination of ability to work at diseases caused by physical factors. Moscow. p 116-124.

Shuvalova, L. A., Ostrovskaia, M. V., Sosunov, E. A., & Lednev, V. V. (1991). The effect of a weak magnetic field in the paramagnetic resonance mode on the rate of the calmodulin-dependent phosphorylation of myosin in solution. *Doklady Akademii Nauk SSSR*, *317*(1), 227-230.

Simonov, A. N., Livshits, V. A., & Kuznetsov, A. N. (1986). EFFECT OF CONSTANT MAGNETIC-FIELDS ON THE FORMATION OF BILAYER LIPID-MEMBRANES. *Biofizika*, *31*(5), 777-780.

Sisken, B. F., Walker, J., & Orgel, M. (1993). Prospects on clinical applications of electrical stimulation for nerve regeneration. *Journal of cellular biochemistry*, *51*(4), 404-409.

Sisken, B. F., Jacob, J. M., & Walker, J. L. (1995). Acute treatment with pulsed electromagnetic fields and its effect on fast axonal transport in normal and regenerating nerve. *Journal of neuroscience research*, *42*(5), 692-699.

St-Pierre, L. S., Parker, G. H., Bubenik, G. A., & Persinger, M. A. (2007). Enhanced mortality of rat pups following inductions of epileptic seizures after perinatal exposures to 5 nT, 7 Hz magnetic fields. *Life Sciences*, *81*(21-22), 1496-1500.

Takashima, S., Onaral, B., & Schwan, H. P. (1979). Effects of modulated RF energy on the EEG of mammalian brains. *Radiation and environmental biophysics*, *16*(1), 15-27.

Tambiev, A. K., Kirikova, N. N., Lapshin, O. M., Betzkii, O. V., Novskova, T. A., Nechaev, V. M., & Petrov, I. Y. (1989). The combined effect of exposure to EMF of millimeter and centimeter wavelength ranges on productivity of microalgae. *Millimeter waves in medicine and biology. N. Devyatkov, editor*, 183-188.

Tessaro, L. W., & Persinger, M. A. (2013). Optimal durations of single exposures to a frequency-modulated magnetic field immediately after bisection in planarian predict final growth values. *Bioelectromagnetics*, *34*(8), 613-617.

Tessaro, L. W., Murugan, N. J., & Persinger, M. A. (2015). Bacterial growth rates are influenced by cellular characteristics of individual species when immersed in electromagnetic fields. *Microbiological research*, *172*, 26-33.

Tiras, K. P., Srebnitskaya, L. K., Ilyasova, E. N., Klimov, A. A., & Lednev, V. V. (1996). The influence of weak combined magnetic field on the rate of regeneration in planarians Dugesia tigrina. *Biofizika*, *41*(4), 826-831.

Tsang, E. W., Koren, S. A., & Persinger, M. A. (2009). Specific patterns of weak (1 microTesla) transcerebral complex magnetic fields differentially affect depression, fatigue, and confusion in normal volunteers. *Electromagnetic biology and medicine*, *28*(4), 365-373.

Tsutsaeva, A. A., Makarenko, B. I., Beznosenko, B. I., Gomosov, V. I., Simonova NYa, K. L., Shatilova, L. E., ... & Lisenko, N. A. (1995, April). Radioprotective effect of microwave action. Millimeter Waves in Medicine and Biology. In *Digest of papers of the 10th Russian Symposium with International Participation* (pp. 24-26).

und Halbach, O. V. B. (2009). Structure and function of dendritic spines within the hippocampus. *Annals of Anatomy-Anatomischer Anzeiger*, *191*(6), 518-531.

Usenko UA, Derjapa UR, Kopanev CI, Panin LE. 1989. Effects of heliogeophysical factors on some professional and physiological functions of aviation operators in Siberia. In: Gnevyshev MN, Ol' AI, editors. Problems of cosmic biology, Vol 65, Biophysical and clinical aspects of heliobiology. Leningrad: Nauka (Science). p 52-65.

VanWijk, R. (2001). Bio-photons and bio-communication. *Journal of Scientific Exploration*, *15*(2), 183-197.

Varró, P., Szemerszky, R., Bárdos, G., & Világi, I. (2009). Changes in synaptic efficacy and seizure susceptibility in rat brain slices following extremely low-frequency electromagnetic field exposure. *Bioelectromagnetics: Journal of the Bioelectromagnetics Society, The Society for Physical Regulation in Biology and Medicine, The European Bioelectromagnetics Association*, *30*(8), 631-640.

Vjalov AM. (1971). Clinical, hygienic and experimental data on the action of magnetic fields in industrial conditions. In: Kholodov YuA, editor. Influence of magnetic fields on biological objects. Moscow: Nauka (Science). p 165-177.

Vladimirskij, B. M., & Kislovskij, L. D. (1995). Cosmophysical periods in European history. *Biofizika*, *40*(4), 856-860.

Volobuev, AN., Trufanov, LA., Ovchinnikov, EL., Konstenkov, AG. (1985). *Influence of static magnetic field on the velocity of propagation of electrical pulse along the nerve fiber.* In: Nonionizing irradiation in phlebological practice. Kujbyshev. pp 79-97.

Whissell, P. D., Tsang, E. W., Mulligan, B. P., & Persinger, M. A. (2009). Prenatal exposures to LTP-patterned magnetic fields: Quantitative effects on specific limbic structures and acquisition of contextually conditioned fear. *International Journal of Neuroscience*, *119*(1), 1-14.

Wiech, K., Ploner, M., & Tracey, I. (2008). Neurocognitive aspects of pain perception. *Trends in cognitive sciences*, *12*(8), 306-313.

Wever, R. (1967). Über die Beeinflussung der circadianen Periodik des Menschen durch schwache elektromagnetische Felder. *Zeitschrift für vergleichende Physiologie*, *56*(2), 111-128.

Wever, R. (1968). Einfluss schwacher elektro-magnetischer Felder auf die circadiane Periodik des Menschen. *Naturwissenschaften*, *55*(1), 29-32.

Wu, H. P. P., & Persinger, M. A. (2011). Increased mobility and stem-cell proliferation rate in Dugesia tigrina induced by 880 nm light emitting diode. *Journal of Photochemistry and Photobiology B: Biology*, *102*(2), 156-160.

Yakovleva, M. I., & Medvedeva, M. V. (1974). *Conditioned Control of Cardiac Activity and Respiration and Morphological Changes in the Brain of Pigeons under the Action of a Constant Magnetic Field (Uslovnoreflektornaya Regulyatsiya Serdechnoi Deyatelnosti Dykhaniya i Morfologicheskie Izmeneniya v Golovnom Mozge Golubei pri Deistvii Postoyannogo Magnitnogo Polya)* (No. NISC-Trans-3569). NAVAL INTELLIGENCE SUPPORT CENTER WASHINGTON DC TRANSLATION DIV.

Yeagley HL. 1947. A preliminary study of physical basis of bird navigation. J Appl Physiol 18:1035-1063.

Zaĭtseva, S. A., & Pudovkin, M. I. (1995). Effect of solar and geomagnetic activity on population dynamics among residents of Russia. *Biofizika*, *40*(4), 861-864.

Zecca L, Ferrario P, Conte GD. 1984. Activation of immune systembypulsedmagneticfieldsafterg-rayirradiation.Bioelectrical Repair and Growth Society (BRAGS), 1981. Transactions of the First Annual Meeting, Vol 4.

Zemskov, V. S., Korpan, N. N., Khokhlich, I. I., Pavlenko, V. A., Nazarenko, L. S., Koval'chuk, A. I., & Stefanishin, I. (1988). Effect of millimeter-band low intensity electromagnetic radiation on the course of wound healing. *Klin. Khir.*, *1*, 31-33.

Chapter 2

2. Parameterizing the Influence of Physiologically Patterned EMF on Forskolin Induced Pheochromocytoma Plasma Membrane Extensions

2.1 Abstract

Previous research has demonstrated the utility of pheochromocytoma (PC-12) cells as a model for the *in vitro* examination and experimentation of neuritogenesis after treatment with forskolin or nerve growth factor (NGF). Electromagnetic fields (EMFs), especially those that have been designed to mimic biological function, have been evidenced to influence, at least functionally, various biological systems. Here, we aimed to determine the most effective EMF pattern, as well as other application parameters, that will optimally influence the proportion of plasma membrane extensions in PC-12 cells treated with a cyclic adenosine monophosphate activator (forskolin). Furthermore, we aimed to determine the biomolecular mechanism that drives the synergism between appropriately patterned EMF and forskolin stimulation in this cell model. Results emphasize that EMF pattern, and not intensity, as well as exposure duration is important for maximizing the synergism between chemical treatment and EMF application. Results demonstrated that EMF pattern, especially when that pattern mimics what naturally occurs in the brain, reliably increases the proportion of plasma membrane extensions. Other EMF parameters, such as exposure duration, intensity, and timing, did not appreciably alter the proportion of cells bearing neuron-like extensions.

2.2. Introduction

Pheochromocytoma (PC-12) cells can be induced to produce plasma membrane extensions that have been previously characterized to have morphological and physiological features similar to that of peripheral neurons (Greene and Tishcler, 1976; Green and Tischler, 1982). These cells are electrically excitable and capable of producing and secreting classical neurotransmitters, such as dopamine and serotonin (Shafer and Artichson, 1991, Satpute et al., 2010) making them an excellent model to investigate the mechanisms of neurogenesis and neuronal activity.

Neurotrophic factors, such as brain-derived neurotrophic factor (BDNF) and nerve growth factor (NGF), are quintessential for the survival and differentiation of developing and maturing neurons. NGF treatment has been shown to produce neurite extensions in PC-12 cells with several different biomolecular pathways identified driving this effect (Loeb et al., 1991; Vaudry et al., 2002; Wooten et al., 1999). Caillaud and colleagues (1995) demonstrated that forskolin, in combination with NGF and epidermal growth factor (EGF), was capable of producing neurite extensions in PC-12 cells. Additional work by Gunning et al., (1981a; Gunning et al., 1981b) and Ritcher-Landsberg and Jastorff (1986) showed that elevations in cyclic adenosine monophosphate (cAMP) could mimic the plasma membrane extensions induced by NGF treatment of PC-12 cells.

Forskolin is a diterpene isolated from the *Coleus forskohlii* root, that is capable of activating adenylyl cyclase in various tissues (Seamon and Daly, 1981, Seamon and Daly, 1983, Seamon et al., 1981). Therefore, forskolin treatment results in increased levels of cyclic-adenosine monophosphate (cAMP) that is followed by activation of protein phosphorylation by cAMP

dependent proteins, most notably, PKA (Park and Kim, 1996). In addition to activating adenylyl cyclase, forskolin can act on potassium-induced depolarization that can partially substitute the action of NGF resulting in the promotion of neurite outgrowth (Hoshi et al., 1988). The activity of forskolin was also shown to act on calcium channel kinetics by increasing calcium influx by activating voltage dependent channels, but does not alter channel expression (Bouron et al., 1999).

There are some conflicting results regarding the molecular mechanism by that forskolin promotes neurogenesis in PC-12 cells although cAMP and ERK activity appear to be involved. For instance, researchers were able to demonstrate that adenylyl cyclase activity led to growth arrest and accumulation of cytoplasmic cAMP ultimately resulted in neurite production in PC-12 cells (Deutsch and Sun, 1992; Greene and McGuire, 1978). Lazarovici et al., (1998) were able to extend these results and observed that the production of neurites of PC-12 cells in response to forskolin was independent of PKA activity. Contrary to these findings, Foley and colleagues (2005) found that stimulation of ERK by forskolin depends on PKA, Rap1, and C3G suggesting that forskolin works via PKA dependent C3G pathway to activate ERK in these cells. In this vein, York et al., (1998) reported that cAMP elevating agents can lead to the activation of ERKs in a Rap1-dependent fashion. Bos et al., (2003) showed that treatment with forskolin stimulates activation of Rap1 via activation of cAMP-dependent PKA activity. Research by Wang et al., (2006) added further evidence that forskolin activated ERK in PC-12 cells that was contingent on PKA activity. Recently, Park et al., (2012) showed that forskolin increased dopamine synthesis by transiently phosphorylating ERK1/2, while sustained activity of ERK1/2 resulted in neurite outgrowth. The effects described were concentration dependent.

cAMP modulates cell survival, proliferation, differentiation, and apoptosis through a cascade involving PKA, ERK1/2, and CREB and this pathway is evident in PC-12 cells (Stork and Schmidt, 2002). Dugan and colleagues (1999) and others (Stork and Schmitt, 2002; Vossler et al., 1997), have showed that sustained activation of ERK phosphorylation by way of Rap-1, subsequent to stimulation by PKA, with B-Raf. NGF treatment also activates prolonged, stable activation of ERK leading to the formation of neuritic outgrowths (York et al., 1998). Park et al (2012) demonstrated that forskolin (at discrete concentrations) was also able to prolong the activation of ERK1/2 leading to the formation of sympathetic-like neurite extensions similar to those observed in PC-12 cells stimulated with NGF. Ritcher-Landsberg and Jastorff (1986) were able to demonstrate that forskolin did not act as a second messenger for NGF-induced neurite production (Garrels and Schubert, 1979; Halegoua and Patrick, 1980; Schubert and Whitlock, 1977; Schubert et al., 1978) but rather that the effects of forskolin and NGF were synergistic suggesting distinct yet complimentary modes of action.

There is ample evidence to suggest the manner, and mechanism, by that cAMP activation via forskolin stimulation can lead to plasma membrane extensions in PC-12 cells. Recently, Zhang et al (2014) demonstrated the potential to circumnavigate direct chemical stimulation by exposing cells to various treatments of electromagnetic field radiation (i.e., light). Under the appropriate conditions, light was able to induce neurite extensions in the absence of NGF, that was contingent upon the activation of Raf/MEK/ERK signalling (Zhang et al., 2014).

Our lab has previously shown that exposures to a time-varying, physiologically patterned, propagating electromagnetic field (EMF), can affect biological systems (Whissel and Persinger, 2007; Ross et al., 2008; Mach and Persinger, 2009; Murugan et al., 2014; Karbowski et al., 2012). Buckner et al, (2015, 2017, 2018) demonstrated that the application of a frequency

modulated EMF (e.g., Thomas) is capable of reducing proliferation of B16-BL6 melanoma cells *in vivo* and *in vitro*. Exposures to the Thomas EMF has also been shown to produce analgesia in rats, influence the change in pH of physio-chemical reactions, is correlated with quantitative electroencephalographic changes associated with altered states of consciousness, affect the growth rates of bisected planaria, mediate the induction of excess correlation between distal pairs of humans, chemiluminescent reactions, and pH deviations (Murugan et al., 2013; Murugan et al., 2015; Dotta et al., 2014, Dotta et al., 2012; Dotta et al., 2015; Dotta et al., 2011; Tessaro and Persinger, 2013).

Martin et al (2003, 2004, 2005a; 2005b) showed that exposure to an EMF modeled after the burst-firing rate of a collection of amygdaloid neurons, was capable of inducing analgesia in rats that was equivalent to 4mg/kg of morphine (Fleming et al., 1994). Burst-firing EMF was demonstrated to ameliorate self-reported mood and depression scores in human participants receiving weekly 1 hour treatments of 1 μT intensity for the duration of 6 weeks (Baker-Price, 2003). Murugan et al (2014) compared the metastatic potential of cancer cell cultures treated with typical pain management therapeutics (e.g., morphine) as compared to cells receiving treatment with the burst-firing EMF, and found that only samples receiving morphine, and not the patterned EMF, had activated proliferation pathways. In addition, Murugan and colleagues (2014) showed that the burst-firing EMF activated mu opioid receptors in order to elicit their effects. Finally, Loney et al (unpublished) recently demonstrated synergisms between sub-micromolar concentrations of forskolin and concomitant burst-firing EMF treatment on the proportion of neurite bearing PC-12 cells. The authors noted that the effects observed were dependent on the available concentration of forskolin with too high a concentration eliminating burst-firing EMF effects. The aim of the following investigation is to demonstrate the specific timing (frequency), exposure duration, intensity, pattern, and application geometry of the

applied burst-firing EMF that were necessary to maximize the proportion of PC-12 cells bearing plasma membrane extensions subsequent to stimulation with sub-micromolar concentrations of forskolin. Furthermore, we aim to identify the potential biomolecular pathways that are activated (or inhibited) when these cells are presented with the most effective field configuration using a pharmacological inhibitor approach.

2.3. Methods

2.3.1. Cell culturing and induction of plasma membrane extensions

Pheochromocytoma (PC-12) cells, derived from the rat adrenal medulla, were grown to confluence on 100-mm stock plates supplemented with standard growth media (85% RMPI-1640, 10% horse serum, 5% fetal bovine serum, 1% antibiotic and antimycotic; v/v equivalents). 50 µL of the cell suspension were inoculated on poly-L-lysine-treated, 35-mm cell culture dishes and allowed to adhere to plates for 24 hours in a standard incubator at standard conditions (37ºC, 95% O_2, 5% CO_2). After appropriate adhesion, growth media was removed and cells were supplemented with 2 mL of serum-free media (RMPI-1640 with 0.5% antibiotic and antimycotic). Cultures were then placed in the exposure incubator, operating at standard conditions, that contained the EMF exposure equipment. Cells were treated with 1 µL of forskolin (final concentration: 0.5 µM) at ten minutes during their respective exposure conditions.

2.3.2.1. Exposure apparatus and burst-firing EMF

The exposure device consisted of a cube of Plexiglas that was 12 cm on each side fitted with three pairs of reed relay solenoids (5VDC Reed Relay, 0.5A at 125VAC; Radio Shack, Sault Ste. Marie, MI; #275-232), that allowed the resulting magnetic field to be presented through all three geometric planes. This EMF application geometry has been previously referred to as the "4-D box" application and has been used in experiments that were successful at reducing tumor progression *in vitro* and *in vivo* (Buckner et al., 2015, 2017, 2018). The resulting burst-firing pattern was generated using a custom built, adjustable digital-to-analog converter (DAC), that converted a series 230 points, ranging from 0 to 256, to voltage equivalents of -5V to +5V (127 = 0V). The DAC was operated using a personal laptop computer whose program software was capable of generating and adjusting the pattern, intensity, point duration (PD), inter-stimulus interval (ISI), and solenoid activity. For exposures, the 4-D box, containing the cell plates, was placed inside a standard tissue culture incubator at 37 ± 0.1 °C and $5 \pm 0.2\%$ CO_2. Photos corresponding to the 4-D application geometry can be found in Appendix A1 and standard exposure set-up can be found in Appendix A2.

2.3.2.2. Effects of burst firing, spatially rotating EMF (sr-EMF), rotating magnetic field (r-MF), and exposure duration on forskolin-induced PC-12 plasma membrane extensions

For this experiment, adherent PC-12 cells were exposed to one of two devices, the 4-D application geometry or the Resonator and either Sham or Field applications, for a duration of 1 or 3 hours. The Resonator generated a r-MF at a frequency of 110 Hz and peak intensity of 70 mG when measured at a distance of 1 m. Technical specifications for the Resonator are provided in Appendix B1 and B2. Cultures were placed at a distance of 1 m as the Resonator

generated physical vibrations in the exposure room that were attenuated to background displacements at 1 m. Sham applications for the 4-D application geometry consisted of uploading the target EMF pattern and placing cells in the exposure device, but no current was passed through the solenoids of the 4-D box. Field applications consisted of simultaneously presenting the burst-firing pattern (PD = 3 msec, ISI = 3 msec) through opposing pairs of solenoids and was rotated along all three spatial axes every 500 msec followed by the simultaneous activation of all three planes for 500 msec. The intensity of the burst-firing EMF was measured to be between 20 and 40 mG (2 – 4 uT) using an AC milliGauss meter (AlphaLabs). The presence of the pattern was verified using a mini-audio amplifier coupled to a magnetic telephone pick-up. Sham applications of the r-MF generating device (Resonator) consisted of plugging the device into the 120 VAC outlet and turning its cooling fan on. Active field exposures consisted of turning the engine that turned a series of static magnets at a rate of 110 Hz. The r-MF generated from the Resonator was verified by way of an AC milliGauss meter (AlphaLabs). Trials were conducted such that in each condition there were N=2 plates exposed in parallel and all replicates (N=3) were completed independently.

2.3.2.3. Determining the difference between rotational or constant application of burst-firing EMF generated through the 4-D exposure application

The aim of this section was to differentiate the contribution of rotation or constant application of the burst-firing EMF pattern on the ability to induce plasma membrane extensions in PC-12 cells treated with forskolin. PC-12 cells were prepared according to the procedures described in section 2.3.1. Cells were either exposed to the burst-firing EMF (PD = 3 msec, ISI = 3 msec) generated through all three pairs of solenoids simultaneously (constant exposure) or to the same pattern that was simultaneously presented through opposing pairs of solenoids that was then

rotated along all three spatial axes every 500 msec followed by the simultaneous activation of all three planes for 500 msec (rotation) using the 4-D exposure apparatus. The peak intensity and duration of exposure to the burst-firing EMF for both the constant and rotational conditions were held consistent between 20 and 40 mG (2 – 4 uT) and 1 hour respectively. The presence and intensity of the burst-firing EMF was verified using a telephone pick-up and mini audio amplifier and an AlphaLabs AC milliGauss meter.

2.3.2.4. The influence of point duration of burst-firing EMF on PC-12 plasma membrane extensions

The effect of specific combinations of PD and ISI had on the proportion of PC-12 cells bearing plasma membrane extensions was examined. The exposure apparatus, peak intensities, EMF pattern, and spatial presentation across solenoids were the same as described in section 2.3.2.2. There were a series of three manipulations with respect to the PD and ISI variables for the burst-firing pattern: 1) PD = 3msec, ISI = 3 msec (positive control), 2) PD = 1, ISI = 1, and 3) PD = 3, ISI = 3000. These combinations of PD and ISI were selected from previous experiments conducted in our laboratory to examine the effectiveness of the burst-firing field on thermal analgesia in rats, amelioration of psychometric measures of depression, induction of mystical experiences in humans, and the generation of excess correlations in physio-chemical reactions (Baker-Price, 2003;Dotta et al., 2015; Martin et al., 2004; Fleming et al., 1994; Tsang et al., 2009; Cook and Persinger, 1997; Meli and Persinger, 2009). The duration of exposure was 1 hour, as results from experiment 2.3.2.2 suggested that there was no significant difference between 1 and 3-hour field applications. For each replicate, there was N=2 plates exposed in parallel and all replicates (N = 3) were conducted independently (i.e., on different days). The presence and intensity of each EMF was verified using an AC

milliGauss meter (AlphaLabs) and mini-audio amplifier coupled to a telephone pick-up. A diagrammatic representation of the burst-firing EMF configuration can be found in Appendix C.

2.3.2.5. Intensity dependence of burst-firing EMF on induced plasma membrane extensions in PC-12 cultures

PC-12 cells were sub-cultured and plated according to the methods detailed in section 2.3.1. and then subjected to exposures in the 4-D box exposure and burst-firing pattern as outlined in section 2.3.2.2. The PD and ISI for the burst-firing pattern used in this experiment were each set to 3 msec respectively. Plates of PC-12 cells were exposed for a duration of 1 hour to one of three intensities: 1) 300 – 500 nT (Low), 2) 2 – 5 μT (Medium), and 3) >10 μT (High). Intensities were verified using an AC milliGauss meter (AlphaLabs) and the presence of the field pattern was confirmed using a mini-audio amplifier coupled to a magnetic telephone pick-up. Plates(N=2) were exposed in parallel and all conditions were independently replicated (N=3).

2.3.2.6. Pattern specificity of EMF application on forskolin-induced PC-12 plasma membrane extensions

The efficacy of the pattern of EMF application on the proportion of plasma membrane extensions in PC-12 cells treated with nanomolar concentrations of forskolin was tested. The exposure apparatus for this investigation consisted of the 4-D box application geometry (section 2.3.2.2.), however there was no rotation in the pattern applied across the solenoids (i.e., all three spatial planes were activated simultaneously). PC-12 cells were sub-cultured and

plated according to our standard protocols outlined in section 2.3.1, before being exposed for a duration of 1 hour to one of the four following EMF conditions: Burst-firing EMF, Reverse Burst-firing EMF, Thomas-EMF, and 7-Hz pulse (690 msec 7-Hz sine wave followed by a 210 msec pause). The reverse burst-firing pattern consisted of the same series of 230 points that made up the burst-firing pattern, however the series of integers were inverted. The Thomas-EMF was generated by converting 859 integer values between 0 and 256 to a corresponding voltage of -5 V to +5V (127 = 0V), producing 18 doublet peaks with gradually increasing intervals between 3 msec (for the first 5 repeats) to 120 msec for the last 5 repeats. The resulting frequency modulation for the Thomas-EMF pattern ranged from 25 Hz for the first 5 to 6 Hz for the last 5 repeats. For all patterned EMF applications, PD and ISI were set to 3 msec respectively. The patterns were all exposed continuously to the cells for a duration of 1 hour, and peak intensities were set between 2 and 4 μT. The intensity and pattern of each respective manipulation was assessed using an AC milliGauss meter (AlphaLabs) and a magnetic telephone pick-up coupled to a mini-audio amplifier. A series of photographic representations of the burst-firing, reverse burst, FM-EMF, and 7 Hz sine wave patterns can be found in Appendix D. There were N=2 plates that were exposed in parallel for each condition and all replicates (N=3) were conducted independently.

2.3.2.7. Identifying the potential biomolecular pathway for the action of burst-firing EMF on forskolin-induced plasma membrane extensions in PC-12 cell cultures using an inhibitor series

PC-12 cell cultures were prepared in accordance with the methods outlined in section 2.3.1. and were exposed for the duration of 1 hour to either sham or burst-firing EMF generated through the 4-D box application geometry. Here, the presentation of the burst-firing EMF was presented in opposing pairs of solenoids and rotated through all three spatial planes at a

frequency of 2 Hz (i.e., 500 msec presentations) before being simultaneously presenting all three planes for 500 msec. PD and ISI were set to 3 msec respectively. The intensity of the burst-firing EMF was verified, by way of an AC milliGauss meter (AlphaLabs) and mini-audio amplifier coupled to a telephone pick-up coil, to fall within the 3 – 5 μT range.

Inhibitors (or suspending media for controls) were injected to PC-12 plates 30 min prior to their respective exposure conditions, maintained for the 1-hour treatment, and then the media removed and replaced with serum-free media. Injections of 1 μL (final concentration 0.5 μM) forskolin were added to plates at 10 minutes into their respective treatment conditions. Following exposure, samples were removed, transported to a different room, and measures were taken for photon emission (see section 2.3.4 for a complete methodology). After emission was assessed, media was removed, replaced with serum free media, and inoculated with 1 μL of forskolin (final concentration 0.5 μM) before being allowed 72 hours for differentiation and morphological assessment. The inhibitors were used at the indicated concentrations: 50 nM SB20219 (Sigma Chemical, Oakville, Canada), 5 μM PD98059, 14 nM bisindolylmaleimide, 10 nM wortmannin, and 36 μM H7 (Calbiochem, San Diego, CA). Plates receiving EMF or sham exposures were conducted in blocks of 6. That is to say that each of the respective inhibitors (5) as well as a control plate (i.e., receiving only forskolin and having its media removed and replaced at the end of the exposure duration) were conducted in a given replicate, and all replicates (N=7) were conducted independently.

2.3.3. Cell morphological measures

In order to assess the efficacy of our various treatments, photos (N=4 per plate) were taken 3 days after receiving EMF exposure using a phase-contrast setting on a light compound

microscope at 100x magnification. The total number of cells were counted for each quadrant and summated for each plate. In addition, cells bearing plasma membrane extensions (i.e., any observable distortion and protrusion whose origin can be traced to the cell body) were counted and reported as a proportion of the total cell count. Additional measures included: the proportion of cells with multipolar and higher order arborizations, number of inter-cellular connections (i.e., synapses), and proportion of cells whose plasma membrane extensions exceeded the diameter of the cell soma at its largest extent.

The data from investigation 2.3.2.2. suggested that there was no impact of exposure duration on the proportion of cells displaying plasma membrane extensions, or other morphological measures, and therefore all subsequent investigations only tested the impact of 1 hour exposures. Furthermore, there was no observable difference in the proportion of cells exhibiting plasma membrane extensions at days 3 and 6 following exposure. Therefore, subsequent morphological measures for investigations 2.3.2.3 – 2.3.2.7. were taken only 3 days after exposure.

2.3.4. Ultra-Weak Photon emission

In conjunction with morphological measures, biophoton emission data was recorded for the experiment outlined in section 2.3.2.7. The aim was to possibly identify 1) differences in emission spectra that were associated with specific biomolecular pathway inhibitors in forskolin treated PC-12 cells and 2) to demonstrate a potential interaction between altered biomolecular pathway activity in these cells when they have been treated with a patterned EMF.

PC-12 cells treated with specific inhibitors in the presence or absence of forskolin (see section 2.3.2.7 for summary of group construction) and either receiving 1 hour of burst-firing EMF or Sham exposures were removed from the exposure incubator and transported to the recording immediately following their respective EMF treatment conditions. The recording room, that housed the measurement unit, was located approximately 3 m away from the cell culture laboratory. A single plate was placed over the aperture of a Model DMC-0089 digital photomultiplier tube (PMT) (SENS-TECH Sensory Technologies; SN:68569). The entire experimental detection system was housed in a darkened wooden box, that was covered by 10 layers (8 cm) of thick cotton cloth to ensure no environmental light pollution would affect the sensitivity of the PMT recordings. The typical dark count or background ambient recording obtained for this PMT were in the range of 0 – 2 photon units per 20 msec (50 – 100 photons per sec). Measurements were acquired using Sens-Tech Counter Timer software (Version 2.8, build: 11) at a sampling rate of 50 Hz. The PMT recordings were stored on a personal laptop computer. Each recording session consisted of a 2-min baseline (empty box) recording, before placing the cells over the aperture of the PMT recording device and the emission measured for another 3 x 1-min sessions. Between baseline and active cell recordings a 2-min light adjustment period was provided to reduce the impact of environmental light pollution during data collection. At the end of the recording period, the cells cultures were returned to the culture lab and placed in a standard incubator for 3 days. Each recording session was conducted in blocks (i.e., N = 1 sample for each inhibitor-forskolin and field condition) and all trials were replicated independently (N=7).

2.3.5. Methods of analyses

2.3.5.1 Cell morphology:

Raw data for morphological measures were converted into a proportion of the total cells counted (feature of interest/total cell count·100%) and were used in subsequent analyses. Unless otherwise specified, all proportions were subjected to a one-way analysis of variance. Subsequent Tukey's post-hoc tests, where applicable, were employed to demonstrate that source(s) of variance were driving the effect.

2.3.5.2 Ultra-Weak Photon Emission:

Raw emission data were imported into Excel for the calculation of the mean and standard deviation (SD) for each of the recording phases (i.e., baseline, cell, post-baseline). Furthermore, raw time-series data was standardized (i.e., z-transformed) and truncated between +/-5 SD to accommodate outliers. Standardized data was then subjected to spectral analysis yielding spectral power densities whose frequency range spanned 0 – 25 Hz in 0.01 Hz bin increments. Spectral data as well as the means and SD for each recording phase were then exported into SPSS for statistical analysis. The, data was grouped in 1 Hz increments (i.e., 1 Hz bin = 1.01 to 1.99) for time-series analysis. Assessment of the mean and SD of the measurement were subjected to a MANOVA with condition [sham v. Burst (3,3)] and inhibitor (6 levels) as between-subjects' factors with measurement period (3 levels) as within subjects' factors. Examination of spectral power densities for frequency patterns were also investigated by way of MANOVA with frequency (25 levels) as within subjects' factors. Relevant post-hoc tests, or other manipulations are discussed in the corresponding results section.

2.4. Results:

2.4.1. Effect of burst-firing EMF and rotating EMF exposure duration on forskolin induced PC-12 plasma membrane extensions

A MANOVA with device, field condition, and duration of exposure as between-subject's variables revealed no within-subject's main effects or interactions for any of the morphological features measured. A 3-way between-subject's analysis of variance was conducted with device (Resonator v. 4-D), duration (1 v. 3 hours) and exposure condition (Sham v. Field) as independent variables with each of the morphological measures as dependent variables. Results revealed a significant two-way interaction of device (Resonator v. 4-D) and exposure condition (Sham v. Field) for the proportion of cells bearing plasma membrane extensions (PME) only [$F_{(1,47)} = 6.25$, $p = .016$, Ω^2-est = .10]. This interaction was abolished when examining morphological measures taken on Day 6 [$F_{(1,47)} = 0.19$, $p>.05$]. Post-hoc one-way analyses of variance were conducted in order to ascertain the source of the interaction and revealed that the significant differences obtained were driven by a greater proportion of PME-bearing cells when exposed to the 4-D burst-firing EMF and proportionally lower PME-bearing cells exposed to the Resonator field condition. (Figure 2.4.1.1).

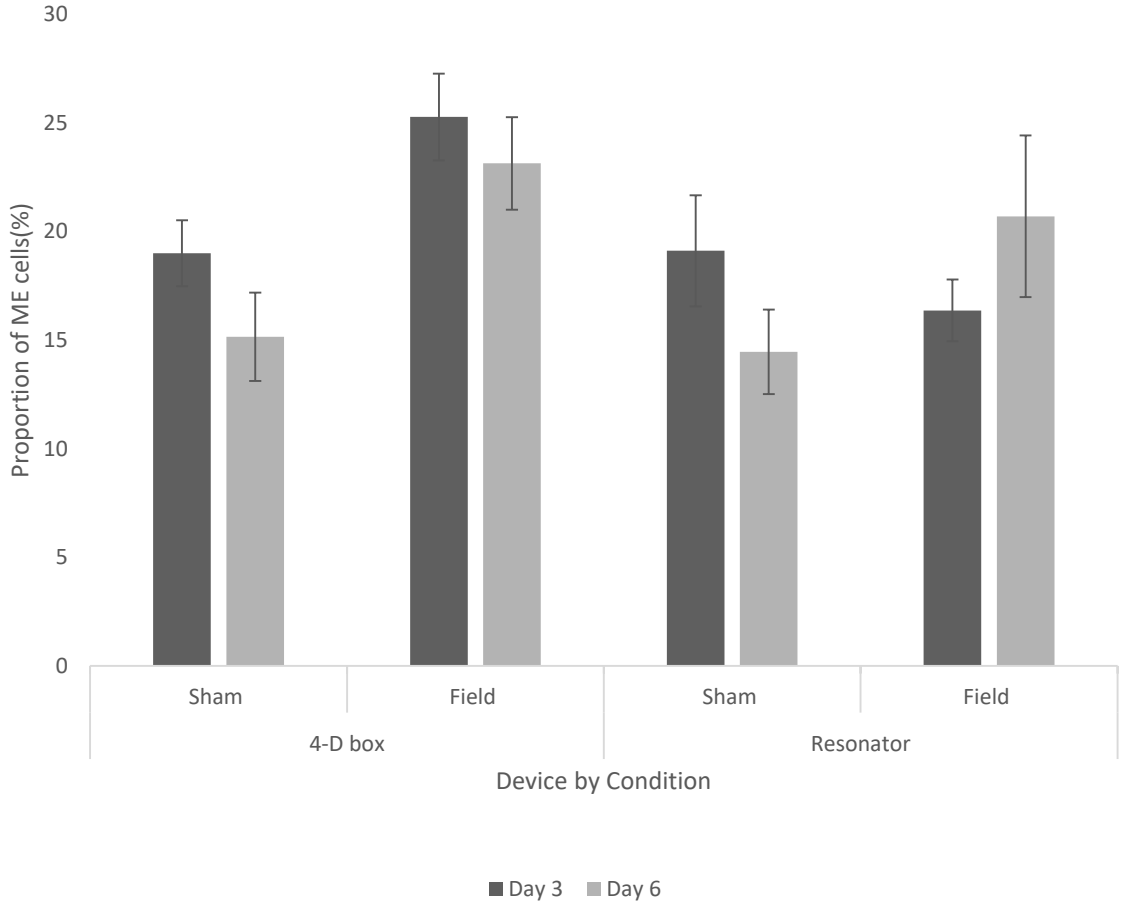

Figure 2.4.1.1: 2-way interaction of device and field condition on the proportion of PME-bearing cells treated with 0.5 µM forskolin Error bars represent standard error of the mean (SEM). Field produced in the 4-D condition was consisted of the burst-firing pattern (PD = 3, ISI = 3) with a peak intensity of 40 mG and was spatially rotated across all three axes at an interval of 2 Hz. Frequency of the Resonator was verified to be 110 Hz and the peak intensity at the exposure distance of 1 m was 70 mG.

Subsequently, one-way analysis of variance was conducted selecting only the 4-D application geometry in order to verify significant differences between 1) exposure condition (Sham v. Field) and 2) day of measure, for PME-bearing cells only. Here, the results indicated significant differences between exposure condition for the proportion of PME-bearing cells on Day 3 [$F_{(1,26)} = 6.48$, $p = .017$, Ω^2-est = 0.21] and Day 6 [$F_{(1,26)} = 7.24$, $p = .013$, Ω^2-est = 0.22] with no difference across days. The results can be seen in Figure 2.4.1.2.

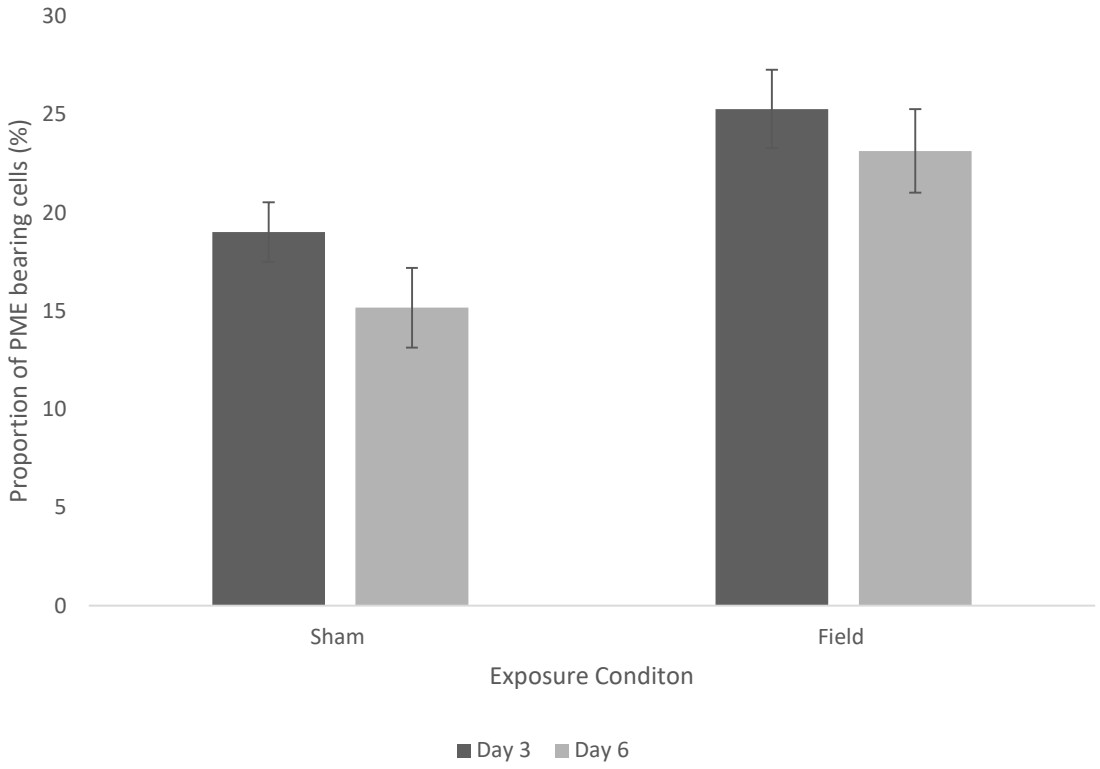

Figure 2.4.1.2: Main effect of the burst-firing pattern (PD = 3, ISI = 3) generated by the 4-D application geometry with 2 Hz spatial rotation across all three axes on the proportion of PME-bearing cells treated with 0.5 µM forskolin. Peak intensity was verified to be 40 mG within the EMF-generating unit. Error bars represent SEM.

Next, we aimed to evaluate any features of the exposure parameters that were unique to the Resonator (r-MF) device. A two-way repeated measures ANOVA with exposure duration (1 and 3 hours) and condition (no field v. field) and time (day 3 and 6 measures) was conducted to statistically validate any effects between treatment conditions and percent of cells bearing neurites, multipolar nerites, long extensions, and synapses. Results indicated a main effect of exposure duration [$F_{(1,20)} = 5.00$ $p = .037$, $p\eta^2 = 0.20$]. Subsequent post-hoc one-way analysis of variance revealed that cells measured 3 days following exposure had a higher proportion of neurite-bearing cells, regardless of exposure condition (sham v. field) when the cells were exposed for a duration of 3 hours [$F_{(1,23)} = 6.61$, $p = .017$, Ω^2-est = 0.23] as can be seen in Figure 2.4.1.3.

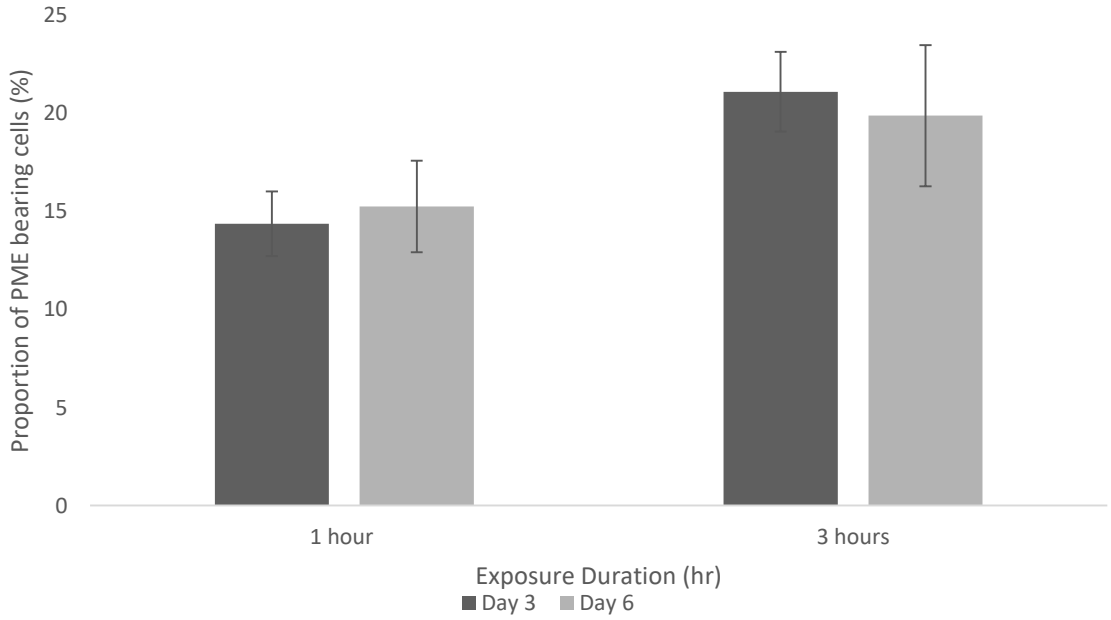

Figure 2.4.1.3: Data represents the change in proportion of cells bearing neurites from PC-12 cells injected with 0.5 µM forskolin and exposed to the Resonator C500 device at 1 m for 1 hour and 3 hours. Error bars represent SEMs.

2.4.2. Determining the difference between rotational or constant application of burst-firing EMF generated through the 4-D exposure application

A one-way analysis of variance was used to compare the spatio-temporal presentation (constant v. rotation) was conducted to statistically validate any differences between morphological measures assessed. Results indicated no significant differences in the proportion of cells bearing PME ($p>.05$) or any other morphological measure between treatment conditions ($p>.05$; Figure 2.4.2.1).

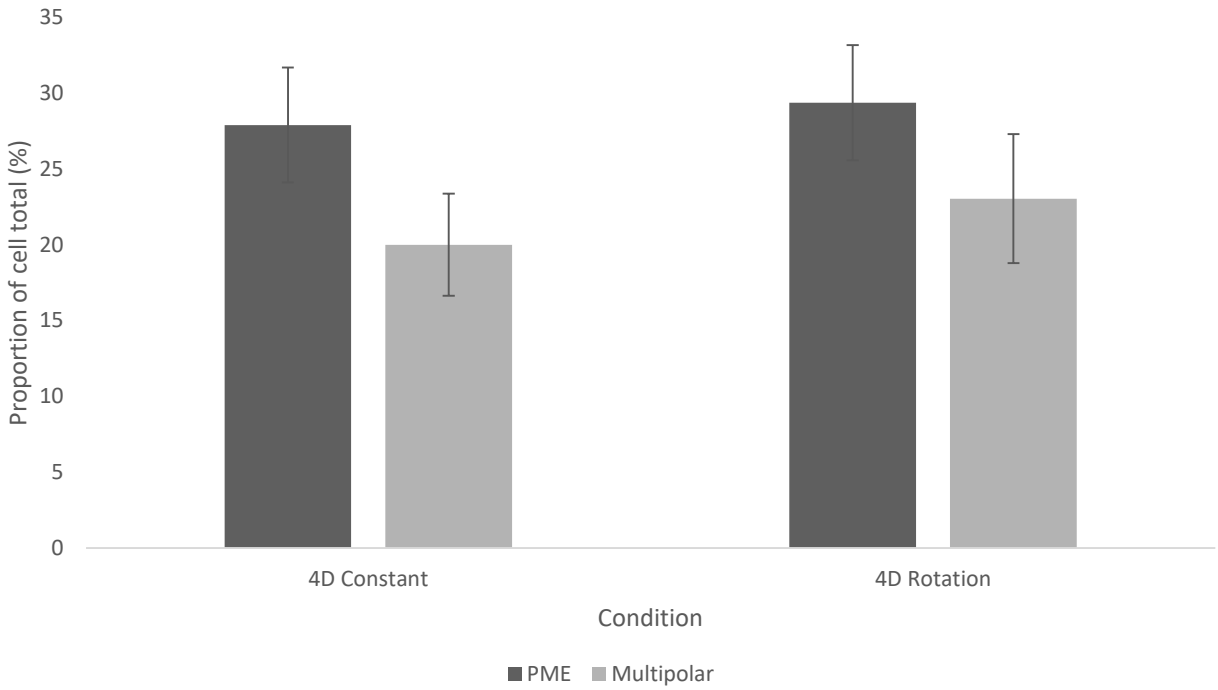

Figure 2.4.2.1: Proportion of cells displaying PME and multipolar PME, two measures that demonstrated differences between EMF patterns, as a function of spatio-temporal pattern of presentation (constant v. rotation) in the 4-D application apparatus. Error bars represent SEMs n=2 plates per trial and N=4 replicates conducted independently.

2.4.3. The influence of point duration of burst-firing EMF on PC-12 plasma membrane extensions

One-way analysis of variance examining the difference in morphological measures as a function of condition (i.e., changing PD and ISI) revealed significant differences for the proportion of PME-bearing [$F_{(3,35)} = 5.83$, $p = .003$, Ω^2-est = 0.35] and multipolar cells [$F_{(3,35)} = 8.27$, $p = 3.24 \cdot 10^{-4}$, Ω^2-est = 0.44]. The differences obtained were driven by greater proportion of PME-bearing and multipolar between burst-firing treated samples and Sham exposures. There was no difference between any of the different combinations of PD and ISI used in this investigation. Results can be observed in the figure 2.4.3.1.

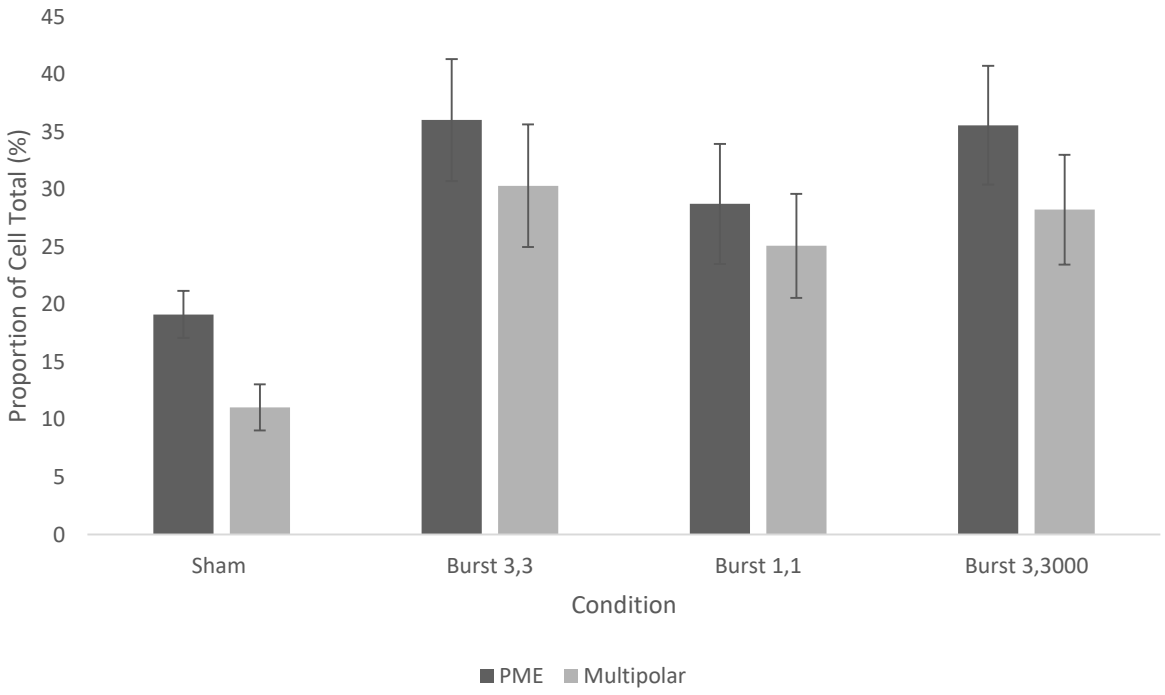

Figure 2.4.3.1: The proportion of PME and multipolar cells as a function of exposure condition. EMF intensity, regardless of PD and ISI fell between 3 and 5 μT. Error bars represent SEM.

2.4.4. Intensity dependence of burst-firing EMF on induced plasma membrane extensions in PC-12 cultures

A one-way ANOVA was conducted to ascertain differences in morphological measures as a function of intensity. Results revealed statistically significant differences in the proportion of PME-bearing cells [$F_{(2,29)} = 6.08$, $p = .003$, Ω^2-est = 0.41] and multipolar cells [$F_{(3,29)} = 12.36$, $p = 3.3 \cdot 10^{-5}$, Ω^2-est = 0.59] by intensity. Tukey's post-hoc analysis revealed that the effects were driven by significantly lower proportions of PME-bearing cells in sham conditions as compared to all other intensities, with the greatest differences obtained between sham exposures and high intensity burst-firing EMF exposures. No differences were obtained between the highest intensity and all other EMF exposure intensities. The findings have been summarized in Figure 2.4.4.1.

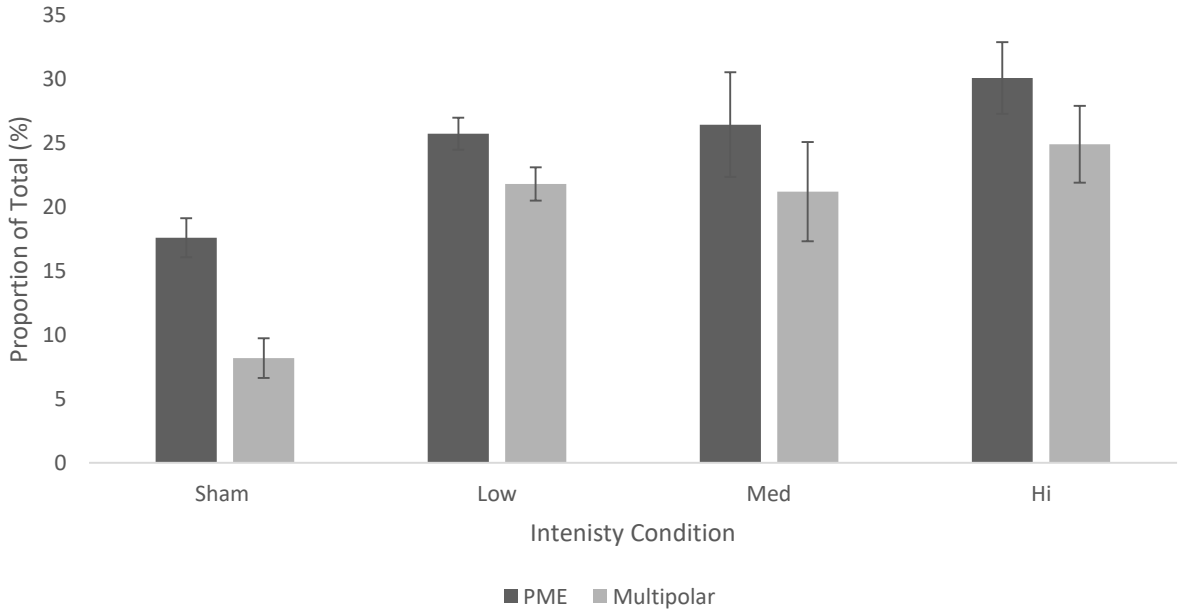

Figure 2.4.4.1: Effects of intensity on the proportion (%) of PME-bearing and multipolar cells treated to Burst-firing EMF (3,3) for 1 hour in combination to 0.5 µM forskolin. Sham

(control); Low (0.3 -0.5 uT); Med (3 – 5 uT); Hi (10^{+} uT). Error bars represent SEM. There were total of N = 3 independent replicates with n = 2 plates for each intensity whilst Sham conditions contained N=6 independent trials with n = 2 plates conducted in parallel.

2.4.5. Pattern specificity of EMF application on forskolin induced PC-12 plasma membrane extensions

Analyses of variance was conducted to verify difference in morphological features as a function of different patterned EMF exposures (5-levels). The results indicated significant differences between the proportion of PME-bearing [$F_{(4,29)} = 3.93$, $p = .031$, Ω^2-est = 0.39] and multipolar cells [$F_{(4,29)} = 4.71$, $p = .006$, Ω^2-est = 0.43] as a function of patterned EMF exposure. Tukey's post-hoc tests demonstrated the effects observed were being driven by the difference in the proportion of PME-bearing cells between Burst and Rev-Burst. There was a significantly greater proportion of multipolar cells when exposed to the burst-firing EMF as compared to both the Rev-burst and Thomas conditions, with the latter pair being no different from each other.

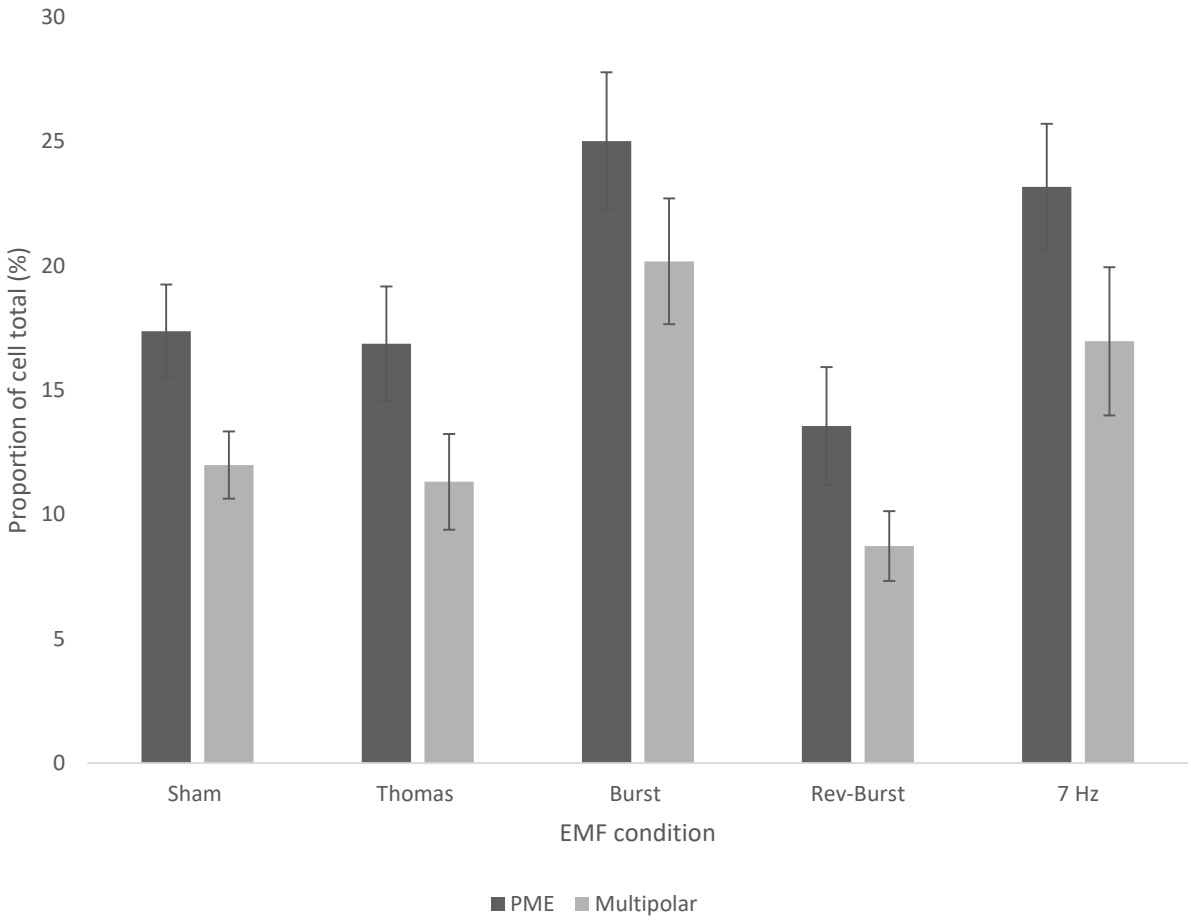

Figure 2.4.5.1: The representation of the differences obtained between varying EMF configurations (patterns) as applied to 0.5 µM forskolin treated PC-12 cells. PD and ISI were 3 msec and verified intensity fell within the range of 2 – 4 µT respectively. The proportion of cell total for plasma membrane extensions (PME) are represented in the dark bars, whilst the proportion of the multipolar cells are represented in the light bars. Error bars correspond to SEMs. N =3 replicates with 2 plates conducted in parallel.

2.4.6. Identifying the potential biomolecular pathway for the action of burst-firing EMF on forskolin induced plasma membrane extensions in PC-12 cell cultures using an inhibitor series

2.4.6.1: Cell Morphology:

At the time of this writing, several (N=7) failed attempts to assess the impact of various inhibitors in the presence of the most effective field condition were conducted. No data has been rendered.

2.4.6.2: Ultra-Weak Photon Emission Spectra:

There were no significant differences between chemical inhibitors or EMF exposure as a function of frequency for mean photon counts, standard deviation of the raw counts, nor the spectral power densities among the 25-Hz bins ($p>.05$). Data was further investigated by examining the mean spectral power densities as well as the standard deviation of spectral power densities divided into frequency bins corresponding to the classical EEG frequencies, (delta :0-3 Hz; theta: 4-7 Hz; alpha:1 8-11 Hz; alpha2: 12-15 Hz; beta1: 16-19 Hz; and beta2: 20-24 Hz). A MANOVA with these variables as dependents and EEG bins as within subjects' factors was used. There were no significant differences in the mean spectral power densities, corresponding to the classical EEG bins, as a function of condition and inhibitor ($p>.05$). However, there was a significant within-subjects' interaction of condition and EEG frequency bins [$F_{(5,360)} = 3.02$, $p = .011$, $p\eta^2 = .04$]. Post-hoc one-way analyses revealed that the differences were being driven by a reduction in low frequency (delta; 0-3 Hz) spectral power density variability when the burst-firing field was present and can be found in Figure 2.4.6.2.1.

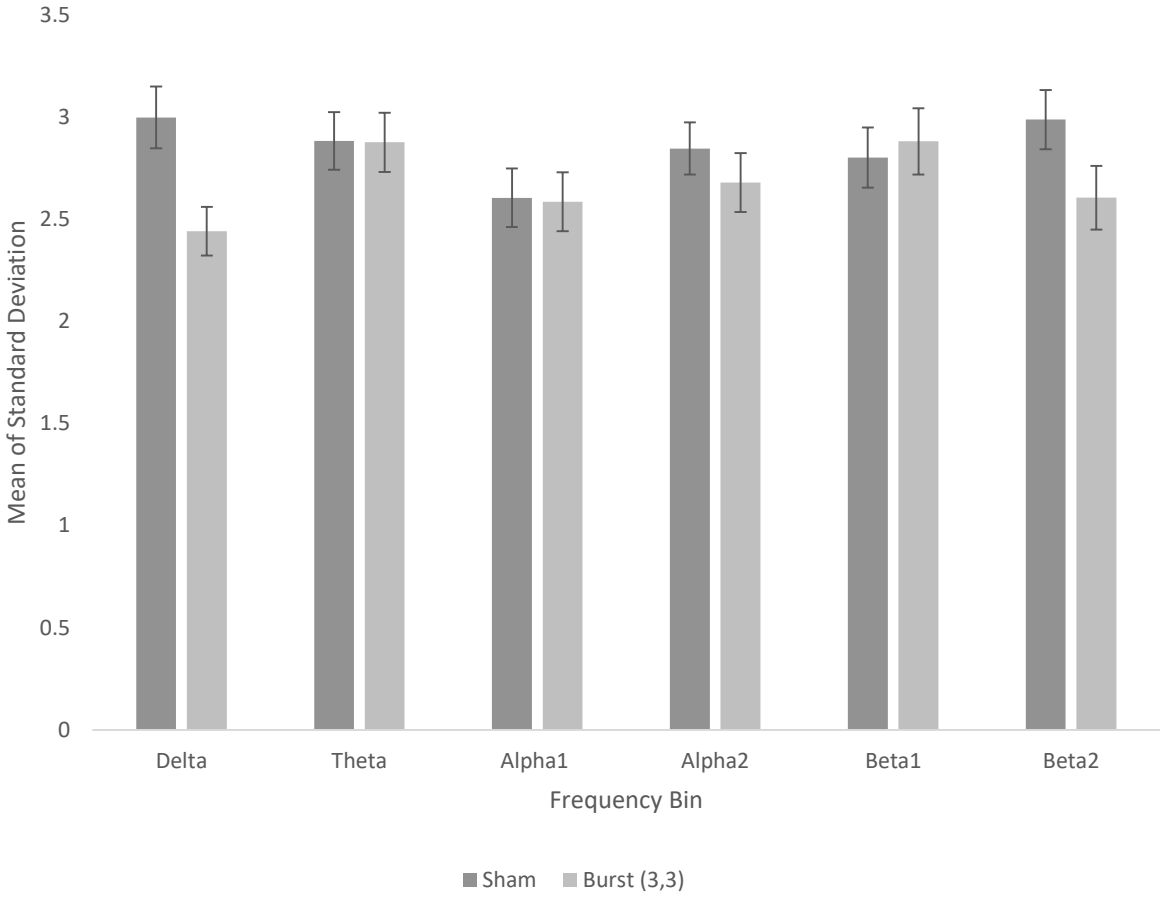

Figure 2.4.6.2.1: Data investigating differences in the standard deviation of spectral power densities (ordinate) organized into classical EEG bands (abscissa). Each frequency bin was the aggregate (mean) corresponding to frequency ranges of: delta :0-3 Hz; theta: 4-7 Hz; alpha:1 8-11 Hz; alpha2: 12-15 Hz; beta1: 16-19 Hz; beta2: 20-24 Hz. Error bars represent SEMs.

2.5. Discussion

In this series of investigations, we aimed to determine the most effective configuration of EMF application parameters that could influence neuritogenesis of PC-12 cells treated with a cAMP activator. These data showed that 1) different forms of electromagnetic (EM) energy differentially influenced PME (neurite outgrowth), 2) there was no difference when cells were exposed to EMF for 1 or 3 hours, 3) the effects on PME was strongly dependent on the temporal organization of an effector field, 4) the burst-firing EMF and 7-Hz sine were the most impactful and, 5) difference in intensity (0.1 to 10 uT) had the same effect on PME.

In terms of source of the EM energy, our results indicated that burst-firing EMF presented through pairs of solenoids arranged across the 3 spatial axes as being able to promote (enhance) neurite formation (operationalized as a change in the proportion of cells bearing PME) when samples of PC-12 cells were also incubated with 0.5 µM forskolin. Conversely, the effects observed when the same experimental protocol was applied to cells that were exposed to a rotating magnetic field (rMF) of comparable intensity, demonstrated a reduction in morphological measures. There is evidence to suggest that different forms of EM energy, generated from different sources can lead to similar or opposite effects. For example, Ossenkopp and Kavaliers (Ossenkopp and Kavaliers, 1987; Kavaliers and Ossenkopp, 1986) demonstrated a sensitization to nociceptive stimuli in animals exposed to a rMF rotated at a frequency of 0.5 Hz with an intensity of 3 G, while analgesic effects were observed by Martin et al. (2004) when rats were exposed to burst-firing EMF of much lower intensities (5 – 10 uT). Furthermore, certain field parameters may enhance abilities while other configurations may lead to extirpation of an effect as evidenced in research examining Ingo Swann's remote viewing capacity (Koren and Persinger, 2002). Mr. Swann possessed the unique capacity to accurately describe the nature and content of images sealed in envelopes and placed in a

separate location. His capacity to accurately described image content was impeded when targets were exposed to a patterned EMF.

The results of these studies show that there is a specificity for EMF pattern in terms of inducing effects, first by altering the gestalt temporal structure of the EMF stimulus (i.e., presentation of different patterns) then by discretely altering the temporal organization of the most effective field (i.e., changing point duration and inter-stimulus interval). In the former case, 3 distinct EMF patterns that have been previously shown to be biologically relevant (burst-firing, Thomas-EMF, and LTP), as well as 2 other targets, the inverted pattern of the effector field (Rev-Burst) and a 7-Hz pulse, were compared. Results revealed that the burst-firing EMF was most successful at positively impacting our measures (i.e., proportion of PME-bearing cells and proportion of cells with multipolar extensions), as compared to other targets. Most notably, there was an inversion of effects (i.e., return to baseline measures) observed when the structure of the target field was reversed. These effects provide evidence that pattern is important when using EMF exposure to affect biological systems and that, even when the energy is the same, the structure of the quanta (stimulus) is different.

The effects of the 7-Hz pulse had a very similar effects on proportion of PME-bearing cells when compared to the burst-firing pattern. PC-12 cells that are induced to differentiate by stimulation with chemical agents respond specifically to dopamine agonism and antagonism insofar that they are classified as peripheral dopaminergic neurons (Hussain et al., 2006; Westerink and Ewing, 2008; Pothos et al., 1998). The effects associated with the burst-firing pattern have been demonstrated to act, at least partially, on u-opioid receptors, and are related to the biomolecular features of dopamine reactions (Thompson et al., 2000; Calon et al., 2000; Greengard et al., 1999). The 7-Hz pulse has some similarity to naturally occurring EM

fluctuations in the environment. For instance, the geomagnetic field (that which arises from the rotation of Earth's fluid iron core) and Schumann harmonics (the consequence of lightning discharges between the Earth's surface and the ionosphere) share this frequency and have been observed to have remarkable impacts on animal behaviour and neurodevelopment (Fournier et al., 2012; Friedman et al., 1965; Persinger, 1999). Although unsubstantiated, it is possible that the 7-Hz pulse activate neuritogenesis in the PC-12 model by mimicking fluctuations in the geomagnetic field, although more rigorous experimental investigations are warranted.

It is interesting to note that the changing the organization of PD and ISI of the burst-firing EMF had no effect on the proportion of PME-bearing cells in the PC-12 model as compared to changing the overall pattern. An analogy to describe what was found can be likened to the information contained within a narrative. In our narrative analogy, we may conceptualize point duration, and alterations in this parameter, as the speed at that the narrative is read whilst the inter-stimulus interval would be analogous to pauses associated with punctuation (commas and periods) of the narrative. The overall information (content) in the narrative does not change if we speed up or slow down the rate at that we read the excerpt nor does the time we take to pause at the appropriate punctuation. In our manipulation, the content (structure) of the signal is maintained but the speed and latency (pauses), between the presentation of the pattern is altered with no change to the message (information) being espoused. Provided this analogy holds, we would expect no differences to be observed. An alternative perspective would be that our investigation only examines physical features of our target system. With this limited tool of investigation, we cannot appreciate subtle changes in the function of the biological substrate that may be elicited by our manipulations. Provided that we examined our system using more functional measures, rather than strictly examining changes in physical structure, differences may arise.

We have emphasized the importance of pattern in the observed effects and provided the analogy of a narrative, describing the function of the EMF pattern, to that the biological system responds. In keeping with this analogy, we will examine the influence of rotation, constant application of the most effective field pattern, and the intensity of this pattern on the proportion of cells bearing PME. When comparing rotated presentations of the burst-firing field (presentation of the pattern in the plane-paired solenoids across 3 spatial axes followed immediately by the simultaneous presentation of all 3-pairs across a rotation frequency of 0.5 Hz) and constant presentation through all 3 pairs of solenoids simultaneously, no differences were determined in morphology. Consider how a recorded narrative that is played through a set of headphones might affect transmission of information. In one instance, the recording is played through both speakers simultaneously while in another situation, the same narrative is constantly alternated between both speakers. Here again, the content of the narrative is not altered and the individual receives all necessary/relevant information. Similarly, the pattern of the EMF is not different (i.e., same content) and in both the rotated and constant conditions the target system receives appropriate stimulation to elicit the observed effects. In these experiments, we observed an intensity-independence between the three levels (low: 300-500 nT; medium: 3-5 uT; high: 10^{+} uT) of application intensity and their capacity to appreciably alter the proportion of PME-bearing cells and those that bear multipolar (higher order arborizations) extensions. There was no difference in morphological measures between the different intensities but differences were observed and described as a marked enhancement in the proportion of cells bearing PME and multipolar extensions when comparing the highest intensity (10^{+} uT) to sham (no field) conditions. If we operationalize intensity as the volume of speech, then it does not matter whether the message is screamed or whispered, the importance lies in the message being articulated. Again, limitations arise as the technology employed does not allow the field strengths to exceed 15 μT. It is possible that higher intensities (~ 100 uT),

that are 10 times greater than the limits of our tool, may render differing results. The investigation described previously would identify 1) threshold effects and 2) power windows that optimally drive this phenomenon.

One aim in this series of investigations was to determine the biomolecular pathway that was most associated with statistical differences of the proportion of cells bearing plasma membrane extensions by way of an inhibitor series. Two measures were utilized in order to determine any potential effects associated with 1) morphological measures (structure) and 2) functional differences as assessed by ultra-weak photon emission (UPE). No data has been successfully collected in order to appropriately assess differences in morphological features as a function of field in combination with specific inhibitors. Results from UPE analyses revealed a burst-firing field effect described as a reduction in the mean variability (standard deviation) of spectral power densities falling within the 0 – 3 Hz range. No effects were determined to be inhibitor specific. Little can be said about discrete differences occurring at the biomolecular level accommodating the observed effects. Despite this lack of mechanistic clarity, data collected comparing 1 and 3-hour exposure durations to the burst-firing EMF revealed statistical differences in the proportion of PME-bearing cells between these two exposure conditions. Three possible mechanisms are suggested: 1) burst-firing EMF promotes the accumulation of secondary signalling molecules (i.e., cAMP) that is maintained over the course of the exposure, 2) burst-firing EMF impacts enzyme kinetics, either speeding up or slowing down the rate-limiting step, leading to the promotion of neurite outgrowth, or 3) downstream enzyme (MEK/ERK) activity is stabilized long-term. Data that refutes the first mechanism was provided by Loney et al., (Unpublished) who demonstrated that the presence of forskolin is essential for field mediated effects and that the burst-firing field alone does not induce plasma membrane extension. Not only does this evidence refute the first mechanism it may also serve

to support the third hypothesis. The scientific literature also suggests that maintained activation of the MEK/ERK pathway is quintessential to the formation of plasma membrane extensions as evidenced in similar studies using nerve growth factor (Loeb et al., 1991; York et al., 1998; Park et al., 2012). One possible manner by that to verify our hypotheses is to investigate greater exposure durations (i.e., more than 24 hours less than 72 hours) and measure PME proportion and length of these corresponding extensions as well as directly assessing cAMP levels using an enzyme-linked assay.

We conclude that the effects of EMF application on PC-12 cells treated with forskolin are contingent upon the pattern of the applied field. Intensity demonstrated no difference between various levels, nor does discretely altering the temporal construction of the pattern. When the inverted configuration of the burst-firing field is presented in combination with forskolin the proportion of cells bearing PME are reduced, burst-firing EMF effects are eliminated. Lastly, although we were unable to directly assess the associated biomolecular pathway related to EMF enhanced neurite outgrowth, we offered alternative means for clarifying the mechanism involved evidenced by differences in proportion of PME-bearing cells exposed for 1 and 3 hour durations.

2.6. References:

Baker-Price, L., & Persinger, M. A. (2003). Intermittent burst-firing weak (1 microTesla) magnetic fields reduce psychometric depression in patients who sustained closed head injuries: A replication and electroencephalographic validation. *Perceptual and Motor Skills*, *96*(3), 965-974.

Bouron, A., Becker, C., & Porzig, H. (1999). Functional expression of voltage-gated Na+ and Ca2+ channels during neuronal differentiation of PC-12 cells with nerve growth factor or forskolin. *Naunyn-Schmiedeberg's archives of pharmacology*, *359*(5), 370-377.

Bos, J. L., De Bruyn, K., Enserink, J., Kuiperij, B., Rangarajan, S., Rehmann, H., ... & Zwartkruis, F. (2003). The role of Rap1 in integrin-mediated cell adhesion.

Buckner, C. A., Buckner, A. L., Koren, S. A., Persinger, M. A., & Lafrenie, R. M. (2015). Inhibition of cancer cell growth by exposure to a specific time-varying electromagnetic field involves T-type calcium channels. *PLoS One*, *10*(4), e0124136.

Buckner, C. A., Buckner, A. L., Koren, S. A., Persinger, M. A., & Lafrenie, R. M. (2017). The effects of electromagnetic fields on B16-BL6 cells are dependent on their spatial and temporal character. *Bioelectromagnetics*, *38*(3), 165-174.

Buckner, C. A., Buckner, A. L., Koren, S. A., Persinger, M. A., & Lafrenie, R. M. (2018). Exposure to a specific time-varying electromagnetic field inhibits cell proliferation via cAMP and ERK signaling in cancer cells. *Bioelectromagnetics*, *39*(3), 217-230.

Caillaud, T., Xu-van Opstal, W. Y., Scarceriaux, V., Billardon, C., & Rostene, W. (1995). Treatment of PC-12 cells by nerve growth factor, dexamethasone, and forskolin. *Molecular neurobiology*, *10*(2-3), 105-114.

Calon, Frédéric, Abdallah Hadj Tahar, Pierre J. Blanchet, Marc Morissette, Richard Grondin, Martin Goulet, Jean-Pierre Doucet et al. "Dopamine-receptor stimulation: biobehavioral and biochemical consequences." *Trends in neurosciences* 23 (2000): S92-S100.

Cook, C. M., & Persinger, M. A. (1997). Experimental induction of the “sensed presence” in normal subjects and an exceptional subject. *Perceptual and Motor Skills*, *85*(2), 683-693.

Deutsch, P. J., & Sun, Y. (1992). The 38-amino acid form of pituitary adenylate cyclase-activating polypeptide stimulates dual signaling cascades in PC-12 cells and promotes neurite outgrowth. *Journal of Biological Chemistry*, *267*(8), 5108-5113.

Dotta, B. T., Buckner, C. A., Lafrenie, R. M., & Persinger, M. A. (2011). Photon emissions from human brain and cell culture exposed to distally rotating magnetic fields shared by separate light-stimulated brains and cells. *Brain research*, *1388*, 77-88.

Dotta, B. T., Lafrenie, R. M., Karbowski, L. M., & Persinger, M. A. (2014). Photon emission from melanoma cells during brief stimulation by patterned magnetic fields: is the source coupled to rotational diffusion within the membrane. *General Physiology and Biophysics*, *33*, 63-73.

Dotta, B. T., Murugan, N. J., Karbowski, L. M., & Koren, S. A. (2015). Rotational frequency matching of the energy of the changing angular velocity magnetic field intensity and the proton magnetic moment produces a ten fold increased excess correlation in pH shifts in spring water. *NeuroQuantology*, *14*(1).

Dotta, B. T., & Persinger, M. A. (2012). "Doubling" of local photon emissions when two simultaneous, spatially-separated, chemiluminescent reactions share the same magnetic field configurations. *Journal of Biophysical Chemistry*, *3*(01), 72.

Dugan, L. L., Kim, J. S., Zhang, Y., Bart, R. D., Sun, Y., Holtzman, D. M., & Gutmann, D. H. (1999). Differential effects of cAMP in neurons and astrocytes role of B-raf. *Journal of Biological Chemistry*, *274*(36), 25842-25848.

Fleming, J. L., Persinger, M. A., & Koren, S. A. (1994). Magnetic pulses elevate nociceptive thresholds: Comparisons with opiate receptor compounds in normal and seizure-induced brain-damaged rats. *Electro-and Magnetobiology*, *13*(1), 67-75.

Foley, John D., Eric W. Grunwald, Paul F. Nealey, and Christopher J. Murphy. "Cooperative modulation of neuritogenesis by PC-12 cells by topography and nerve growth factor." *Biomaterials* 26, no. 17 (2005): 3639-3644.

Fournier, N. M., Mach, Q. H., Whissell, P. D., & Persinger, M. A. (2012). Neurodevelopmental anomalies of the hippocampus in rats exposed to weak intensity complex magnetic fields throughout gestation. *International Journal of Developmental Neuroscience*, *30*(6), 427-433.

Friedman, H., Becker, R. O., & Bachman, C. H. (1965). Psychiatric ward behaviour and geophysical parameters. *Nature*, *205*(4976), 1050-1052.

Garrels, J. I., & Schubert, D. (1979). Modulation of protein synthesis by nerve growth factor. *Journal of Biological Chemistry*, *254*(16), 7978-7985.

Greene, Lloyd A., and Jeffrey C. McGuire. "Induction of ornithine decarboxylase by nerve growth factor dissociated from effects on survival and neurite outgrowth." *Nature* 276, no. 5684 (1978): 191.

Greene, L. A., & Tischler, A. S. (1982). PC-12 pheochromocytoma cultures in neurobiological research. In *Advances in cellular neurobiology* (Vol. 3, pp. 373-414). Elsevier.

Greene, L. A., & Tischler, A. S. (1976). Establishment of a noradrenergic clonal line of rat adrenal pheochromocytoma cells that respond to nerve growth factor. *Proceedings of the National Academy of Sciences*, *73*(7), 2424-2428.

Greengard, P., Allen, P. B., & Nairn, A. C. (1999). Beyond the dopamine receptor: the DARPP-32/protein phosphatase-1 cascade. *Neuron*, *23*(3), 435-447.

Gunning, P. W., Landreth, G. E., Bothwell, M. A., & Shooter, E. M. (1981). Differential and synergistic actions of nerve growth factor and cyclic AMP in PC-12 cells. *The Journal of Cell Biology*, *89*(2), 240-245.

Halegoua, S., & Patrick, J. (1980). Nerve growth factor mediates phosphorylation of specific proteins. *Cell*, *22*(2), 571-581.

Hoshi, T., Garber, S. S., & Aldrich, R. W. (1988). Effect of forskolin on voltage-gated K+ channels is independent of adenylate cyclase activation. *Science*, *240*(4859), 1652-1655.

Hussain, S. M., Javorina, A. K., Schrand, A. M., Duhart, H. M., Ali, S. F., & Schlager, J. J. (2006). The interaction of manganese nanoparticles with PC-12 cells induces dopamine depletion. *Toxicological sciences*, *92*(2), 456-463.

Karbowski, L. M., Harribance, S. L., Buckner, C. A., Mulligan, B. P., Koren, S. A., Lafrenie, R. M., & Persinger, M. A. (2012). Digitized quantitative electroencephalographic patterns applied as magnetic fields inhibit melanoma cell proliferation in culture. *Neuroscience Letters*, *523*(2), 131-134.

Kavaliers, Martin, and Klaus-Peter Ossenkopp. "Stress-induced opioid analgesia and activity in mice: inhibitory influences of exposure to magnetic fields." *Psychopharmacology* 89, no. 4 (1986): 440-443.

Koren, S. A., & Persinger, M. A. (2002). Possible disruption of remote viewing by complex weak magnetic fields around the stimulus site and the possibility of accessing real phase space: A pilot study. *Perceptual and Motor Skills*, *95*(3), 989-998.

Lazarovici, P., Jiang, H., & Fink, D. (1998). The 38-Amino-Acid Form of Pituitary Adenylate Cyclase-Activating Polypeptide Induces Neurite Outgrowth in PC-12 Cells that Is Dependent

on Protein Kinase C and Extracellular Signal-Regulated Kinase but not on Protein Kinase A, Nerve Growth Factor Receptor Tyrosine Kinase, p21ras G protein, and pp60c-srcCytoplasmic Tyrosine Kinase. *Molecular Pharmacology, 54*(3), 547-558.

Loeb, D. M., Maragos, J., Martin-Zanca, D., Chao, M. V., Parada, L. F., & Greene, L. A. (1991). The trk proto-oncogene rescues NGF responsiveness in mutant NGF-nonresponsive PC-12 cell lines. *Cell, 66*(5), 961-966.

Mach, Quoc Hao, and Michael A. Persinger. "Behavioral changes with brief exposures to weak magnetic fields patterned to stimulate long-term potentiation." *Brain research* 1261 (2009): 45-53.

Martin, L. J., S. A. Koren, and M. A. Persinger. "Thermal analgesic effects from weak, complex magnetic fields: critical parameters." *Electromagnetic biology and medicine* 24, no. 2 (2005): 65-85.

Martin, L. J., & Persinger, M. A. (2003). Spatial heterogeneity not homogeneity of the magnetic field during exposures to complex frequency-modulated patterns facilitates analgesia. *Perceptual and motor skills, 96*(3), 1005-1012.

Martin, L. J., & Persinger, M. A. (2004). Thermal analgesia induced by 30-min exposure to 1 μT burst-firing magnetic fields is strongly enhanced in a dose-dependent manner by the α2 agonist clonidine in rats. *Neuroscience letters, 366*(2), 226-229.

Martin, L. J., and M. A. Persinger. "The influence of various pharmacological agents on the analgesia induced by an applied complex magnetic field treatment: a receptor system potpourri." *Electromagnetic Biology and Medicine* 24, no. 2 (2005): 87-97.

Meli, S. C., & Persinger, M. A. (2009). Red light facilitates the sensed presence elicited by application of weak, burst-firing magnetic fields over the temporal lobes. *International Journal of Neuroscience, 119*(1), 68-75.

Murugan, Nirosha J., Lukasz M. Karbowski, Robert M. Lafrenie, and Michael A. Persinger. "Temporally-patterned magnetic fields induce complete fragmentation in planaria." *PloS one* 8, no. 4 (2013): e61714.

Murugan, N. J., L. M. Karbowski, R. M. Lafrenie, and M. A. Persinger. "Maintained exposure to spring water but not double distilled water in darkness and thixotropic conditions to weak (~ 1 μT) temporally patterned magnetic fields shift photon spectroscopic wavelengths: Effects of different shielding materials." *Journal of Biophysical Chemistry* 6, no. 01 (2015): 14.

Murugan, N. J., Karbowski, L. M., & Persinger, M. A. (2014). Serial pH increments (~ 20 to 40 milliseconds) in water during exposures to weak, physiologically patterned magnetic fields: implications for consciousness. *Water, 6*, 45-60.

Murugan, N. J., Karbowski, L. M., & Persinger, M. A. (2014). Weak burst-firing magnetic fields that produce analgesia equivalent to morphine do not initiate activation of proliferation pathways in human breast cells in culture. *Integrative Cancer Science and Therapeutics*, *1*(3), 47-50.

Ossenkopp, K. P., & Kavaliers, M. (1987). Morphine-induced analgesia and exposure to low-intensity 60-Hz magnetic fields: inhibition of nocturnal analgesia in mice is a function of magnetic field intensity. *Brain Research*, *418*(2), 356-360.

Park, K. H., Park, H. J., Shin, K. S., Choi, H. S., Kai, M., & Lee, M. K. (2012). Modulation of PC-12 cell viability by forskolin-induced cyclic AMP levels through ERK and JNK pathways: an implication for L-DOPA-induced cytotoxicity in nigrostriatal dopamine neurons. *Toxicological Sciences*, *128*(1), 247-257.

Park, Tae-Ju, and Kyong-Tai Kim. "Cyclic AMP-independent inhibition of voltage-sensitive calcium channels by forskolin in PC-12 cells." *Journal of neurochemistry* 66, no. 1 (1996): 83-88.

Persinger, M. A. (1999). Wars and increased solar-geomagnetic activity: aggression or change in intraspecies dominance?. *Perceptual and motor skills*, *88*(3_suppl), 1351-1355.

Pothos, E. N., Przedborski, S., Davila, V., Schmitz, Y., & Sulzer, D. (1998). D2-Like dopamine autoreceptor activation reduces quantal size in PC-12 cells. *Journal of Neuroscience*, *18*(15), 5575-5585.

Richter-Landsberg, C., & Jastorff, B. (1986). The role of cAMP in nerve growth factor-promoted neurite outgrowth in PC-12 cells. *The Journal of cell biology*, *102*(3), 821-829.

Ross, M. L., Koren, S. A., & Persinger, M. A. (2008). Physiologically patterned weak magnetic fields applied over left frontal lobe increase acceptance of false statements as true. *Electromagnetic biology and medicine*, *27*(4), 365-371.

Satpute, R. M., Hariharakrishnan, J., & Bhattacharya, R. (2010). Effect of alpha-ketoglutarate and N-acetyl cysteine on cyanide-induced oxidative stress mediated cell death in PC-12 cells. *Toxicology and industrial health*, *26*(5), 297-308.

Schubert, D., M. La Corbiere, C. Whitlock, and W. Stallcup. (1978). Alterations in the surface properties of cells responsive to nerve growth factor.

Schubert, D., & Whitlock, C. (1977). Alteration of cellular adhesion by nerve growth factor. *Proceedings of the National Academy of Sciences*, *74*(9), 4055-4058.

Seamon, K. B., & Daly, J. W. (1981). Forskolin: a unique diterpene activator of cyclic AMP-generating systems. *Journal of cyclic nucleotide research*, *7*(4), 201-224.

Seamon, K. B., & Daly, J. W. (1983). Forskolin, cyclic AMP and cellular physiology. *Trends in Pharmacological Sciences*, *4*, 120-123.

Seamon, K. B., Padgett, W., & Daly, J. W. (1981). Forskolin: unique diterpene activator of adenylate cyclase in membranes and in intact cells. *Proceedings of the National Academy of Sciences*, *78*(6), 3363-3367.

Shafer, T. J., & Atchison, W. D. (1991). Transmitter, ion channel and receptor properties of pheochromocytoma (PC-12) cells: a model for neurotoxicological studies. *Neurotoxicology, 12*(3), 473-492.

Stork, Philip JS, and John M. Schmitt. "Crosstalk between cAMP and MAP kinase signaling in the regulation of cell proliferation." *Trends in cell biology* 12, no. 6 (2002): 258-266.

Tessaro, L. W., & Persinger, M. A. (2013). Optimal durations of single exposures to a frequency-modulated magnetic field immediately after bisection in planarian predict final growth values. *Bioelectromagnetics, 34*(8), 613-617.

Thompson, A. C., Zapata, A., Justice, J. B., Vaughan, R. A., Sharpe, L. G., & Shippenberg, T. S. (2000). κ-Opioid receptor activation modifies dopamine uptake in the nucleus accumbens and opposes the effects of cocaine. *Journal of Neuroscience, 20*(24), 9333-9340.

Tischler, A. S., & Greene, L. A. (1978). Morphologic and cytochemical properties of a clonal line of rat adrenal pheochromocytoma cells that respond to nerve growth factor. *Laboratory investigation; a journal of technical methods and pathology, 39*(2), 77-89.

Tischler, A. S., Greene, L. A., Kwan, P. W., & Slayton, V. W. (1983). Ultrastructural effects of nerve growth factor on PC 12 pheochromocytoma cells in spinner culture. *Cell and tissue research, 228*(3), 641-648.

Tischler, A. S., Ruzicka, L. A., & Perlman, R. L. (1990). Mimicry and inhibition of nerve growth factor effects: interactions of staurosporine, forskolin, and K252a in PC-12 cells and normal rat chromaffin cells in vitro. *Journal of neurochemistry*, *55*(4), 1159-1165.

Tsang, E. W., Koren, S. A., & Persinger, M. A. (2009). Specific patterns of weak (1 microTesla) transcerebral complex magnetic fields differentially affect depression, fatigue, and confusion in normal volunteers. *Electromagnetic biology and medicine*, *28*(4), 365-373.

Vaudry, D., Stork, P. J. S., Lazarovici, P., & Eiden, L. E. (2002). Signaling pathways for PC-12 cell differentiation: making the right connections. *Science*, *296*(5573), 1648-1649.

Vossler, M. R., Yao, H., York, R. D., Pan, M. G., Rim, C. S., & Stork, P. J. (1997). cAMP activates MAP kinase and Elk-1 through a B-Raf-and Rap1-dependent pathway. *Cell*, *89*(1), 73-82.

York, R. D., Yao, H., Dillon, T., Ellig, C. L., Eckert, S. P., McCleskey, E. W., & Stork, P. J. (1998). Rap1 mediates sustained MAP kinase activation induced by nerve growth factor. *Nature*, *392*(6676), 622.

Wang, Z., Dillon, T. J., Pokala, V., Mishra, S., Labudda, K., Hunter, B., & Stork, P. J. (2006). Rap1-mediated activation of extracellular signal-regulated kinases by cyclic AMP is dependent on the mode of Rap1 activation. *Molecular and cellular biology*, *26*(6), 2130-2145.

Westerink, R. H. S., & Ewing, A. G. (2008). The PC-12 cell as model for neurosecretion. *Acta Physiologica*, *192*(2), 273-285.

Whissell, P. D., & Persinger, M. A. (2007). Emerging synergisms between drugs and physiologically-patterned weak magnetic fields: implications for neuropharmacology and the human population in the twenty-first century. *Current neuropharmacology*, *5*(4), 278-288.

Wooten, Marie W., M. Lamar Seibenhener, Guisheng Zhou, Michel L. Vandenplas, and T. H. Tan. "Overexpression of atypical PKC in PC-12 cells enhances NGF-responsiveness and survival through an NF-κB dependent pathway." *Cell death and differentiation* 6, no. 8 (1999): 753.

Zhang, Kai, Liting Duan, Qunxiang Ong, Ziliang Lin, Pooja Mahendra Varman, Kijung Sung, and Bianxiao Cui. "Light-mediated kinetic control reveals the temporal effect of the Raf/MEK/ERK pathway in PC-12 cell neurite outgrowth." *PloS one* 9, no. 3 (2014): e92917.

Chapter 3

3 The Influence of Physical Application Geometry on PC-12 Cell Morphology and B16-BL6 Ultra-Weak Photon Emission Spectra

3.1 Abstract:

There has been little attention paid to the contribution that physical application geometry (the structure through which current is passed) plays in the bio-effectivity of exposure to patterned electromagnetic fields. In this study, we compared EMF generated from 4 unique geometric structures on 2 biological model systems: 1) morphological changes in PC-12 cells treated with forskolin and exposed to burst-firing EMF for 1 hour and 2) the production of ultra-weak photons (UPE) by B16-BL6 cells treated with a frequency modulated (i.e., Thomas) EMF. The unique geometric exposure devices were constructed by wrapping copper wire around structured frames representing Helmholtz, Hoberman, Rodin, and Toroid geometries. Results showed that the physical structure of EMF-generating devices influenced the proportion of neuron-like outgrowths in PC-12 cells exposed to sham and burst-firing EMF. Furthermore, exposure of B16-BL6 cells to the Thomas-EMF presented using distinct EMF-generating devices was able to influence the raw and spectral UPE profiles. These findings herein support the adage that, as in biology, structure dictates function, even when it is applied to the equipment used in EMF research.

3.2. Introduction:

Research has demonstrated the ability of exposure to weak, physiologically patterned and time-varying electromagnetic fields (EMFs) to affect biological systems. Buckner et al., (2015) showed that exposures to a frequency modulated (FM) field, also known as the Thomas-EMF, reduced cancer cell growth *in vitro* and *in vivo*. Exposure to this FM-EMF was able to enhance calcium influx through T-type calcium channels as the mechanism of action (Buckner et al., 2015, 2017, 2018). In addition, Dotta et al., (2016b) had previously identified that spectral power characteristics of ultra-weak photons emitted from B16-BL6 cells that could 1) differentiate between cancerous and non-cancerous tissues, 2) could identify differences between cells receiving exposures to EMFs compared to sham treatments, and 3) identified the potential utility of using ultra-weak photon emission as a tool to measure biomolecular

pathways using exclusion filters that were congruent with Cosic's resonant recognition mode (Dotta et al., 2011, 2014, 2016a, 2016b).

Experimental evidence has shown that different patterns (temporal organizations of current injections delivered to the EMF-generating device) are capable of eliciting different outcomes in biological systems. For instance, an asymmetric FM-EMF (i.e., Thomas) is capable of reducing proliferation of B16-BL6 cells while the presentation of an EMF modeled after the burst-firing of a collection of amygdaloid neurons, does not. However, exposures to the burst-firing EMF has been shown to reduce nociceptive responses in rats challenged with thermal nociceptive stimuli as effectively as 4 mg/kg equivalent morphine (Fleming et al., 1994). The Thomas-EMF was also effective at reducing nociceptive responses in rats but it was less effective than the burst-firing EMF (Martin et al., 2004). Exposure to burst-firing EMF was found to be correlated with increased positive self-reported mood states from individuals presenting with symptoms of mild-to-moderate depression (Baker-Price and Persinger 1996; Baker-Price and Persinger, 2003). Murugan et al., (2014) showed that exposures of breast cancer cells to burst-firing EMF could be a useful alternative pain-management program for individuals receiving treatment for cancer. Traditional pain intervention strategies (i.e., morphine) may increase the potential of developing metastases especially in the later stages of cancer progression (Simon and Arbo, 1986). Here, Murugan and colleagues co-cultured cancerous and healthy cells and treated samples with either morphine or burst-firing EMF and showed that morphine, and not exposures to burst-firing EMF, activated biomolecular pathways associated with proliferation. Loney et al., (unpublished) demonstrated that exposures to burst-firing EMF enhanced the proportion of neurite bearing PC-12 cells subsequent to sub-micromolar levels of a cyclic-adenosine monophosphate (cAMP) activator; forskolin. The previous chapter in this thesis described experiments that were able to

demonstrate pattern specificity, intensity, exposure duration, and timing (pattern frequency) were important components needed to optimize the proportion of neurite bearing cells in a PC-12 model of neurogenesis using a different piece of equipment; the 4-D application system.

Evidence supports the assertion that pattern is quintessential for EMF exposures to appreciably influence the function of biological systems. In normal systems, such as the processes associated with memory, pattern is also important. For instance, long-term potentiation (LTP), a feature of learning and memory consolidation, can be operationalized as the persistent and stable enhancement of synaptic strengths (or connectivity) following stimulation (Frey and Morris, 1997; Malenka and Nicoll, 1999) and has been associated with electromagnetic processes (Komaki et al., 2014; Haas and Rose, 1982; Rose et al., 1988)**.** Mach and Persinger (2009), postulated that rats exposed to a digitized version of an LTP pattern at crucial time points in memory acquisition and retrieval would show differences on memory-based tasks. The results of their experiments indicated an enhancement of memory performance for LTP-patterned EMF treated animals that were exposed after training but a reduction in performance if they were exposed to the LTP patterned EMF prior to training. Unlike Thomas-EMF treatments, LTP-EMF was not capable of reducing proliferation in cancer cells. However, Dotta et al., (2014) demonstrated that isolated samples microtubules exposed to LTP-patterned EMF were capable of re-emitting this same pattern (as assessed by the spectral characteristics of ultra-weak photon emission) as compared to other patterned EMF treatments. The ability of microtubules to emit photons was specific for the LTP pattern while the most conspicuous effects approached the theoretical constructs detailed by Hameroff and Penrose in their orchestrated objective reduction theory of consciousness (Hameroff and Penrose, 2014).

Evidence supports the underlining importance that the pattern of the applied EMF plays in relation to its capacity to affect biological systems. Despite the breadth of knowledge detailing the importance of EMF pattern, little attention has been given to the contribution made by the physical structure through that the resultant EMF is generated. The importance of assessing the relevance of physical application geometry (i.e., different configurations around that copper wire is wound and the through that current is passed) can be supported by discussing the structural difference between static magnets and EMFs generated from current loops.

The intensity (amount) of electromagnetic force exerted upon an object to do work of a static magnetic results from the combined organizations (alignment) of magnetic dipoles contained within the ferromagnetic material (Burke, 2012). Under the appropriate conditions, these dipoles can either be made to align, by way of an external "magnetizing" field, or be unaligned (demagnetized) by heating the material to the point where it begins to luminesce; its Currie temperature (Burke, 2012). Generally, we describe the amount of electromagnetic force available to do work by field lines. Field lines are magnetic force vectors (flux lines) that extend from the magnetic North pole and enter the magnetic South pole and are present in both bar and horseshoe magnets. The distance traveled along a bar magnet is greater than the distance between adjacent poles of a horseshoe magnet that in turn may affect the quality (constraints) of the field lines. A change in the constrictions of magnetic field lines of force (either by convergence or divergence) will impact the intensity of the static magnet. When an EMF is generated by passing a current through a conducting wire, the resultant magnetic field is perpendicular and circumferential to the direction in that the current is traveling and follows the Biot-Savart law. Changing the shape of the wire by wrapping it along an axis (i.e., a coil) results in a solenoid that has a much different field configuration and parameters (i.e., intensity) as compared to a solitary length of wire. Adding to this, if one were to wrap a length of

conducting wire in a direction perpendicular to the circumference of a non-conducting loop, the resulting field configuration would take a doughnut shaped or toroidal field structure. Furthermore, Helmholtz demonstrated that two electrically coupled (connected) circular coils of wire with an equal number of wrappings that are physically separated by a distance equivalent to the radius of the paired coils, generates a constant EMF contained within the cylindrical volume, when current is passed through it and describes a structure named a Helmholtz coil.

The physical structure of an EMF-generating device can change or impact the characteristics of the resulting EMF. Despite these differences, little research has been conducted examining the role that physical geometry plays in the biological efficacy of exposures to weak, physiologically patterned EMFs. Here we propose two investigations using well defined biological systems (i.e., cancer cells) that predictably respond to the application of unique patterned EMFs. The first investigation aims to identify differences obtained in the morphology and proportion of neurite-bearing PC-12 cells after exposure to the combination of burst-firing EMF and sub-micromolar concentrations of a cAMP activator; forskolin. In addition to qualitative morphological differences, we will assess the ultra-weak photon emission spectra (i.e., measures of discrete individual differences) from PC-12 cells exposed to burst-firing EMF presented through 4 unique application geometries 3 days after treatment. The target day was selected as data from the previous chapter suggested that 72 hours is required in order to observe differences in neurite outgrowth in this cell line. In our second investigation, discrete differences in ultra-weak photon emission spectral profiles were examined for B16-BL6 cells exposed to Thomas-EMF (as this patterned has been shown to significantly decrease their proliferation) generated through the same 4 unique physical application geometries. These investigations will allow us to identify any potential differences that can be elicited as a

function of geometric structure of an EMF-generating device in global and discrete measures relevant to biological systems.

3.3. Methods

3.3.1. Cell culture and induction of plasma membrane extensions in PC-12 cells

Pheochromocytoma (PC-12) cells, derived from the rat adrenal medulla, were grown to confluence on 100-mm stock plates supplemented with standard growth media (85% RMPI-1640, 10% horse serum, 5% fetal bovine serum, 1% antibiotic and antimycotic; v/v equivalents). 50 µL of cell suspensions were inoculated on poly-L-lysine-treated, 35-mm cell culture dishes and incubated for 24 hours in a standard incubator at standard conditions (37ºC, 95% O_2, 5% CO_2) allowing the cells to adhere. On the day of the experiment, growth media was removed and the cells were supplemented with 2 mL of serum-free media (RMPI-1640 with 0.5% antibiotic and antimycotic). Cultures were then placed in an exposure incubator, operating at standard conditions, that contained the EMF exposure devices.

3.3.2. EMF exposure conditions for PC-12s

For this investigation, PC-12 cells were exposed to either Sham or burst-firing EMF generated through 1 of 4 physical application geometries (Helmholtz, Hoberman, Rodin, or Toroid; Appendix E1-E4) for the duration of 1 hour. The burst-firing EMF was generated from a digital file programmed for 230 points ranging from 0 to 256, that were converted to voltage equivalents of -5V to +5V (127 = 0V) by way of a custom constructed, adjustable digital-to-analog converter and modified mini-audio amplifier that supplied current to each of the

respective physical application geometries. PD and ISI were set to 3 and 3000 msec respectively. Field intensity was verified using an AC milliGauss meter (AlphaLabs) and field pattern was verified using a mini-audio amplifier coupled to a telephone pick-up coil. The intensity of the pattern fell between 300 and 500 nT. The cells were treated with 1 µL of forskolin (final concentration: 0.5 µM) or DMSO (vehicle) at ten minutes into their respective exposure conditions. The control conditions consisted of plates of cells that received only forskolin or DMSO. For each condition, there were 2 plates that were conducted in parallel and all replicates (N =3) were conducted on separate days. An example of the experimental exposure set-up is provided in Appendix E5

3.3.3. Cell morphological measures

In order to assess the efficacy of our various treatments, photos (N=4 per plate) were taken 3 days after exposure using a phase-contrast light compound microscope at 100x magnification. The total number of cells were counted for each quadrant and summated for each plate. In addition, cells bearing plasma membrane extensions (i.e., any observable distortion or protrusion whose origin can be traced to the cell body; PME) were counted and reported as a proportion of the total number of cells. Other pertinent morphological features were measured including: the proportion of cells with multipolar and higher order arborizations, the number of inter-cellular connections (i.e., synapses), and proportion of cells whose plasma membrane extensions exceeded the largest diameter of their cell soma. Morphological measures were taken immediately following the recordings of biophoton emission.

3.3.4. Ultra-Weak Photon emission measurements for PC-12 cells

The plates of PC-12 cells that had been treated with forskolin or vehicle (DMSO) and that received either sham or burst-firing EMF exposures through one of the four target EM physical application geometries were removed from the growth incubator and transported to the recording room. The recording room, that housed the photon measurement device is located approximately 3 m away from the cell culture laboratory. A single plate was placed onto the aperture of a Model DMC-0089 digital photomultiplier tube (PMT) (SENS-TECH Sensory Technologies; SN:68569). The entire experimental detection system and culture plate was housed in a darkened wooden box, that was covered by 10 layers (8 cm) of thick cotton cloth to ensure no environmental light pollution would affect the sensitivity of the PMT recordings. The typical dark counts or background ambient recordings obtained for this PMT were in the range of 0 – 2 photon units per 20 msec (50 – 100 photons per sec). Measurements were acquired using Sens-Tech Counter Timer software (Version 2.8, build: 11) at a sampling rate of 50 Hz and were recorded and stored on a personal laptop computer. Each recording session was divided into three recording phases: 1) a 2-min pre-baseline period (6000 points), 2) a 5-min active cell recording period (i.e., when dish was placed over the aperture of the recording device; 15000 points), and 3) a 2-min post baseline recording period (6000 points). Each recording phase was separated by a 2-min light adjustment period to reduce the impact of environmental light pollution during data collection. PMT measures were obtained prior to the morphological measures and were taken 3 days following chemical treatment and EMF exposure. For each recording session there were 2 plates per condition, and all conditions were independently replicated in triplicate (N=3).

3.3.5. Cell culture of B16-BL6 mouse melanoma cells

Mouse melanoma (B16-BL6) cells were obtained from Dr. Carly Buckner and Dr. Robert Lafrenie from the Health Sciences North Cancer Research Institute in Sudbury, Ontario. The cells and were cultured on 100-mm plates and maintained in DMEM media supplemented with 10% fetal bovine serum, 100 U/ml penicillin G, 100 μg/ml streptomycin sulfate and 250 ng/ml amphotericin B and maintained in a water jacketed incubator with standard settings (37°C, 95% oxygen, 5% CO_2). Stock cultures were split every 3-5 days at a ratio of approximately 1:5. For the experiments, sub-cultures derived from stock plates were added to plates at a final cell concentration of 10^6 cells/per 35-mm plate and incubated 4 – 6 hours to allow adherence in standard conditions prior to experimentation.

3.3.6. EMF exposure conditions for B16-BL6 cells

A single 35-mm plate containing ~10^6 B16-BL6 cells was removed from the cell culture laboratory and transported to the exposure and the measurement room approximately 3 m away. Samples were placed inside of 1 of the 5 EMF physical application geometries [cells only (controls), Helmholtz, Hoberman, Rodin, or Toroid] and on top of the aperture of a Model DMC-0089 digital photomultiplier tube (PMT) (SENS-TECH Sensory Technologies; SN:68569). The apparatus was kept in a darkened box covered with 10 layers (8 cm) of black cotton cloth. The B16-BL6 cells were exposed to the Thomas-EMF with both the PD and ISI set to 3.25 msec and at an intensity range of 300-500 nT. We chose this patterned EMF as it had been previously demonstrated to significantly increase calcium uptake in the B16-BL6 cell line as early as 15-min into exposure, as well as reducing growth in B16-BL6 cells following repeated exposure (Buckner et al., 2015, 2018). The Thomas-EMF was generated by

converting a digital file of 859 integer values between 0 and 256 to a corresponding voltage of -5 V to +5V (127 = 0V), producing 18 doublet peaks with gradually increasing intervals between 3 msec (for the first 5 repeats) to 120 msec for the last 5 repeats. The resulting frequency modulation for the Thomas-EMF pattern ranged from 25 Hz for the first 5 to 6 Hz for the last 5 repeats. The Thomas-EMF pattern was presented for a duration of 30-min through a custom constructed, adjustable digital-to-analog converter and modified mini-audio amplifier that supplied current to each of the respective physical application geometries. The intensity, as verified by an AC milliGauss meter (AlphaLabs), was between 300 – 500 nT.

3.3.7. Ultra-Weak Photon Emission Measurements for B16-BL6 cells

A single 35 mm plate containing ~10^6 B16-BL6 cells was removed from the cell culture laboratory and transported to the exposure and the measurement room approximately 3 m away. Samples were placed inside of 1 of the 5 EMF physical application geometries (cells only, Helmholtz, Hoberman, Rodin, or Toroid) and on top of the aperture of a Model DMC-0089 digital photomultiplier tube (PMT) (SENS-TECH Sensory Technologies; SN:68569) in a darkened box covered with 10 layers (8 cm) of black cotton cloth. The experimental set-up was constructed to allow detection of changes in ultra-weak photon emission from cells whilst they were simultaneously exposed to a weak, time-varying EMF. Measurements of ultra-weak photon emission were acquired using Sens-Tech Counter Timer software (Version 2.8, build: 11) at a sampling rate of 50 Hz and data were recorded and stored on a personal laptop computer. The recording phases consisted of 3, 1-min long measurements at a sampling rate of 50 Hz. There were 5 measurements periods that were recorded for each experiment: background baseline period, pre-exposure cell baseline period (i.e., pre-exposure sham), 3 periods during the exposure [beginning (minutes 1 – 3), middle (minutes 15 – 18), and end

(minutes 27-30)], and post-exposure cell baselines period (post-exposure shams). For this experiment, pre-exposure and post-exposure cell baseline measures also served as the Sham exposure controls for statistical comparisons. Prior to the commencement of the pre-exposure cell baselines, a 5-min adjustment period was allowed to accommodate recondite variance associated with ambient light pollution.

3.3.8. Methods of analyses

3.3.8.1. Cell Morphology:

The raw data obtained for morphological measures were converted into the proportion of the total cells counted (variable of interest/total cell count·100%) and were used in subsequent analyses. In addition, three separated variables were computed corresponding to the ratio of multipolar bearing cells, synaptic connections, and the long extensions relative to the number of cells bearing plasma membrane extensions. Ratio values allow for the appropriate assessment of a greater degree of complexity as a function of exposure condition. Unless otherwise specified, all proportions were subjected to a *one-way* analysis of variance. Subsequent Tukey's *post-hoc* tests, where applicable, were employed to demonstrate that source(s) of variance were driving the effect.

3.3.8.2. Ultra-Weak Photon Emission – PC-12 Cell Experiment:

Raw photon emission data taken 3 days after exposures to sham or burst-firing EMF in combination with 0.5 μM forskolin were imported in MatLab processing software to allow the computation of the mean and standard deviation (SD) of photon counts for each of the

recording phases (i.e., baseline, cell, post-baseline). Furthermore, raw time-series data was standardized (i.e., z-transformed) and truncated between +/-5 SD to accommodate outliers for each 1 min recording. Standardized cell photon emission was then subjected to spectral analysis yielding spectral power densities whose frequency range spanned 0 – 25 Hz in 0.01 Hz bin increments. Spectral data as well as the mean number of photons and SD of photon count for each recording phase were then exported to SPSS for statistical analysis. Here, spectral data was then grouped in 1 Hz increments (i.e., 1 Hz bin = 1.01 to 1.99) for time-series analysis. Spectral data, examining the frequency range of 0 – 24 Hz in 1 Hz increments, were subjected to a Multi-variate analysis of variance (MANOVA) with field (sham v. burst-firing EMF) and geometry (Helmholtz, Hoberman, Rodin, Toroid) as between-subject's factors and frequency (25 levels) as a within-subject's measures. A one-way analysis of variance was conducted to ascertain differences between mean photon counts and the standard deviation of photon counts as a function of geometry.

3.3.8.3. Ultra-Weak Photon Emission – B16-BL6 Experiment:

Raw photon count data was imported into MatLab processing software to allow the computation of means and SDs for each of the 3, 1-min recordings corresponding to the background baseline, pre-exposure cell baseline, 3 periods during the exposure [beginning (minutes 1 – 3), middle (minutes 15 – 18), and end (minutes 27-30)], and post-exposure cell baselines measurement periods. Raw time-series data for the aforementioned recording phases were standardized, truncated between +/- 5 SDs, and spectrally analyzed. The corresponding spectral power densities had a frequency range that spanned 0 – 25 Hz in 0.01 Hz bin increments. All computed data was entered into SPSS for statistical analysis. Data for the 0.01 Hz bins were aggregated into 25, 1 Hz bins (i.e., 1 Hz = 1.01 – 1.99 Hz) to reduce the number

of potentially spurious effects. To investigate overall changes in mean photon counts and standard deviation of these measures, serial one-way ANOVAs were conducted with appropriate alpha-wise correction.

Spectral power densities for each of the 25, 1 Hz (0-24 Hz) bins were subjected to serial MANOVAs controlling for pre-exposure sham, EMF treatment, and post-exposure sham measurement periods with geometry (4 levels) as between-subjects' measures and frequency (25 levels) as within-subjects' measures. Relevant post-hoc analyses were conducted in order to ascertain the driving factors between statistically relevant findings and are discussed within their respective sub-sections.

3.4. Results

3.4.1. PC-12 Cell morphology

PC-12 cell treated with forskolin and EMF presented using different geometries showed differences in the proportion of cells with multipolar extensions depending on the particular geometry. The results of a *one-way* ANOVA examining the proportion of cells bearing plasma membrane extensions (PME), multipolar cells, inter-cellular contacts, and long extensions by condition (9-levels: controls receiving only chemical stimulation, 2 field conditions across 4 application geometries), revealed significant differences for multipolar cells [$F_{(8,54)}$= 3.04, p =.008, Ω^2-est = 0.36], inter-cellular contacts [$F_{(8,54)}$= 2.21, p =.044, Ω^2-est = 0.28], and long extensions [$F_{(8,54)}$= 2.96, p =.009, Ω^2-est= 0.34] as a function of EMF exposure condition. Furthermore, significant differences were obtained in the ratios of multipolar to PME-bearing cells [$F_{(8,54)}$ = 12.98, p =$1.46 \cdot 10^{-9}$, Ω^2-est = 0.69], synapses to PME-bearing cells [$F_{(8,54)}$ =

4.90, $p = 2.06 \cdot 10^{-4}$, Ω^2-est = 0.46], and long extensions to PME-bearing cells [$F_{(8,54)} = 4.88$, $p = 2.12 \cdot 10^{-4}$, Ω^2-est = 0.46]. Graphs showing the differences obtained for multipolar cells and the ratio of multipolar cells to PME-bearing cells as a function of condition can be observed in figures 3.4.1.1 and 3.4.1.2 respectively.

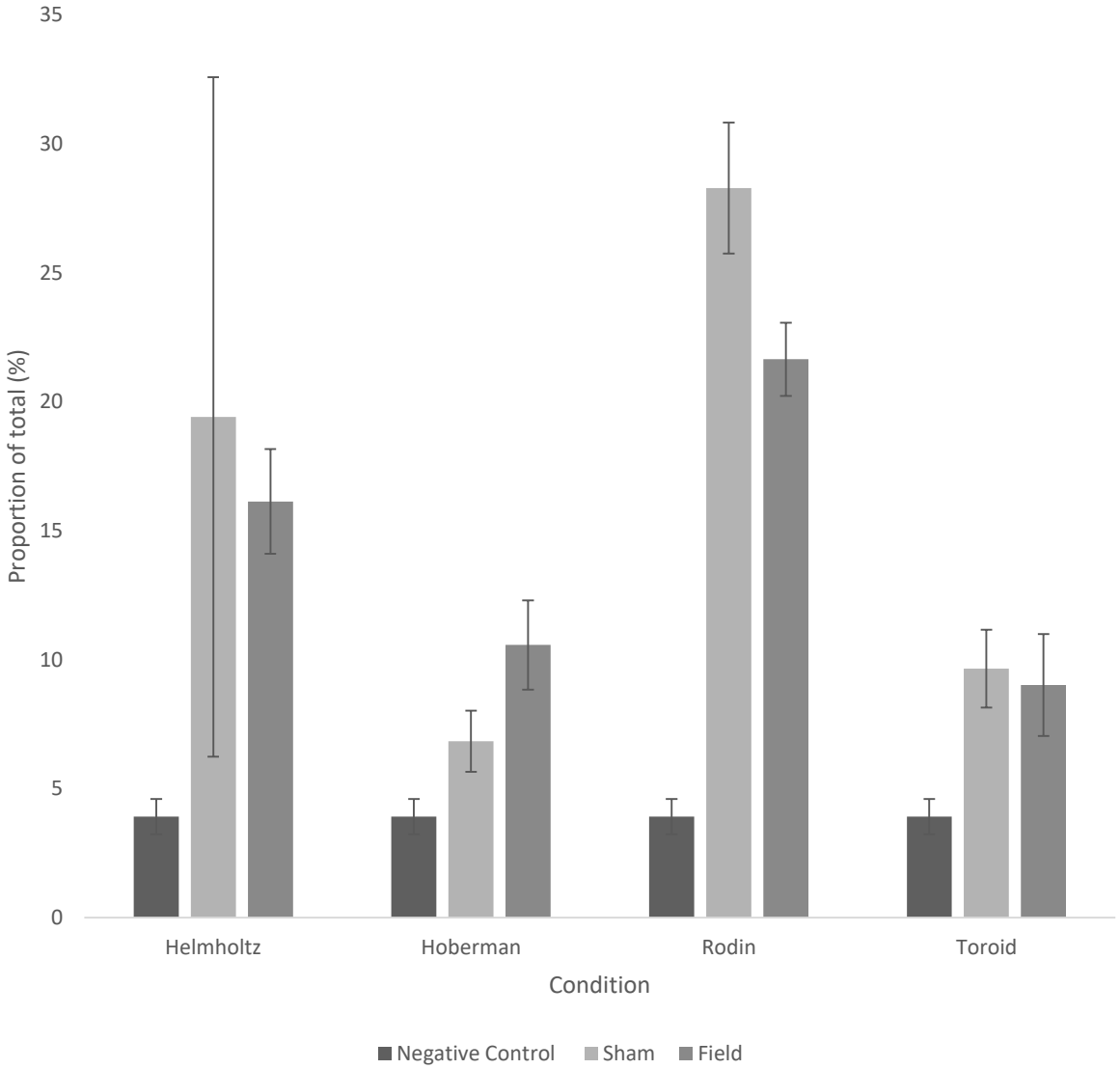

Figure 3.4.1.1: Data examining the proportion of cells bearing multipolar plasma membrane extensions as a function of exposure condition and geometry. Field exposure consisted of 1 hour of burst-firing with PD = 3 msec and ISI = 3000 msec, at an intensity range of 300-500 nT. Error bars represent SEMs.

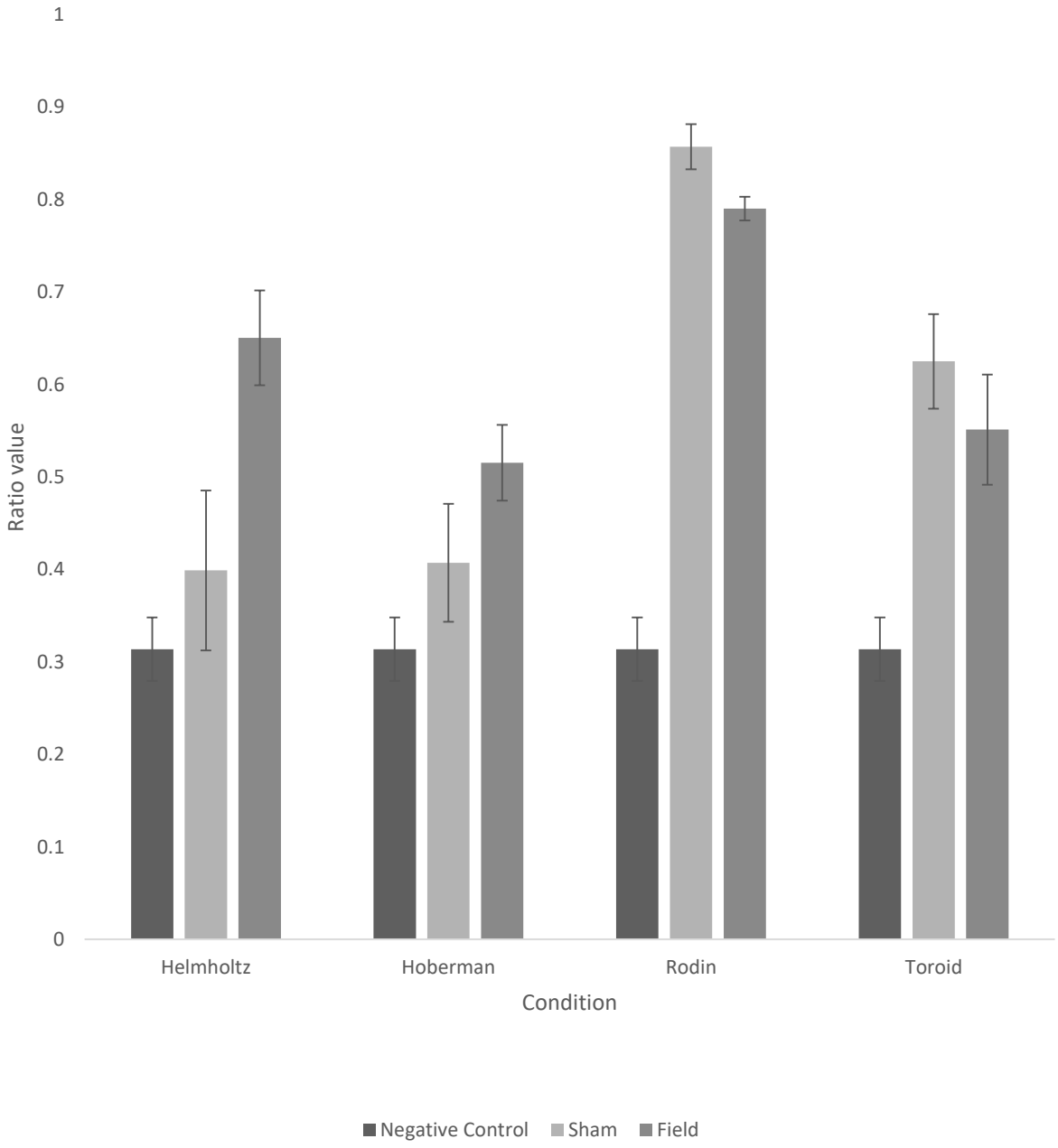

Figure 3.4.1.2: Differences obtained in the ratio (Y-axis) of the number of multipolar cells relative to PME-bearing cells as a function of geometry (X-axis) and exposure condition. Field exposure consisted of 1 hour of burst-firing with PD = 3 msec and ISI = 3000 msec, at an intensity range of 300-500 nT. Error bar represent SEMs.

Differences in morphological features of the PC-12 cells treated with forskolin and exposed to burst-firing EMF presented through different geometries were shown for the proportion of cells with PME, multipolar extensions, inter-cellular contacts, and long extensions were tested using *one-way* analyses of variance. Only differences where $p<.0125$ were considered significant after alpha-level correction. There were no differences observed in any of the morphological measures for the Helmholtz and Toroid geometries as a function of condition. However, there were differences in the proportion of PME-bearing cells [$F_{(2,18)} = 6.93$, $p = .007$, Ω^2-est = 0.46], and multipolar cells [$F_{(2,18)} = 7.58$, $p = .005$, Ω^2-est = 0.49], as a function of condition for the Hoberman geometry. Meanwhile, measures for PME [$F_{(2,18)} = 29.02$, $p = 5.0 \cdot 10^{-6}$, Ω^2-est = 0.78], multipolar cells, [$F_{(2,18)} = 61.24$, $p = 3.17 \cdot 10^{-8}$ Ω^2-est = 0.88], synapses [$F_{(2,18)} = 46.37$, $p = 2.19 \cdot 10^{-7}$, Ω^2-est = 0.85], and long extensions [$F_{(2,18)} = 6.44$, $p = .009$, Ω^2-est = 0.45], demonstrated differences as a function of exposure condition within the Rodin geometry. Data corresponding to the proportion of PME-bearing cells and proportion of multipolar cells for each geometry across the different exposure conditions can be found in figures 3.4.1.3 – 3.4.1.6.

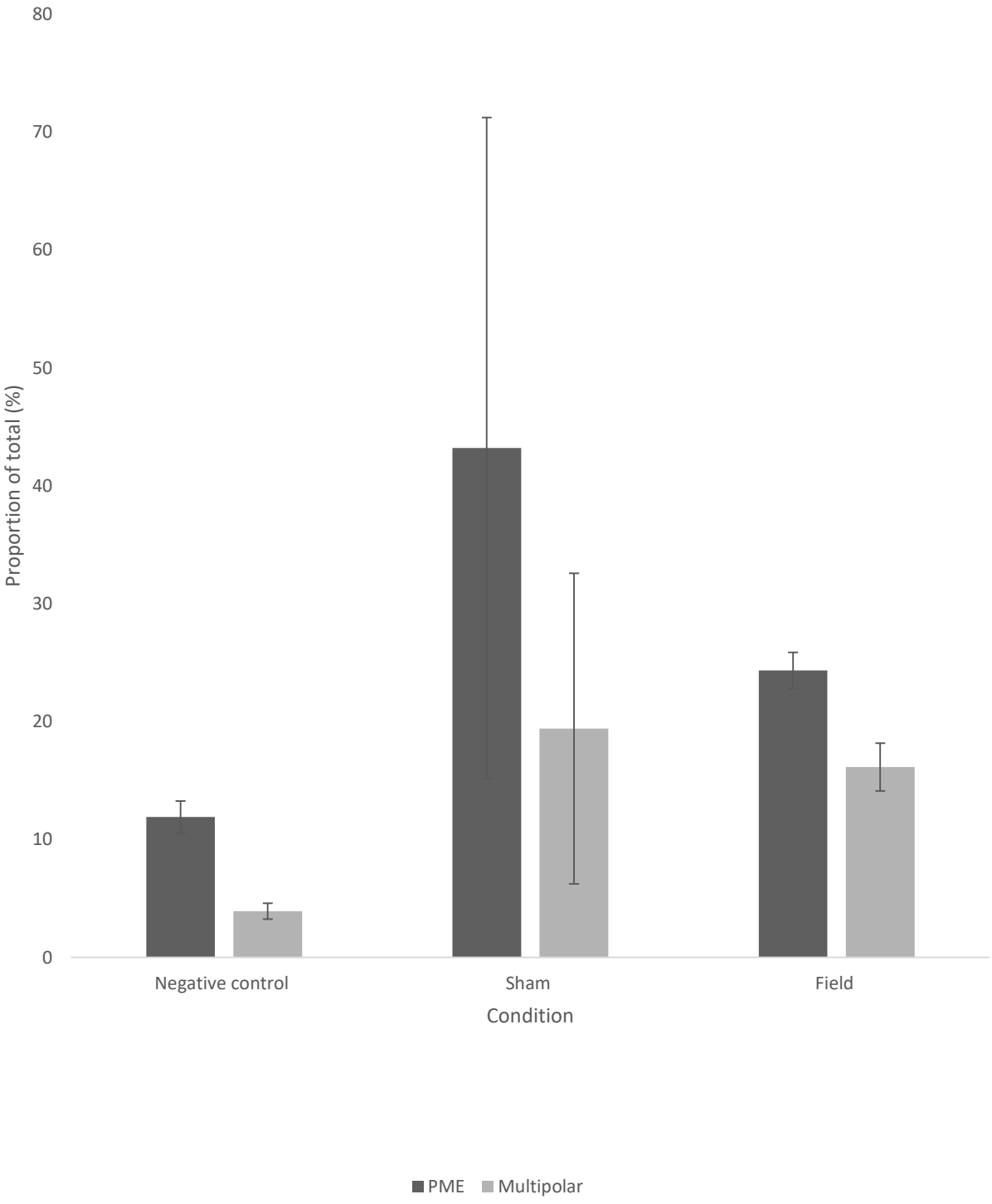

Figure 3.4.1.3: Differences in the proportion of cells bearing PME and multipolar extensions for the Helmholtz geometry. Field exposure consisted of 1 hour of burst-firing with PD = 3 msec and ISI = 3000 msec, at an intensity range of 300-500 nT. Error bar represent SEMs. No significant differences were obtained at the $p<.0125$ level.

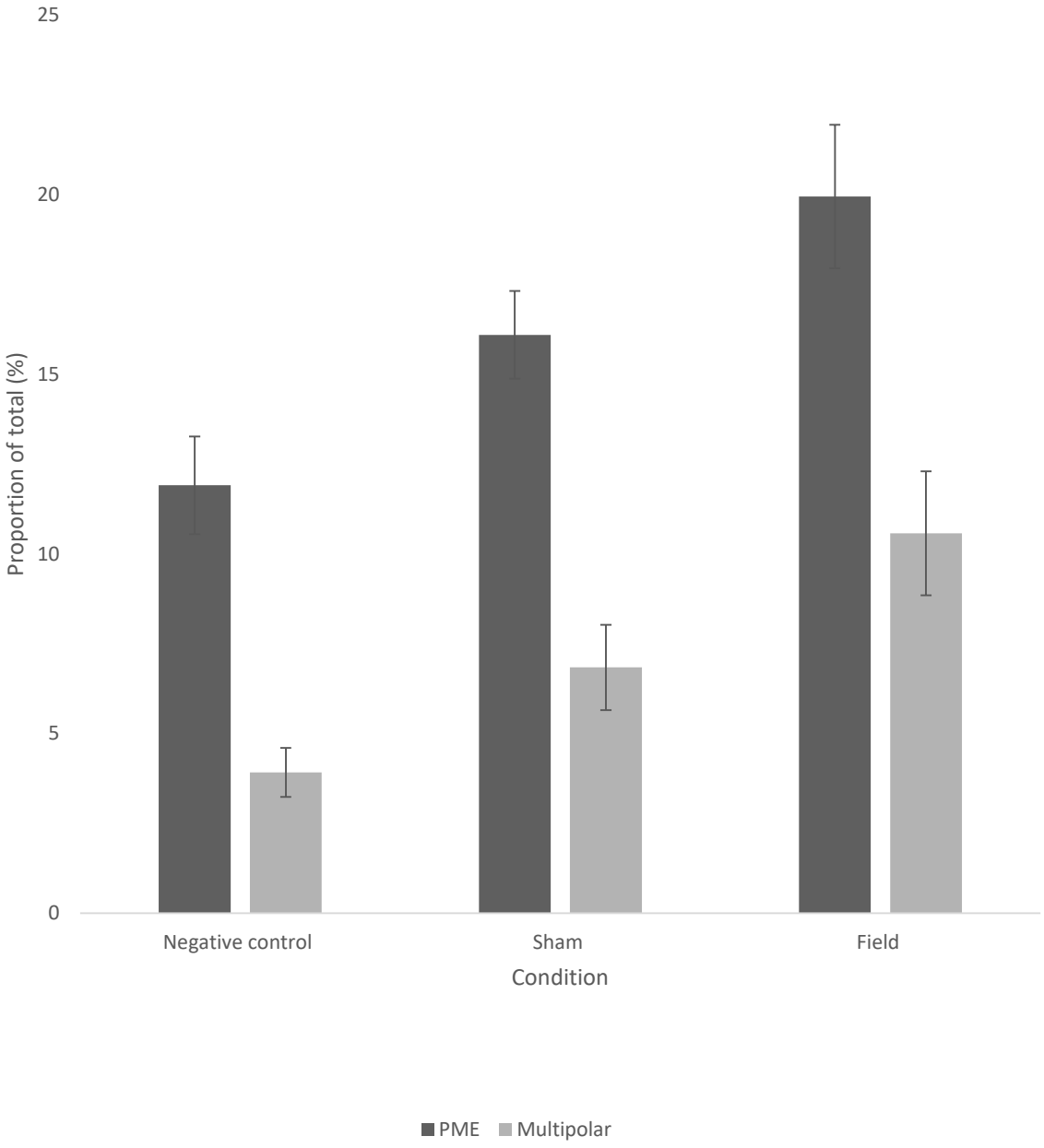

Figure 3.4.1.4: Differences in the proportion of cells bearing PME and multipolar extensions for the Hoberman geometry. Field exposure consisted of 1 hour of burst-firing with PD = 3 msec and ISI = 3000 msec, at an intensity range of 300-500 nT. Error bar represent SEMs. Differences between field and negative control, but not between sham exposures, were driving the observed effects.

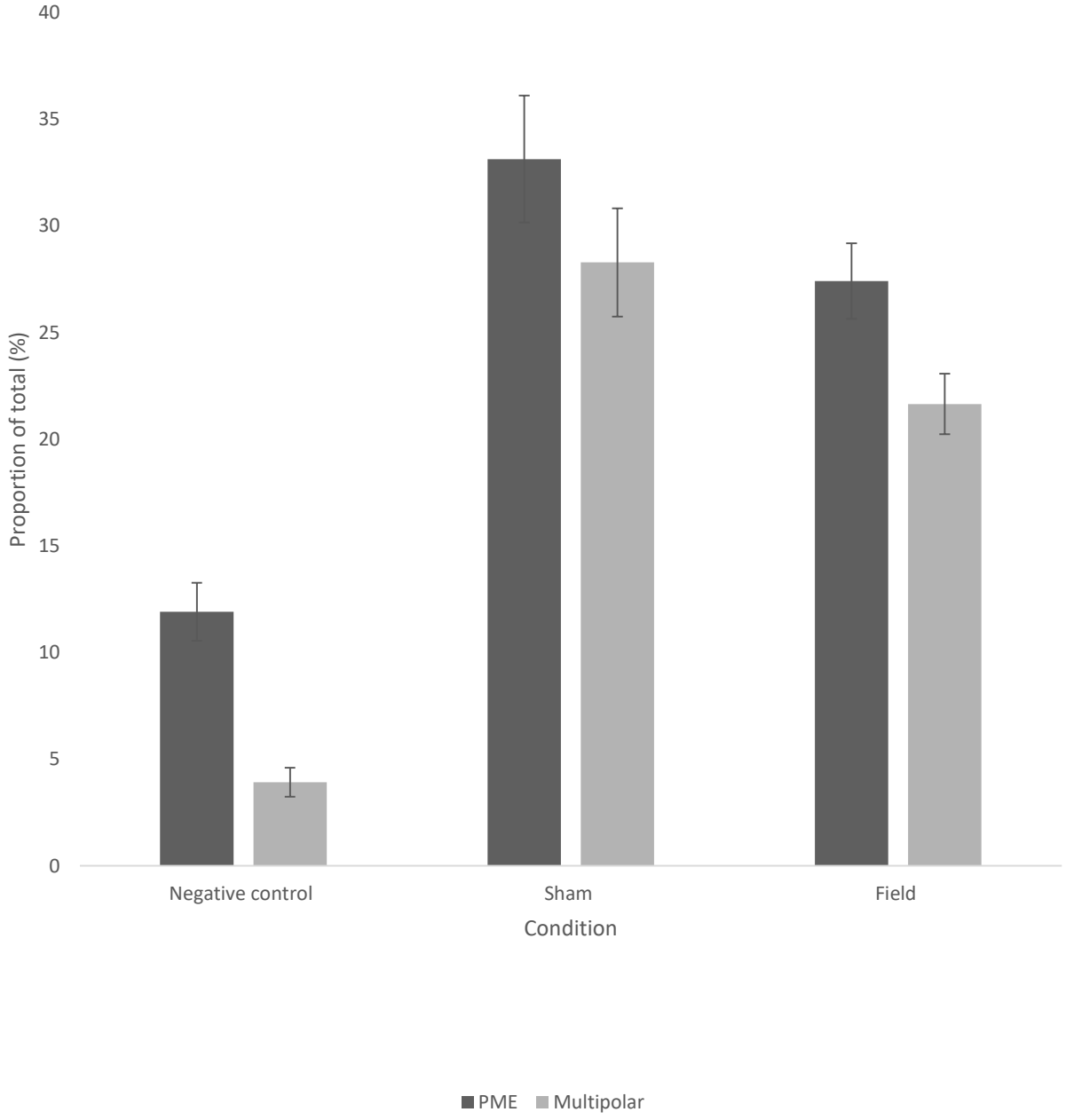

Figure 3.4.1.5: Differences in the proportion of cells bearing PME and multipolar extensions for the Rodin geometry. Field exposure consisted of 1 hour of burst-firing with PD = 3 msec and ISI = 3000 msec, at an intensity range of 300-500 nT. Error bar represent SEMs. Differences observed were being driven by sham and field conditions as compared to negative controls.

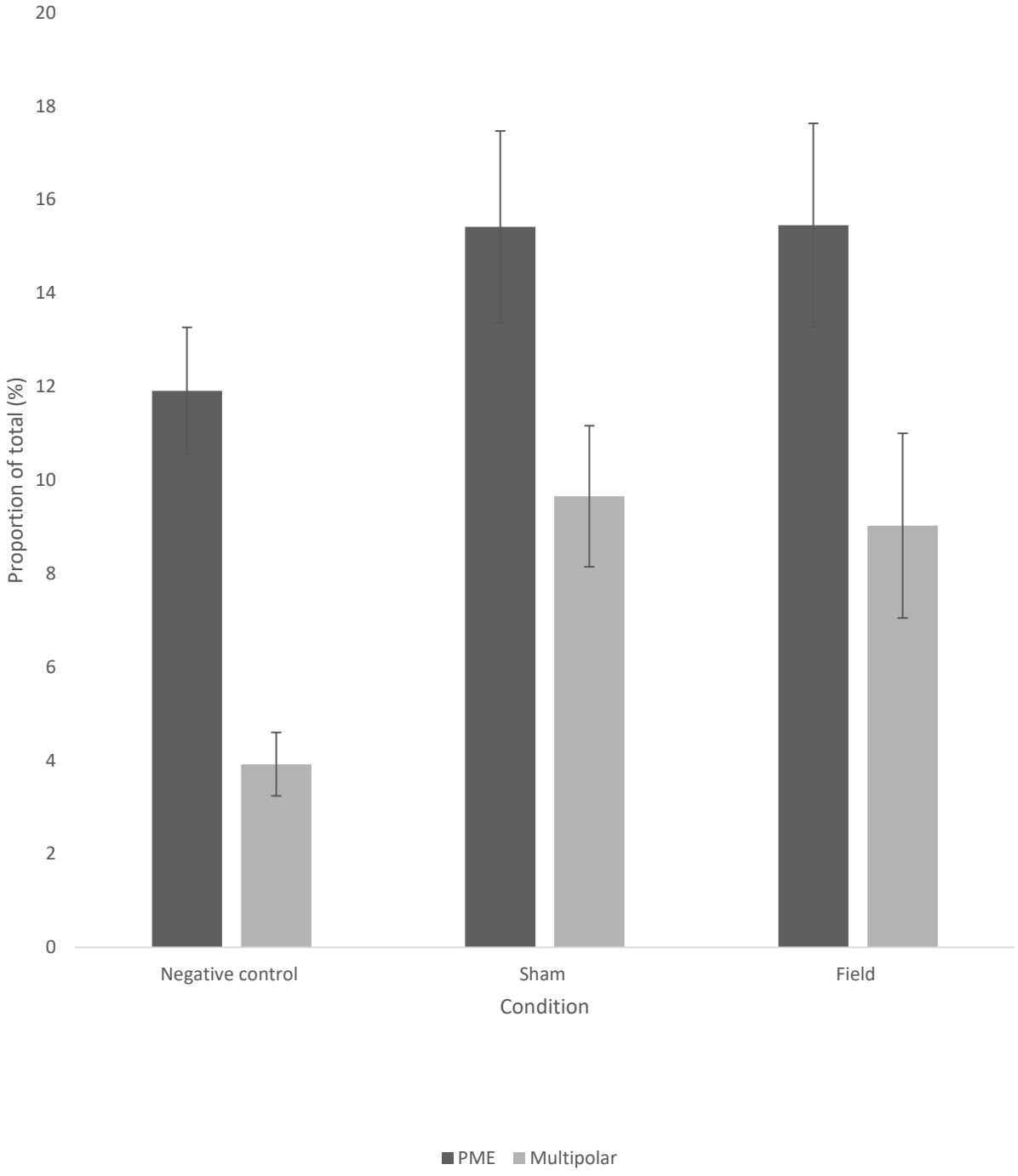

Figure 3.4.1.6: Differences in the proportion of cells bearing PME and multipolar extensions for the Toroid geometry. Field exposure consisted of 1 hour of burst-firing with PD = 3 msec and ISI = 3000 msec, at an intensity range of 300-500 nT. Error bar represent SEMs. No differences were obtained.

3.4.2. Ultra-Weak Photon emission measurements for PC-12 cells

The number of photons emitted by the PC-12 cells cultures collected by PMT measures were z-transformed and truncated between +/-5 SD prior to being spectrally analyzed and divided into 0.1 Hz increment bins. The means and SDs of photons emitted for each condition were also computed for each recording session. Differences in photon emission were analyzed for both global (mean and SD of recording) and discrete (1 Hz bins and classical EEG bands) using a MANOVA with chemical (DMSO v. Forskolin), Field (control, sham, Burst), and physical application geometry as between-subject's factors. None of the discrete measures were shown to be different between treatments. However, it was shown that the mean photon counts when cells were present, irrespective of field condition or chemical treatment showed a difference between geometries [$F_{(4,\ 101)} = 8.04$, $p = 1.2 \cdot 10^{-5}$, Ω^2-est = 0.25]. Post-hoc analysis of homogenous sub-groups identified mean photon counts for the PC-12 cells exposed to the Rodin coil and Helmholtz coil (all groups combined) as being lower than that of cells exposed to the Hoberman coil or controls. Follow-up multiple nonparametric tests (Mann-Whitney U) confirmed the findings of parametric equivalents, as homogeneity of variance was violated. Field effects (data not shown) were demonstrated to have impacted the standard deviation of the recording phase but was not impacted by physical application geometry.

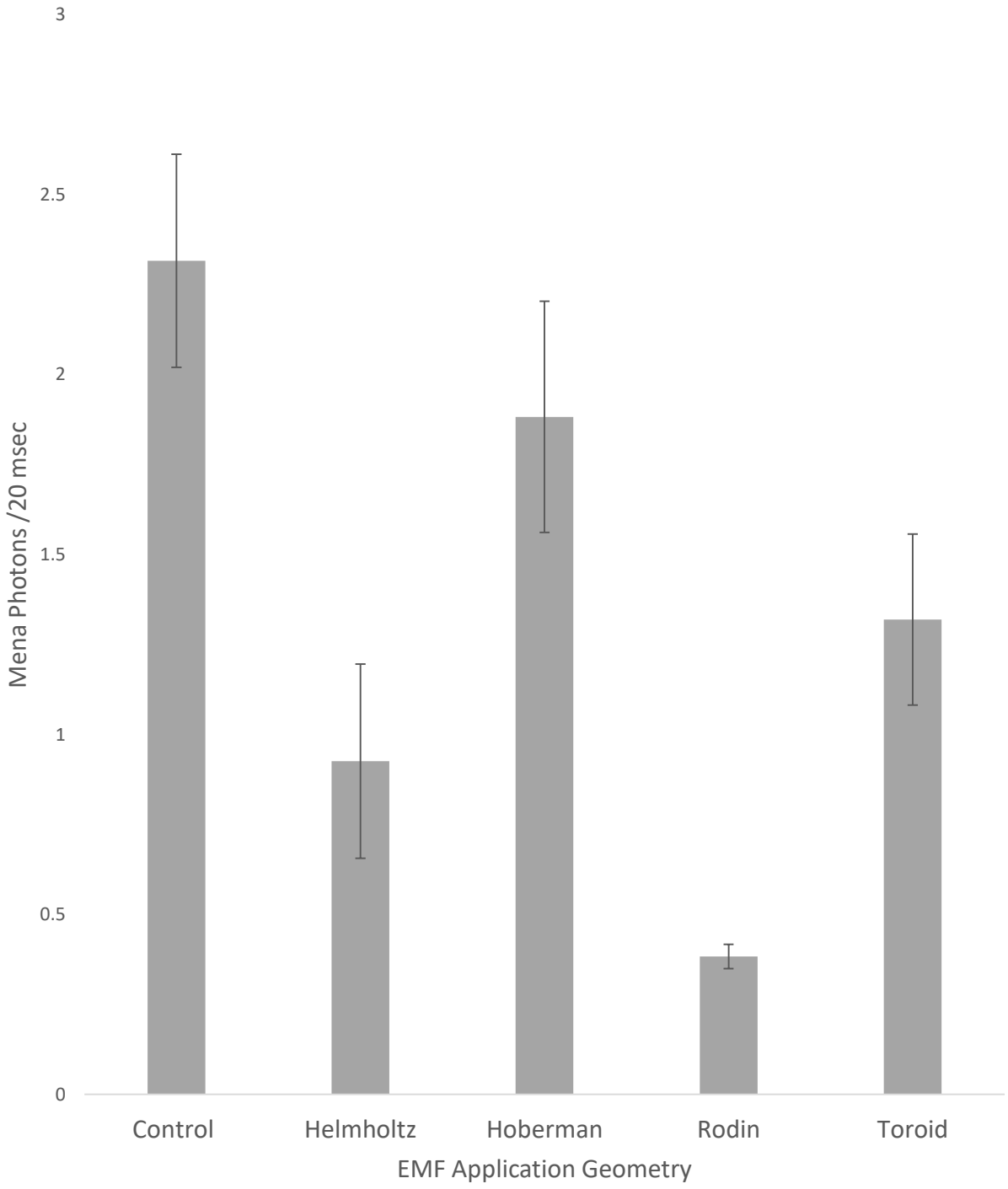

Figure *3.4.2*: Differences obtained between physical application geometry as assessed by PMT spectra emission 3 days following treatment. All groups were combined in this analysis. Error bars represent SEMs. (N=3).

3.4.3. Ultra-Weak Photon Emission Measurements for B16-BL6 cells

The data from the mean photon counts and SD of the recording segment were extracted from each of the 3, 1-min recording measures from 3 observation periods during baseline, pre-exposure sham, field recording (minutes 1-3; 15-18; 27-30), and immediately following exposure (post-exposure sham) and imported into Excel. The data was standardized and truncated between +/-5 SD to accommodate outliers and separately organized in a between-subjects' and a within-subjects' manner before being exported into SPSS for statistical analysis.

For the dataset organized as between-subjects' cases, 3 separate *one-way* analyses of variance were conducted to examine the differences in the mean photon counts and SD of the photon counts for the 3 periods of observation: pre-exposure sham, overall field effect, and post-exposure sham. Significance was considered at the $p<.02$ level. There was no difference in mean photon counts ($p=.041$) nor the standard deviation of photon counts ($p=.049$) for the post-exposure sham conditions between geometries, after alpha-level correction. In contrast, there were significant differences in mean photon counts [$F_{(3,35)} = 5.52$, $p = .004$, Ω^2-est = 0.34] and in the SD of photon counts [$F_{(3,35)} = 4.54$, $p = .009$, Ω^2-est = 0.30] in pre-exposure sham treated B16-BL6 cells. Tukey's post-hoc analyses confirmed that the differences were being driven by higher values for the Hoberman condition as compared to the Toroid and Helmholtz conditions. Analysis of the combined field effects demonstrated significant differences for mean photon counts [$F_{(3,107)} = 8.18$, $p = 6.1 \cdot 10^{-5}$, Ω^2-est =0.19] and the SD of photon counts [$F_{(3,107)} = 6.37$, $p = .001$, Ω^2-est =0.16] as a function of geometry. The mean photon counts and SD of photon counts for the Hoberman condition had significantly higher values as compared to all other geometries. Results are summarized in figures 3.4.3.1 and 3.4.3.2.

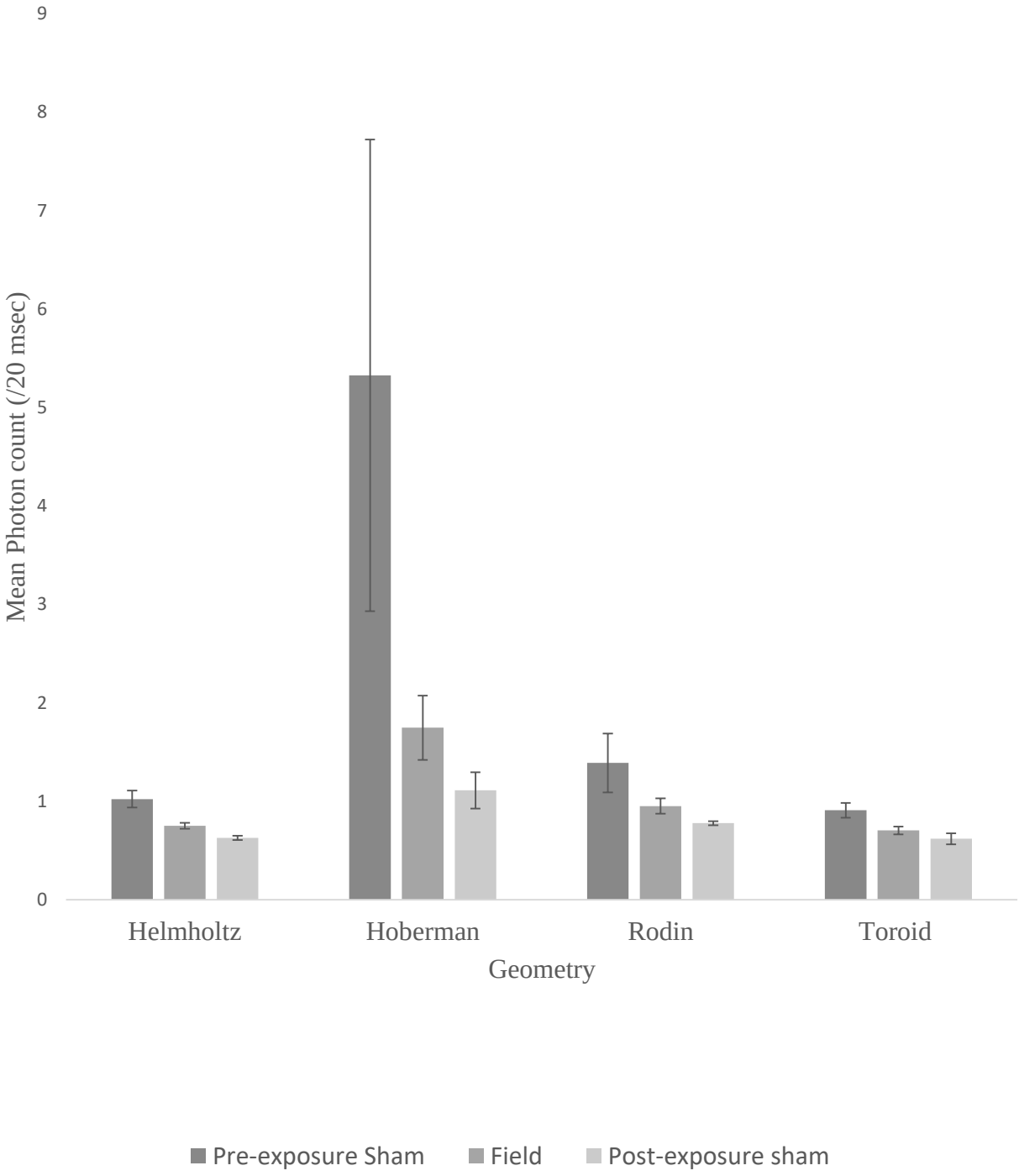

Figure 3.4.3.1: Mean photon counts, per 20 msec (ordinate), as a function of geometry (abscissa). Bars (left to right) correspond to measurement periods observing photon emission during pre-exposure sham, total field exposure, and post-exposure sham. Error bars represent SEMs.

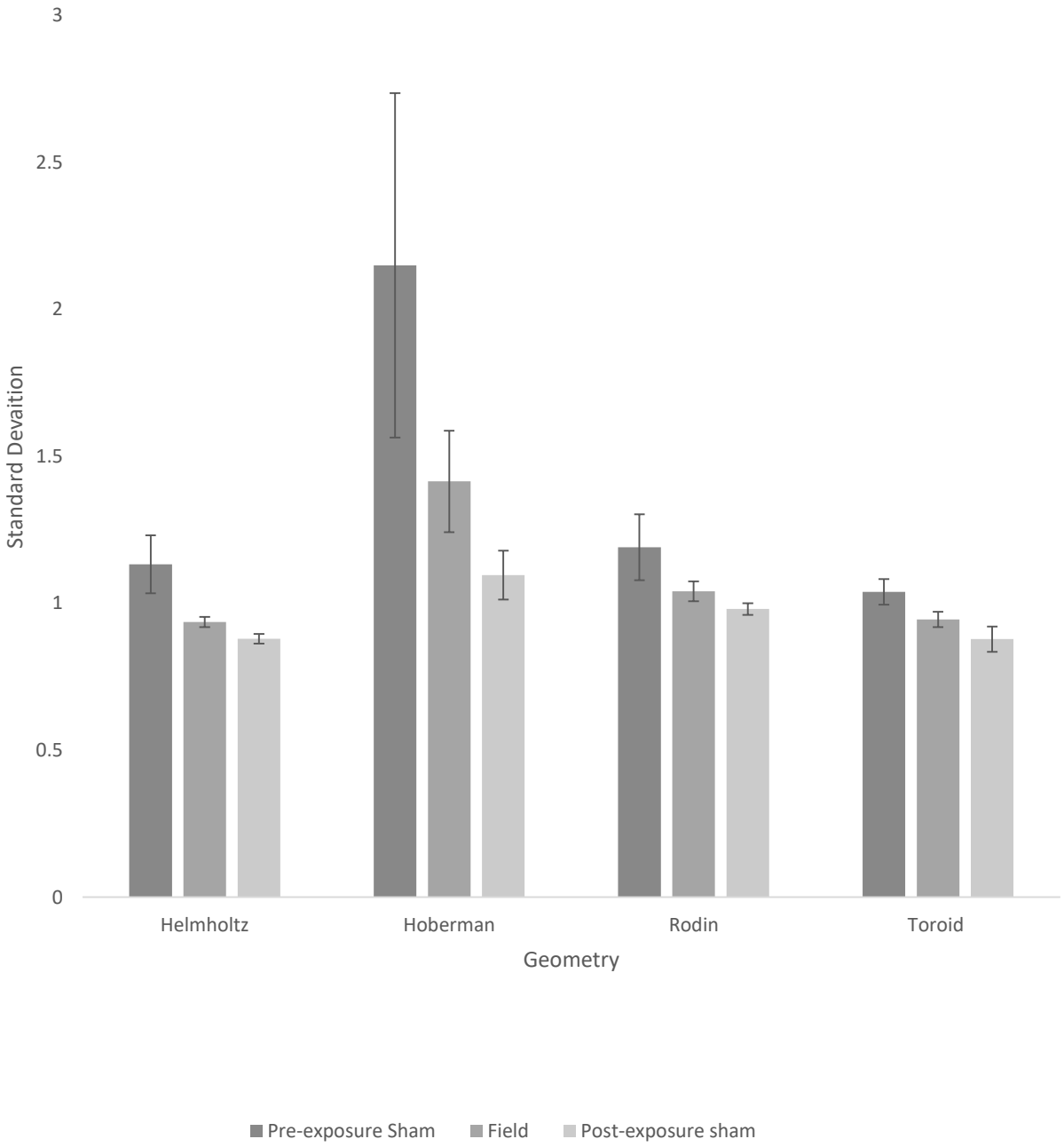

Figure 3.4.3.2: Differences in the standard deviation (ordinate) of measurement periods for the pre-exposure sham, total field exposure, and post-exposure baselines (represented as bar going from left to right) as a function of EMF physical application geometry (abscissa). Error bars represent SEM values.

The frequency-specific attributes of photon emission associated with each geometry during the three target phases of recording (pre-exposure sham, field, post-exposure sham) were investigated using 3 separate MANOVAs to assess spectral power density (SPD) values for 25, 1 Hz frequency bins (1 Hz bin = spectral frequencies between 1.00 to 1.99 Hz) with geometry (4 levels) as the between-subjects' factors and frequency (25 levels) as the within subjects' variables. Results were considered significant at the $p<.02$ level after alpha wise correction. Investigations examining pre-exposure sham conditions revealed a significant within subjects' interaction of geometry by frequency of photon emission [$F_{(72,768)} = 3.52$, $p<.001$, $p\eta^2 = 0.25$], while no such interaction was determined in post-exposure baselines ($p=.89$), however this interaction was maintained during the field exposure portion of the experiment [$F_{(72,2496)} = 2.01$, $p <.001$, $p\eta^2 = .05$). Post-hoc analyses using one-way analyses of variance aimed to investigate which frequencies that were different between each geometry during the pre-exposure sham and active field conditions, as subtle distinctions between physical application geometry was most salient to this investigation.

Post-hoc examinations of pre-exposure sham conditions identified the 3- and 10-Hz frequency bins as being significantly different between geometries: the Helmholtz and Hoberman conditions had lower SPD values compared to the Rodin geometry for 3- Hz bin; while the 10-Hz bin had lower SPD values for the Hoberman and Helmholtz geometries but higher SPD values for the Toroid condition. There were also differences in the frequency of photon emission for B16-BL6 cells exposed to the active EMF condition and post-hoc analyses demonstrated differences in SPD values for the 3- and 16-Hz frequency bins. The differences obtained in the 3-Hz frequency bin showed SPD values in the Hoberman and Helmholtz conditions that were significantly lower than the SPD values in the Rodin condition. Differences in the 16-Hz bin were being driven by significantly lower SPD values in the

Hoberman condition as compared to the Rodin condition. Data associated with the most salient findings are presented in figure 3.4.3.3 and 3.4.3.4.

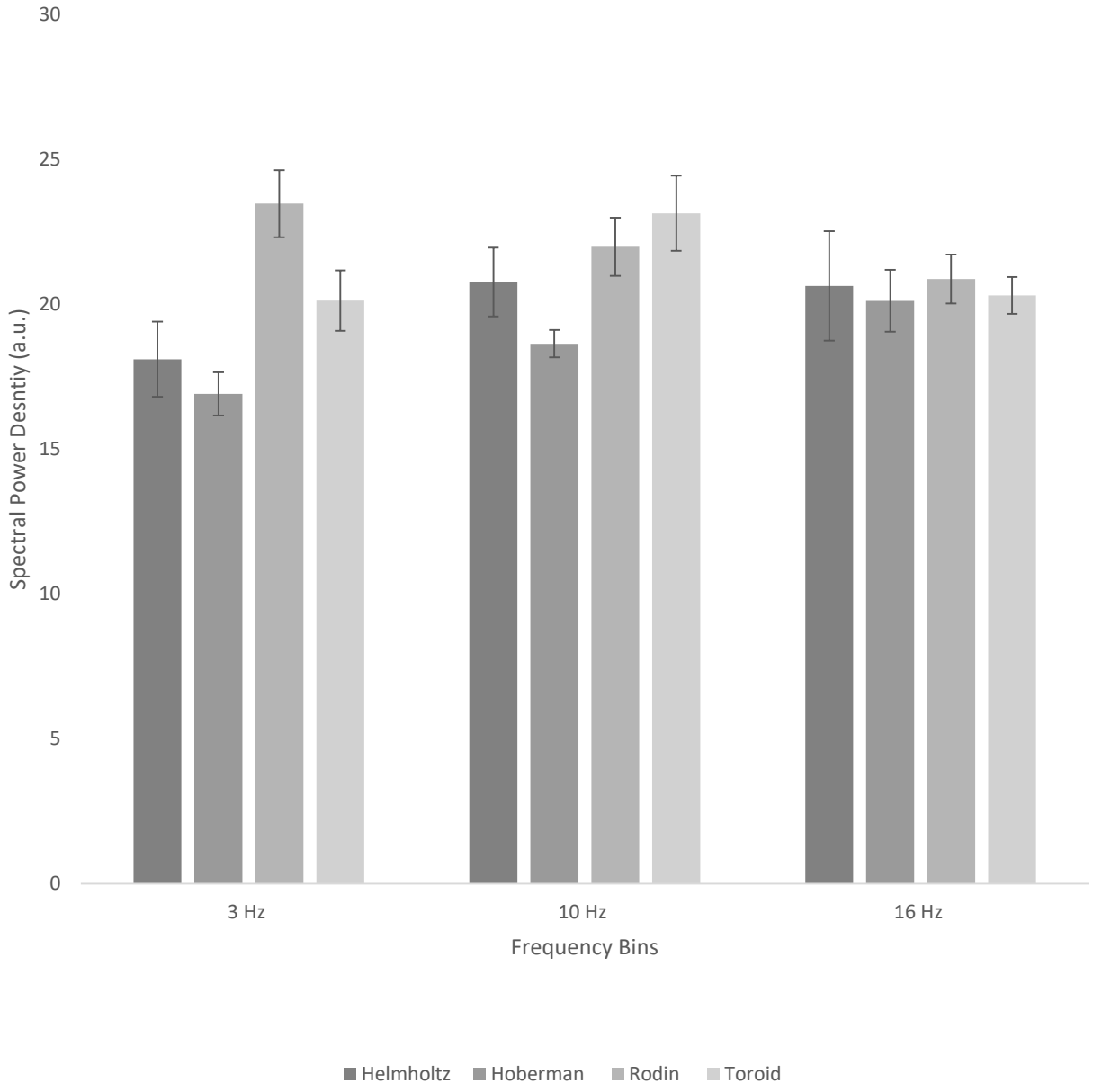

Figure 3.4.3.3: Spectral power density (arbitrary units; ordinate) differences for 3 distinct frequency bins (3, 10 and 16 Hz) comparing the 4 different EMF application geometries during the pre-exposure sham condition. Geometries are represented as bars in alphabetical order from left to right. Error bars represent SEM values. (N=3).

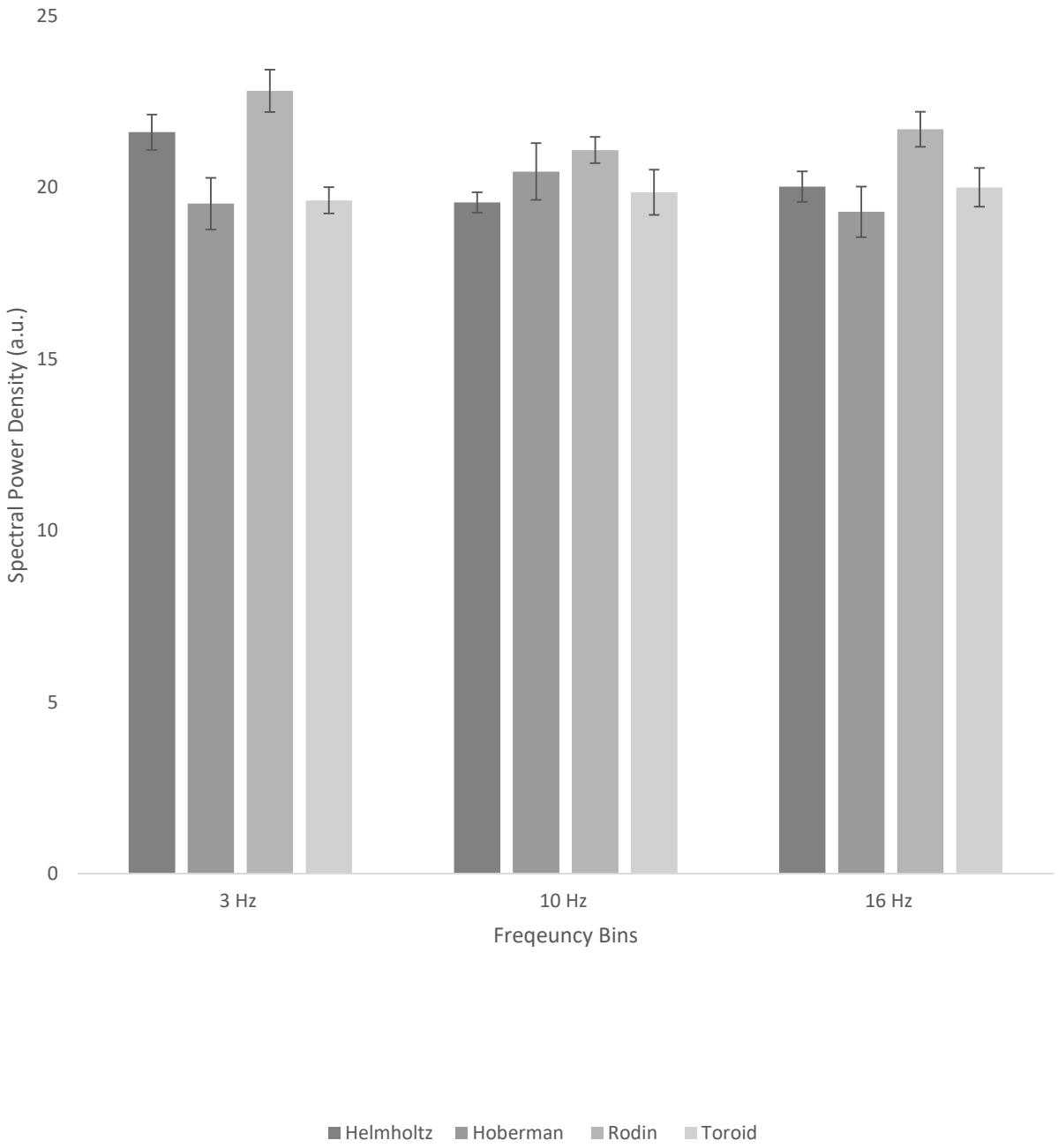

Figure 3.4.3.4: Spectral power density (ordinate; arbitrary units) differences as a function of 3 distinct frequency bins (abscissa) comparing the 4 different physical application geometries (bars; alphabetical order left-to-right) during the Thomas-EMF application. Error bars represent SEM values. (N=3).

Differences in 1) mean photon counts across observation periods as a function of manipulation and 2) SD across observation periods as a function of manipulation, and 3) the spectral power densities across observation periods as a function of manipulation for data organized in a within-subjects' manner were investigated using serial MANOVAs. In all three cases, there were no significant differences obtained for mean photon counts, standard deviation, or spectral power density (with 25-Hz bin frequencies) as a function of manipulation (pre-exposure sham, Thomas-EMF exposure, or post-exposure shams; $p>.05$). Based upon the results of analyses conducted on this data organized as between-subjects' observations, the classification accuracy for frequency alterations within salient experimental manipulations was examined. Four step-wise discriminant analyses were used to classify between a single geometry by comparing that target to all other geometries using a single-step entry method. This methodology only identifies the largest source of variance in order to differentiate between targets and was conducted only on spectral characteristics analyzed from each of the recording segments: pre-exposure sham, Thomas-EMF, post-exposure sham. Results demonstrated, moderate accuracy in differentiating between 2 out of 4 unique geometries. Results are summarized in table 3.4.3.1:

Table 3.4.3.1: Summary of multiple, single-step (Max-steps = 1) discriminant analyses. Data presented aimed to identify unique statistical features that distinguish between various geometric configurations of EMF application geometry. Relevant (statistically significant effects) findings are bolded for convenience.

Geometry	Variable Entered	Wilks-λ	X^2 – value	p-value	Cross-validated Accuracy
Helmholtz	Pre-exposure sham; 2-Hz bin	.686	3.58	.058	75%
Hoberman	**Post-exposure sham; 12-Hz bin**	**.440**	**7.80**	**.005**	**83.3%**
Rodin	----------	----------	- ----------	- ----------	----------
Toroid	**Thomas-EMF; 16-Hz bin**	**.256**	**13.03**	**$3.06 \cdot 10^{-4}$**	**100%**

3.5. Discussion:

The experiments in this chapter have demonstrate that there are unique subtleties that can be used to distinguish physical application geometry as a factor important on EMF exposures. For example, when changes in the morphological features of PC-12 cells, such as PME, are used as the outcome, 2 structural geometries that were wound with copper wire, the Helmholtz coil and Toroid, did not have an effect when cells were exposed to both forskolin and burst-firing EMF. In contrast, the two remaining geometries, the Hoberman and Rodin, did demonstrate unique differences in morphology in PC-12 cells treated with 0.5 µM forskolin and exposed to burst-firing EMF corresponding to changes in the proportion of cells bearing PME or multipolar extensions. Exposures to the burst-firing EMF generated using the Hoberman configuration showed an increase in the proportion of cells bearing plasma membrane extensions (PME) and multipolar extensions when the field was present as compared to

forskolin treatment alone (control). Burst-firing EMF generated using the Rodin coil was associated with a reduction in the proportion of cells bearing PME and multipolar extensions relative to sham exposure conditions (i.e., no field present) although both conditions were associated with significantly greater changes in C12 morphology as compared to control conditions.

When using the emission of ultra-weak photons from forskolin-treated PC-12 cells cultures as the endpoint exposure to EMF using different geometries and field conditions (sham v. burst-firing EMF) taken three days after their treatments, only those cells that received exposure by the Rodin coil, be it sham or field, demonstrated a net reduction in mean photon counts. Comparatively, the cells that were exposed to either the sham or burst-firing EMF conditions generated through the Hoberman geometry had mean photon counts that trended towards control measures. There is some evidence, from our experiments, to suggest that the lower the overall photon count, the greater the proportion of differentiated cells.

Data examining ultra-weak photon emission (UPE) profiles from cultures of melanoma cells were able to successfully differentiate between the 4 different application geometries. In this study were reported a net increase in background mean photon counts, relative to all other geometries, for the Hoberman condition during pre-field (sham) recordings. Similar increases in the standard deviation of the photon emission was also seen. Persinger et al., (2013) demonstrated that a reduction in the local static magnetic field intensity corresponded to an increase in spontaneous UPE emitted from a subject's head. If true, the net increase in local magnetic activity, as is the case when the appropriate field is being generated through any device, would result in a net decrease in overall photon intensity. In all instances observed, for all geometries, when the field was activated there was a net reduction in both the mean photon

counts and the standard deviation of the counts that supports the findings previously reported. It is interesting that when the field has been removed, the counts do not immediately return to baseline conditions. This effect may be accommodated by results obtained by Karbowski et al., (2016). In their experiments, B16-BL6 cells were exposed to patterned pulses of light while being simultaneously exposed to a patterned EMF prior to having their UPE profiles measured. There was an increase in the overall UPE intensity corresponding to the wavelength of light that was presented to cells and that enhancement was sustained for approximately 70 min after a 60 min exposure. The energy that was released during this time frame was calculated to fall within the range of energy that was contained within the EMF that was simultaneously exposed with the light pulses. In the experiments presented in this chapter we did not expose B16-BL6 cells to patterned light pulses, but the net reduction in photon intensity and variability may also serve to represent a change in the applied EMF energy. If correct, the it is assumed that, provided our observation accommodated the length of exposure, the UPE counts would return to baseline around 40 min after the field (Thomas) was terminated.

In addition to the mean photon counts and standard deviation, we showed that the spectral power differences emitted from the cells (i.e., B16-BL6 cells) were able to successfully differentiate between application geometries during sham (pre-field) and Thomas – EMF exposures. The spectral characteristics were binned in 1 Hz increments and it was shown that 3 distinct frequency bins, 3, 10, and 16 Hz, that represent harmonics of calcium ion cyclotron resonance were differently affected by application geometry. (McLeod et al., 1987; Blackman et al., 1994; Vorobyov et al., 1998**).** This observation is further supported by the data indicating that exposures of cells to the Thomas-EMF acts on calcium signalling, and is congruent with previous findings (Buckner et al., 2018). Finally, the data could be used to successfully

discriminate between a selected target geometry, as compared to all others, based upon unique UPE spectral characteristics during unique periods of observation.

These results, taken together, suggest that application geometry does in fact paly a role, albeit minor, in the bio-effectivity of exposures to patterned EMF, at least in the cells lines studied. Furthermore, discrete differences can be observed in cell morphology (e.g., PC-12 cells) and correlates with function (i.e., UPE) that can differentiate between different physical structures through that a patterned EMF has been presented. The evidence collected supports the idea that structure dictates function even when examining the nature of the application geometry of patterned EMFs and warrants further exploration.

3.6. References:

Baker-Price, L. A., & Persinger, M. A. (1996). Weak, but complex pulsed magnetic fields may reduce depression following traumatic brain injury. *Perceptual and motor skills*, *83*(2), 491-498.

Baker-Price, L., & Persinger, M. A. (2003). Intermittent burst-firing weak (1 microTesla) magnetic fields reduce psychometric depression in patients who sustained closed head injuries: A replication and electroencephalographic validation. *Perceptual and Motor Skills*, *96*(3), 965-974.

Blackman, C. F., Blanchard, J. P., Benane, S. G., & House, D. E. (1994). Empirical test of an ion parametric resonance model for magnetic field interactions with PC-12 cells. *Bioelectromagnetics: Journal of the Bioelectromagnetics Society, The Society for Physical Regulation in Biology and Medicine, The European Bioelectromagnetics Association*, *15*(3), 239-260.

Buckner, C. A., Buckner, A. L., Koren, S. A., Persinger, M. A., & Lafrenie, R. M. (2015). Inhibition of cancer cell growth by exposure to a specific time-varying electromagnetic field involves T-type calcium channels. *PLoS One*, *10*(4), e0124136.

Buckner, C. A., Buckner, A. L., Koren, S. A., Persinger, M. A., & Lafrenie, R. M. (2017). The effects of electromagnetic fields on B16-BL6 cells are dependent on their spatial and temporal character. *Bioelectromagnetics*, *38*(3), 165-174.

Buckner, C. A., Buckner, A. L., Koren, S. A., Persinger, M. A., & Lafrenie, R. M. (2018). Exposure to a specific time-varying electromagnetic field inhibits cell proliferation via cAMP and ERK signaling in cancer cells. *Bioelectromagnetics*, *39*(3), 217-230.

Burke, H. E. (2012). *Handbook of magnetic phenomena*. Springer Science & Business Media.

Dotta, B. T., Buckner, C. A., Cameron, D., Lafrenie, R. M., & Persinger, M. A. (2011). Biophoton emissions from cell cultures: biochemical evidence for the plasma membrane as the primary source. *General Physiology and Biophysics*, *30*(3), 301.

Dotta, B. T., Murugan, N. J., Karbowski, L. M., Lafrenie, R. M., & Persinger, M. A. (2014). Shifting wavelengths of ultraweak photon emissions from dying melanoma cells: their chemical enhancement and blocking are predicted by Cosic's theory of resonant recognition model for macromolecules. *Naturwissenschaften*, *101*(2), 87-94.

Dotta, B. T., Lafrenie, R. M., Karbowski, L. M., & Persinger, M. A. (2014). Photon emission from melanoma cells during brief stimulation by patterned magnetic fields: is the source coupled to rotational diffusion within the membrane. *General Physiology and Biophysics*, *33*, 63-73.

Dotta, B., Buckner, C., & Lafrenie, R. (2016a). Photon Emissions as differential indicators for different components of protein kinase A (PKA) in transfected murine melanoma cells. *Arch can Res*, *4*(3), 10-21767.

Dotta, B. T., Karbowski, L. M., Murugan, N. J., Vares, D. A. E., & Persinger, M. A. (2016b). Ultra-weak Photon Emissions Differentiate Malignant Cells from Non-Malignant Cells In Vitro. *Archives of Cancer Res*, *4*(2).

Dotta, B. T., Vares, D. A., Buckner, C. A., Lafrenie, R. M., & Persinger, M. A. (2014). Magnetic field configurations corresponding to electric field patterns that evoke long-term potentiation shift power spectra of light emissions from microtubules from non-neural cells. *Open Journal of Biophysics*, *4*(04), 112.

Fleming, J. L., Persinger, M. A., & Koren, S. A. (1994). Magnetic pulses elevate nociceptive thresholds: Comparisons with opiate receptor compounds in normal and seizure-induced brain-damaged rats. *Electro-and Magnetobiology*, *13*(1), 67-75.

Frey, U., & Morris, R. G. (1997). Synaptic tagging and long-term potentiation. *Nature*, *385*(6616), 533-536.

Haas, H. L., & Rose, G. (1982). Long-term potentiation of excitatory synaptic transmission in the rat hippocampus: the role of inhibitory processes. *The Journal of physiology*, *329*(1), 541-552.

Hameroff, S., & Penrose, R. (2014). Consciousness in the universe: A review of the 'Orch OR'theory. *Physics of life reviews*, *11*(1), 39-78.

Karbowski, L. M., Murugan, N. J., & Persinger, M. A. (2016). Experimental evidence that specific photon energies are “stored” in malignant cells for an hour: the synergism of weak magnetic field-LED wavelength pulses. *Biology and Medicine*, *8*(1), 1.

Komaki, A., Khalili, A., Salehi, I., Shahidi, S., & Sarihi, A. (2014). Effects of exposure to an extremely low frequency electromagnetic field on hippocampal long-term potentiation in rat. *Brain research*, *1564*, 1-8.

Mach, Quoc Hao, and Michael A. Persinger. "Behavioral changes with brief exposures to weak magnetic fields patterned to stimulate long-term potentiation." *Brain research* 1261 (2009): 45-53.

Malenka, R. C., & Nicoll, R. A. (1999). Long-term potentiation--a decade of progress?. *Science*, *285*(5435), 1870-1874.

Martin, L. J., Koren, S. A., & Persinger, M. A. (2004). Thermal analgesic effects from weak, complex magnetic fields and pharmacological interactions. *Pharmacology Biochemistry and Behavior*, *78*(2), 217-227.

McLeod, B. R., Smith, S. D., & Liboff, A. R. (1987). Calcium and potassium cyclotron resonance curves and harmonics in diatoms (A. Coeffeaformis). *Journal of Bioelectricity*, *6*(2), 153-168.

Murugan, N. J., Karbowski, L. M., & Persinger, M. A. (2014). Weak burst-firing magnetic fields that produce analgesia equivalent to morphine do not initiate activation of proliferation

pathways in human breast cells in culture. *Integrative Cancer Science and Therapeutics*, *1*(3), 47-50.

Persinger, M. A., Dotta, B. T., Saroka, K. S., & Scott, M. A. (2013). Congruence of energies for cerebral photon emissions, quantitative EEG activities and~ 5 nT changes in the proximal geomagnetic field support spin-based hypothesis of consciousness. *Journal of Consciousness Exploration & Research*, *4*(1).

Rose, G. M., David M. Diamond, K. Pang, and T. V. Dunwiddie. "Primed burst potentiation: lasting synaptic plasticity invoked by physiologically patterned stimulation." In *Synaptic plasticity in the hippocampus*, pp. 96-98. Springer, Berlin, Heidelberg, 1988.

Simon, R. H., & Arbo, T. E. (1986). Morphine increases metastatic tumor growth. *Brain research bulletin*, *16*(3), 363-367.

Vorobyov, V. V., Sosunov, E. A., Kukushkin, N. I., & Lednev, V. V. (1998). Weak combined magnetic field affects basic and morphine-induced rat's EEG. *Brain Research*, *781*(1-2), 182-187.

Chapter 4

4 Physical Characterization of the Nature of Electromagnetic Field Application Geometry

4.1 Abstract:

The role played by physical application geometry as a facet of electromagnetic field (EMF) exposure is an underdeveloped concept that has been subjected to limited experimentation. Provided that the concept of structure dictates function is relevant to EMF exposure it is suggested that an investigation of the physical properties of EMF geometry are necessary. In this study, we provide a series of investigations aimed to determine the salient effects that physical application geometry plays in terms of producing bio-effective EMFs. Results are suggestive of the idea that unique constructions can appreciably (statistically) alter background, ambient static (DC) EMF intensity, especially when the structure approaches a dome-like geometry. Further experimentation demonstrated no statistically significant differences for other physical measures although this does not rule out the importance of individual differences. The observed effects have been likened to alterations in the signal-to-noise ratio or Weber's concept of the just noticeable differences as a potential mechanism of action.

4.2. Introduction:

The greatest tool developed by human kind has been the scientific method. Systematic evaluation of systems (physical, chemical, biological, etc.) and their corresponding reactions to precise/accurate manipulations of contributing factors have provided a detailed, although not an exhaustive, understanding of the description of the Nature of the physical world. One of the cornerstone ideas underlying many systems is the assertion that structure dictates function.

By extension, the structure of the experiment can influence the function of the system under observation. The aforementioned statement is best exemplified in terms of the double slit experiment for electrons and photons, whereby the parameters of the experiment can suggest, based on the interpretation of the results, that the observed stimuli either behave as a particle or a wave (Bach et al., 2013; Eibenberger et al., 2013; Selleri, 1992).

With respect to biological systems, the concept that structure dictates function can be used in our examination of the brain. For example, the structure of the hippocampus can be likened to two concentric ring-like, intercalated c-like structures that condenses into nanometer separations allowing for the transition from electrical impulses to chemical representations of the same information. Furthermore, the hippocampus has demonstrated the ability to undergo adult neurogenesis within its subdivisions of the cornu ammons (CA) fields, as well as possessing Schaffer collaterals allowing for re-entrant processes and prolongation of the same stimulus along its consolidatory path to more crystallized long-term representations (i.e., memory) (Riedel and Micheau, 2001; Morris et al., 2007). Additional examples of structure dictating function, at the level of the brain, include Heschl's gyrus and the lateral geniculate nucleus of the thalamus. Heschl's gyrus, along its course, has a tonotopic representation of the frequencies of sound sensed by the ear, in the medial – lateral and anterior –posterior axes, where high frequencies are presented most medially (and posterior) while low frequencies are represented more laterally (and posterior) **(**Humphries et al., 2010; Talavage et al., 2004). The observed organization of Heschl's gyrus is reflected, although inverted, in the cochlea that discriminates frequencies and translates them to corresponding nervous impulses. With respect to the lateral geniculate nucleus (LGN) of the thalamus, it is composed of 6 layers, alternating between grey and white layers, that can be subdivided into the magnocellular components (inner layers 1, 2) and the parvocellular portions (outer layers 3 to 6) (Reid and Shapley, 1992;

Garey and De Courten, 1983; Crosby et al., 1962). The magnocellular division of the LGN is responsible for colour-blind vision and rapid conduction, whilst the parvocellular layers are associated with lower velocity conduction and are associated with the conduction of colour vision (Crosby et al, 1962; Parent, 1996). Visual processing and perception, to allow for binocular vision, has divided the visual fields into ipsilateral and contralateral features, that are structurally maintained at the level of the LGN whereby layer 2,3, and 5 process ipsilateral visual information and layers 1,4, and 6 process contralateral information along with its integration into primary, secondary, and tertiary visual areas (BA 17, 18, 19, etc.) (Crosby et al., 1962; Parent, 1996). Outside the brain, we can demonstrate the concept of structure dictating function in a number of organ systems. In examining the stomach, whose role in digestion is the acidification of foodstuffs that have been passed by way of the esophagus (another specialized tube structure whose function is to pass food along to the stomach (Thibodeau et al., 2004). Acidification during digestion of the food supply is derived from specialized cells oxyntic (parietal) cells that allow for the production and release of hydrochloric acid in the lumen of the stomach (Forte et al., 1981; Sedar and Friedman, 1961). As a consequence of the acidifying function of the stomach, there are biological fail-safes that have evolved including goblet cells that can secrete an alkaline mucus (Jass and Filipe, 1981; Thibodeau et al., 2004) so that the acidic environment does not destroy the epithelial lining of the organ and ultimately having the acidic solution leak into adjacent structures (organs) and digest the animal from the inside out. An additional function of the stomach, required to promote digestion, is churning, a process arising from the peristaltic contraction of muscle fibers embedded within the structural layering (tunics) of the organ.

It has been shown that exogenous application of discrete physiologically relevant (i.e., functional) stimuli can impact the structure of the system for that the stimulus is directed. For

instance, Mach and Persinger (2009) demonstrated that the application of a weak intensity EMF, patterned to mimic LTP in hippocampal slices, facilitated learning of an inhibitory task for animals that were exposed to this field during the task but a reduction in spatial memory in trained animals that were exposed 30 min before or after training. The authors theorized that the observed differences were being driven by hippocampal saturation. Comparatively, the application of a burst-firing EMF, derived from the activity of a collection of amygdaloid-hippocampal cells, has demonstrated functional changes that mimic the activity recorded from the mesial basal temporal lobe structures including: visual sensations, ego-alien intrusions, and the sensed presence (Cook and Persinger, 1997; Persinger and Healey, 2002; Persinger, 2003). Although we typify the alterations that result from the application of a patterned EMF as a functional alteration, it is truly the temporal construction or arrangement of parameters such as stimulus (point) duration, inter-stimulus interval, and intensity that have been shown cause the observed effects. It was only through systematic and rigorous investigation and experimentation, the application of our most valuable tool, that has allowed temporal structure of EMFs to be fully appreciated.

We have argued that just as temporal structure of EMFs can alter the biological function of systems so too should the physical structure in that the EMF is being presented have an effect. Some research has pointed to some validity/fidelity of the idea that the structure of the of the EMF-generating device can alter the effectiveness of the patterned EMF. For example, Martin and Persinger (2003) provided evidence that the physical structure through that an EMF is generated is important when examining the analgesic response in rats exposed to burst-firing EMF presented through a simple solenoid (heterogeneous field) versus a Helmholtz coil (homogeneous field). Results showed that maximum analgesia was obtained when the biologically relevant field was presented by the heterogeneous field-generating device. In the

previous chapter, we demonstrated that unique structural organizations of EMF-generating devices, had effects on photon emission measures by B16-BL6 cells and PC-12 cells treated with 0.5 µM forskolin, as well as in the morphological features of the treated PC-12 cells. Given this evidence it would be prudent to discern to what degree the physical application geometry contributes to the observed effects of EMF exposures on biological systems.

In this group of experiments, we have rigorously assessed the physical attributes of 4 distinct EMF-generating devices. Herein we suggest comparing changes measured in the static, ambient magnetic environment in response to different geometric configurations bound in copper wire to Faraday-like cages, as well as to the ability of unique geometries wrapped in copper wire to respond to weak environmental magnetic fields, to deflect or impede an incident, biologically relevant propagating EMF, and to contribute to changes in exposure conditions for that effects have been previously demonstrated by assessing static magnetic field changes.

4.3. Methods:

4.3.1. Physical Description of the Electromagnetic Application Geometries:

The devices corresponding to the following geometries were each constructed using 100-ft (~33 m) of 18 AWG primary, insulated copper wire. A total of 4 different electromagnetic (EM) physical application geometries were created and are identified as: Helmholtz, Hoberman, Rodin, and Toroid coils. Photos of the corresponding physical application geometries are included in **Appendix E1 – E4**.

Geometry#1: Helmholtz coil

The Helmholtz coil was fabricated out of two independent coils that were each wrapped continuously with 50-ft of wire wound around two fused 25.4 cm diameter plastic crochet hoops. The independent coils were then mounted to a wooden frame (L: 29.2 cm, W: 21.6 cm) that served as the base of the apparatus. The coils were mounted and separated by a block of wood (13.34 cm) affixed at the superior pole. The construction of the base and the upper mount were completed using Elmer's carpenter's glue. The coils were separated by their radius (12.7 cm) in order to replicate the original design proposed by Herman von Helmholtz, the original creator of this geometry. Resistance of the entire coil was assessed to be 0.8 Ohms by way of a Victor 70C digital multimeter.

Geometry #2: Hoberman coil

The Hoberman coil was derived from a collection of six overlapping plastic, circular rings that, as a whole, results in an icosododecahedron with 20 triangular faces and twelve pentagonal faces with a maximal diameter of 30.48 cm. For our purposes, the original Hoberman sphere was bifurcated, wrapped with electrical tape, and finally wrapped in one continuous fashion with 100-ft of 18 AWG primary, insulated copper wire. The resulting Hoberman coil has a base diameter of 30.48 cm and a dome height of 15.7 cm accommodating 10 triangular and 6 pentagonal faces. Coil resistance was 4.5 Ohms as measured by a Victor 70C digital multimeter.

Geometry #3: Rodin coil

The Rodin coil was constructed by fusing 2, 25.4 cm diameter plastic, circular crochet hoops, and continuously wrapping them with 50-ft of wire in a counter-clockwise fashion parallel to the circumferential plane. Following the completion of the circumferential wrapping, the Rodin coil was then perpendicularly wrapped with the remaining 50-ft of wire. Conceptually, the resulting aggregate encompassed an inner solenoid wrapped by an outer toroid. The resulting leads of the inner solenoid and outer toroid were soldered together to form a single input lead so as to activate both components simultaneously. The resulting resistance of the Rodin coil, as measured by a Victor 70C digital multimeter, was 0.4 Ohms.

Geometry #4: Toroid coil

The Toroid coil was created by wrapping 100-ft of wire around a plastic, circular 25.4 cm diameter crochet hoop. Wrappings were perpendicular to the circumference of the plastic backbone and were wrapped in a counter-clockwise fashion. The resulting resistance of the Toroid coil was 1.0 Ohms as verified by a Victor 70C digital multimeter.

Comparator Geometries:

In addition to the four primary target, physical application geometries, there were 8 different comparator geometries that were developed in order to assess and compare the differences obtained between background static magnetic field intensities measured in the various application geometries. Our working hypothesis was that any difference, or resulting change in the intensity of the background magnetic field would arise in the same way that changes in

the field are observed in a Faraday cage. A Faraday cage is built from specific materials (i.e., copper alloys) with a physical structure that causes attenuation of a magnetic field as measured in the "cage". Here we constructed 8 different Faraday-like containers using 25.4 cm diameter plastic salad dishes. One salad dish served as a physical control (i.e., no copper wrappings), while the remaining 7 salad bowls were covered with either a copper foil mesh or a copper weavemesh. Four devices were generated using copper foil mesh corresponding to 25, 50, 75 and 100% surface area coverage. Three devices were created using the copper weavemesh that included 25, 50, and 100% surface area coverings. The copper weavemesh described by the manufacturer (FerrierWire) to be used in electromagnetic interference and radio frequency (EMIRFI) shielding, filtering, and straining applications had a wire diameter of 0.04 cm, with a wire opening diameter of 0.08 cm. All copper foil mesh and copper weavemesh applications were affixed to the plastic salad containers using Elmer's glue. Photographic representations of each of the 8 comparator geometries can be found in Appendix F.

4.3.2. Determining The Change in the Earth's Static Magnetic Field Intensity as a Function of Physical Application Geometry:

The static intensity of the horizontal and orthogonal vectors of Earth's electromagnetic field (EMF) were measured using a tri-axial, vector FMV400 fluxgate magnetometer from MacIntyre Electronic Design Associates (MEDA). The magnetometer has a sensitivity of 1 nT with a range that extends to +/-100,000 nT (1 Gauss) with a +/-0.25% accuracy and an upper limit sampling rate of 1 Hz using the associated software platform. Data was collected in two different locations at Laurentian University, Sudbury, ON (longitude 80.78 W, latitude 46.62 N). The first locus of measure (N1; Neurochemistry) is situated in the basement laboratory of Laurentian University's Science II building. The second locus (N2; consciousness laboratory

chamber) was an acoustic chamber and Faraday cage in the basement of Laurentian University's Science II building that was separated from N1 by approximately 30 m. Data was collected from all 12 different geometric organizations of copper wire and copper mesh coverings (4 primary geometries and 8 comparator geometries). The measurement periods were divided into three, 5-minute segments that included a pre-geometry baseline, a geometry present test measure, and a post-geometry baseline measure. All data were acquired at a sampling rate of 1 Hz and all trials were conducted independently. Values for the angles of magnetic declination and inclination were manually recorded at the outset and at the termination of each recording period. For each of the four primary target geometries, as well as the 7 comparator geometries, there was a minimum of an N =3 measurements at each of the two loci. Photos of the experimental setup for the measurement set-up in location N1 (neurochemistry) are provided in Appendix G.

4.3.3. Determining the Change in the Static Vectorial Intensity of an Incident, Time-Varying EMF as a Function of Physical Application Geometry

Data was acquired using a tri-axial, FMV400 vector fluxgate magnetometer with a sampling rate of 1 Hz and was recorded using a personal laptop computer and associated software. The FMV400 magnetometer was placed at a distance of 30 cm from the opening of a 38 cm X 33 cm X 27 cm plastic milk crate that was wrapped in a single layer with 305 m of 30 AWG primary, insulated copper wire. The milk crate coil served as the source generator for the inducing, exogenous, frequency modulated (FM) EMF and will be herein referred to as the inducing coil. The pattern of the inducing FM-EMF (also called the Thomas-EMF) was generated by converting 859 integer values between 0 and 256 to a corresponding voltage of -5 V to +5V (127 = 0V) using a digital-to-analog converter that supplied current to the inducing

coil. The resulting FM-EMF consisted of 18 doublet peaks, where each singlet peak was 6 msec in duration, with gradually increasing intervals between 3 msec (for the first 5 repeats) to 120 msec for the last 5 repeats. The resulting frequency modulation for the FM-EMF pattern ranged from 25 Hz for the first 5 repeats to 6 Hz for the last 5 repeats. The duration of that each point of the 859 integer series was presented through the inducing coil was set to 3 msec and served as the point duration (PD). The inter-stimulus interval (ISI), that corresponds to the temporal delay between successive presentations of the 859-point pattern was also set to 3 msec. The cycle duration for the 859-point series FM-EMF was approximately 2.58 s when the PD and ISI were set to 3 msec respectively. The resulting FM-EMF was continuously presented during the induction phase. A diagrammatic representation of the FM-EMF pattern can be found in **Appendix H1**.

The experimental design for this investigation consisted of five, 2-minute recording periods that were organized in an A-B-A-B-A design. For this experiment, the recording period designated by 'A' indicated that the inducing field was not present (i.e., the equipment was on but no current was applied to the inducing coil) while the recording period designated 'B' indicated that the inducing field was active (i.e., current was being supplied to the inducing coil). There were five devices representing different EM application geometry conditions that were placed directly over the recording magnetometer; control (no geometry), Helmholtz, Hoberman, Rodin, and Toroid. Each EM application geometry condition was replicated across 10 independent trials (N=10). A photo and schematic representation of the experimental set-up has been provided and can be found in **Appendix H2**.

4.3.4. Assessing the Change in Induced Voltage through Various Physical Application Geometries in a Faraday Cage and Acoustic Chamber

The goal of this investigation was to discern the capacity of each geometry to act as an induction coil as a means of assessing the peak frequencies, and the intensity, of Earth's geomagnetic field. Previous research has demonstrated that the discrete, reliable fundamental and harmonic frequencies of the Earth's magnetic field are a consequence of lightning discharge between the Earth's surface and the inner layer of the ionosphere, associated with geomagnetic activity (Williams, 1992; Cherry, 2002; Schlegel and Füllekrug, 1999)**.** Here, we aim to investigate whether the structural geometry of the recording device can impact the ability to detect or interfere with the geomagnetic fundamental and harmonic frequencies.

All four magnetic geometry devices (the Helmholtz, Hoberman, Rodin, and Toroid devices) were simultaneously measured for discrete fluctuations in geomagnetic harmonic frequencies. The magnetic geometry devices attached to a Mitsar Model 201 quantitative electroencephalographic (QEEG) amplifier by way of silver-silver chloride cup sensors coupled to alligator clips that were directly attached to the copper wound coils. Data was acquired from all 4 geometries simultaneously and measured at a sampling rate of 500 Hz, using WinEEG software with low cut filter set to DC, high cut filter set to 30 Hz, and a notch filter between 55 -75 and 110 -130 Hz for the duration of 30 minutes. There were N=8 independent trials conducted between 20:00 and 23:00 DST local time. All recordings were conducted in an acoustic chamber and Faraday cage that has been previously demonstrated to reduce the static component of Earth's magnetic field by approximately 50% (Persinger et al., 2015)**.** A pictorial representation of the experimental set-up is provided in **Appendix I.**

4.3.5. Characterizing the Change in the Static EM Background Intensity as a Function of Application Geometry in a Standard Incubator

To examine the effects of our target EMF geometry devices on cell culture environments, we first assessed the output capacity of each magnetic geometry device in a standard exposure incubator. The standard incubator had an atmospheric composition of 95% oxygen and 5% CO_2 that was maintained at 37ºC and was located on the 7th floor of the Science II building at Laurentian University, Sudbury, ON (longitude 80.78 W, latitude 46.62 N). For recordings, the FMV400 fluxgate magnetometer was positioned in the center of the incubation unit. Measurements of the horizontal and orthogonal magnetic vector intensities were sampled at 1 Hz increments, with the inner and outer doors of the incubator closed, over the course of the experiment. The experimental measurement period consisted of an A-B-A-B-A repeated measures observation alternating between Sham (A: no field) and Burst (B: field) cycled at 5-minute intervals. There were five magnetic application geometries (Control/no EM geometry, Helmholtz, Hoberman, Rodin, and Toroid) that were placed directly over the recording magnetometer during the recording sessions. Each geometry (with the exception of the control condition) was connected to a DAC that produced a burst-firing pattern of current that generated an EMF through the respective coils for the field condition.

The burst-firing EMF was generated from 230 points ranging from 0 to 256, that were converted to voltage equivalents of -5V to +5V (127 = 0V) by way of a custom constructed, adjustable digital-to-analog converter and modified mini-audio amplifier. The point duration (PD) and inter-stimulus interval (ISI) for this pattern were set to 3 and 3,000 msec, respectively. EMF intensities resulting from the application of current into the respective physical EM application geometries were verified using an AC milliGauss meter (AlphaLabs) that was set

such that the effective intensities ranged from 300 – 500 nT. The duration of the 230-point burst-firing pattern with PD set to 3 msec was 690 msec while the cycle duration lasted 3.69 s. For each combination of physical EM application geometry (Control, Helmholtz, Hoberman, Rodin, and Toroid devices) and field presentation (burst-firing field or no field) a total of N=5 independent replicates were conducted. A diagrammatic representation of the experimental set-up can be found in **Appendix J**.

4.3.6. Methods of analyses:

4.3.6.1. Determining The Change in Earth's Static Magnetic Field Intensity as a Function of Physical Application Geometry:

Raw data for the strength of the magnetic field was collected for the X, Y, and orthogonal components of the Earth's magnetic field and was assessed at 1 Hz. Additional data including the angle of inclination, declination, and the computed Resultant Earth's EMF intensity were recorded. All data pertaining to EMF measures were root-mean-square transformed to assess the time-varying average and imported into SPSS for statistical analysis. We aimed to measure the difference in the intensity of the background geomagnetic EMF fluctuations between when the geometry device was present versus absent. Therefore, difference scores were computed for each of the magnetic vectors (X, Y, orthogonal, and Resultant) in reference to pre-exposure baselines (e.g., prior to the application of the target geometry over the recording device) for each of the geometry devices.

Normality tests revealed several outliers (> 3 STD) that were subsequently removed prior to analysis. The resulting sample size for each geometry was N= 9 for Helmholtz, N = 10 for the Hoberman, N = 11 for the Rodin, and N = 12 for the Toroid. Measures were taken in 2 distinct locations [Neurochemistry (N1) and the and the chamber in the consciousness laboratory (N2)] as outlined in the methods section. A number of comparator devices were created that consisted of varying degrees of copper weavemesh (0, 25, 50, 75, and 100% coverage; N1, N2) wrapped around plastic salad bowls, as well as devices where copper fly mesh was wrapped at varying concentrations around plastic salad bowls (0, 25, 50, and 100%; N1, N2). These comparator geometries were subjected to the same data processing as the target geometries.

4.3.6.2. Determining the Change in the Static Vectorial Intensity of an Incident, Time-Varying EMF as a Function of Physical Application Geometry

The data corresponding to the intensity of the X, Y, and orthogonal vectors, as well as computed Resultant intensities, for measurement either in the presence or following the removal of the inducting field was subjected to a root-mean-square transformation. In addition, the standard deviation of the cycled inducting field was also computed for each condition. All computed variables were entered into SPSS for statistical analysis. Here we aimed to assess a number of parameters and ascertain any differences for the following comparisons: 1) between root-mean-square intensity measures for the magnetic vectors of pre and post exposure measures, 2) between the mean of the change of intensity when the inducing field was present versus absent for each the magnetic vectors, 3) between the standard deviation when the inducting field was present, and 4) the change in deviation when the inducting field was present and absent as a function of geometry. Statistical analyses to confirm differences between geometries was assessed by way of a *one-way* analysis of variance. Data examining the

differences between recording phases were first explored using a MANOVA with intensity as dependent variables, geometry as the between-subject's variables, and recording phase as the within subject's factors. Any significant findings were further evaluated by systematically conducting paired samples t-tests controlling for each geometry with a consideration for significance when $p<.001$ after alpha level correction.

4.3.6.3. Assessing the Change in Induced Voltage through Various Physical Application Geometries in a Faraday Cage and Acoustic Chamber

Data corresponding to the simultaneous recording of the 4 distinct EMF application geometries in the Faraday cage were extracted using two different methods, 1) 60-second raw recordings were extracted and spectrally analyzed within the WinEEG platform, and 2) 60-second raw recordings were manually extracted, imported into SPSS, standardized (i.e., z-transformed), and subjected to spectral analysis. Both extraction methods were conducted on 3 different time points within the 30-minute recording period corresponding to minutes 1, 15, and 30 of the raw record. Extraction method 1 yielded power measures (uV^2/Hz) for 6 distinct frequency bins akin to the classical EEG frequencies: delta (1 – 4 Hz), theta (4 – 7 Hz), alpha (8 – 13 Hz), beta 1 (14 – 20 Hz) beta 2 (21 – 30 Hz), and gamma (30^+ Hz). In addition to power measures, peak frequency values for each of the classical EEG bins were extracted and their means for the 3 recording phases were computed for comparisons. The date for the power derived from extraction method 1 was entered into a MANOVA with geometry as the between-subject's factors and frequency bin (6) and phase of measurement (3) as the within subject's factors. The computed mean for the peak frequencies were entered into a *one-way* analysis of variance to determine any differences between geometry devices. For extraction method 2, the resultant spectral data was binned into 1 Hz increments between 1 and 50 Hz (1 Hz = 1.00 Hz to 1.99

Hz) for each of the recording phases before being subjected to a MANOVA with geometry as the between-subject's factors and frequency (50) and recording phase (3) as the within subject's factors. Tukey's post-hoc tests were employed to discern the driving factors when *one-way* analyses of variance were considered significant while serial *one-way* analyses of variance and paired samples t-tests served as the post-hoc analyses to discern driving forces when MANOVAs were conducted.

4.3.6.4 Characterizing the Change in the Static EM Background Intensity as a Function of Application Geometry in a Standard Incubator

Three independent replicates measuring changes in the background intensity were completed for each condition. The data was extracted, imported into Excel for computation of the root-mean-square and standard deviation values for the intensity of each magnetic vector (X, Y, orthogonal, and Resultant) for the duration of the 5-minute recording segments and subsequently exported into SPSS for statistical analysis. Any global changes between each of the recording segments (i.e., field off v. field on) were of interest and therefore were compared to the mean of each intensity for the respective segments. Data was subjected to multivariate analysis of variance with appropriate post-hoc analyses to determine the source of any interaction.

4.4. Results

4.4.1. Determining The Change in Earth's Static Magnetic Field Intensity as a Function of Physical Application Geometry:

One-way analysis of variance examining the change in the RMS and mean intensities for the X, Y, Z and resultant field vectors revealed significant differences in the intensity of the orthogonal component [$F_{(3,42)} = 4.63$, $p = .007$, Ω^2-est = 0.26] and resultant [$F_{(3,42)} = 5.03$, $p = .005$, Ω^2-est = 0.28] for the Earth's field as a function of geometry. Post-hoc analysis suggested that the effect was being driven by the difference in the change of the orthogonal and resultant intensities between the Hoberman geometry and the Helmholtz and Toroid geometries as can be seen in figure 4.4.1.1. Of note, similar results were obtained when looking at mean intensity measures. In order to assess significant within-subject's changes in each of the magnetic field parameters. Paired samples t-tests were conducted that revealed that only the Hoberman geometry demonstrated significant ($p<.05$) differences in the mean orthogonal and resultant intensities when comparing the geometry present condition to the pre-baseline condition. In addition, using the same type of analysis to examine the change in intensities from geometry present condition to the post-exposure measures, only the Hoberman geometry demonstrated an overshoot in intensity for the Z [$t_{(9)} = -5.75$, $p = 2.76 \cdot 10^{-4}$, MD = -50.14] and resultant [$t(9) = -5.39$, $p = 4.37 \cdot 10^{-4}$, MD = -54.45] intensity vectors.

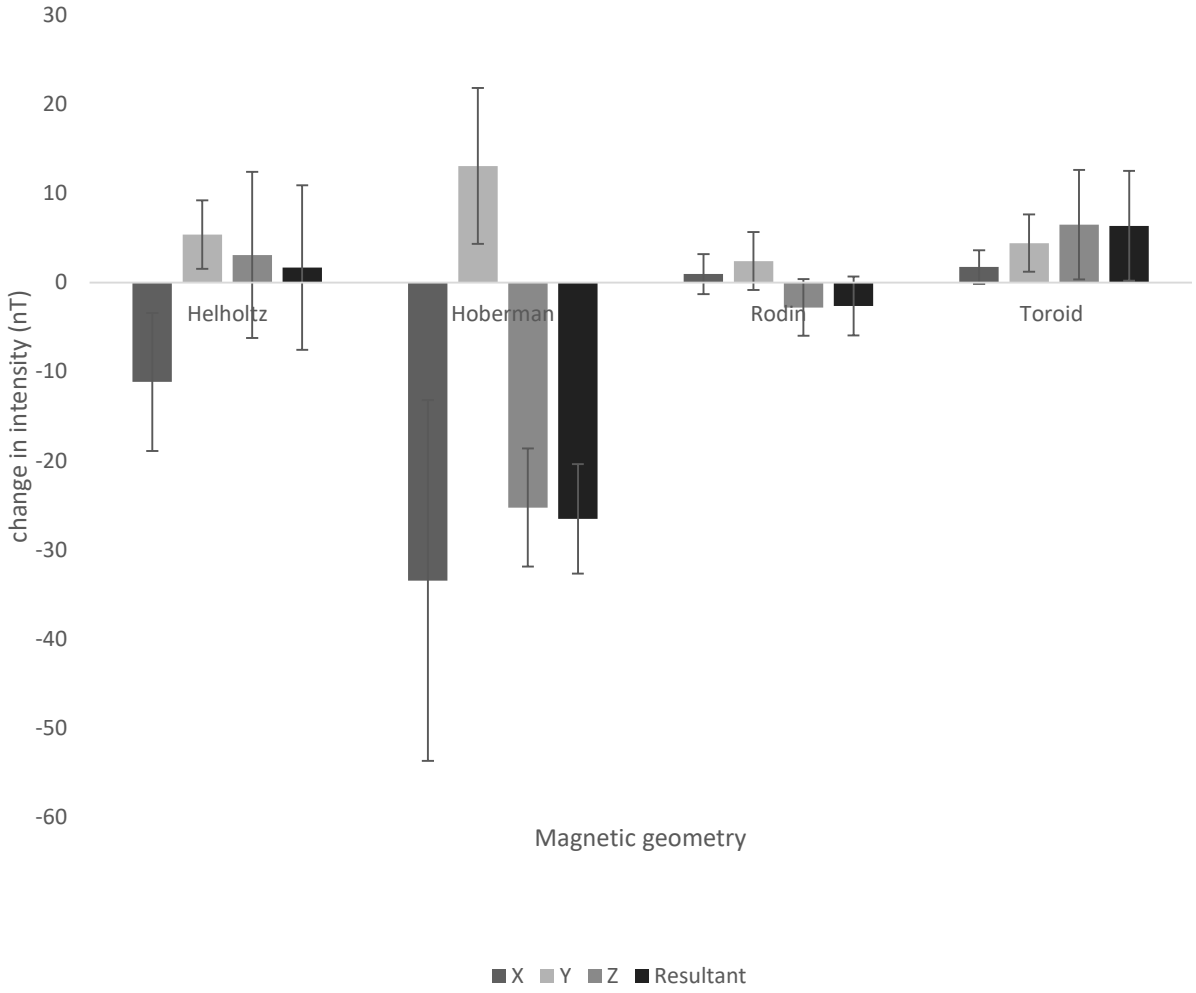

Figure 4.4.1.1: The change in intensity (nT) of the X, Y, Z, and resultant coordinates for Earth's static magnetic field as a function of magnetic geometry. Error bars represent SEMs.

Measure of the magnetic field vectors showed that there was a difference in the change of the static geomagnetic field as a function of the geometry device used for the experiment. After outlier removal (SD>+/-3), there were significant differences observed for the change in the intensity of the orthogonal component [$F_{(12,85)} = 1.98$, $p = .038$, Ω^2-est = 0.25] and the resultant [$F_{(12,85)} = 2.192$, $p = .021$, Ω^2-est = 0.26] intensity of Earth static magnetic field as can be observed in Figure 4.3.1.2. The differences obtained were due to a greater reduction in Earth

static magnetic field (Z and R) were measured with the Hoberman geometry as compared to the 75% covered mesh covered salad bowl.

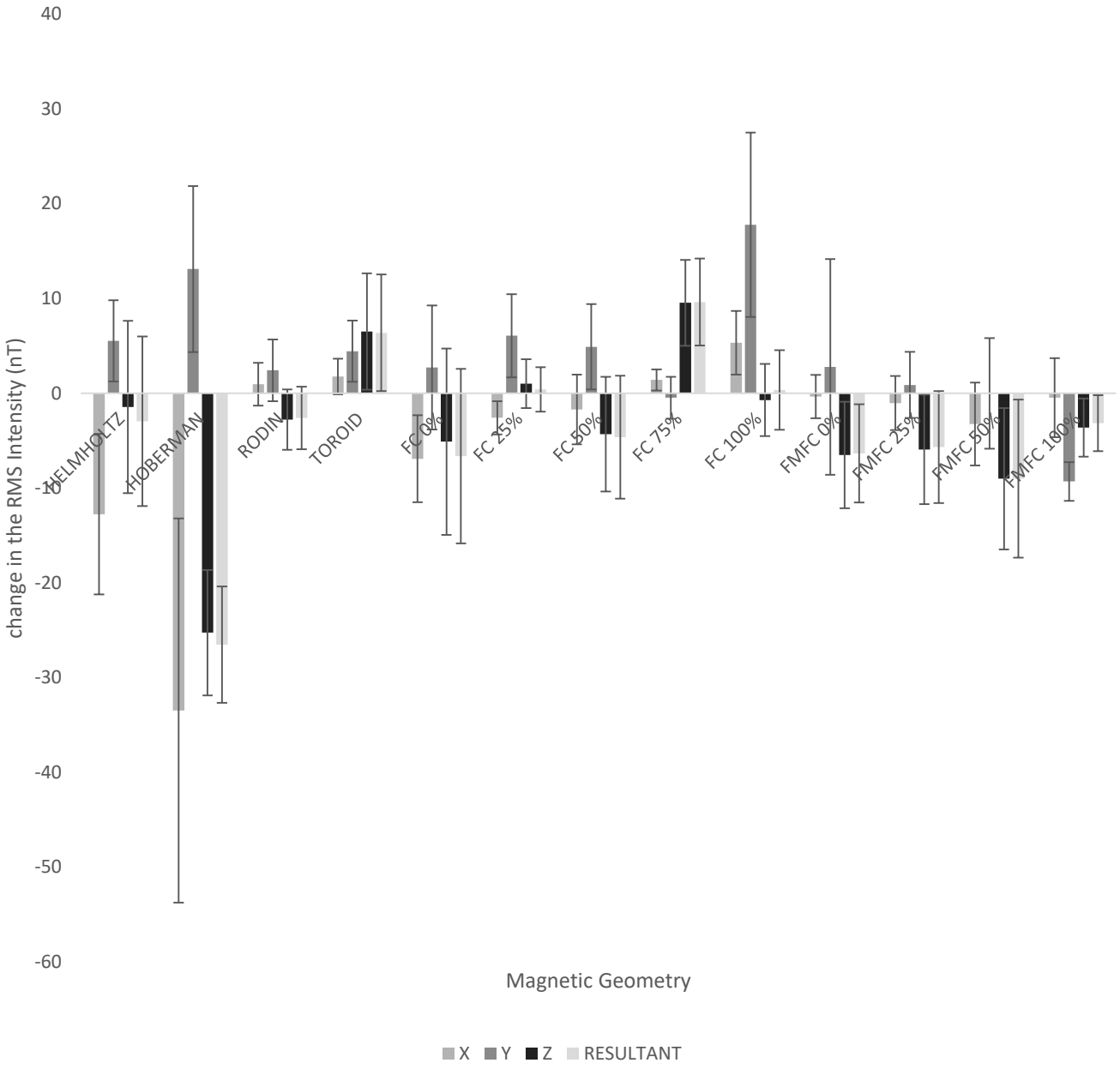

Figure 4.4.1.2: The change of root-mean-square intensity in the rectangular coordinates (X, Y, Z, and Resultant) of Earth's static magnetic field. Error bars represent SEMs. FC refers to copper mesh covered salad bowls, whilst FMFC refers to fly-mesh encapsulated salad bowls. Minimum N=4 for each measure. Each bar has a minimum of 2 different locations embedded within it.

4.4.2. Determining the Change in the Static Vectorial Intensity of an Incident, Time-Varying EMF as a Function of Physical Application Geometry

A comparison of the differences in the mean intensity shifts between when the induced field was present versus when it was absent, the degree of deviation of the mean when the inducting field was present, and the change in deviation between the presence and absence of the inducing field yielded no statistically significant results ($p > .05$) as a function of the geometry device (table 4.4.2.1). Differences in the spatial organization (intensity) contained within each magnetic geometry device was assessed by comparing the pre- to the post-experimental baselines. Exploratory MANOVA demonstrated differences in recording phases for the Y [$F_{(2,64)} = 698.72$, $p < .001$, $\eta^2 = 0.96$], Z [$F_{(2,64)} = 457.50$, $p < .001$, $\eta^2 = 0.93$], and Resultant [$F_{(2,64)} = 456.88$, $p < .001$, $\eta^2 = 0.93$] EMF intensity vectors. Paired samples t-test results demonstrated that there were no significant differences between pre- and post-experimental manipulations as a function of geometry device when alpha level corrections were applied (table 4.4.2.2.).

Table 4.4.2.1: Summary of the means and SEMs (brackets) for the standard deviation (SD) for when the inducting field was active, the change background intensity (field on v. off), and the change in the standard deviation (field on v. off) for each magnetic vector as a function of geometry.

	Field SD (SEM)			**Mean change intensity (SEM)**				**Mean change in SD (SEM)**		
	X-axis	Y-axis	Z-axis	X-axis	Y-axis	Z-axis	Resultant	X-axis	Y-axis	Z-axis
Control	4.06 (0.71)	35.37 (0.97)	19.81 (0.77)	-1.55 (1.50)	-56.28 (3.47)	-34.60 (2.22)	-36.43 (2.39)	0.39 (1.14)	19.93 (1.86)	8.83 (2.45)
Helmholtz	3.78 (0.86)	36.06 (1.59)	20.61 (1.37)	-0.27 (1.48)	-60.59 (1.89)	-32.27 (2.94)	-34.03 (2.92)	1.00 (1.10)	22.79 (1.02)	11.86 (1.68)
Hoberman	2.86 (0.46)	34.24 (0.65)	19.19 (0.99)	1.21 (2.83)	-57.96 (1.34)	-28.61 (3.03)	-30.09 (3.28)	0.86 (0.37)	21.26 (0.78)	11.85 (0.63)
Rodin	3.49 (0.67)	35.56 (1.30)	19.77 (0.96)	-0.12 (1.39)	-53.63 (3.76)	-31.09 (1.73)	-32.64 (1.87)	1.71 (0.46)	21.21 (1.35)	11.94 (0.83)
Toroid	3.10 (0.59)	33.11 (1.23)	18.34 (1.08)	-1.79 (1.98)	-59.35 (5.75)	-33.88 (2.44)	-35.83 (2.57)	0.46 (1.07)	14.11 (5.18)	10.54 (1.67)

Table 4.4.2.2: The mean difference, in nT, between static background magnetic field intensity comparing the pre-exposure baseline to post-exposure baseline conditions as a function of geometry.

	Y-axis			Z-axis			Resultant		
	Mean Diff	T-statistic	P-value	Mean Diff	T-statistic	P-value	Mean Diff	T-statistic	P-value
Control	6.04	1.76	.011	6.43	3.25	.014	6.54	3.00	.020
Helmholtz	8.45	2.48	.048	7.31	2.07	.084	7.60	2.05	.087
Hoberman	6.85	2.02	.083	.066	.018	.986	-0.34	-0.087	.933
Rodin	0.95	0.151	.885	4.93	2.66	.032	4.87	2.93	.022
Toroid	1.89	0.279	.792	4.41	2.54	.143	4.27	1.64	.162

Significance was considered when $p<.001$ after alpha-level correction. Data explored after significant within-subject's time effect was revealed by way of exploratory MANOVA.

4.4.3. Assessing the Change in Induced Voltage through Various Physical Application Geometries in a Faraday Cage and Acoustic Chamber

There were no differences in power and the frequency as a function of the different application geometries for measures of induced voltage through the different magnetic geometry devices measured simultaneously. Data corresponding to classical WinEEG extractions were subjected to a MANOVA with the classical EEG bins and the measurement period as the within-subject's factors was conducted for both differences in frequency and power. Neither measure demonstrated a significant main effect for geometry, either as a between-subject's measure or within-subjects' measure. These effects were not significant when considering the arithmetic

mean of the 3 observation periods. Peak frequencies and power (SPD)for each of the geometries can be observed in table 4.4.3.1.

Table 4.4.3.1: Displays the mean power (SPD; uV^2/Hz) and frequency (Hz) across the three recording phases (beginning, middle, end) of the 30-minute continuous recording across N=7 independent trials. SEMs are reported within the brackets.

	Classical EEG Frequency Bins											
	Delta		Theta		Alpha		Beta1		Beta2		Gamma	
Geometry	*f*	SPD	*f*	SPD	*f*	SPD	*f*	SPD	*f*	SPD	*f*	SPD
Helmholtz	3.68 (0.15)	36.34 (31.67)	4.06 (0.14)	89.86 (79.55)	9.85 (0.15)	127.50 (89.34)	18.35 (0.62)	49.06 (29.27)	20.54 (0.27)	64.15 (33.85)	30.97 (0.65)	25.20 (11.65)
Hoberman	3.72 (0.12)	90.99 (86.48)	3.92 (0.01)	164.99 (141.39)	9.80 (0.15)	147.67 (118.81)	18.75 (0.32)	41.17 (30.10)	20.80 (0.42)	65.70 (42.49)	33.19 (1.43)	24.60 (16.17)
Rodin	3.91 (0.00)	14.34 (9.27)	4.20 (0.18)	74.60 (48.14)	9.74 (0.34)	73.82 (35.50)	18.26 (0.61)	38.62 (17.97)	21.89 (1.06)	121.26 (58.25)	32.89 (1.45)	68.68 (39.01)
Toroid	3.35 (0.41)	95.36 (47.38)	3.97 (0.06)	396.71 (256.25)	9.29 (0.41)	396.03 (212.10)	18.22 (0.82)	62.19 (18.31)	20.74 (0.41)	147.21 (50.25)	32.97 (1.31)	46.92 (13.81)

The raw data extracted according to method 2 was processed for each of the 3 observation periods (min 1, 15, and 30) from a 30-minute measurement across N=7 independent trials. The data was standardized, and subjected to spectral analysis prior to being divided into 50, 1 Hz bins (1 Hz bin = spectral frequencies 1.00 – 1.99 Hz) and then subjected to MANOVA for spectral power density (SPD) by geometry (4 levels) with each observation period (3 levels) and the frequency (50 levels) as within-subjects' factors. This analysis revealed no between- or within-subjects' effect of geometry ($p>.05$) but a main effect for frequency [$F_{(49,1127)} = 20.49$, $p <.001$, $p\eta^2 = 0.47$). Data not shown.

4.4.4. Characterizing the Change in the Static EM Background Intensity as a Function of Application Geometry in a Standard Incubator

Serial (3) MANOVAs were used to identify differences in the background vector intensity measured in a standard incubator when the burst-firing EMF pattern was presented through each of the magnetic geometry devices versus when the field was absent. Analyses of the identified significant within-subjects' field effects for the X-axis [$F_{(1,8)} = 6.02$, $p = .040$, $\eta^2 = 0.43$] and the orthogonal [$F_{(1,8)} = 51.50$, $p< .001$, $\eta^2= 0.87$] but not for the Resultant or the Y-axis ($p>.05$) vectors. The data is summarized in table 4.4.4.1. Furthermore, we found no difference in the mean SD for the burst-firing EMF versus no field conditions for any of the geometries. Serial MANOVAs revealed no significant within-subject's field effect for the orthogonal magnetic vector ($p>.05$), but did reveal significant within-subjects' main effects for the field vectors in the X-axis [$F_{(1,8)} = 6.20$, $p= .038$, $\eta^2= 0.44$] and Y-axis [$F_{(1,8)} =19.20$, $p = .002$, $\eta^2= 0.71$], table 4.3.4.2. There were no geometry-specific effects noted.

Table 4.4.4.1: Mean intensities (nT) comparing the field and no field being generated through each EMF physical application geometry. There is an enhancement when the field is on.

	X-axis				Z-axis			
	Mean (SEM)	MD(SEM)	T-stat	P-value	Mean (SEM)	MD(SEM)	T-stat	P-value
No field	74772.25 (676.12)	-4.23 (1.34)	-3.16	.007	80714.20 (140.48)	6.72 (1.38)	4.86	$2.52 \cdot 10^{-4}$
Field	74776.48 (675.39)				80707.48 (140.77)			

Table 4.4.4.2: Mean of the SD for 5-min recordings of intensity for each of the magnetic vectors. MD refers to the mean difference obtained from the statistical analysis.

	X-axis				Y-axis				Z-axis			
	Mean (SEM)	MD(SEM)	T-stat	P-value	Mean (SEM)	MD(SEM)	T-stat	P-value	Mean (SEM)	MD(SEM)	T-stat	P-value
No field	7.60 (0.41)	1.32 (0.7)	2.33	.040	11.38 (1.33)	-6.04 (1.49)	-4.06	.002	27.31 (2.33)	-0.63 (0.64)	-0.97	.352
Field	6.27 (0.31)				17.42 (1.11)				27.93 (7.22)			

4.5. Discussion:

The results determined in this series of investigations support the idea that differences between physical application geometries can have subtle and discrete effects on magnetic field presentations. Here, we have demonstrated that specific geometries, primarily the Hoberman or dome-like structure, can influence the static (DC) background electromagnetic intensity. These observations were specific for vector direction and the resultant change caused a reduction of approximately 20-30 nT. Although these are relatively weak changes, these features are important because similar intensity fluctuations in geomagnetic storm intensity have been associated with a myriad of behavioural and biological effects (Persinger and Saroka, 2014; Mulligan and Persinger, 2012; Michon and Persinger, 1997; Suess and Persinger, 2001; Persinger, 2001; O'Connor and Persinger, 1997; Bureau and Persinger, 1995; Booth and Persinger, 2005). For example, changes in geomagnetic storm activity has been associated with changes in mood, spontaneous death following induced limbic seizures, and the occurrence of parapsychological phenomena. The mechanism of action, although undetermined in these investigations, is hypothesized to be due to a reduction in ambient noise leading to an increase in the signal-to-noise, or clarity, of the applied signal. Consider the analogy of a room full of people who are all engaged in conversation. The ability to discern a single individual's content amongst the cacophony would be almost incomprehensible. However, if the multitude of difference conversations are reduced to whisper levels and the selected individual's voice remained at a constant volume (i.e., normal talking level), the ability to appreciate their message, as compared to all others, would be enhanced.

It is prudent to determine the relative reduction in energy contained within this system. The equation to determine the energy contained within a volume of a magnetic field is defined by:

$$E = \frac{B^2}{2\mu} \cdot V$$

Where E is the energy ($kg \cdot m^2 s^{-2}$), B is the magnetic field intensity, in Tesla ($kg \cdot A^{-1} s^{-2}$), μ is the permeability of free space ($1.256 \cdot 10^{-6}\ kg \cdot m \cdot A^{-2} s^{-2}$) and V is the volume ($m^3$).

The volume of a dome is defined by:

$$V = 1/6\pi h\ (3a^2 + h^2)$$

Where V is the volume (m^3), h is the height of the dome (m), and the a is the radius of the base (m)

For the Hoberman sphere used in these experiments, the height was 0.15 m and radius of 0.15 m and would yield a volume equal to $7.065 \cdot 10^{-3}\ m^3$. If the resulting change in magnetic field intensity contained within this volume is 20 nT ($2.0 \cdot 10^{-8}\ kg \cdot A^{-1} s^{-2}$), then the energy would be within the order of $1.13 \cdot 10^{-12}$ J. The observed reduction in overall energy is the able to provide the opportunity for any exogenous sources to be detected in terms of Weber's concept of the just noticeable difference that is based upon the reference sensory level as defined by the equation:

$$k = \frac{\Delta I}{I}$$

Where k is a constant, based upon the system under observation, *I* is the original intensity of the stimulus, and ΔI is change in intensity required for the change to be perceived.

A proportional reduction in the original intensity of the stimulus, or the ambient environmental sources acting on the system under observation, would result in a net reduction in the change required in order for the system to "perceive" or respond to the difference applied to it. Here, a reduction in ambient geomagnetic intensity would lower the threshold for the intensity of an applied EMF that is required to have an appropriate effect on the system. Thus, weaker fields would be more impactful provided our hypothesis is correct.

In terms of the ability to effectively shield, or impede, the propagation of an inducting field we have demonstrated that these geometries have minor influences on the variability (standard deviation) of the inducing field's intensity although these effects do not rise to statistical significance. Reduction in variability, in this manner, can be likened to a homogenization of the incoming signal content or to a reduction in complexity of the generated signal. In either case, the fidelity of the incoming signal is reduced and may lose some of its effective qualities as it is impacted by the geometry during its propagation. In this same experiment, small differences, albeit not statistical, were measured between pre- and post-induction measures and may be indicative of a EM storing capacity within different arrangements/configurations of copper wire. Verification is required to further detail and elaborate on this assertion. One experimental feature that may assist in answering this question would be to examine continuous and prolonged induction exposures since intermittent presentations may not have appropriately saturated the local EM containment environment.

Discrete differences were observed between frequency components and power measures when the physical application geometries were measured for voltage fluctuations over the course of a 30-min observation while immersed in a reduced geomagnetic environment. Here again, differences were not statistical. These discrete alterations between the magnetic geometry devices around that copper wire was wound may result in standing waves or resonant cavities that would differ depending on the shape the object, and could be detected as very small differences in intensity or SPD. While these differences did not rise to statistical significance the idea that there are any differences between geometries may be salient. One could postulate that the impact of structure, especially for those structures that significantly overlap, would be discrete and could be obfuscated by statistical tools. Examples, from cosmology and biology, can be used to defend this point of view.

Consider the distortion of the fabric of space-time caused by the presence of large masses interspersed throughout the Universe, and modeled by Einstein's equation for general relativity:

$$R = \frac{8 \pi G}{c^4} T$$

Where R is the curvature (m^{-2}), G is the gravitational constant ($6.67 \cdot 10^{-11}$ $m^3 \cdot kg^{-1}s^{-2}$), c is the speed of light ($3.0 \cdot 10^8 m \cdot s^{-1}$) and T is the stress energy tensor ($kg \cdot m^{-1}s^2$).

Of importance is the stress-energy tensor, and its relation to the energy, and ultimately mass, of the stellar body. If, for example, we compared the space-time distortion of our sun to another star with twice the mass but roughly the same volume, although the change in R is twice that for the

larger star, the overall change in curvature even though it is real and exists is so small that statistically it would be irrelevant. However, even these minute changes in local space-time curvature can be shown to significantly impact the paths of orbiting bodies and the bending of light around the star. In a more biologically relevant context, if we examine lethal doses of certain pharmaceuticals, like fentanyl, and compare them to therapeutic dosages, the difference of a few micrograms is the difference between effective pain management and death. The difference of a few micrograms to a dose of 2 mg would be statistically inconsequential but the resulting effects (i.e., death) would be remarkably impactful.

In our last investigation, there were no differences obtained between each unique magnetic geometry device when a biologically relevant field was being generated through these devices. What was determined, however, was that there was a reduction in the intensity in the orthogonal vector with a concomitant enhancement in the Y-axis intensity when the field was present. These changes were ubiquitous across geometries. When variability was assessed, we observed a trend toward homogeneity (decreased variability) in the X-axis vector, with an associated trend toward heterogeneity (increased variability) in the Y-axis vector but we did not detect any change in the orthogonal vector.

We liken our findings to a change in the signal-to-noise ratio when the field is present. Here, the noise is operationalized as the mean intensity, while the signal is described as the variability. However, rather than the analogy of a conversation we adopt the metaphor of a choir performing to a talkative audience. When the choir is not performing, conversations within the audience dominate but when the choir commences its performance the crowd begins to quiet down (overall

reduction in intensity). As the performance progresses, one begins to appreciate harmonies being vocalized by certain members of the choir (homogenization of signal as measured by a reduction in variability in our experiment) while other portions of the choir are disharmonious singing unique notes (heterogeneity or increased variability in the signal). Taken together, and finishing the analogy, the intermingling of harmonies from one area of the choir combined with the disharmonious aspects of another, as a gestalt, leads to a beautiful aggregate of enchanting melodies.

In summary, unique geometric configurations of aggregates of copper wire built to serve as magnetic field generating devices demonstrate unique characteristics in terms of their effects on altering the ambient EM environment. These changes allow for reduced environmental noise in the order of 20-30 nT, allowing for a reduction in the intensity of change required for the system to identify and respond just noticeable effects. Applied EMF stimuli through these geometries may not be different depending in the application investigated. Further research may reveal statistical features of EM storing capacity, under different experimental conditions, as well as demonstrating unique frequency and power distributions of induced voltage fluctuations.

4.6 References:

Bach, R., Pope, D., Liou, S. H., & Batelaan, H. (2013). Controlled double-slit electron diffraction. *New Journal of Physics*, *15*(3), 033018.

Booth, J. N., Koren, S. A., & Persinger, M. A. (2005). Increased feelings of the sensed presence and increased geomagnetic activity at the time of the experience during exposures to transcerebral weak complex magnetic fields. *International Journal of Neuroscience*, *115*(7), 1053-1079.

Bureau, Y. R. J., & Persinger, M. A. (1995). Decreased latencies for limbic seizures induced in rats by lithium-pilocarpine occur when daily average geomagnetic activity exceeds 20 nanoTesla. *Neuroscience letters*, *192*(2), 142-144.

Cherry, N. (2002). Schumann Resonances, a plausible biophysical mechanism for the human health effects of Solar. *Natural Hazards*, *26*(3), 279-331.

Cook, C. M., & Persinger, M. A. (1997). Experimental induction of the "sensed presence" in normal subjects and an exceptional subject. *Perceptual and Motor Skills*, *85*(2), 683-693.

Crosby, E. C. T., Humphrey and EW Lauer 1962 Correlative Anatomy of the Nervous System.

Eibenberger, S., Gerlich, S., Arndt, M., Mayor, M., & Tüxen, J. (2013). Matter–wave interference of particles selected from a molecular library with masses exceeding 10000 amu. *Physical Chemistry Chemical Physics*, *15*(35), 14696-14700.

Forte, J. G., J. A. Black, T. M. Forte, T. E. Machen, and J. M. Wolosin. "Ultrastructural changes related to functional activity in gastric oxyntic cells." *American Journal of Physiology-Gastrointestinal and Liver Physiology* 241, no. 5 (1981): G349-G358.

Garey, L. J., & De Courten, C. (1983). Structural development of the lateral geniculate nucleus and visual cortex in monkey and man. *Behavioural Brain Research*, *10*(1), 3-13.

Humphries, C., Liebenthal, E., & Binder, J. R. (2010). Tonotopic organization of human auditory cortex. *Neuroimage*, *50*(3), 1202-1211.

Jass, J. R., & Filipe, M. I. (1981). The mucin profiles of normal gastric mucosa, intestinal metaplasia and its variants and gastric carcinoma. *The Histochemical journal*, *13*(6), 931-939.

Mach, Quoc Hao, and Michael A. Persinger. "Behavioral changes with brief exposures to weak magnetic fields patterned to stimulate long-term potentiation." *Brain research* 1261 (2009): 45-53.

Martin, L. J., & Persinger, M. A. (2003). Spatial heterogeneity not homogeneity of the magnetic field during exposures to complex frequency-modulated patterns facilitates analgesia. *Perceptual and motor skills*, *96*(3), 1005-1012.

Michon, A. L., & Persinger, M. A. (1997). Experimental simulation of the effects of increased geomagnetic activity upon nocturnal seizures in epileptic rats. *Neuroscience Letters*, *224*(1), 53-56.

Morris, R., Amaral, D., Bliss, T., & OKeefe, J. (2007). The hippocampus book. *Anderson, P*, 872.

Mulligan, B. P., & Persinger, M. A. (2012). Experimental simulation of the effects of sudden increases in geomagnetic activity upon quantitative measures of human brain activity: validation of correlational studies. *Neuroscience Letters*, *516*(1), 54-56.

O'connor, R. P., & Persinger, M. A. (1997). Geophysical variables and behavior: LXXXII. A strong association between sudden infant death syndrome and increments of global geomagnetic activity—possible support for the melatonin hypothesis. *Perceptual and motor skills*, *84*(2), 395-402.

Parent, A. (1996). *Carpenter's human neuroanatomy*. Williams & Wilkins.

Persinger, M. A. (2001). The neuropsychiatry of paranormal experiences. *The Journal of neuropsychiatry and clinical neurosciences*, *13*(4), 515-524.

Persinger, M. A., & Healey, F. (2002). Experimental facilitation of the sensed presence: Possible intercalation between the hemispheres induced by complex magnetic fields. *The Journal of nervous and mental disease*, *190*(8), 533-541.

Persinger, M. A. (2003). The sensed presence within experimental settings: implications for the male and female concept of self. *The Journal of Psychology*, *137*(1), 5-16.

Persinger, M. A., & Saroka, K. S. (2014). Quantitative support for convergence of intrinsic energies from applied magnetic fields and "noise" fluctuations of Newton's gravitational value within the human brain. *International Letters of Chemistry, Physics and Astronomy*, *19*(2), 181-190.

Persinger, M. A., Dotta, B. T., Karbowski, L. M., & Murugan, N. J. (2015). Inverse relationship between photon flux densities and nanotesla magnetic fields over cell aggregates: Quantitative evidence for energetic conservation. *FEBS open bio*, *5*(1), 413-418.

Reid, R. C., & Shapley, R. M. (1992). Spatial structure of cone inputs to receptive fields in primate lateral geniculate nucleus. *Nature*, *356*(6371), 716.

Riedel, G., & Micheau, J. (2001). Function of the hippocampus in memory formation: desperately seeking resolution. *Progress in Neuro-Psychopharmacology and Biological Psychiatry*, *25*(4), 835-853.

Schlegel, K., & Füllekrug, M. (1999). Schumann resonance parameter changes during high-energy particle precipitation. *Journal of Geophysical Research: Space Physics*, *104*(A5), 10111-10118.

Sedar, A. W., & Friedman, M. H. F. (1961). Correlation of the fine structure of the gastric parietal cell (dog) with functional activity of the stomach. *The Journal of Cell Biology*, *11*(2), 349-363.

Selleri, F. (Ed.). (1992). *Wave-particle duality* (p. 187). London: Plenum Press.

Suess, L. A. H., & Persinger, M. A. (2001). Geophysical variables and behavior: XCVI.“Experiences” attributed to Christ and Mary at Marmora, Ontario, Canada may have been consequences of environmental electromagnetic stimulation: implications for religious movements. *Perceptual and motor skills*, *93*(2), 435-450.

Talavage, T. M., Sereno, M. I., Melcher, J. R., Ledden, P. J., Rosen, B. R., & Dale, A. M. (2004). Tonotopic organization in human auditory cortex revealed by progressions of frequency sensitivity. *Journal of neurophysiology*, *91*(3), 1282-1296.

Thibodeau, G. A., Patton, K. T., & Wills. (2004). *Structure & function of the body*. St Louis: Mosby.

Williams, E. R. (1992). The Schumann resonance: A global tropical thermometer. *Science*, *256*(5060), 1184-1187.

Chapter 5

5.1 General Discussion

Throughout the experiments presented, we have described unique features that were associated with the temporal structure of electromagnetic fields and the material (physical) sources from that these field are generated. In our discovery, we have characterized the effectiveness of burst-firing EMF, a pattern that was derived from the activity of amygdaloid-hippocampal cells, and its synergisms with respect to sub-micromolar concentrations of forskolin in a cell model of neuritogenesis. In this endeavour, we were successful at determining the most appropriate pattern as well as discussing the relevance of exposure duration, identified the role of intensity and timing, and attempted, albeit in vein, to demonstrate the biomolecular course of action that accommodates the observed changes with respect to concomitant treatments to burst-firing EMF and chemical stimulation with forskolin. We have likened our findings to that of a well constructed narrative and presented this as an analogy for the resonance-like phenomenon that has been attributed to what we have measured. Caution is recommended in interpreting these results and utilizing this analogy as more data may provide conflicting evidence suggestive of a more appropriate mechanism.

Our findings suggest that the pattern (described as the content of a narrative) of EMF exposure is important to the activation of PC-12 cells to respond with extensions of their plasma membrane (i.e., neurites) secondary to chemical stimulation with forskolin. While the volume (intensity) and the speed at that the narrative is read (alterations in the point duration and inter-stimulus delay, or successive presentations of the same pattern) contribute very little to the effectiveness of the

patterned EMF, at least in this model of observation. Duration of exposure also seems to mitigate and contribute, at least in part, to the effectiveness of the target pattern with trends towards a greater proportion of plasma membrane extensions measured with longer durations. If one assumes, as is the case with list-learning tasks or rote memorization, that the greater the number of iterations of the important information the more likely that the message is to be appropriately interpreted and remembered. It was also determined that different forms of EMF energy (i.e., rotating EMF vs. patterned EMF generated through solenoids) produce different results. If we continue with the analogy of a narrative of instructions that direct a system to respond in a certain way, then we can consider the form of EMF energy as the "language" of the narrative. Consider that we liken the system of observation to the auditory cortex of an individual whose primary language of communication and comprehension is English with no exposure to other languages. Then, and only then, if the language of instruction is presented in English will they respond congruently to the directions presented and accurately perform whatever task is requested. However, if the same set instructions were presented to the English speaker in German, the likelihood that the individual will accurately complete the task is reduced. Similarly, if the energy or the form of the EMF is incorrect or incongruent with the system that it is designed to affect that system may respond in an unpredictable manner or will not react to the stimulus.

What was also determined was that distinct apparatuses wrapped in copper wire to create unique geometric configurations through that patterned EMFs are generated, can impact the effectiveness of said field. The changes observed with respect to unique structures around that copper wire is wrapped either enhanced or reduced the proportion of plasma membrane extensions in a PC-12 model of neuritogenesis, as well as affecting measurements of ultra-weak photon emission (UPE)

from melanoma cultures. In some way, the physical nature of the EMF-generating device has impacted correlates of function (i.e., differentiation and UPE spectral profiles), in such a way that the differences obtained can identify the equipment used during the experiment.

We have argued, at least from the perspective of biology, that structure dictates function and provided a series of examples that supported this assertion. Considering that the geometric configuration around that copper wire is wrapped may impact the biological relevance of an applied EMF further investigation is required. If we adapt our analogy of a narrative or language and shift it to the perspective of creating music by way of an instrument, we may be able to shed some light on these features. Consider an acoustic guitar and a guitarist who is instructed to repeatedly play a series of musical scales. In a standard setting, with standard equipment, each of the notes ring clearly and produce harmonious and concordant tones. Now, if we were to introduce an altered instrument whose housing was cuboid rather than bulbous in shape, and the artist was asked to play the same scales again the perception of the notes would be different and may be interpreted as discordant. Changes in the structure will ultimately change the function, even slightly. The greater the change in a structure the greater the noticeable difference.

Our results suggest that unique geometric organizations around that copper wire is wrapped, especially when that shape approaches a dome, can reduce the ambient, static magnetic background. Furthermore, the individual geometries respond in subtle, albeit not statistically significant, manners to a myriad of physical manipulations. This would suggest that the geometries used in the experiments respond in a manner similar to that of individual differences. Again, we have defended that even though the observed differences may be small and statistically

insignificant, that they are not inconsequential. As a whole, this project demonstrates, at least provisionally, that the equipment employed as the source generator for EMFs is important to the bio-effectivity of the pattern of that EMF. Future endeavours should aim to identify whether the complexity of the physical application geometry can influence 3-dimensional models, as all investigations conducted in this thesis examined the relevance in electromagnetic field physical application geometry in 2-dimensional samples.

5.2 Implications and Future Directions

The results demonstrated in this thesis have shown the potential to use patterned EMF in combination with forskolin to promote neurite outgrowth in PC-12 cells. The implications of such work would constitute the foundation for EMF-mediated therapeutic intervention especially in Parkinson's disease (PD). A hallmark neurophysiological correlate of PD is the deterioration of midbrain dopaminergic cells most notably within the substantia nigra (Lang and Obeso, 2004**)**. Reconstituting dopamine supplies, either by promoting cell survival or with cell replacement, would be of marked benefit to the individual. It is important to note that PC-12 cells induced to form neurites as demonstrated in the model outlined in this document, have been shown to respond to dopamine stimulation and actively undergo dopamine neurotransmission (Kozminki et al., 1998; Loder and Melikian, 2003; Ohare-Imaizumi et al., 1991; Pothos et al., 1998). Cell replacement, either by direct injection or vector assisted implantation, with PC-12 cells followed by treatment with forskolin or nerve growth factor (NGF) in combination with exposures to burst-firing EMF may serve as a cost-effective alternative for the treatment of PD. However, *in vivo* studies would have to be conducted in order to assess the efficacy of this methodology.

Prior to *in vivo* analysis, functional features of PC-12 cells induced to promote neuritogenesis by way of forskolin and burst-firing EMF exposures, must be identified. In this vein, it would be prudent to assess any and all alterations in dopamine synthesis and neurotransmission and typify these reactions as approximating normal, healthy functioning cells. In so doing, we would be able to examine whether burst-firing EMF exposure is represented functionally in the activity of these cells by assessing pulse-rate using patch-clamp technology. These investigations may demonstrate the influence that point duration and inter-stimulus interval have on the activity of these cells, a feature that may have been overshadowed by solely measuring morphology. Comparing EMF treated samples to what is normally occurring in fully functional systems would allow us to potentially tailor our treatments to best suit the requirements of the system. Functional analysis (i.e., assessing firing rate, dopamine concentration, dopamine response reactions, etc.) of these cells would not only rule out changing the temporal structure of the applied pattern, it would also demonstrate the potential contribution of intensity.

An additional feature in PD is neurodegeneration subsequent to L-DOPA treatment as well as the naturally occurring changes associated with disease progression **(**Meredith et al., 2008; Zhang et al., 2005**)**. It would be of interest then to challenge our PC-12 cells induced to generate neurites when presented with the combination of forskolin an burst-firing EMF with L-DOPA or MPP^+ (a chemical agent that induces PD-like symptoms *in vivo*) and measure cell integrity and survival as some data has been collected has shown that induced PC-12 cells respond by undergoing apoptosis when challenged with L-DOPA (Park et al., 2012; Velez-Pardo et al., 1997; Walkinshaw and Waters, 1995) and MPP^+ (Xu et al., 2017; Santos et al., 2015; Zhu et al., 2012). These

investigations would provide insight to the neuroprotective value of burst-firing EMF on these cells. Based on the findings in this latter study, we may design additional experiments, such as the investigation of burst-firing EMF treatment following forskolin or NGF induced neuritogenesis, as an adjunct therapy to L-DOPA treatment or as a standalone treatment regime for neuroprotection against neurodegeneration.

Although the data collected here has implicated pharmaco-magnetic synergisms for neurite formation, no underlying mechanism has been identified. We propose additional investigations to effectively discern the biomolecular mechanism of action in a step-wise fashion. In the first phase, completing a treatment course with burst-firing EMF and inhibitors, as outlined in Chapter 2, would serve as a screening method for the identification of downstream effects that drive the observed morphological changes. In the second phase, manipulating specific targets identified by first phase experiments such that they become constitutively active/inactive and exposing these systems to our pharmaco-magnetic stimulations would be revealing. These latter investigations would provide more insight to other potential chemical agents that could be used as a more cost-effective replacement for forskolin. Additionally, identifying the appropriate pathway of action and sequential timing of the events within the cascade leading to neurite outgrowth, would allow for the development of specifically patterned EMF configurations and application regimes that could completely circumnavigate chemical manipulation. Our data collection was also limited in duration (1 hour exposures) to the burst-firing EMF and single treatments of forskolin. We suggest further exploration into the duration of EMF exposure by assessing lengthier treatments (i.e., 6, 12, and 24 hours), multiple EMF exposures over the course of neurite development (i.e., 6 hours per day for 3 days), multiple stimulations with forskolin (i.e., 0.5 μM a day for 3 days), and the

combination of such manipulations. The aim, again, is to ultimately demonstrate the utility of patterned EMF exposures to best maximize neurite production, higher order branching, and inter-cellular contacts, as a means to identify the effective treatment regime necessary to assist in PD management.

5.3 References

Kozminski, K. D., Gutman, D. A., Davila, V., Sulzer, D., & Ewing, A. G. (1998). Voltammetric and pharmacological characterization of dopamine release from single exocytotic events at rat pheochromocytoma (PC-12) cells. *Analytical chemistry*, *70*(15), 3123-3130.

Lang, A. E., & Obeso, J. A. (2004). Challenges in Parkinson's disease: restoration of the nigrostriatal dopamine system is not enough. *The Lancet Neurology*, *3*(5), 309-316.

Loder, M. K., & Melikian, H. E. (2003). The dopamine transporter constitutively internalizes and recycles in a protein kinase C-regulated manner in stably transfected PC-12 cell lines. *Journal of Biological Chemistry*, *278*(24), 22168-22174.

Meredith, G. E., Sonsalla, P. K., & Chesselet, M. F. (2008). Animal models of Parkinson's disease progression. *Acta neuropathologica*, *115*(4), 385-398.

Ohara-Imaizumi, M. I. C. A., Nakazawa, K., Obama, T. O. M. O. K. O., Fujimori, K., Takanaka, A. K. I. R. A., & Inoue, K. A. Z. U. H. I. D. E. (1991). Inhibitory action of peripheral-type benzodiazepines on dopamine release from PC-12 pheochromocytoma cells. *Journal of Pharmacology and Experimental Therapeutics*, *259*(2), 484-489.

Park, K. H., Park, H. J., Shin, K. S., Choi, H. S., Kai, M., & Lee, M. K. (2012). Modulation of PC-12 cell viability by forskolin-induced cyclic AMP levels through ERK and JNK pathways: an

implication for L-DOPA-induced cytotoxicity in nigrostriatal dopamine neurons. *Toxicological Sciences*, *128*(1), 247-257.

Pothos, E. N., Przedborski, S., Davila, V., Schmitz, Y., & Sulzer, D. (1998). D2-Like dopamine autoreceptor activation reduces quantal size in PC-12 cells. *Journal of Neuroscience*, *18*(15), 5575-5585.

Santos, N. A. G., Martins, N. M., Sisti, F. M., Fernandes, L. S., Ferreira, R. S., Queiroz, R. H. C., & Santos, A. C. (2015). The neuroprotection of cannabidiol against MPP+-induced toxicity in PC-12 cells involves trkA receptors, upregulation of axonal and synaptic proteins, neuritogenesis, and might be relevant to Parkinson's disease. *Toxicology in Vitro*, *30*(1), 231-240.

Velez-Pardo, C., Jimenez Del Rio, M., Verschueren, H., Ebinger, G., & Vauquelin, G. (1997). Dopamine and iron induce apoptosis in PC-12 cells. *Pharmacology & toxicology*, *80*(2), 76-84.

Walkinshaw, G., & Waters, C. M. (1995). Induction of apoptosis in catecholaminergic PC-12 cells by L-DOPA. Implications for the treatment of Parkinson's disease. *The Journal of clinical investigation*, *95*(6), 2458-2464.

Xu, J., Gao, X., Yang, C., Chen, L., & Chen, Z. (2017). Resolvin D1 attenuates Mpp+-induced Parkinson disease via inhibiting inflammation in PC-12 cells. *Medical science monitor: international medical journal of experimental and clinical research*, *23*, 2684.

Zhang, W., Wang, T., Pei, Z., Miller, D. S., Wu, X., Block, M. L., ... & Zhang, J. (2005). Aggregated α-synuclein activates microglia: a process leading to disease progression in Parkinson's disease. *The FASEB Journal*, *19*(6), 533-542.

Zhu, Q., Wang, J., Zhang, Y., & Sun, S. (2012). Mechanisms of MPP+-induced PC-12 cell apoptosis via reactive oxygen species. *Journal of Huazhong University of Science and Technology [Medical Sciences]*, *32*(6), 861-866.

Appendices

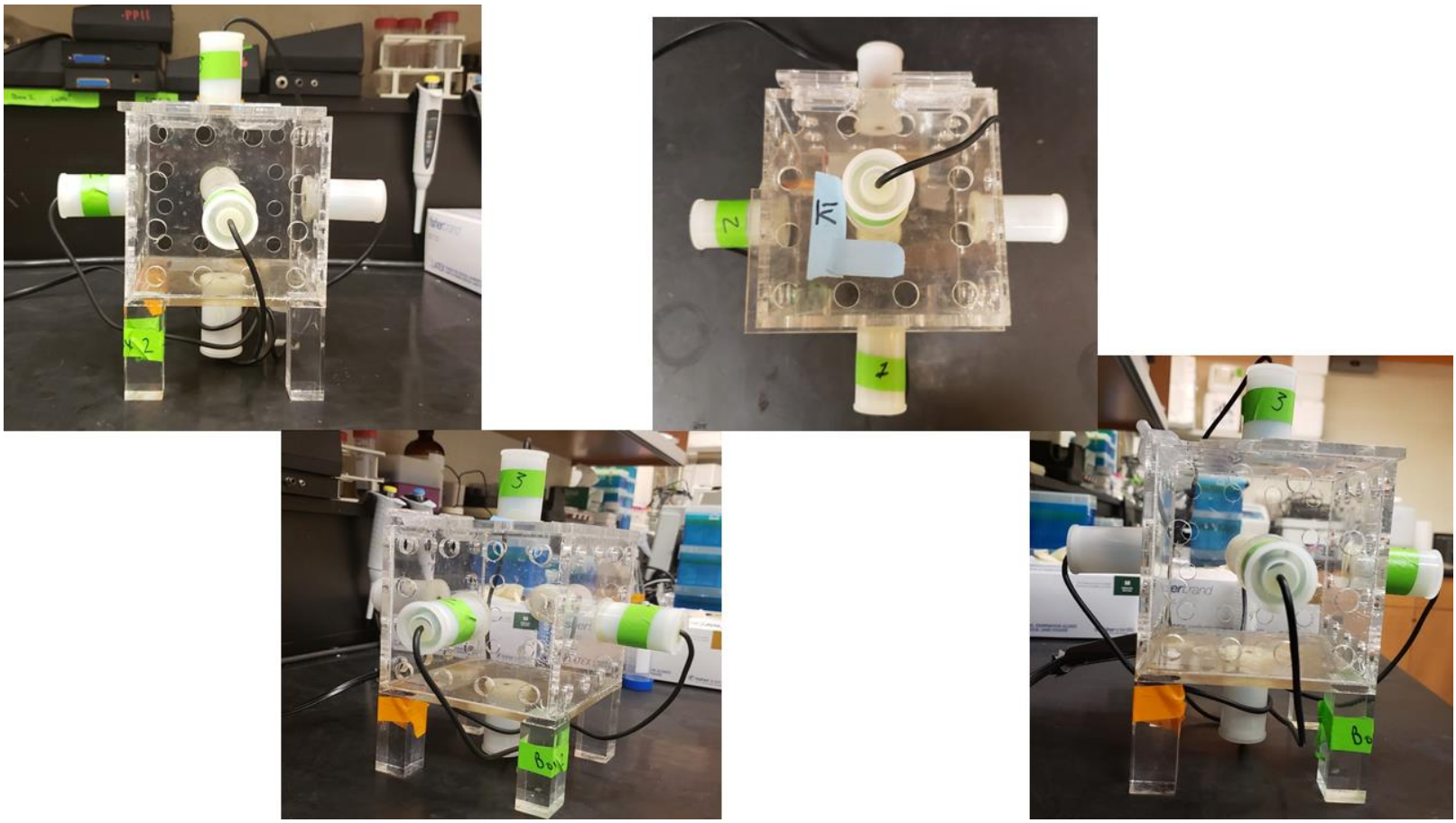

Appendix A1: Photographic representation of the 4-D exposure apparatus from different points of view. Front (top left); Top (Top right), Corner (bottom left), side (bottom right).

Appendix A2: Photographic representation of the 4-D application geometry with corresponding computer generated patterned EMF (computer) and custom built digital-to-analog converter (DAC; blue box).

Appendix B1: Photo of the Resonator.

Appendix B2: Technical specifications and description of the Resonator

(12) United States Patent

Shallcross

US009156709B2

(10) Patent No.: US 9,156,709 B2

(45) Date of Patent: Oct. 13, 2015

U.S.C. 154(b) by 1186 days.

(21) Appl. No.: 12/096,063

(22) PCT Filed: Dec. 6, 2006

(86) PCT No.: PCT/CA2006/001984

§ 371 (c)(1),
(2), (4) Date: Jun. 4, 2008

(87) PCT Pub. No.:

(Continued)

FOREIGN PATENT DOCUMENTS

CA 2526977 Al 4/2006
CA 2488776 Al 6/2006

OTHER PUBLICATIONS

---

(54) MULTI-ROTATOR MAGNETIC RESONATOR EMBODYING SACRED GEOMETRY

(76) Inventor: Kim Shallcross, Milton (CA)

(*)

7/2000 Saho et al. Notice: Subject to any disclaimer, the term of this8/2000 Saho et al. patent is extended or adjusted under 351/2001 Kim

W02007/065257

PCT Pub. Date: Jun. 14, 2007

(65) Prior Publication Data

US 2008/0296162 Al Dec. 4, 2008

(30) Foreign Application Priority Data

Dec. 6, 2005 (CA) _____ 2526977

(51) Int. Cl.

C02F 1/48 (2006.01)

C02F 1/00 (2006.01)

A 61N 2/06 (2006.01)

(56) References Cited

U.S. PATENT DOCUMENTS

5,942,961 A *
6,093,318 A
6,103,113 A
6.171.490 B1

8/1999 Srail et al. 335/284

A61N 2/12 (2006.01)

HOIF 7/02 (2006.01)

(52) U.S. Cl.
CPC . C02F 1/005 (2013.01); A61N2/06 (2013.01); A61N2/12 (2013.01); C02F 1/481 (2013.01), HOIF 7/0294 (2013.01)

(58) Field of Classification Search
CPC ..... C02F 1/005; C02F 1/48; C02F 1/481 :C02F 1/482; 2/06; A61N 2/12 USPC .....
335/306; 210/222Q23•, 600/9 See application file [Or complete search history.

Wikipedia: Magnet Therapy, Dec. 2, 2011, pp. I-5.·
Wikipedia: Magnetic water treatment, Dec. 2, 2011, pp. I-4.· Pitkänen, About Strange Effects Related to Rotating Magnetic Systems, pp. 1-13 (undated).

(Continued)

Primary Examiner — Ramon Barrera
(74) Attorney, Agent, or Firm — Harness, Dickey & Pierce, P.L.C.

(57) ABSTRACT

A magnetic resonator is provided that has a support structure and a plurality of roller assemblies mounted thereto for rotation about respective axes ofrotation that are generally parallel one to another. Drive means are coupled to the roller assemblies to rotate each of the roller assemblies about its respective axis of rotation relative to the support structure. Each roller assembly houses a plurality of magnets disposed along respective axes of the roller assemblies. The plurality of magnets are grouped in a plurality of first and second arrangements with a first arrangement being interspersed between a pair of second arrangements. At least one of the first and second arrangements incorporates a pattern or shape based on sacred geometry.

11 Claims, 7 Drawing Sheets

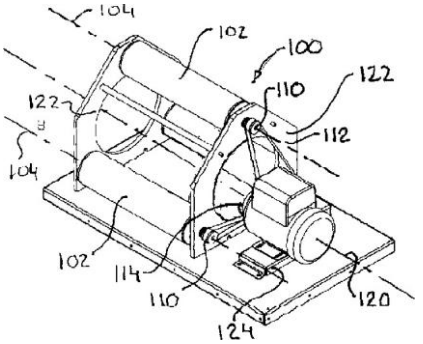

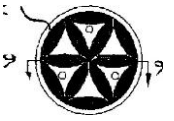

132

(56) References Cited

U.S. PATENT DOCUMENTS

6,208,497 B1 3/2001 Seale et al.
6,277,275 B1 8/2001 Yoshifusa et al.
6,323,647 Bl 11/2001 Anderson et al. 6 B211/2009 Shallcross

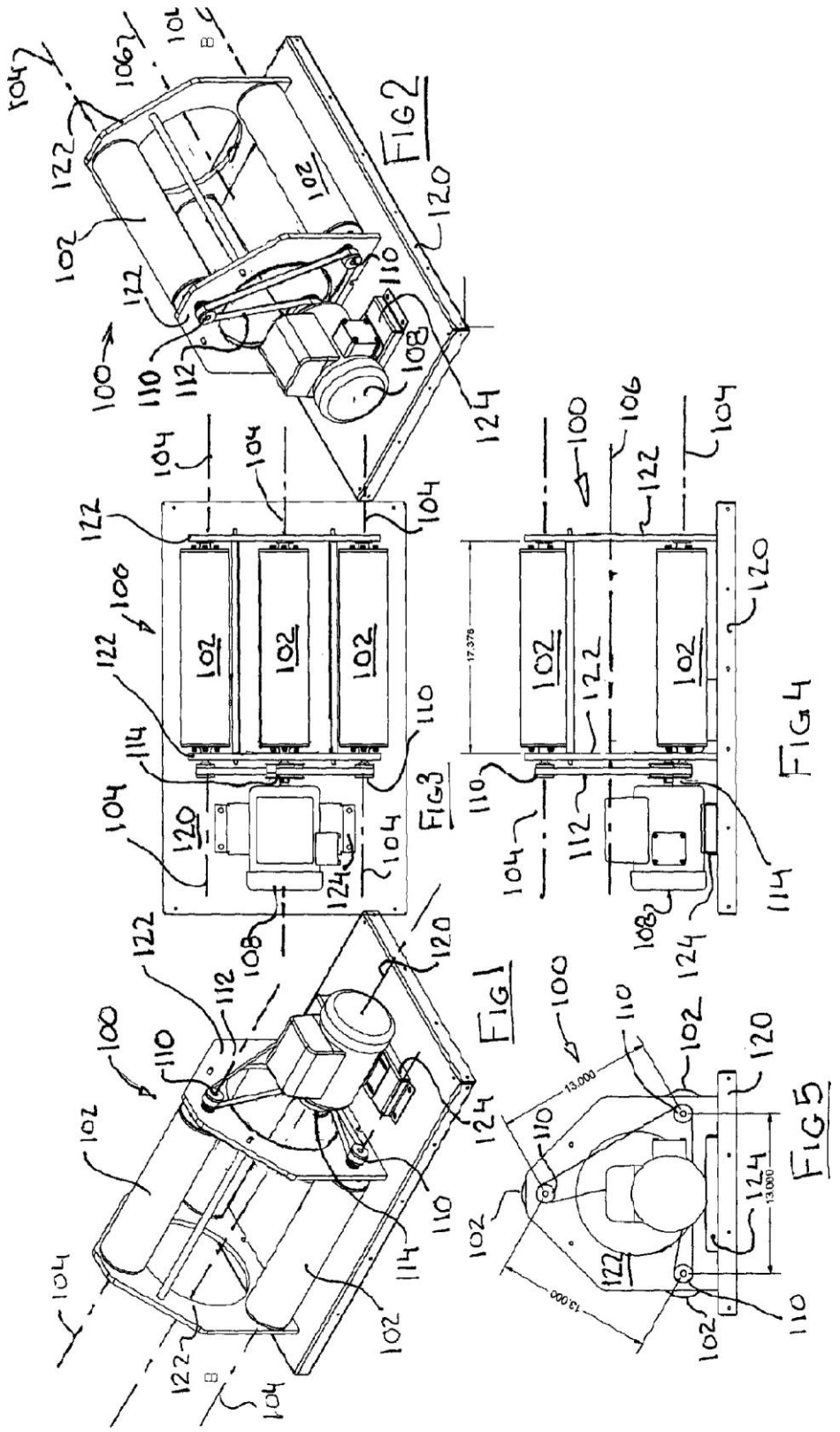
FIG1
FIG2
FIG3
FIG4
FIG5
100
102
104
106
108
110
112
114
120
122
124
17.378
13.000

of

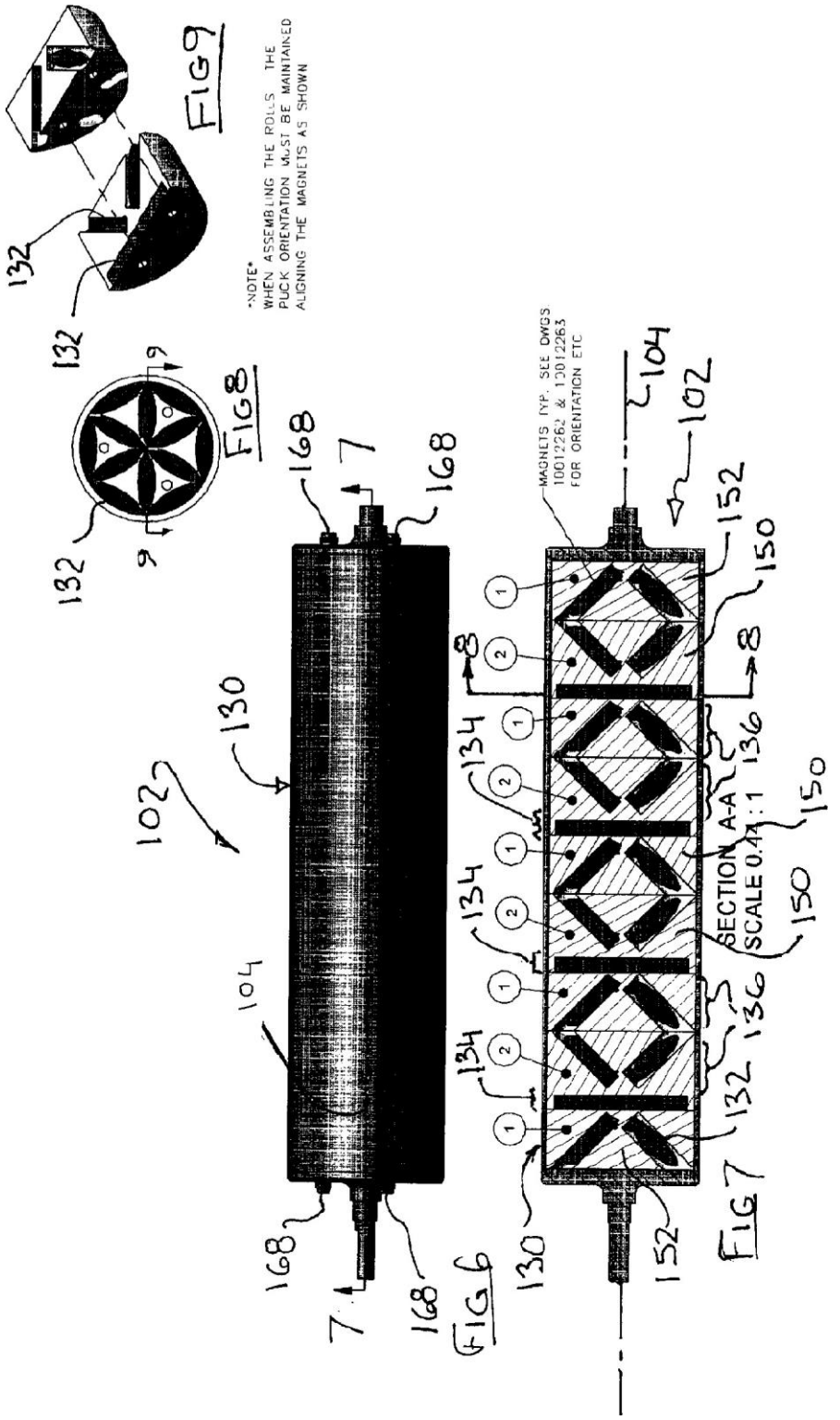
132
132
FIG 9
NOTE
WHEN ASSEMBLING THE ROLLS THE PUCK ORIENTATION MUST BE MAINTAINED ALIGNING THE MAGNETS AS SHOWN
132
9
9
FIG 8
168
7
168
102
130
104
168
7
168
FIG 6
MAGNETS TYP. SEE DWGS 10012262 & 10012263 FOR ORIENTATION ETC
104
102
152
150
8
8
134
136
SECTION A-A
SCALE 0.4 : 1
150
134
136
132
130
152
FIG 7

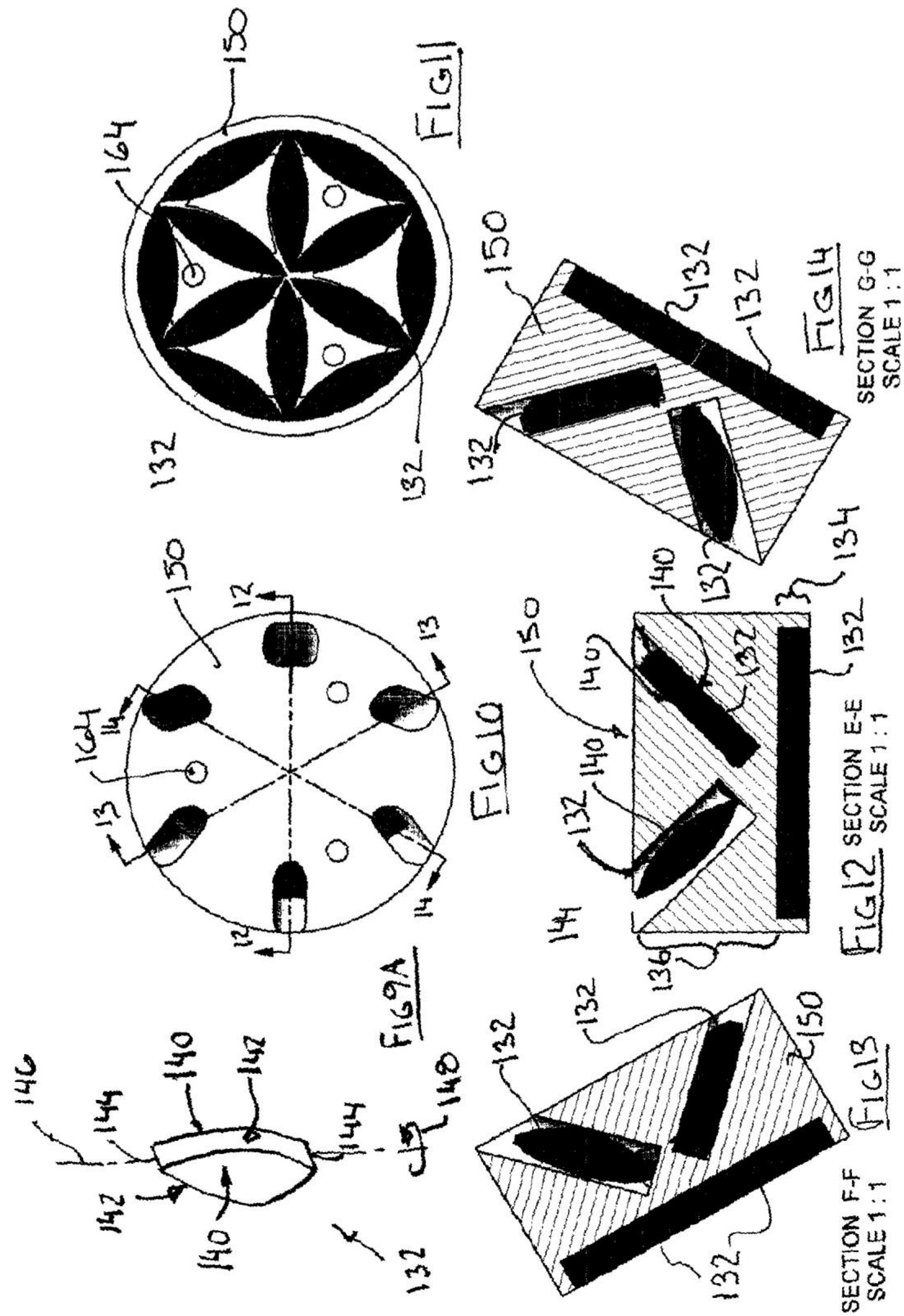
FIG 9A
FIG 10
FIG 11
FIG 12 SECTION E-E SCALE 1:1
FIG 13 SECTION F-F SCALE 1:1
FIG 14 SECTION G-G SCALE 1:1

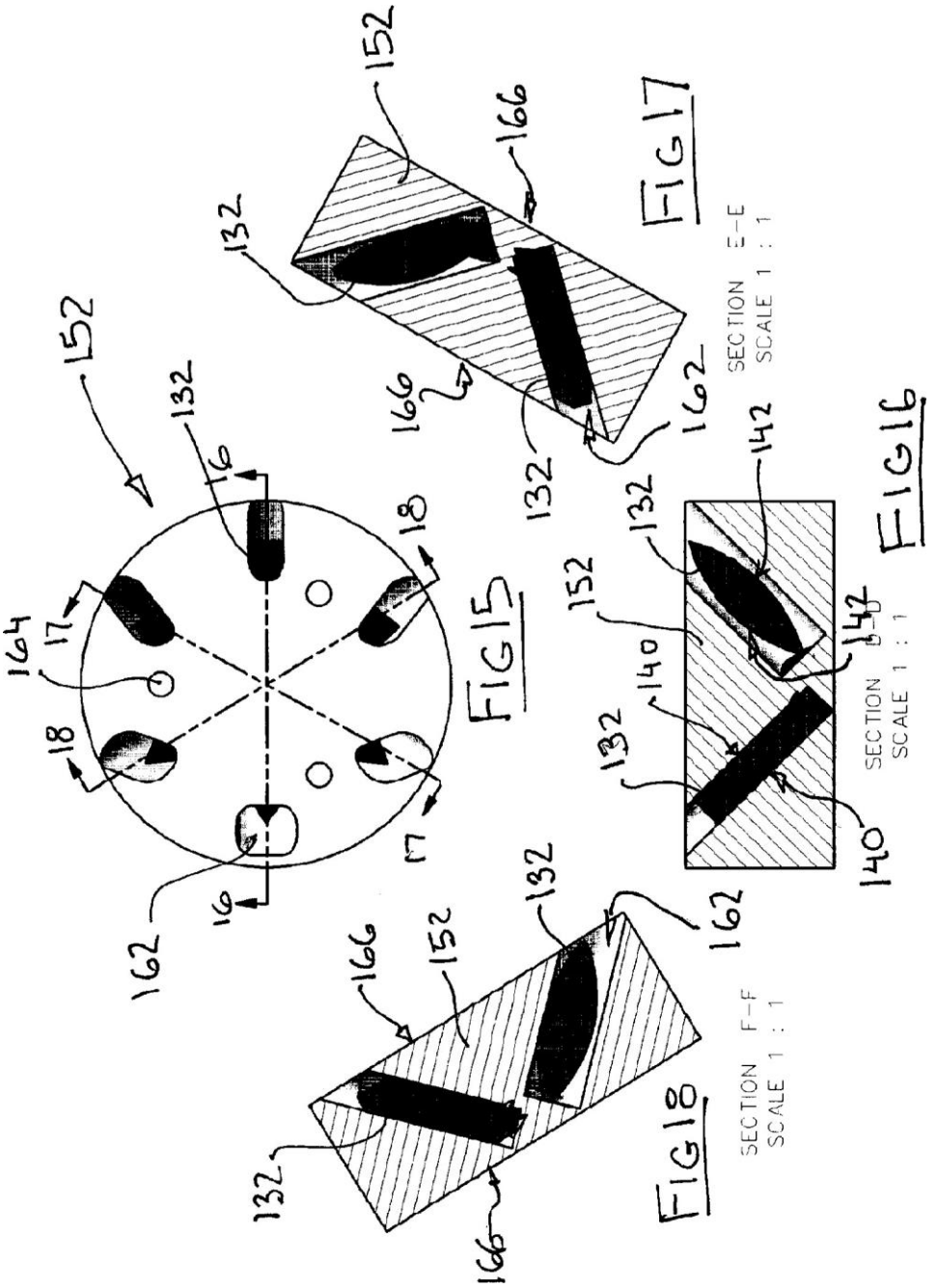

FIG 15

FIG 16

FIG 17

FIG 18

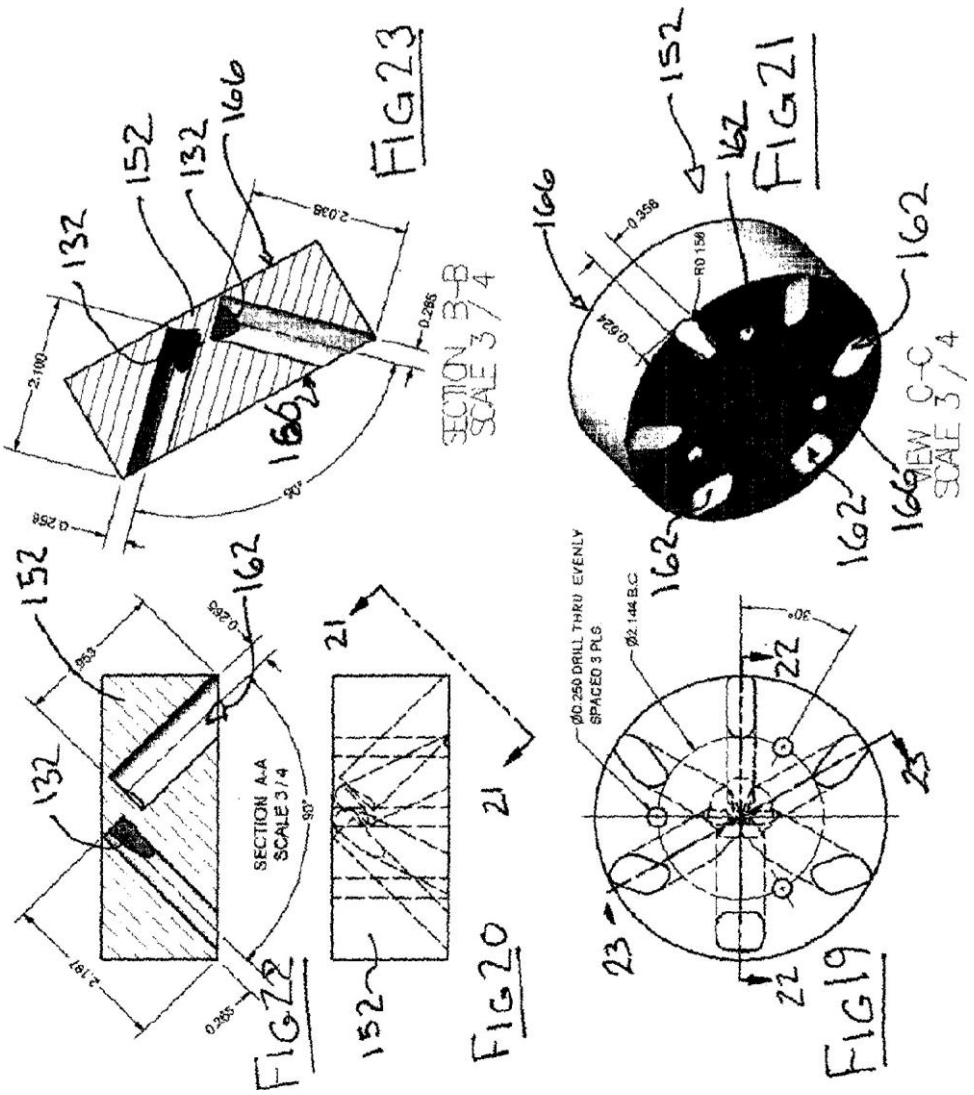

FIG 22

FIG 20

FIG 23

FIG 19

FIG 21

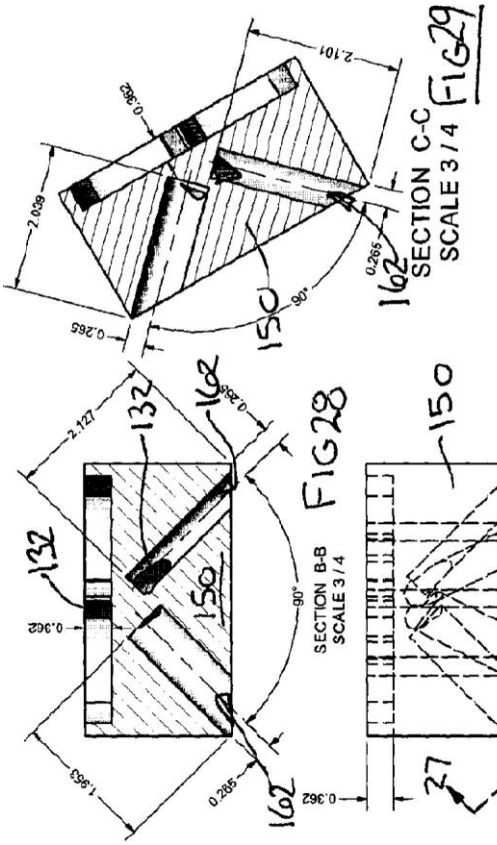

FIG29 FIG28 FIG26

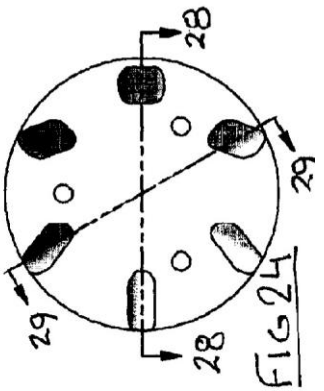

FIG24

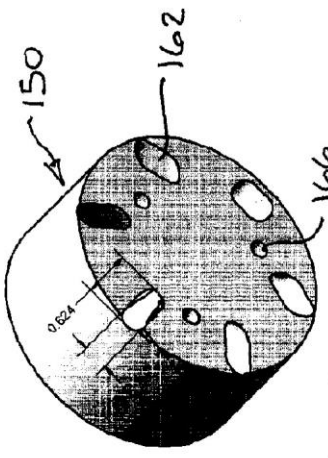

FIG27

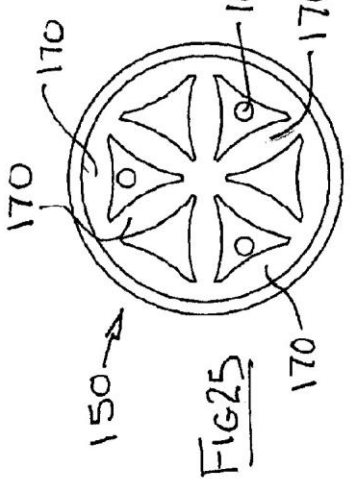

FIG25

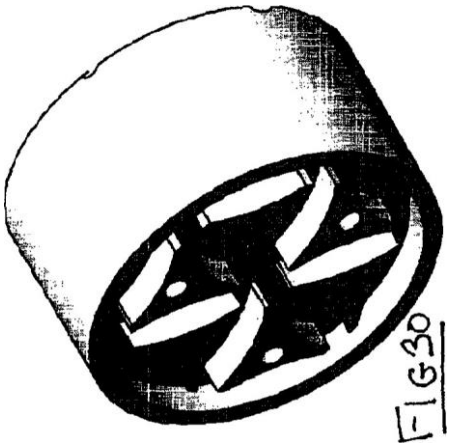

FIG 30

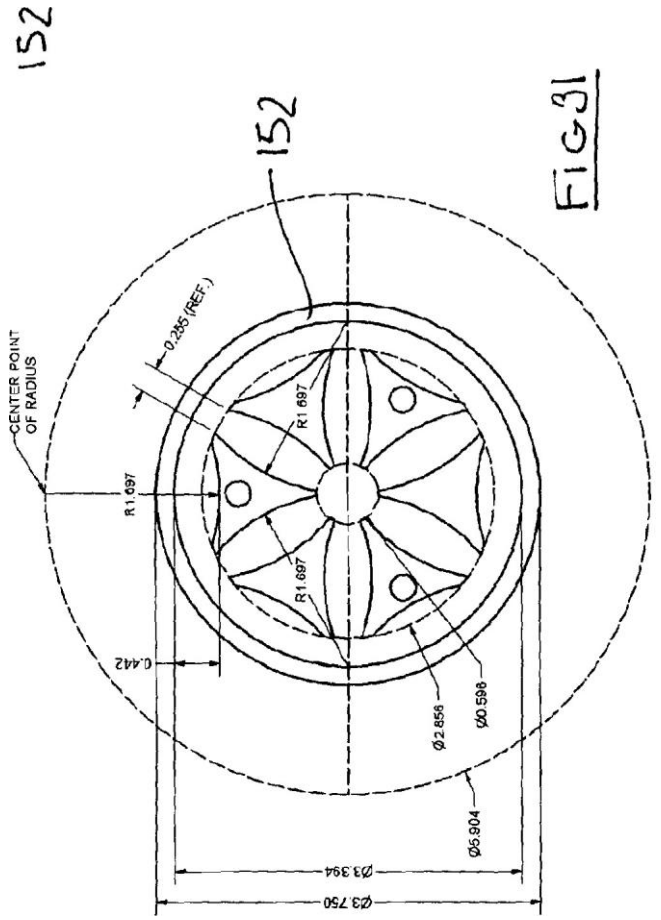

FIG 31

NOTE: DXF AVAILABLE FROM ENGINEERING

MULTI-ROTATOR MAGNETIC RESONATOR EMBODYING SACRED GEOMETRY

CROSS-REFERENCE TO RELATED APPLICATION

This application is the U.S. national phase of PCT Appln. No. PCT/CA2006/001984 filed Dec. 6, 2006, that claims priority to Canadian application 2,526,977 filed Dec. 6, 2005.

FIELD OF THE INVENTION

The present invention relates to devices that utilize magnetic fields arising from the rotation of magnets, that devices may be useful in the field ofpurilication and healing.

BACKGROUND OF THE INVENTION

A variety of devices have been proposed for the purpose of purifying water through the use of magnetic fields. Most purifying devices are stagnant magnets, few are rotating and require contact with one or more rotating magnets within a vessel containing the water to be purified. In contrast, Applicant has previously invented magnetic purification devices that require only that the substance to be purified be near the device. Applicant's earlier inventions are exemplified in Applicant's Canadian Patent Application Nos. 2,488,776 and 2,526,977.

Sacred geometrical patterns are patterns constructed using the sacred geometrical ratios, such as exemplified by the "Seed of Life" pattern, used in the description of preferred embodiments set out below. Other sacred geometrical shapes and patterns include, without limitation, pentagons, pentagrams, hexagrams, equilateral triangles, squares, rectangles with sides having a 2: I ratio, vesicapisces and 3-dimensional structures such as the pyramid and the cathara grid. Other shapes, patterns and structures will be known to those versed in sacred geometry.

SUMMARY OF THE INVENTION

In very general terms, the present invention recognizes that a significantly more eflèctive field may be realized in a magnetic resonator embodying sacred geometry by repeating a magnetic pattern based on sacred geometry axially along a rotating roller and by utilizing a plurality of rollers arranged parallel to one another.

More particularly, a magnetic resonator is provided that has a support structure and a plurality of roller assemblies mounted thereto for rotation about respective axes of rotation that are generally parallel one to another. Drive means are coupled to the roller assemblies to rotate each of the roller assemblies about its respective axis of rotation relative to the support structure. Each roller assembly houses a plurality of magnets disposed along respective axes of the roller assem-

Applicant's earlier inventions recognize that using a plurality of magnets arranged in patterns that conform to "sacred geometry" (that is discussed in more detail below) is significantly more effective than the simple rotation of a bar magnet. Nevertheless, despite Applicant's advances to date, there is a desire for even more efficient and compact devices for purifying such things as food, water, air and soil and direct application to human and animal body surfaces for healing.

The term "sacred geometry" does not refer to any religious significance. In contrast, the term "sacred geometry" is a well-known term of art that refers to a number of basic geometrical patterns and sequences that reoccur in nature. While some of the patterns may have been used in religious rituals because of the belief that such patterns have a fundamental connection with nature and humanity, this is not the locus of the present invention.

There are numerous publications that discuss sacred geometry. Exemplary ones include The Ancient Secret of the Flower of Lilè (W. I and Il) by 'Drunvalo Melchizedec and the Internet (see [Or example http:/www.intent.com/sg) and the reader is relèrred to those [Or a more in-depth study of sacred geometry.

Very broadly, sacred geometry generally relates to patterns blies. The plurality of magnets are grouped in a plurality of first and second arrangements with a first arrangement being interspersed between a pair of second arrangements. At least one of the first and second arrangements incorporates a pattern or shape based on sacred geometry.

The first arrangement of magnets may be a "seed of life" pattern.

The second arrangement of magnets may include a plurality of magnets disposed generally equidistantly about the respective axes of rotation in a generally pyramid or cone-shaped pattern or shape with a vertex of the pyramid or cone facing the first arrangement.

The magnets in the second arrangement may have discernible front and rear faces on opposite sides of a longitudinal axis. The magnets may be arranged with the longitudinal axes lying along the pyramid or cone shape. Each magnet may be rotated by an equal amount in a common direction from its neighbour whereby diametrically opposed magnets have their respective front and rear Faces Facing in generally perpendicular directions.

The magnets in the first and second arrangements may have generally planar front and rear Faces joined by curved side Faces that meet at opposite ends 10 present a lens-like profile when viewed from the front or rear Faces and a generally

and figures created or embodying one of live basic geometrical ratios: Pi, •V2, •x/5, •x/3, and Phi.

Pi is the ratio of the diameter of the circle to its circumlèrence.

A/2 is the length of a diagonal of a square with sides of length I .

A/5 the length of the a diagonal of a rectangle with sides of length I and length 2.

A/3 is the length of the chord connecting the points of 60 intersection of two circles each having a radius l, where the circumlèrence of each intersects the centre of the other.

Phi is (l +/5)/2 and is a naturally occurring ratio prevalent in animal and plant skeletal structures. It is also retèrred 10 as the "golden ratio". Most naturally occurring fractal patterns, such as snowflakes, tree shapes and so on, 10110w the golden ratio.

rectangular profile when viewed from the side face, with the longitudinal axis of each lens extending through its ends.

The magnets may be mounted in support blocks having recesses lòrmed therein (Or receiving and orienting the magnets.

The support blocks may be cylindrical and housed in roller assemblies comprising a tubular shell of a non-magnetic material. Retainers may be provided that act between the shell and the support blocks 10 constrain the support blocks against rotation relative 10 the shell.

The magnetic resonator may have three roller assemblies spaced equidistantly about a common axis.

The magnets may be arranged with their north and south poles alternating.

The magnetic resonator may have lour first arrangements of magnets and nine second arrangements of magnets.

Each second arrangement may include six magnets.

3

DESCRIPTION OF DRAWINGS

FIG. 1 is a perspective view from above showing a top, a side and an end of a magnetic resonator according to the present invention with its outer cover removed;

FIG. 2 is a view corresponding to FIG. 1 but showing the

4

drums illustrated, mounted for rotation about respective rotational axes 104 generally parallel to each other.

The roller assemblies 102 and their respective axes are also parallel to and spaced equally about a common axis 106.

Three roller assemblies 102 are illustrated arranged with their respective axes 104 arranged to correspond to the cor-

opposite side;

FIG. 3 is a top plan view of the magnetic resonator of FIGS. 1 and 2;

FIG. 4 is a front elevation corresponding to FIG. 3•

FIG. 5 is an end elevation of the magnetic resonator of

FIGS. 1 and 2;

FIG. 6 is a plan or elevational view of a roller assembly of

a resonator unit according to the present invention (as the

roller assemblies illustrated are cylindrical, plan and eleva-

(ional views would be similar);

FIG. 7 is a sectional view of the roller assembly taken on

line 7-7 ofFIG. 6•

FIG. 8 is a sectional view of the roller assembly of FIG. 6

corresponding to line 8-8 of FIG. 7 and showing a magnet

holder according to the present invention;

FIG. 9 is a sectional view of the magnet holder of FIG. 8

taken on line 9-9 of FIG. 8•

FIG. 9A is a perspective view of a "lens" shaped magnet

according to the present invention;

FIG. 10 is a front elevation of a magnet holder according to

the present invention for holding 1 8 magnets;

FIG. 11 is a rear elevation of the magnet holder of FIG. 10•

FIG. 12 is a section on line—12-12 of FIG. 10•

FIG. 13 is a section on line 13-13 ofFIG. 10•

FIG. 14 is a section on line 14-14 ofFIG. 10•

ners of an equilateral triangle when viewed from the end, such

as in FIG. 5.

A prototype magnetic resonator 100 built according to such an arrangement has provided beneficial results in test-

ing. It is however expected that other numbers and arrange-

ments of rollers may work. Certainly beneficial results, albeit

a smaller resonant field is achievable with a single roller assembly 102.

Each of the roller assemblies 102 contains magnets

arranged according to a pattern conforming to sacred geom-

etry as described in detail further below.

The roller assemblies 102 are rotated about their respective

axes 104 by any suitable motive power means or rotator to

create a resonant magnetic field. A suitable rotator, as illus-

trated, may include a motor 108 rotatably coupled to the

rotator assemblies 102 by a drive belt 112 that rides on and

frictionally engages driven pulleys 110 mounted to the rotator

assemblies 102. A driving pulley 114 mounted to an output

shaft of the motor 108 and presses against the drive belt 112

to frictionally engage the belt 112.

It will be appreciated that the pulley and belt arrangement

is exemplary and may be substituted with other drive assem-

blies such as a sprocket and chain assembly or a gear drive

assembly, to mention but two alternatives.

The balance of the structure illustrated in FIGS. 1 through

5 is mostly support structure for the mounting and support of

FIG. 15 is a front elevation of a magnet holder according to the present invention for holding 6 magnets;

FIG. 16 is a section on line 16-16 ofFIG. 15•

FIG. 17 is a section on line 17-17 ofFIG. 15•

FIG. 18 is a section on line 18-18 ofFIG. 15•

FIG. 19 is a front elevation showing hidden detail of a magnet holder according to the present invention for holding six (6) magnets.

FIG. 20 is a top plan view of the magnet holder of FIG. 19'

FIG. 21 is a perspective view ofthe magnet holder of FIGS. 19 and 20 taken from the direction of line 21-21 of FIG. 2()•

FIG. 22 is a section on line 22-22 ofFIG. 19;

FIG. 23 is a section on line 23-23 ofFIG. 19;

FIG. 24 is a front elevation of a magnet holder according to the present invention [Or holding eighteen (18) magnets;

FIG. 25 is a rear elevation ofthe magnet holder of FIG. 24;

FIG. 26 is a top plan view ofthe magnet holder ofFIG. 24;

FIG. 27 is a perspective view ofthe magnet holder ofFIGS. 24, 25 and 26 taken from the perspective ofline 27-27 ofFIG. 26;

FIG. 28 is a section on line 28-28 of FIG. 24;

FIG. 29 is a section on line 29-29 of FIG. 24;

FIG. 30 is a perspective view of a magnet holder according to the present invention (Or holding eighteen (18) magnets;

the components described above. The support structure illustrated includes a base 120 to that roller assembly support plates 122 are secured to extend generally perpendicularly therefrom. The roller assembly support plates would typically house bearings into that respective ends of the roller assemblies 102 are journalled for low friction rotational support.

The motor 108 may be supported on the base 120 by an adjustable motor mount 122 to allow for tensioning of the drive belt 112 by moving the motor 108.

A non-magnetic cover (not illustrated) may be provided over the magnetic resonator 100 for aesthetics and to protect against inadvertent contact with any moving parts.

The roller assemblies 108 and parts thereof are illustrated in detail in FIGS. 6-31. Each roller assembly 108 has a generally cylindrical shell 130 of a non-magnetic material (Ibr example aluminium) inside of that is disposed an array of lens-shaped magnets 132 disposed generally axially thereal-ong.

"Non-magnetic" as used herein is intended to relèr to a material that doesn't significantly interlère with the magnelic field associated with the magnets 132.

The array of magnets 132 generally comprises two arrangements. A first arrangement 134 is a radially disposed "seed of lilè" pattern as shown in FIG. 8.

and

FIG. 31 is a front elevation ofthe magnet holder ofFIG. 30 showing representative radii of curved portions of FIG. 30.

DESCRIPTION OF PREFERRED EMBODIMENTS

A magnetic resonator according to the present invention is generally indicated by relèrence in the accompanying illustrations. The magnetic resonator basically comprises a plurality of roller assemblies 102, such as the cylindrical

first arrangement 134. In other words, the magnets 132 of the second arrangement 136 diverge from the rotational axis 104 away from the adjacent first arrangement 134.

As can be seen in FIGS. 9 through 16, each of the magnets 132 of each second arrangement 136 has a slightly different orientation than the remaining magnets 132 of the second arrangement 136. As mentioned above, each magnet 132 has a generally lens-like shape in that it has generally parallel planar side faces 140 and curved front and rear faces 142 that meet at opposite edges 144 as can be seen in FIG. 9A. A lens axis 146 extends through each lens 132 between the edges 144 equidistant from the side faces 140.

A second arrangement 136 generally comprises six magnets equidistantly spaced about the rotational axis 104 of the roller 102 in a generally conical layout. In other words, one end of each ofthe magnets 132 is closer to the rotational axis 138 than is its opposite end. Hence the magnets 132 of the second arrangement 136 either converge or diverge relative 10 the rotational axis 138 (depending on one's frame of relèrence).

A second arrangement 136 is located adjacent each first arrangement with the magnets 132 of each second arrangement 136 being closest 10 the rotational axis 104 adjacent the

Use of the resonator 100 doesn't require that the object to be treated surround the roller assemblies 102. Being adjacent thereto is generally sufficient and accordingly, in the case of fluids all that is required is that a non-magnetic conduit for the fluid pass by the resonator 100. It is believed that purification time will depend on the substance being purified and the overall size of the resonator 100. For water purification using a resonator 100 having rollers of about 17 inches in length and about 4 inches in diameter it is believed that approximately 0.03 seconds would be required for killing a virus. PCB 's may require about 20 minutes. Accordingly it should be apparent that a continuous flow operation (as contrasted with a batch

Each lens 132 in the second arrangement 136 is oriented as
if it has been rotated about 30 ^{0} (thirty degrees) about its lens
axis 146 relative to the immediately adjacent lenses 132. The
arrow indicated by relèrence 148 in FIG. (DA illustrates the
rotation. FIGS. 12 through 14 and 15 through 18 illustrate the
resulting orientations. Note for example that one of the two
lenses 132 apparent in FIG. 12 (to the left as illustrated)
presents its side face parallel to the plane of the page whereas
the other (to the right as illustrated) has its side faces 140
perpendicular to the plane of the page. FIG. 16 illustrates the
reverse arrangement.

The magnets 132 are held in their respective positions by
respective 18 magnet and 6 magnet holders 150 and 152.
FIGS. 10 through 14 and 24 through 31 illustrate the former
and FIGS. 15 through 23 illustrate the latter. Quite simply the
magnet holders 150 and 152 are non-magnetic blocks with
suitable recesses for receiving the magnets 132 to align and
hold them in their desired positions.

The 18 magnet holders 150 hold both a first arrangement
134 and a second arrangement 136 of magnets 132. The 6
magnet holders 152 hold only a second arrangement 136 of
magnets. It should be borne in mind that the magnet holders
150 and 152 are merely exemplary as no doubt other secure-
ment means are viable. For example the entire array could be
operation) may be viable at least for some applications.

The above description focuses upon the use of a "seed of
lilè" pattern. The seed of lilè is but one geometric pattern
that incorporates the reoccurring ratios or sequences Ibund
in nature that are collectively referred to as "sacred geom-
etry". It is believed that the inherent ratios of the sacred
geometry associated with the "seed of life" has a strong
influence on the effectiveness of the resulting magnetic field.
Accordingly, it stands to reason that beneficial results would
also be achieved by selecting other of the geometric patterns
within the sacred geometry group.

The magnets 132 should be as strong as reasonably pos-
sible. Accordingly rare earth magnets are presently preferred
in view of their high strength to size ratio. Whilst this is a
preference it is not a requirement. Other forms of permanent
magnets or even electromagnets may be used. Preferably the
magnets 132 are symmetrically disposed to minimize rota-
tionally induced vibration during use. The magnets are pref-
erably arranged in alternating north-south orientation, but this
may be changeable.

The resonator 100 of the present invention is believed to
have practical application as a means to purify water or food
by killing pathogens and breaking down toxins. The resonator
100 also may have practical application in direct application

cast into a suitable potting material such as a thermosetting or thermal setting polymer or a chemically setting resin such as epoxy.

Reference is now made to FIGS. 20 through 23 illustrating a six magnet holder 152. The 6 magnet holder 152 has a generally cylindrical body 160 having a plurality of recesses 162 each of that accommodates a single magnet 132.

Each ofthe recesses 162 is configured to receive its respective magnet in a desired orientation by closely engaging the side Faces 140 of the magnet 132.

Locating holes 164 are provided between opposite Faces 166 ofthe 6 magnet holder 152 to align with locating rods or bolts 168 (see FIG. 6) that extend through the roller assembly 102. The locating holes 164 align the magnet holders 150 and 152 and secure the magnet holders 150 and 152 to the balance of the roller assemblies (Or rotation therewith.

Relèrence is now made 10 FIGS. 24 through 31 that illustrate 18 magnet holders 150. The 18 magnet holders are similar to the 6 magnet holders on one side but, on the opposite side, include lilrlher recesses 170 Ibr receiving and holding the magnets 132 ofthe first arrangement 134. As with the 6 magnet holder 152, locating holes 164 are provided to align with locating rods or bolts 168 and retain the 18 magnet holder 150 in a desired orientation within the roller assembly 104.

to a human body and animals to assist in restoring circulation, treating inflammation, ulceration, viral and bacterial infections and as a general tonic. The resonator 100 may also be useful for reducing environmental toxins in air, water, food and soil. Preliminary tests are believed to be able to show the breakdown of toxic compounds (such as in automobile exhaust) into smaller and less harmlill constituent elements such as IC, CO, NO and S O .

The above invention is described in an illustrative rather than a restrictive sense. Variations may be apparent to persons skilled in such arrangements without departing from the spirit and scope of the invention as defined by the claims set out below.

PARTS LIST

100 resonator

102 roller assembly

104 axis (roller assembly)

106 common axis (of roller assemblies)

108 motor

110 driven pulleys

112 drive belt

114 drive pulleys

120 base

In use, the motor 108 is activated 10 rotate the roller assemblies 1 02 via the drive bell 1 12. The desired speed al that the rollers 102 rotate may vary depending upon the purpose tor that the resonator is 10 be used. For example, it is believed that running the roller assemblies 102 al 3,500 10 rpm may prove 10 be beneficial in water purification applications.

122 support plates

124 adjustable motor mount

130 shell (roller)

132 magnets

134 first arrangement (seed of lilè)

136 second arrangement (conical)

138 rotational axis (roller assembly)

140 side face (lens)

142 front and rear faces (lens)

144 edges (lens)

146 lens axis

148 arrows (showing rotational displacement of lens)

150 18 magnet holder

152 6 magnet holder

162 recesses (for holding magnets)

164 locating holes

166 opposite faces (of body)

168 rods or bolts (extending through roller assembly)

170 recesses in 150 for holding first arrangement of magnets

The invention claimed is:

1. A magnetic resonator comprising: a support structure; a plurality of roller assemblies mounted to said support structure for rotation about respective axes of rotation that are generally parallel to one another; drive means coupled to said roller assemblies for rotating each of said roller assemblies about its respective axis of rotation relative to said support structure; each said roller assembly housing a plurality of magnets disposed along said respective axes; said plurality of magnets are grouped in a plurality of a first and second

along said pyramid or cone shape; each said magnet is rotated by an equal amount in a common direction from its neighbour whereby diametrically opposed magnets have respective of said front and rear faces facing in generally perpendicular directions.

4. The magnetic resonator of claim 3 wherein: said magnets in said first and second arrangements have generally planar side faces joined by curved front and rear faces that meet at opposite ends to present a lens-like profile when viewed from the said front or rear faces and a generally rectangular profile when reviewed from said side faces; and, said longitudinal axis of each said lens extends through said ends.

5. The magnetic resonator of claim 4 wherein: said magnets are mounted in support blocks having recesses IUrmed therein for receiving and orienting said magnets.

6. The magnetic resonator of claim 5 wherein: said support blocks are cylindrical; said roller assemblies have a tubular shell of a non-magnetic material housing said support blocks; and, retainers are provided that act between said shell and said support blocks to constrain said support blocks against rotation relative to said shell.

arrangements in distinct, non-identical patterns, with a first arrangement being interspersed between a pair of said second arrangements; at least one of said first and second arrangements incorporating a pattern or shape based on a seed of life pattern.

2. The magnetic resonator of claim 1 wherein: said second arrangement of magnets includes a plurality of said magnets disposed generally equidistantly about said respective axes of rotation in a generally pyramid or cone-shaped pattern or shape with a vertex of said pyramid or cone facing said first arrangement.

3. The magnetic resonator of claim 2 wherein: said magnets in said second arrangement of magnets have discernible front and rear faces on opposite sides of a longitudinal axis; said magnets are arranged with said longitudinal axes lying

7. The magnetic resonator of claim 6 further comprising:

three of said roller assemblies spaced equidistantly about a common axis.

8. The magnetic resonator of claim 7 wherein at least some of said magnets are arranged with their respective north and south poles alternating.

9. The magnetic resonator of claim 8 further comprising:

four of said first arrangements and nine of said second arrangements, along each said roller.

10. The magnetic resonator of any one of claim 1 wherein each said second arrangement has six (6) magnets.

11. The magnetic resonator of claims 1 wherein said drive means is arranged to rotate said rollers at from 3,500 to 4 000 revolutions per minute ("rpm").

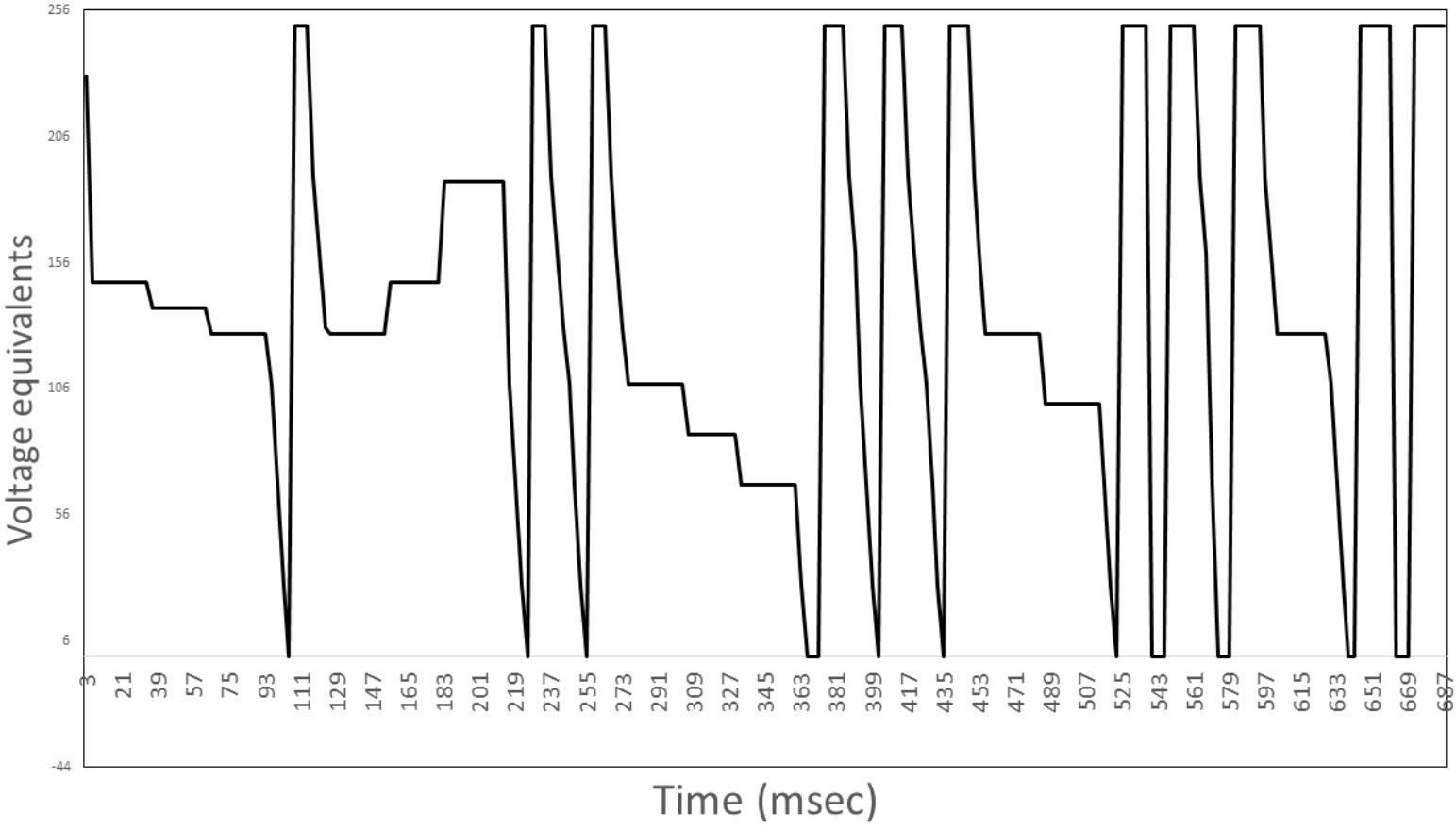

Appendix C: Graphical representation of the burst-firing EMF pattern.

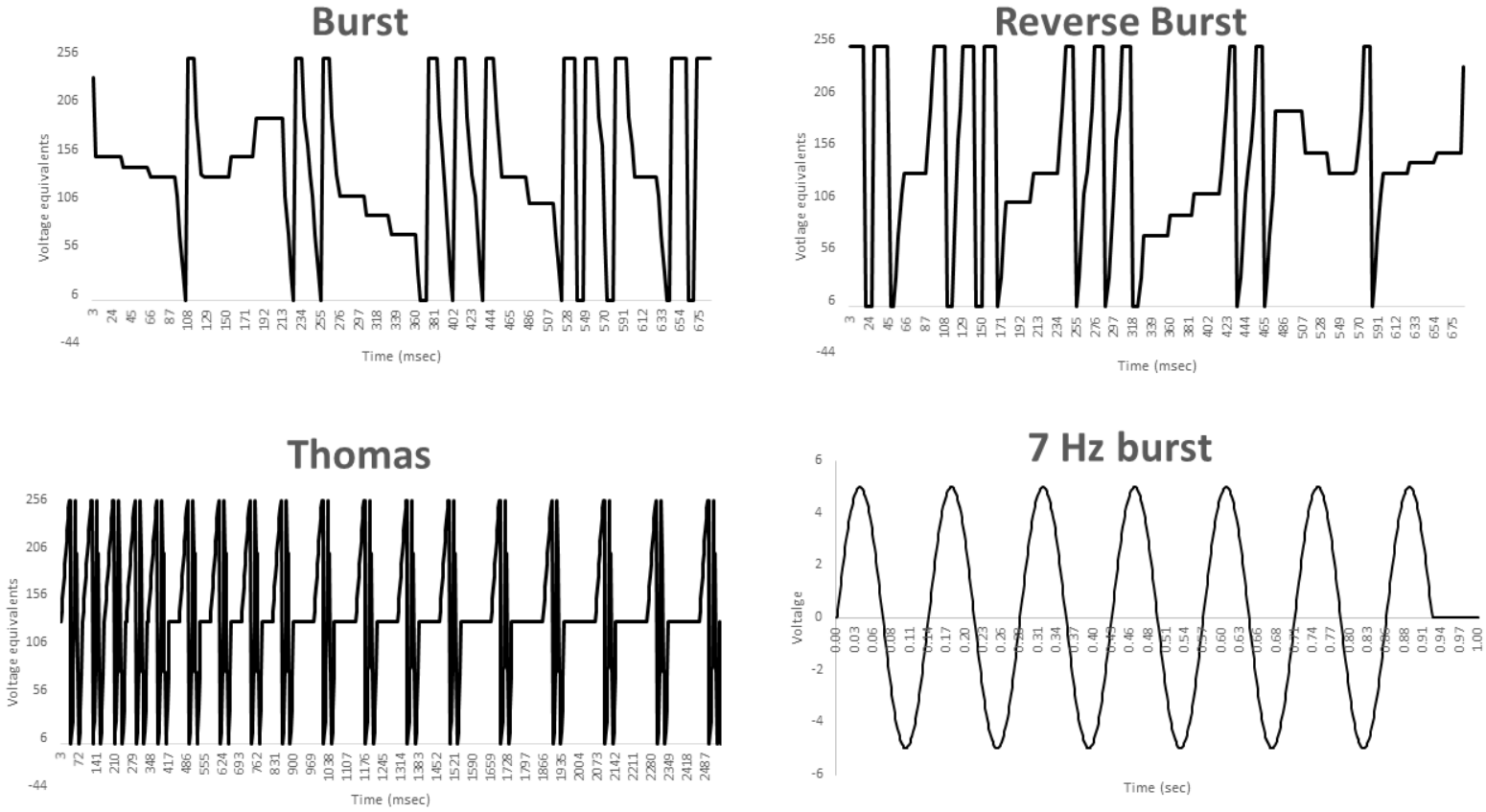

Appendix D: Graphical representation of the burst-firing (top left), reverse burst firing (top right), Thomas (bottom left), and 7-Hz burst (bottom right) patterns.

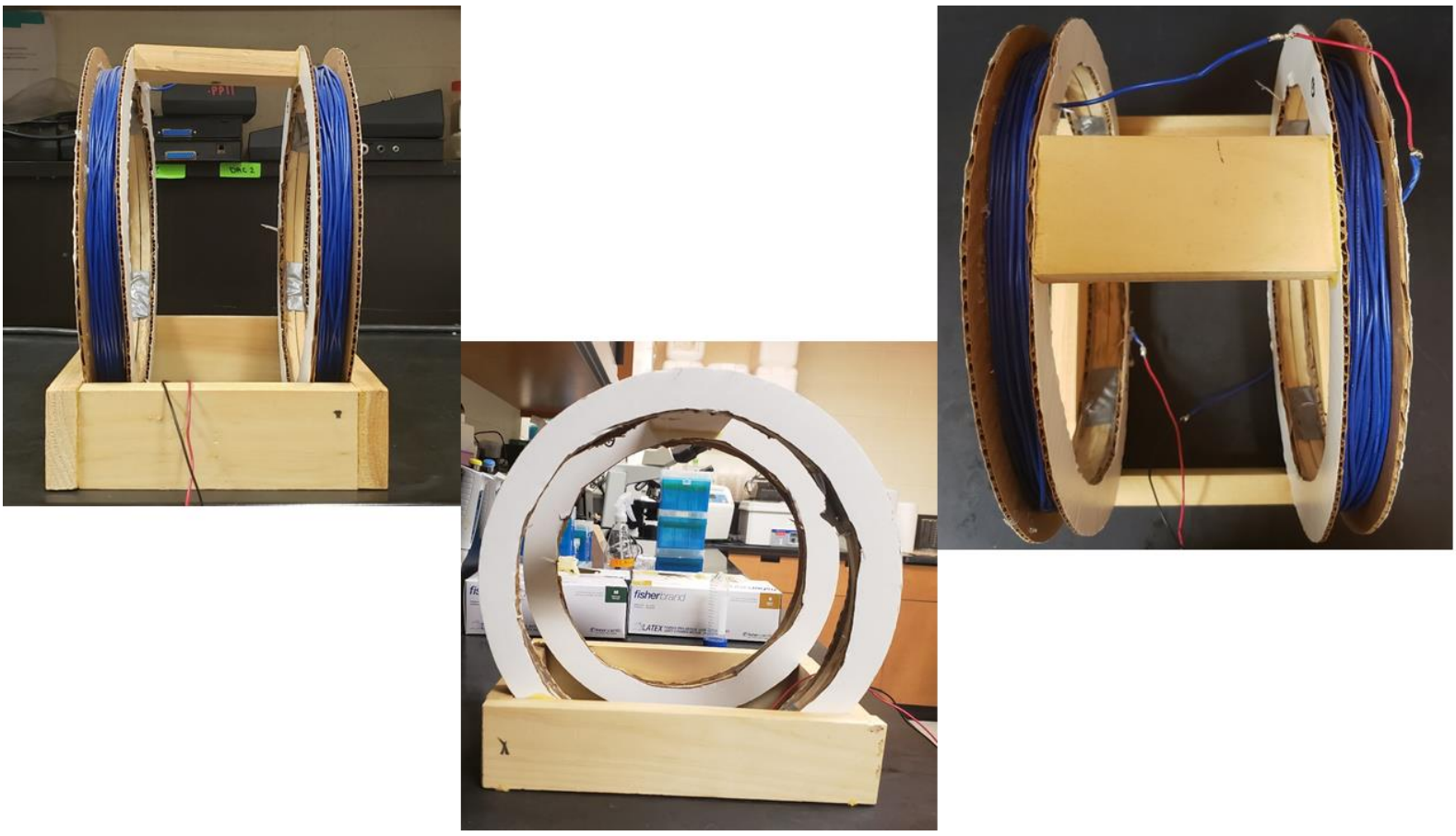

Appendix E1: Photographic representation of the Helmholtz geometry from various perspectives. Front view (top left), Top view (top right), Left-sided view (bottom, middle).

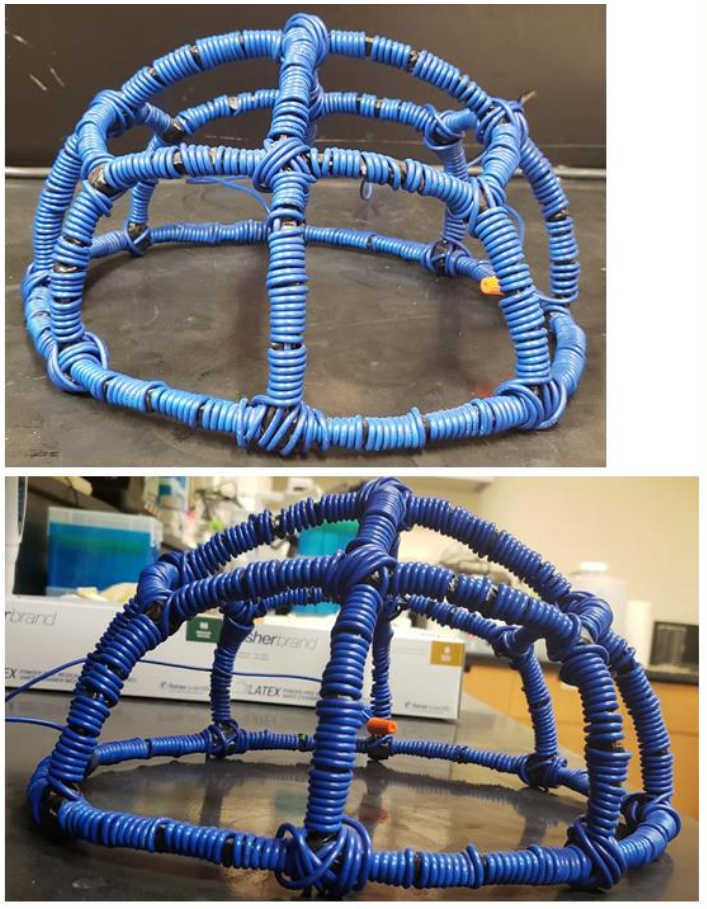

Appendix E2: Photographic representation of the Hoberman geometry taken from various perspectives. Front view (top left), Top view (right), Left-sided view (bottom left).

Appendix E3: Photographic representation of the Rodin geometry taken from different perspectives. Front view (top left), Top view (right), Left-sided view (bottom left).

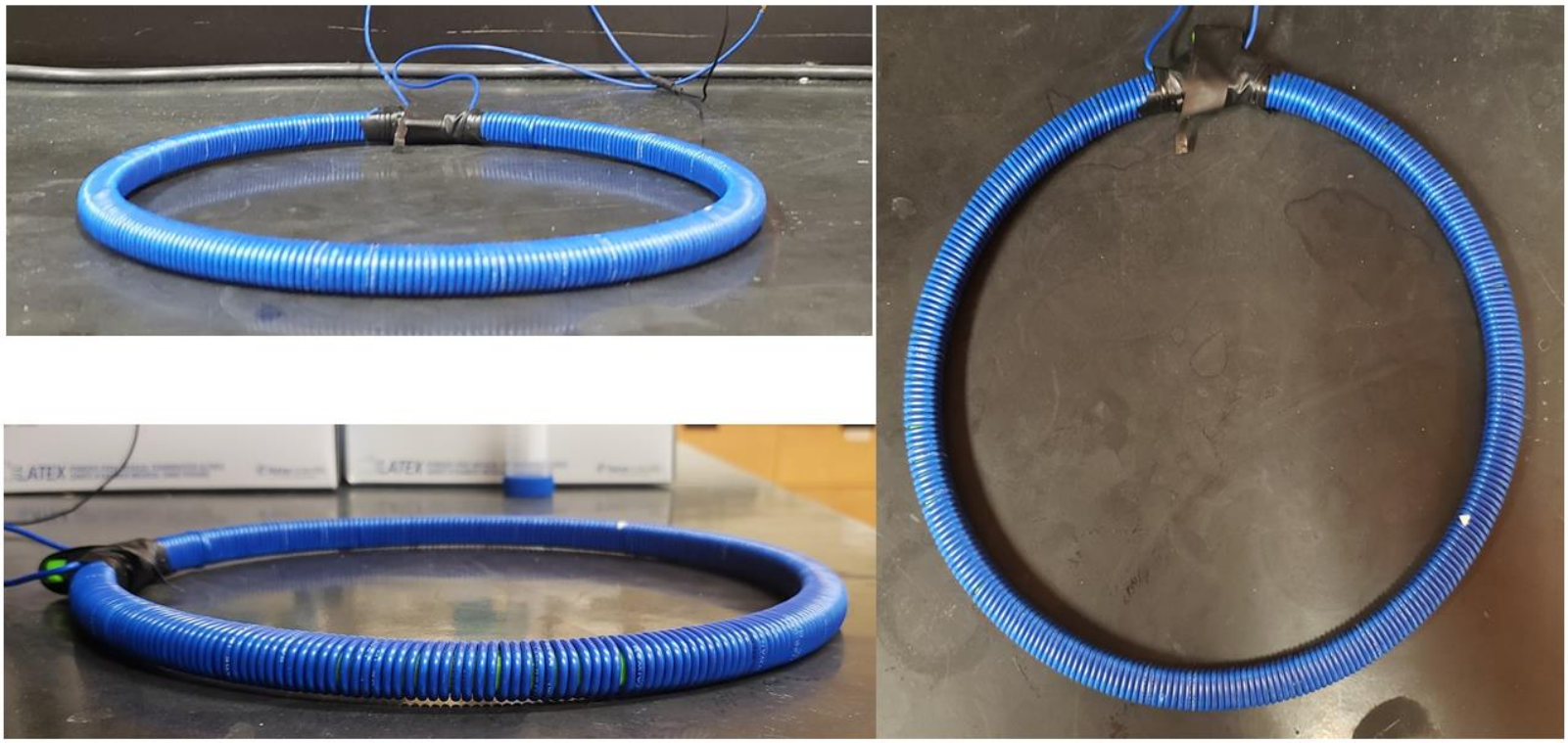

Appendix E4: Photographic representation of the Toroid geometry taken from different perspectives. Front view (top left), Top view (right), Left-sided view (bottom left).

Appendix E5: Pictographic representation of PC-12 exposure conditions to various magnetic field generating devices (i.e., application geometries). The example provided demonstrates the Hoberman geometry in the context of the experimental set-up.

Appendix F: Photographs of the Faraday-bowls. Weavemesh (top row) and fly mesh (bottom row) constructs ranging from left-to-right in terms of overall coverage.

Appendix G: Photographic representation of experimental set-up for the measurement of background, ambient fluctuations in the Earth's magnetic field with the Hoberman geometry as an example.

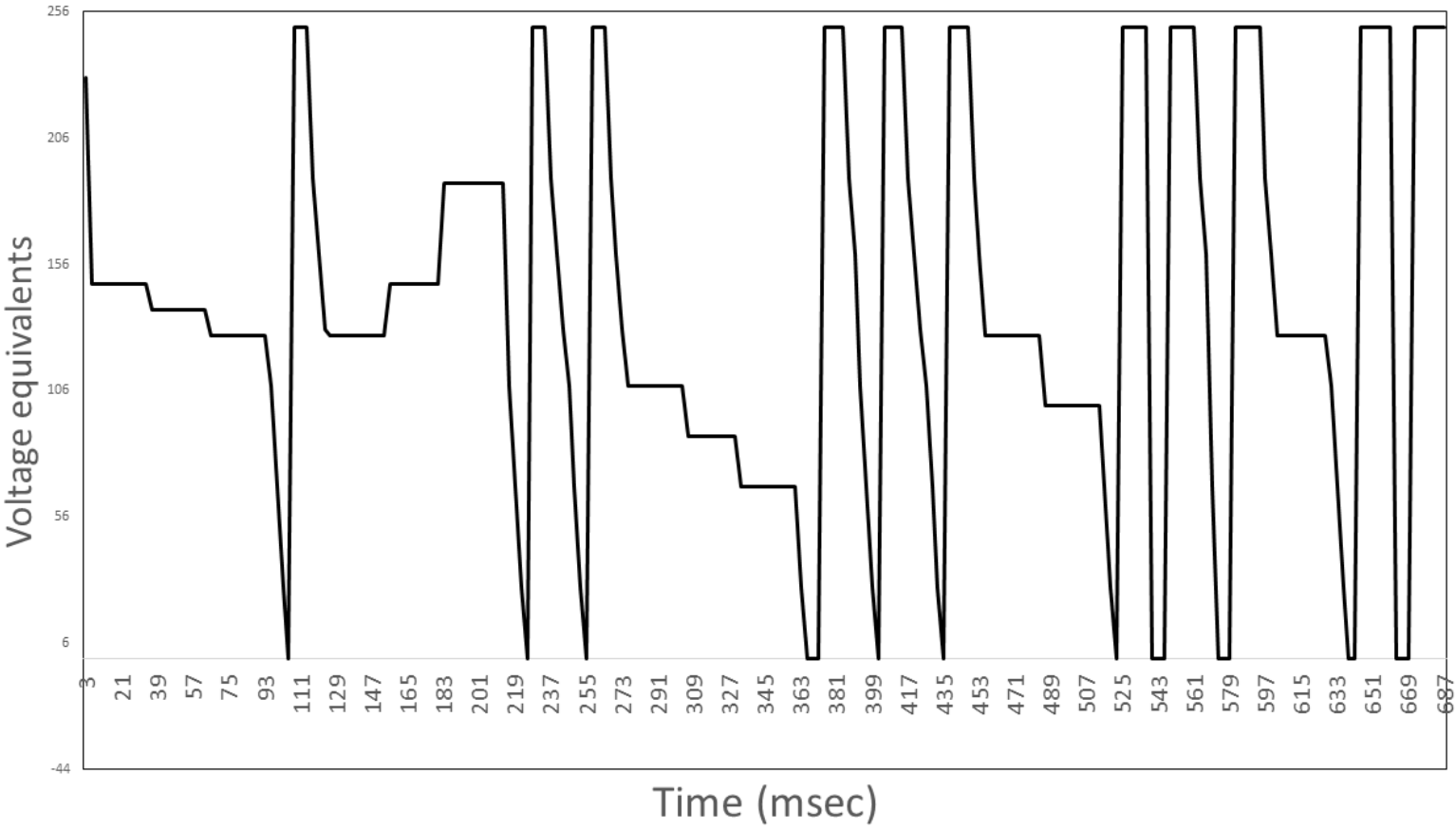

Appendix H1: Graphical representation of the Thomas-EMF pattern.

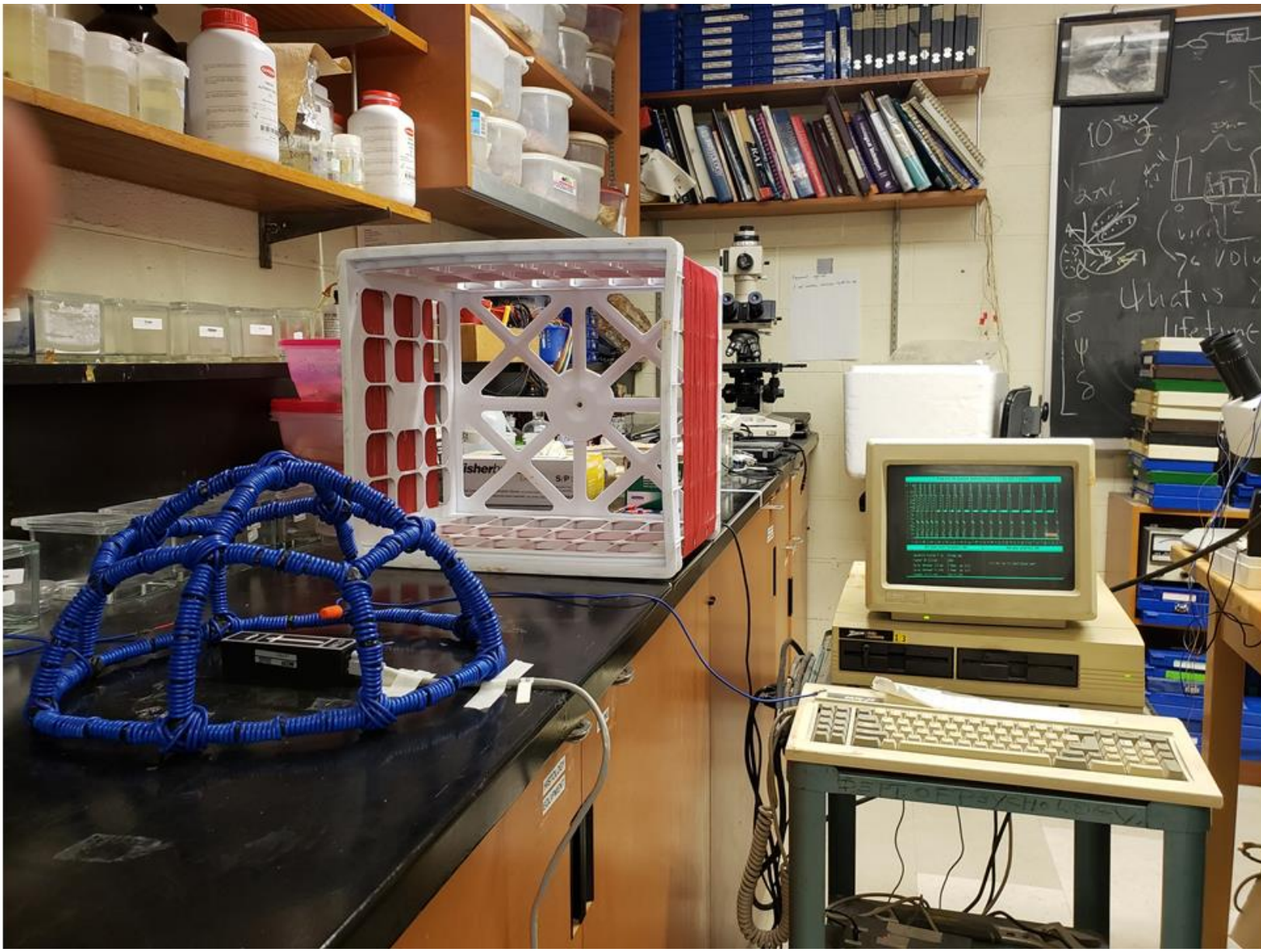

Appendix H2: Photographic representation of the experimental set-up for exogenous field induction trials with the Hoberman geometry serving as an example.

Appendix I: Photograph of the experimental set-up for the measurement of background voltage fluctuations induced the various EMF coils in a Faraday cage and acoustic chamber.

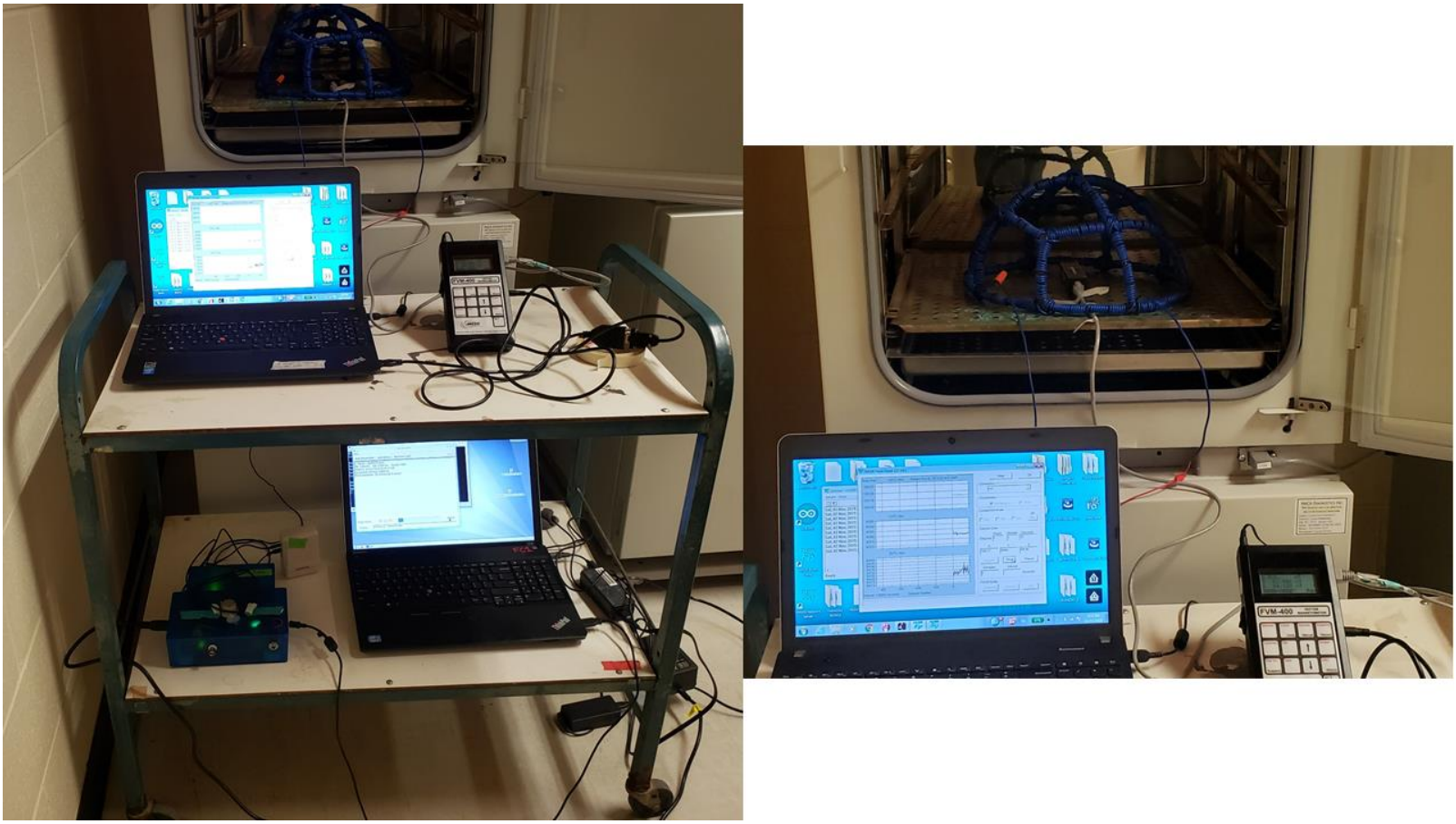

Appendix J: Photograph of the experimental set-up for measuring fluctuations in static magnetic field measures in a standard incubator when the burst-firing EMF is generated through different application geometries. Here, the Hoberman geometry is used as an example.